Characterization and prospective applications of melanin from black fungi in environmental biotechnology

Cristy Alejandra Medina-Armijo

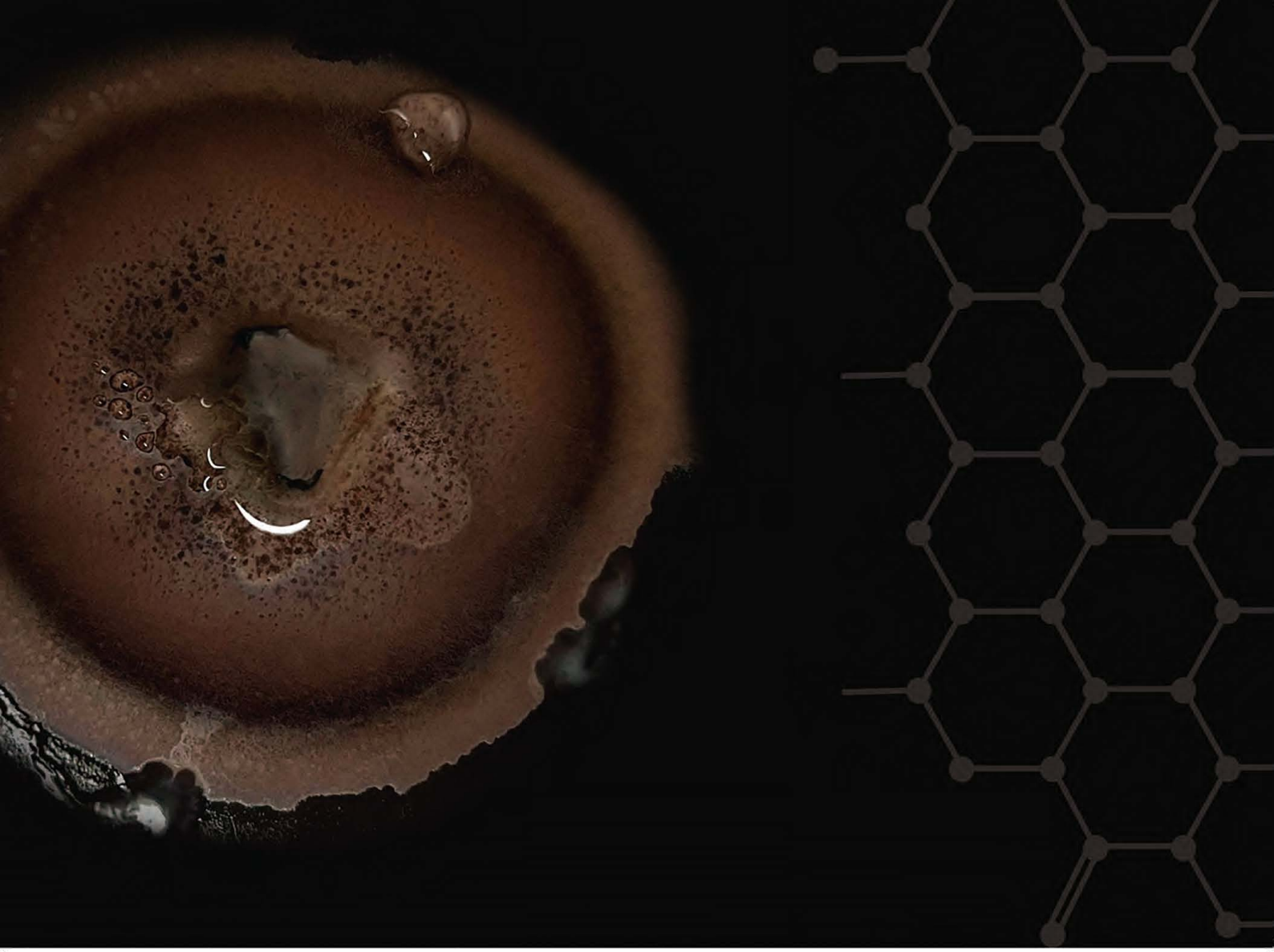

PhD. Dissertation

Characterization and prospective applications of melanin from black fungi in environmental biotechnology

Cristy Alejandra Medina-Armijo

UNIVERSITAT DE BARCELONA

IRTA
Institut
de Recerca i Tecnologia
Agroalimentàries

Barcelona, May 2024

UNIVERSITAT DE BARCELONA

FACULTAT DE FARMÀCIA I CIÈNCIES DE L'ALIMENTACIÓ

Characterization and prospective applications of melanin from black fungi in environmental biotechnology

Cristy Alejandra Medina-Armijo

Barcelona, May 2024

Doctorate Programme of Environmental Biotechnology

Faculty of Pharmacy and Food Sciences

Characterization and prospective applications of melanin from black fungi in environmental biotechnology

Cristy Alejandra Medina-Armijo

Supervised by:
Dr. Francesc X. Prenafeta Boldú and Dr. Marc Viñas Canals

Institute of Agrifood Research and Technology (IRTA)

Programme of Sustainability in Biosystems

Thesis submitted to fulfill the requirements for the doctoral degree at the University of Barcelona.
Barcelona, May 2024

"The future belongs to those who believe in the beauty of their dreams."

Eleanor Roosevelt

Agradecimientos

Finalmente, esta etapa se cerrará pronto. Sé que el doctorado es solo uno de los desafíos que tendré que superar durante mi vida, pero lo recordaré como uno de los hitos de mayor exigencia mental. Por eso, me gustaría expresar mi gratitud a todos aquellos que me brindaron la posibilidad de completar esta tesis en particular, así como el apoyo académico en general que recibí durante mi tiempo de doctorado en IRTA-Torre Marimon. Ante todo, me gustaría enviar mi más profundo agradecimiento a mis directores Francesc Prenafeta-Boldú y Marc Viñas Canals, por presentarme un tema tan interesante para el proyecto de doctorado y brindarme todas las condiciones necesarias para realizarlo y completarlo en IRTA. Agradezco su invaluable guía y consejo durante todos estos años. Aún más que eso, estoy agradecido por su paciencia, inquietudes, apoyo y comprensión en mi viaje de doctorado. También deseo enviar mis sinceros agradecimientos Yolanda Lucas y Anna Puerta por su invaluable ayuda técnica, apoyo en el laboratorio y sobre todo por la motivación de aprender y emprender nuevos retos y su desinteresada ayuda.

A todo el grupo de Sostenibilidad en Biosistemas, por todos los momentos en el laboratorio, las risas, los llantos, el estrés, las charlas, las comidas y tantos momentos compartidos tratando de mejorar el mundo. Mil gracias a mis compañeros de doctorado, especialmente a Marlene y Lucía, un pequeño grupo donde podíamos desahogarnos del trabajo, comprendernos y ayudarnos mutuamente. Son las mejores. Tampoco puedo dejar de agradecer a Miriam Guivernau y Laura Tey por su gran ayuda en momentos críticos, especialmente por el apoyo moral que se necesita cuando uno se siente perdido. Su gestión para solucionar los problemas es indiscutible. Gracias también por su conocimiento e ideas brillantes y por su constante disposición a ayudar. Quisiera agradecer a la Dra. Belén Fernández por toda su ayuda con el análisis de gases, por el tiempo que dedicó a resolver mis dudas, en varias ocasiones. Su ayuda fue invaluable, mil gracias.

Finalmente quiero dar las gracias a mi querida familia a mis padres, por su apoyo incondicional, sus ánimos y sus payasadas liberadoras. Son una fuente constante de inspiración para mí. A mi hermana Ale, todos tus consejos de química experimental fueron clavados para desarrollar mi tesis. Siempre presente en la habitación favorita de mi corazón, siempre remando juntas eres tremenda, la mejor hermana. Por supuesto a mi Alex, mi persona favorita, debería escribir otra tesis para darte los agradecimientos, las palabras se van a quedar cortas. Gracias por ser un pilar en los mejores y peores momentos. Siempre estas, siempre nos cuidas a mí y a toda la tropa (Negra, Otto, Marramiau y Kity). Cada camino que tomamos juntas lo hacemos el mejor, siempre hay flores en nuestras vidas. No podría haber terminado esta tesis sin tu gran apoyo.

¡Gracias totales!

TABLE OF CONTENTS

INDEX OF FIGURES

Chapter 1.

Chapter 3.

Chapter 4.

Chapter 5.

Chapter 6.

INDEX OF TABLES

Chapter 1

Chapter 3

Chapter 4

Chapter 5

Summary

Black fungi comprise a diverse group of ascomycetes characterized by their dark pigmentation due to the presence of melanin within their cells. This melanization process confers black fungi with a remarkable adaptability to a broad spectrum of harsh environments, including extreme temperatures, pH, water activity, and pressure values, as well as high levels of UV/ionizing radiation, and exposure to toxic chemicals. Over the past decade, fungal melanin has garnered increasing interest for its potential applications in organic semiconductors and bioelectronics, drug delivery systems, photoprotective materials, and environmental remediation processes. Despite significant advancements in these fields, the large-scale practical use of melanin remains limited, primarily due to the restricted availability and high cost associated with its natural sources. Furthermore, the complex physicochemical properties of melanin, coupled with its low solubility in water and organic solvents, hamper both its study and practical utilization.

This thesis investigated the metallotolerance of a collection of 34 strains of black fungi isolated from hydrocarbon-rich environments. Two metallotolerant strains belonging to *Exophiala mesophila* and *Rhinocladiella similis* were selected for subsequent biosorption experiments on As(V) and Cr(VI), as respective models of environmentally relevant metalloid and a heavy metal. The sorption efficacy of *E. mesophila* melanin extracts was studied in more detail and the sorption isotherm and kinetics were determined for Cr(VI). The results revealed high inter- and intraspecific variability in metallotolerance, suggesting the existence of additional physiological mechanisms beyond melanization that enable these fungi to cope with the toxic effects of metals and metalloids. A significant difference in the maximum Cr(VI) adsorption capacity (q_{max}) was observed between alive fungal biomass, dead biomass, and he fungal melanin extracts (alive biomass and extracted melanin, qmax: 95.26 vs. 544.84 $mgCr^{6+}\ g^{-1}$).

A protocol for the production of *E mesophila* biomass and for the optimized extraction of melanin was developed to obtain sufficient yields of this biomaterial for subsequent fundamental and applied research. Fungal melanin was then characterized by using an array of spectrophotometric techniques (UV-Vis, FTIR, and EPR) and by cyclic voltammetry (CV). The utilization of tricyclazole, a specific inhibitor of the biosynthesis of the melanin type most black fungi have been associated to (built from 1,8-dihydroxynaphthalene monomers), allowed us to identify, OH, COOH and C=O as the primary groups involved in Cr(VI) binding mechanisms during adsorption processes by whole cells of *E. mesophila*. Additionally, bioelectrochemical assessment of melanin revealed electrochemical properties as semiconductor, as well as a synergistic electroactive interaction with *Geobacter sulfarreduscens*. Cyclic voltammetry of melanin extracts incubated with and without cell suspensions of the electroconductive bacterium *Geobacter sulfurreducens* were indicative of novel semiquinone/hydroquinone redox transformations. This melanin interactions may play an important role in cation exchange for the adsorption of metals and in microbial interspecies electron transfer processes, which were intrinsically linked to quinone and semiquinone moietieslecules in the melanin.

The mechanisms of metallotolerance of *E. mesophila* to As(V) and Cr(VI) exposure were studied by combining high throughput biochemical and transcriptome analyses. FTIR analyses revealed changes particularly affecting the content of amide I and II bands (proteins), phospholipids (associated with membranes and DNA), and lipids. The main upregulated metabolic pathways associated to metallotolerance included the enhanced expression of genes related to protective and transport mechanisms, such as cassette ABC transporters, vacuolar transport, NADPH-

dependent Cr(VI) reduction and storage, and antioxidant enzymes (SOD and CAT) to mitigate reactive oxygen species (ROS) production. Additionally, we identified upregulation of various DNA repair pathways and protein synthesis. Novel applications of fungal melanin, aimed at mitigating the emissions of greenhouse gases were investigated. Melanin extracts from *E. mesophila* were compared with other (semi) conductor materials (biochar and magnetite) to assess its influence on carbon cycling and cumulative methane emissions in anaerobic microcosms with soil from postharvest rice fields, amended with rice straw mimicking the postharvest season, when significant amounts of methane are emitted in rice paddy fields. Individual melanin and biochar amendments resulted in a significant reduction of cumulative methane emission (29% and 10% of depletion, respectively ($p < 0.0001$), compared to the control without conductive materials) after 130 days of incubation. This reduction could be attributed to the potential of fungal melanin and biochar to stimulate direct interspecies electron transfer (DIET) mechanism in anoxic soils. Upon melanin application, linear discriminant analysis effect size (LEfSe) revealed a differential and significant presence of putative electroactive bacteria belonging to the genera *Geobacter* and *Pseudopelobacter*,as well as methanogenic archaea (*Methanosarcinia*), which could be outcompeted by the DIET mechanisms of other methanogenic populations with higher methane generation rates in the absence of melanin and biochar. The observed effect suggests that melanin may shorten the lag phase for methane production but ultimatelly lead to a lower overall emission rate. Compound specific isotope analysis of the emitted methane and carbon dioxyde ($\delta^{13}C\text{-}CH_4$, $\delta^{13}C\text{-}CO_2$ and $\delta^{2}H\text{-}CH_4$) revealed that the main methanogenic pathway in the melanin/biochar amended microcosms proceeded through methylotrophic/acetotrophic archaea, instead of hydrogenotrophic pathway predominant in all soil microcosms.

Resumen

Los hongos negros (Black fungi) constituyen un grupo diverso de ascomicetos caracterizados por su pigmentación oscura debido a la presencia de melanina dentro de sus células. Este proceso de melanización confiere a los hongos negros una notable adaptabilidad a un amplio espectro de ambientes hostiles, incluyendo temperaturas extremas, pH, actividad del agua y valores de presión, así como altos niveles de radiación UV/ionizante y exposición a productos químicos tóxicos. En la última década, la melanina fúngica ha despertado un creciente interés por sus potenciales aplicaciones en semiconductores orgánicos y bioelectrónica, sistemas de administración de fármacos, materiales fotoprotectores y procesos de biorremediación ambiental. A pesar de los avances significativos en estos campos, la aplicación industrial a gran escala sigue siendo limitada. Esto se debe principalmente a la disponibilidad restringida y al alto costo asociado con la producción de melanina sintética. Además, las complejas propiedades fisicoquímicas de la melanina, junto con su baja solubilidad en agua y solventes orgánicos, dificultan tanto su estudio como su uso práctico.

Esta tesis investigó la metalotolerancia de una colección de 34 cepas de hongos negros aisladas de ambientes ricos en hidrocarburos. Se seleccionaron dos cepas metalotolerantes pertenecientes a *Exophiala mesophila* y *Rhinocladiella similis* para posteriores experimentos de biosorción sobre As(V) y Cr(VI), como modelos representativos de un metaloide y un metal pesado ambientalmente relevantes. La eficacia de sorción de los extractos de melanina de *E. mesophila* se estudió con mayor detalle, determinándose la isoterma y la cinética de sorción para Cr(VI). Los resultados revelaron una alta variabilidad inter e intraespecífica en la metalotolerancia, lo que sugiere la existencia de mecanismos fisiológicos adicionales a la melanización que permiten a estos hongos afrontar los efectos tóxicos de metales y metaloides. Se observó una diferencia significativa en la capacidad máxima de adsorción de Cr(VI) (qmax) entre la biomasa fúngica viva, la biomasa muerta y los extractos de melanina fúngica (biomasa viva y melanina extraída, *qmax*: 95.26 vs. 544.84 mg Cr^{6+} g^{-1}).

Se desarrolló un protocolo para la producción de biomasa de *Exophiala mesophila* y la extracción optimizada de melanina con el objetivo de obtener rendimientos suficientes de este biomaterial para posteriores estudios fundamentales y aplicados. La melanina fúngica se caracterizó mediante un conjunto de técnicas espectrofotométricas (UV-Vis, FTIR y EPR) y voltamperometría cíclica (CV). La utilización de triciclazol, un inhibidor específico de la biosíntesis del tipo de melanina que se ha asociado a la mayoría de los hongos negros (construida a partir de monómeros de 1,8-dihidroxinaftaleno), permitió identificar a los grupos OH, COOH y C=O como los principales implicados en los mecanismos de unión de Cr(VI) durante los procesos de adsorción por células enteras de *E. mesophila*. Además, la evaluación bioelectroquímica de la melanina reveló propiedades electroquímicas de semiconductor, así como una interacción sinérgica electroactiva con *Geobacter sulfurreducens*. La voltamperometría cíclica de extractos de melanina incubados con y sin suspensiones celulares de la bacteria electroconductora *Geobacter sulfurreducens* indicó la existencia de novedosas transformaciones redox de semiquinona/hidroquinona. Estas interacciones de la melanina podrían desempeñar un papel importante en el intercambio catiónico para la adsorción de metales y en los procesos de transferencia electrónica interespecies microbianos, los cuales están intrínsecamente relacionados con las moléculas de grupos quinona y semiquinona presentes en la melanina.

Los mecanismos de metalotolerancia de *Exophiala mesophila* frente a la exposición a As(V) y Cr(VI) se estudiaron mediante la combinación de análisis bioquímicos y transcriptómicos de alto

rendimiento. Los análisis de espectroscopia infrarroja con transformada de Fourier (FTIR) revelaron cambios que afectaban particularmente al contenido de las bandas de amida I y II (proteínas), fosfolípidos (asociados a membranas y ADN) y lípidos. Las principales rutas metabólicas reguladas al alza y asociadas a la metalotolerancia incluyeron una mayor expresión de genes relacionados con mecanismos de protección y transporte, como transportadores ABC de casete, transporte vacuolar, reducción y almacenamiento de Cr(VI) dependiente de NADPH y enzimas antioxidantes (SOD y CAT) para mitigar la producción de especies reactivas del oxígeno (ROS). Además, se identificó la regulación positiva de diversas rutas de reparación del ADN y la síntesis de proteínas.

Se investigaron novedosas aplicaciones de la melanina fúngica dirigidas a mitigar las emisiones de gases de efecto invernadero. Se compararon extractos de melanina de *E. mesophila* con otros materiales (semi)conductores (biochar y magnetita) para evaluar su influencia en el ciclo del carbono y las emisiones acumuladas de metano en microcosmos anaeróbicos con suelo de arrozales postcosecha. Se agregó paja de arroz para simular la estación postcosecha, cuando se emiten cantidades significativas de metano en los arrozales. Las enmiendas individuales de melanina y biocarbón dieron lugar a una reducción significativa de la emisión acumulada de metano (29% y 10% de disminución, respectivamente ($p < 0,0001$), en comparación con el control sin materiales conductores) después de 130 días de incubación. Esta reducción podría atribuirse al potencial de la melanina fúngica y el biochar para estimular el mecanismo de transferencia directa de electrones entre especies (DIET) en suelos anóxicos.

Tras la aplicación de melanina, el análisis del efecto del tamaño (LEfSe) mediante análisis discriminante lineal reveló una presencia diferencial y significativa de bacterias putativamente electroactivas pertenecientes a los géneros *Geobacter* y *Pseudopelobacter*, así como arqueas metanogénicas (*Methanosarcinia*). Estas poblaciones podrían ser superadas por los mecanismos DIET de otras poblaciones metanogénicas con mayores tasas de generación de metano en ausencia de melanina y biochar. El efecto observado sugiere que la melanina puede acortar la fase de latencia para la producción de metano, pero en última instancia, conducir a una tasa de emisión global más baja. El análisis de isótopos específicos de los compuestos del metano y dióxido de carbono emitidos ($\delta^{13}C\text{-}CH_4$, $\delta^{13}C\text{-}CO_2$ y $\delta^{2}H\text{-}CH_4$) reveló que la principal ruta metanogénica en los microcosmos modificados con melanina/biochar procedía de arqueas metilotróficas/acetotróficas, en lugar de la ruta hidrogenotrófica predominante en todos los microcosmos del suelo.

Structure of the Thesis

The thesis comprehensively reviews the current state of knowledge regarding black fungi and their melanin and investigates the prospects for in the context of bioremediation and their electroconductivity properties. This review provides a foundation for the original research work and findings presented subsequently.

The thesis is structured as follows:

Chapters 3 and 4: These chapters offer a comprehensive overview of:

Metallotolerance and bioremediation capabilities of black fungi.

Medina-Armijo, C., Isola, D., Illa, J., Puerta, A., Viñas, M., and Prenafeta-Boldú, F. X. (2024). The metallotolerance and biosorption of As(V) and Cr(VI) by black fungi. J. Fungi. 10, 47 10, 47. doi: 10.3390/jof10010047.

Melanin: its isolation from natural sources, various synthesis routes (chemical, electrochemical, and sorption onto melanin polymers).

Medina-Armijo, C., Yousef, I., Berna, A., Puerta, A., Esteve-Núñez, A., Viñas, M., et al. (2024). Characterization of melanin from *Exophiala mesophila* with the prospect of potential biotechnological applications. Front. Fungal Biol. 5, 1390724. doi: 10.3389/ffunb.2024.1390724.

Chapters 5 and 6: These chapters are currently under preparation for publication and focus on:

Biochemical and transcriptomic mechanisms underlying heavy metal tolerance in black fungi.

The application of melanin as an electroconductive material facilitating electron transfer for methane mitigation.

The thesis concludes with a general discussion and overall conclusions, along with an outlook for future research directions.

Chapter 1

General Introduction

This introduction provides a comprehensive overview of the fundamental properties of fungal melanin and its significance within the context of heavy metal bioremediation treatments. Particular emphasis is placed on the state of the art of knowledge regarding black fungi as promising candidates for bioremediation applications.

This chapter is currently undergoing preparation for submission as a review article.

Fungal melanin: unveiling natural functions and pioneering bio-based engineering for the bioremediation of heavy metals polluted waters.

Cristy Armijo-Medina[1], Daniela Isola[2], Hugo Madrid[3], Francesc X. Prenafeta-Boldú[1].

[1]Program of Sustainability in Biosystems, Institute of Agrifood Research and Technology (IRTA), Caldes de Montbui, Barcelona, Spain.

[2]Department of Economics, Engineering, Society and Business Organization (DEIM), University of Tuscia, 01100 Viterbo, Italy; isola@unitus.it

Abstract

Melanin, a term encompassing a diverse class of indole/quinone-based natural pigments, is ubiquitously distributed among living organisms from humans to bacteria. However, it is among the eukaryotic organisms, specifically the Black fungi, that melanin stands out for its unparalleled ability to store and synthesize this pigment. Notably, this polymer confers unique properties, such as antioxidant and photoprotection, enabling these fungi to thrive in extreme environments. Fungal melanin possesses a unique structure that imparts remarkable physicochemical properties, rendering it a promising biomaterial with potential technological applications. This review summarizes the advancements in heavy metal chelation using Black fungi and fungal melanin, with a particular emphasis on the physicochemical properties of melanin, particularly its metal chelation and electroconductivity capabilities.

Key Words: Black fungi; DHN-melanin; metal-binding; bioremediation; biosorption; biomaterial; bioelectroconductivity.

1. Introduction

Black fungi are a diverse group of darkly pigmented ascomycetes due to the presence of melanin in their cells, which contributes to a characteristic demiataceous appearance when cultured under laboratory conditions. Althought it is not well defined in phylogenetic therms, black fungi primarily belong to the orders *Chaetothyriales* (*Chaetothyriomycetes*), as well as *Cladosporiales*, *Capnodiales* and *Dothideales* (*Dothidiomycetes*). It has been proposed that these two independent groups evolved in response to similar mass extinction events that expanded arid continental masses and forced fungi to colonize naked rock surfaces (Gueidan et al., 2011). The dothideomycetes appeared about 362 million years ago during the late Devonian, after the so-called Ordovician-Silurian (O-S) extinction event, while the *Chaetothyriale*s order emerged around 229 million years ago, during the Middle Triassic period, following the Permian-Triassic (P-T) mass extinction. The P-T extinction is notable for the abundance of fungal spores preserved in the fossil record (Visscher et al., 1996). These eras were characterized by extreme terrestrial and marine conditions, fostering the development of fungi capable of thriving in harsh environments, including thermotolerance, resistance to high ultraviolet radiation, and the ability to flourish under the nutrient-limiting conditions of exposed rock surfaces.

Melanization has endowed black fungi with exceptional adaptability to a wide range of extreme environments, including hot (Selbmann et al., 2015; Isola et al., 2016) and arid climates (Madrid et al., 2023), polar regions (Onofri et al., 2008), and exposure to deleterous doses of UV/ionizing radiation (Pulschen et al., 2015), and toxic chemicals (Medina-Armijo et al., 2024a). Consequently, they can thrive on rock and building surfaces and even survive in space conditions or in environments contaminated with hydrocarbons, heavy metals, or radioactive material (Dadachova et al., 2008; Zupančič et al., 2016; Prenafeta-Boldú et al., 2018; Medina Armijo et al., 2024). Some species can also act as opportunistic pathogens in invertebrates (Zupančič et al., 2016).

Besides melanization, these fungi exhibit a remarkable physiological adaptability and morphological variation and are generally characterized by asexual reproduction. The multitude of species exhibit filamentous growth, yeast and budding cells, as well meristematic structures, depending on the environmental conditions (Teixeira et al., 2017). However, the most distinguishing feature of black fungi is the prominent accumulation of melanin pigment on the cell wall and/or melanosome-like structures in the cytoplasm (Prota, 1992). Their remarkable resilience is attributed to the protective role of melanin, which shields cells from environmental damage, and their ability to accumulate protective compounds such as mycosporines, carotenoids, polyalcohols, betaine, and trehalose (Selbmann et al., 2013; Ametrano et al., 2019). Previous reports on melanin content of black fungi range from 0.9-1.2% for *Exophiala pisciphila* (Chaetothyriales) to 21-25% for *Cenococcum geophilum* (Dothidiomycetes) of their fungal biomass, expressed in dry weight terms (refs). Recently, we were able to extract and purify melanin from *E. mesophila* equivalent to a yield of 12.5% of its dry weight biomass (refs).

Due to the exceptional adaptability of black fungi, they are typically found in antropized environments (Prenafeta-Boldú et al., 2021). These fungi are easily isolated from surfaces in the built environment that are subjected to fluctuating humidity and temperatures, which are also exposed to cleaning products, such as bathrooms, saunas, and kitchens (wet cells). In fact, it has been proposed that the colonization of built environments is mediated by the drinking water network and enrichment in appliances like domestic humidifiers, dishwashers, and washing machines (Zupančič et al., 2016). Interestingly, many species of black fungi have also been found in toxic environments contaminated with gasoline, solvents, creosote-treated wood, glues, plastics, and other petroleum and coal derived substances (Seyedmousavi et al., 2011a; Isola et al., 2021; Medina-Armijo et al., 2024).

Black fungi, particularly those from the Herpotrichiellaceae family (Chaetothyriales) first garnered scientific attention due to their remarkable ability to metabolize volatile aromatic hydrocarbons like toluene and styrene as their sole carbon and energy source (Prenafeta-Boldú et al., 2006). This metabolic capacity makes them promising candidates for bioremediation applications in highly contaminated environments. Early studies evaluated the use of black fungi in biofilters for the treatment of waste gases containing volatile alkylbenzenes (Cox et al., 1993; Prenafeta-Boldú et al., 2008). The most common "biofilter species" growing on alkylbenzenes reported eversince belong to the genera *Exophiala* and *Cladophialophora*, as reviewed recently (Prenafeta-Boldú et al., 2019). Biochemical and genomic studies have sholwn the involvement of cytochrome P-450 monooxygenases in the initial hydrocarbon oxydation (Cox et al., 1996), which occurs at the alkyl side-chain and explains the apparent unability of these fungi to assimilate unsubstituted aromatic hydrocarbons such as benzene (Prenafeta-Boldú et al 2001). More recent genomic studies with *C. inmunda* growing on toluene demonstrated the overexpression of cytochrome P-450 genes (Blasi et al., n.d.). The extremophilic traits of these fungi enables them to

tolerate acidic and dry conditions, which typically occur in air biofilters (Prenafeta-Boldú et al., 2004; Moreno et al., 2019).

As mentioned before, the complete melanization of the mycelium is a defining trait of the black fungi. Melanin comprises a diverse group of dark polymeric pigments that are found throughout all kingdoms of life, which holds significant scientific interest for potential in innovative biotechnological applications. In black fungi, melanin is thought to be a contributing factor to their extremophilic ecophysiology, due to the role of melanin as a protective shield against various biotic and abiotic stresses. Despite enhancing the survival and competitive advantage of these fungi in certain environments, melanin is not essential for their growth and development (Bell and Wheeler, 1986). One of the primary functions of fungal melanin is its ability to interact with and neutralize reactive oxygen species (ROS). This unique property confers resilience against oxidative stress, and tolerance to high concentrations of toxic compounds, including heavy metals and metalloids (Kogej et al., 2007). The melanin polymeric structure exhibits a cross-linked arrangement, where diverse functional groups like hydroxyl (-OH), carboxyl (-COOH), and amine (-NH), are linked through short C-C bonds (Eisenman and Casadevall, 2012). This intricate architecture imparts unique properties to melanin, such as the capacity to bind metals (Tran-Ly et al., 2020a), while π-π interactions confers melanin with electrical conductivity (PrKumar et al., 2016), and the ability to capture radiation energy and transform it into delocalized electrons and heat (Dadachova et al., 2007). The exploration of the unique charactristics of melanin is promoting an emerging field of research on advanced melanin-based techniques in areas such as for the bioremediation of heavy metal pollution and for the development of functional biomaterials and bioelectrical devices.

This chapter presents an up-to-date review on the biodiversity of metallotolerant black fungi and on the advancements for the application of these fungi for the bioremediation of heavy metals. A specific focus is put on the utilization of fungal melanin as an economical and environmentally friendly biomaterial. We explored the physicochemical properties of fungal melanin and potential novel biotechnological innovations of melanin-derived products.

2. Black fungi as heavy metal bioremediation agents

The lingering deposition of heavy metals and metalloids (HM) in soil and water, a legacy of rapid industrialization in the 20th and 21st centuries, poses a significant threat to global health of humans and the ecosystems (Zhang and Wang, 2020). Unlike biodegradable organic pollutants, HM are persistent contaminants that accumulate in the food chain, amplifying their toxicity and risk to living organisms. Their unsuitability to degradation by natural processes further exacerbates the problem, making the contamination by HM a complex and enduring challenge.

Biological processes for the remediation of HM-contaminated water have been widely studied in recent decades due to the ability of several organisms, including fungi, to induce the bioaccumulation, biomineralization, biosorption, and biotransformation of HM. These processes can be engineered and applied using *in situ* (treatment at the site of contamination) or ex situ (the contaminated site is excavated or pumped and treated away from the point of contamination) remediation techniques. Biological remediation technologies, collectively known as bioremediation, are often an environmentally friendly alternative and can be more cost-effective than conventional physical and chemical techniques. Bioremediation microbial agents must be readily culturable and produce relatively high biomass yields, express the desired bioactive traits at viable rates, and be safe to use in terms of potential biohazard. Consequently, these

microorganisms must be adapted to the bioremediated site conditions and tolerate the presence of toxic pollutants.

Fungi have evolved complex and diverse mechanisms to cope with heavy metal toxicity. These mechanisms encompass antioxidant pathways involving catalase (CAT), peroxidase (POD), glutathione (GSH), and superoxide dismutase (SOD) enzymes, along with metal transport systems mediated by ATP-binding cassette (ABC) transporters (Zhao et al., 2014). Along with these traits, intense melanization positions several black fungi as promising candidates for scalable bioremediation processes. Black fungi have demonstrated remarkable tolerance and adaptation to highly contaminated environments, classifying them among the most extremophilic eukaryotes, and melanin has a high affinity for chelating several metal ions. These unique characteristics strengthens the potential of black fungi as bioremediation agents for heavy metal removal.

A few studies have explored the biosorption of heavy metals by black fungi in-vitro (Table 1). One of the most extensively studied species is *Aureobasidium pullulans* (Dothideales). Suh et al. (1999) reported that *A. pullulans* exhibited a higher Pb(II) accumulation compared to Saccharomyces cerevisiae. Scanning electron microscopy and energy dispersive X-ray analysis revealed that Pb(II) accumulated in the cell inner wall and was attributed to the presence of extracellular polymeric substances (EPS). Additionally, the Pb(II) equilibrium uptake by *A. pullulans* was found to be depend on the amount of excreted EPS rather than on the initial cell dry weight (Suh et al., 1999b, 1999a). Three strains of *A. pullulans* demonstrated significant tolerance to cadmium, the tolerance was accompanied by alterations in lipid composition upon exposure to pullulan or pectin (Čertík et al., 2005). During the cultivation of *A. pullulans* strain CH-1 on an acid hydrolysate derived from Vlasina Lake peat, various metals, including Cu(II), Fe(III), Zn(II), Mn(II), Pb(II), Cd(II), Ni(II), and Cr(VI), were effectively sorbed by the fungus (Radulovicáradulovicá et al., 2007). Ghaedi et al. (2014) investigated the kinetics of Pb(II), Cu(II), Ni(II), and Co(II) metal ion sorption by *A. pullulans*. Parameter data from the fited Langmuir and Freundlich models revealed that *A. pullulans* exhibited a remarkable metal-binding capacity. Recently, *A. pullulans* biomass was used in kinetic Cr(VI) sorption assays, which yielded capacities of 485.7 mg g^{-1}(Fahry et al., 2023). Another study demonstrated the exceptional tolerance to As(V) of a strain of *Exophiala sideris* isolated from a creosote-contaminated environment, wich displayed 50% inhibitory concentrations (IC50) up to 10 g-As(V) L^{-1} (Seyedmousavi et al., 2011b). These findings suggest that black fungi have evolved genetic adaptations for metallotolerance, making them well-suited for biotechnological applications involving high metal concentrations.

Interestingly, certain strains the species *Exophiala psiciphila* species, which is found quite ubiquitously in waterous environments and has been identified as an opportunistic pathogen of cold-bloded animals, has also been isolated as a dark septate endophyte able to efficiently colonize the roots of several plants growin in soils contaminated with heavy metals. Maize plants inoculated with the strain *E. psiciphila* H93 were able to tolerate Pb(II), Zn(II), and Cd(II) better than uninoculated plants, mitigating the harmful effects of the heavy metal-induced stress, and promoting maize growth under such conditions (Li et al., 2011). Biosorption studies in liquid cultures of *E. pisciphila* showed that this fungus accumulated 20% Pb, 15.6% Zn(II), and 3.6% Cd of dry weight of biomass (Zhang et al., 2008). Zhao et al. (2015) investigated the tolerance of *E. psiciphila* to cadmium stress conditions from a genomic perspective, and identified 575 differentially expressed genes, 40% of which were involved in well-known heavy metal tolerance pathways. The main mechanisms described were metal ion binding and transport, organic acid

metabolism and transport, reactive oxygen species scavenging, redox homeostasis, transcription factor production, sulfate assimilation, DNA repair, and cell wall integrity maintenance (Zhao et al., 2015). Additionally, genes encoding for glutathione S-transferases (GST), enzymes involved in xenobiotic detoxification and oxidative stress response, were also studied. This research identified 24 GST genes classified as EpGST from the transcriptome of the metaltolerant *E. pisciphila*. The regulation of EpGST upon exposure to Pb(II), Cd(II), Cu(II), and Zn(II). These results indicate that *E. pisciphila* harbored a diverse of GST genes and the up-regulated EpGSTs are closely related to the heavy metal tolerance of *E. pisciphila* (Shen et al., 2015).

The biomass from representatives of *Cladosporium* (*Capnodiales*) has been extensively studied for its heavy metal sorption capability. Some examples include *Cladosporium resinae* on Cu(II) (de Rome and Gadd, 1987) and *Cladosporium cladosporioides* on gold and silver (Pethkar et al., 2001). *Cladosporium cladosporioides* also removed Pb(II) and Cd(II) from aqueous extracts of *Nordastachys jatamansi* and *Vitis vinifera*, medicinal plants with significant therapeutic value (Pethkar et al., 2001). Fan et al., 2012, studied the biosorption of azure blue tint from an aqueous solution using the *Cladosporium* Ch2-2 strain. The presence of Mg(II) and EDTA in the tint positively influenced the dye biosorption process with this strain (Fan et al., 2012). In other researches, *Cl. cladosporiodes* was found to be a highly efficent agent to biosorb Cu (II) (Carmo et al., 2013), and Mota et al. (2020) identified *Cl. halotolerans* to effectively remove manganese Mn(II) from a liquid medium. Furthermore, the secretion of extracellular laccases by *Cl. halotolerans*, which were apparently Mn-independent, pointed to the ability of this fungus to oxidize Mn^{2+} to Mn^{3+} complexes in the presence of organic acids. Table 1 summarizes a comparison of different parameters related to the adsorption of heavy metals by melanized and non-melanized fungi in aqueous solution from previous published studies.

Tabla 1. Comparison of parameters related to the biosorption of heavy metals by black fungi (Chaetothyriales, Dothideales) and by other non-melanized species.

Fungal species	Phylogenetic group	Metal	Initial Concentration (mg L^{-1})	Sorption Efficiency (%)	Sorption capacity (mg g^{-1})	pH	Reference
		Pb(II)	0.025	90	216	6.0 -7.0	(Suh et al., 1999)
Aureobasidium pullulans	Dothideales	Pb(II)	2.25	-	25	5.0	(Ghaedi et al. 2014) (
		Ni(II)			45		
		Cu(II)			64		
		Co(II)			43		
		Cr(VI)	10	-	486	5.0	(Fahry et al. 2023)
		Cu(II)	0.02	-	364	5.0	(Fomina and Gadd 2003)
		Cd(II)			734		
Aureobasidium pullulans	Dothideales	Cu(II)	-	62.2	-	6.0	(Radulovicáradulovicá et al. 2007)
		Fe(II)		97.3			
		Zn(II)		62.0			
		Mn(II)		24.0			
		Pb(II)		4.2			
		Cd(II)		51.7			
		Ni(II)		35.8			
		Cr(VI)		44.4			
Cladophialophora exuberants	Chaetothyriales	Cu(II)	1250	89.2	-	5.0	(Silva et al. 2023)
		Pb(II)	625	95.7			
Cladosporium halotolerans	Cladosporiales	Mn(II)	50	96	-	6.5	(Mota et al. 2020)

Cladosporium cladosporioides	Cladosporiales	Cu(II)	4.8	97		3.0	(do Carmo et al. 2013)
Cladosporium cladosporioides	Cladosporiales	Cu(II)	50	-	7.7	6.0	(X. Li et al. 2009)
Cladosporium cladosporioides	Cladosporiales	Cr(VI)	504	-	492	1.0	(Garza-González et al. 2017)
Cladosporium cladosporioides	Cladosporiales	Cu(II) Cd(II)			338 548		
Cladosporium herbarum	Cladosporiales	Cu(II)	0.02	-	590	5.0	(Fomina and Gadd 2003)
Cladosporium resinae	Cladosporiales	Cu(II) Cd(II)			697 450		
Cladosporium sp.	Cladosporiales	Cr(VI)	20	99		5.3	(Modkovski et al. 2020)
		Cd(II)	100	-	2.6	6.0	(Mohammadian Fazli et al. 2015)
Exophiala sp.	Chaetothyriales	Cr(VI)	200	99.61		7.0	(Lim, Lee, and Lee 2008)
Exophiala sp.	Chaetothyriales	Cu(II) Pb(II) Cr(VI) Ni(II) Zn(II)	200	99.28 97.67 91.94 99.77 99.61	-	7.0	(Lee, Lim, and Lee 2008)
Rinocladiella simillis	Chaetothyriales	Cr(VI) As(V)	20 20			6.5	(Medina-Armijo et al., 2024)
Aspergillus niger	*Eurotiales*	Cr(VI)	50	-	6.6	-	(Dursun, Uslu, and Cuci 2003)
		Cr(VI)	400	-	117.3	2.0	(Khambhaty et al., 2009)

Asperfillus flavus	*Eurotiales*	Hg(II)	10	97.5	6.5	5.5 -7.0	(Kurniati et al. 2014)
Botrytis cinerea	*Helotiales*	Pb(II)	350	97		4.0	(Akar, Tunali, and Kiran 2005)
Candida albicans	*Saccharomycetales*	Zn (II)	100	22		5.0	(Coelho et al. 2015)
		Co(II)	200	37		4.0	
		Cr(V)	50	76		1.0	
		Hg(II)	100	36		5.5	
Candida fabianii	*Saccharomycetales*	Cr(VI)	100	18.9		2.0 - 4.0	(Bahafid, Joutey, and Sayel 2013)
Candida tropicalis	*Saccharomycetales*	Cr(VI)	100	29.1			
Saccharomyces cerevisiae	*Saccharomycetales*	Cr(VI)	50	-	23.6	2.5	(Sathvika et al. 2015)
		Cr(VI)		-	32.6	1.0	(Özer and Özer 2003)
Trichoderma asperellum	*Hypocreales*	Cd(II)	200	76.2	10.7	9.0	(Mohsenzadeh and Shahrokhi 2014)
Trichoderma brevicompactum	*Hypocreales*	Pb(II)		97.5	6.1	6.6–4.8	(Zhang et al. 2020)

3. Melanin types and interactions with metals

Melanin encompasses a diverse range of structuraly diferent yet functionally similar dark biological pigments, that display black, brown, red, and yellow hues, and exhibit a remarkable resistance to solvents and bleaching agents. Melanin classification is based on the molecular precursor from which it is synthesized. (i) Eumelanin (black to brown) is biosynthesized from L-tyrosine, which is converted into L-3,4-dihydroxiphenylalanine (DOPA-melanin), the oxidation of which leads to two primary monomers, 5,6-dihydroxyindole (DHI) and 5,6-dihydroxyindole-2-carboxylic acid (DHICA). Its synthesis involves catecholamine oxidation, reactive quinone intermediates, and polymerization of the resulting indoles. (ii) Pheomelanin (yellow and red) comprises two types of benzothiazines synthesized in the presence of sufficient cysteine. (iii) Allomelanins, the most diverse group, include pyomelanins (light-brown) produced through the oxidation and polymerization of 1,8-dihydroxynaphthalene (DHN), tetrahydroxynaphthalene (THN), and cathecol via the pentaketide synthetase instead of tyrosine (Figure 1 summarizes the melanin synthesis pathways).

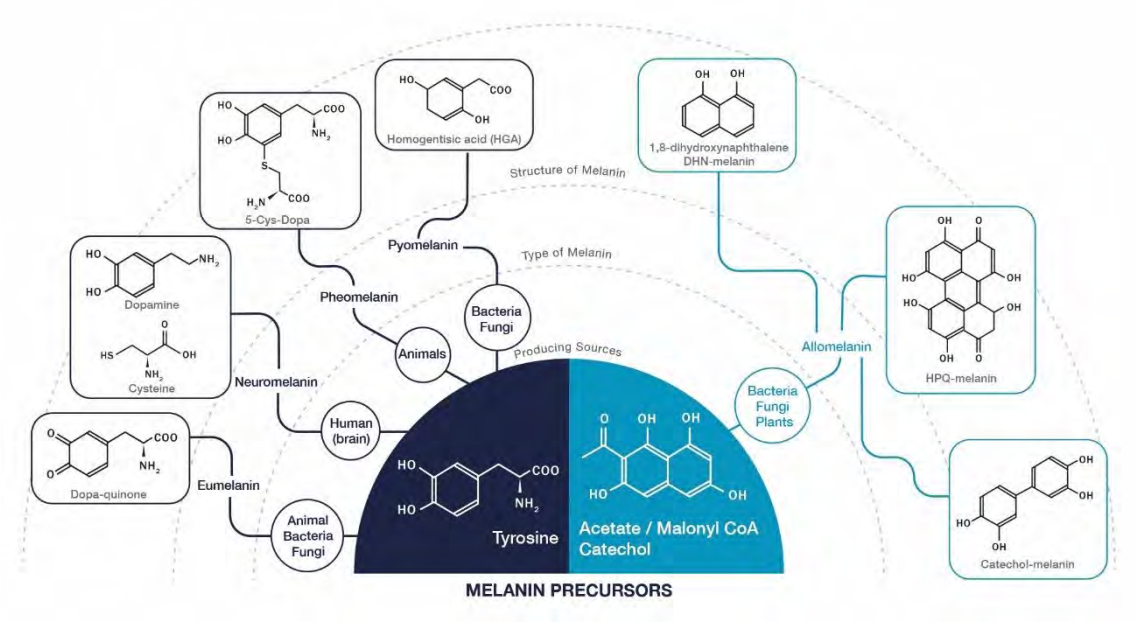

Figure 1. Types of melanin, according to their chemical precursors, building blocks and organisms related with their synthesis.

Melanin's unique structure arises from the assembly of various molecules and functional groups, including phenolic, indolic, carboxylic, and amine compound units, linked by strong, short-distance carbon-carbon bonds, which confers melanin with a negative charge and hydrophobic properties (Prota, 1992). Melanin is also characterized by unpaired electrons that can be detected using electron paramagnetic resonance (EPR), manifesting as a stable free radical signal (Enochs et al., 1993). Despite forming finely dispersed dark suspensions in water, these macromolecules are virtually insoluble in most solvents. Notably, melanin resist degradation by acid hydrolysis, yet it demonstrates an apparent solubility in alkaline solutions like NaOH or KOH, which is a crucial property for its isolation (Crippa et al., 1990). Melanin exhibits specific chemical properties

that distinguish it from other biological pigments and polymers. It has the ability to directly reduce ammonium solutions of silver nitrate, resulting in a grey-colored reaction product. Upon treatment with an oxidizing agent (H_2O_2), melanin extracts decolorize. Additionally, melanin reacts with polyphenols, such as $FeCl_3$, to form a brown precipitate (Selvakumar et al., 2008).

In most black fungi, dihydroxynaphthalene melanin (DHN-melanin) has been reported as the most prevalent type of melanin. Its biosynthetic pathway begins with the endogenous production of acetyl-CoA or malonyl-CoA as precursor molecules. The initial step involves the formation of 1,3,6,8-tetrahydroxynaphthalene (1,3,6,8-THN) catalyzed by polyketide synthases (PKS). This is followed by a series of reduction and dehydration reactions that yield various intermediates, including scytalone, 1,3,8-trihydroxynaphthalene, vermelone, and ultimately 1,8-dihydroxynaphthalene (DHN), which polymerizes to form melanin (Eisenman and Casadevall, 2012). At the structural level, the main difference between DHN-melanin and other melanins is the parcial or complete absence of amide groups. Fungal melanin shows similarities to soil humic acids in terms of volatile compounds released during pyrolysis and amino acids released upon acid hydrolysis (Fogarty and Tobin, 1996). Also, as humic acids, melanin possesses abundant carboxylic groups, enabling it to bind metal ions through ion exchange. This binding affinity is influenced by pH, as the release of H^+ ions play a crucial role in determining the availability of binding sites.

Several mechanisms might exist by which metal binding by fungal melanins could confer a survival advantage to black fungi. If a metal is present at toxic concentrations, melanin can act as a chelating agent, lowering the concentration of the metal into the cell. Conversely, if the metal is essential for cellular physiology but is present in low amounts in the environment, melanin may serve as a storage site for the metal (Fogarty and Tobin, 1996).

Pioneering studies explored metal interactions with melanin by comparing albino mutants to their melanin-containing counterparts. In a study by Gadd and de Rome (1988), extracellular melanin and intact biomass from albino strains of *Cladosporium resinae* and *Aureobasidium pullulans* were investigated for their Cu(II) binding capacity. The results revealed a direct correlation between melanin content and Cu(II) adsorption, with the *A. pullulans* wildstrain exhibiting significantly higher binding than its albino mutant. This effect was even more pronounced in *C. resinae*, where melanin extracts adsorbed nearly the double amount of Cu(II), compared to melanized fungal biomass, and almost the triple of the amount when compared to the corresponding albino strain: 120, 180, and 350 nmol mg^{-1} dry weight, respectively (Rome and Gadd, 1987).

Numerous studies have investigated the interactions between melanized fungi and heavy metals, particularly in response to copper exposure. It has been established that copper preferentially binds to Carboxyl in catechol melanin at pH values below 5, while at pH values above 6, melanin binds copper primarily through phenolic hydroxyl groups (Saiz-Jimenez and Shafizadeh, 1984; Fogarty and Tobin, 1996). Electron spin resonance studies revealed the ability of melanins from *Epicoccus* sp. and *Penicillium* sp. to bind copper and iron and suggested that fungi may play a significant role in metal binding similar to soil and compost humic acids (Żądło and Sarna, 2019). Transmission electron microscope (TEM) and dense electron microscopy techniques have revealed the presence of either melanin granules or a matrix extending outward from the cell walls of melanized fungi (Bell and Wheeler, 1986; Butler et al., 2005; Zhang et al., 2018). Caesar-Tonthat et al. (1995) through TEM analysis, observed that upon copper addition to the medium of *Gaeumannomyces graminis*, the culture exhibited an enhanced cell wall melanin accumulation.

Ban et al. (2023) investigated the interactions between melanin and copper oxide nanoparticles (CuO-NPs) using electron-dense analysis in a system combining synthetic CuO-NPs and *Exophiala salmonis*. They observed the accumulation of nanoparticles The expression of 1,3,6,8-tetrahy- droxynaphthalene reductase (*Arp2*) in the melanin synthesis pathway increased under the stress of CuO-NPs. Notably, fungal cells exhibited deformation and irregularities in shape under the stress condicions induced by 50 mg L^{-1} of 150 nm CuO-NPs.

Specific inhibitors of melanin biosynthesis are valuable tools for studying the predominant melanin type and its interactions with metals. Tricyclazole (5-methyl-1,2,4-triazolo[3,4-b] benzothiazole) is used as a fungicide because it disrupts the DHN-melanin biosynthesis pathway by inhibiting the reductases. These enzymes are essential for converting 1,3,6,8-tetrahydroxynaphthalene (1,3,6,8-THN) to scytalone and 1,3,8-trihydroxynaphthalene (1,3,8-THN) to vermelone. There are many examples in the literature about the effects and applications of tricyclazole on black fungi. Potisek et al. (2021) reported that tricyclazole inhibited melanization in two *Cadophora* isolates, leading to a significant decrease in the proportion of Cd-O-C coordination (indicative of Cd binding to melanin) and highlighted the melanin's contribution to Cd tolerance in these fungi. However, Zhan et al. (2016) observed contrasting results; while tricyclazole reduced growth and sporulation in *Exophiala pisciphila*, it did not affect its capacity to accumulate, suggesting that other mechanisms might contribute to Cd sorption in this species. Notably, the Fourrier-transformed infrared spectroscopy (FTIR) profiles of *E. pisciphila* mycelium samples remained similar after tricyclazole treatment, indicating the presence of functional groups like hydroxyl, amine, and carboxyl, which might be involved in Cd binding. Additionally, research on L*eptodontidium* sp., *Cadophora* sp., and *Phialophora mustea* suggests that melanin may not be the only factor that provides protection against the toxic effect of Cd and Zn in all melanized fungi, and these metals might bioaccumulate through other mechanisms like intracellular chelation or vacuolar sequestration (Berthelot et al., 2020.). These contrasting findings highlight the need for further investigation into the diverse roles of melanin and the binding abilities of different fungal species towards various metals.

Some notable studies have been published on the genes involved in metallotolerance metal-binding features of fungal melanin. The deletion of the copper-transporting ATPase gene BcCCC2, in mutants of *Botrytis cinerea* reduced melanization and sclerotium formation (Saitoh et al., 2010). A recent study of *Cladophialophora exuberans* identified 14 genes related to heavy metal assimilation, including 11 for copper (FRE7, CTR, SOD1, CRM1, CCC2, ATX1, COX17, COX11, CCS1, SCO1, PIC2) and 3 for lead (YOR1, YCF1, HMT1). These genes are involved in heavy metal homeostasis and activate in response to metal presence, encoding proteins that are essential for transport, storage, detoxification, oxidative stress management, and cellular repair (Silva et al., 2023).

4. Mechanisms of metal-binding to fungal melanin

Fungal melanins possesses a unique set of properties and structural features that grant them with an exceptional capacity for capturing various heavy metals. Understanding their adsorption behavior and mechanisms is key to further improving their performance. Melanin's adsorption of metal ions is primarily driven by electrostatic interactions between its negatively charged functional groups, mainly carboxyl, hydroxyl and amine (COOH-, OH-, NH-), and the metal ions (Mauro et al., 2017.; Manirethan et al., 2020; Mota et al., 2020; Fahry et al., 2023). However, the solution’s pH and the adsorbent's point of zero charge (PZC) significantly influence these

interactions. Other factors, such as the presence of competing metal ions, might also affect the availability of binding sites for the target heavy metal or metalloid. Furthermore, the adsorption of cationic or oxidized anionic metal species that should be subjected to electrostatic repulsion indicates that additional mechanisms, like ion exchange, reduction, or multiple mechanisms in combination, might play a role in the complex adsorption behavior of fungal melanin.

The functional groups of melanin contribute to metal binding through various mechanisms, enhancing its ability to bind ions with greater negative charges. Functional groups within its structure facilitate binding through various mechanisms, particularly for ions with higher negative charges. Additionally, melanin possesses high polyionicity, cross-linking, and a heterogeneous structure (Steven et al., 2007), further enhancing its binding capacity. Moreover, its remarkable redox reactivity allows it to act as a buffer against environmental stressors (Szpoganicz et al., 2002). This protective ability involves the oxidation of free radicals into semiquinone and quinol monomers, which also act as metal binding sites (Polymers, 2021). Additionally, melanin's π-conjugated structure contributes to its electrical conductivity. Notably, the C=O stretching band frequency reflects the strength of the π bond formed between the metal and the carbonyl group. This interaction also manifests in the observed double-layer interaction in fungal melanin, as evidenced by electrochemical characterization, highlighting its enhanced electrostatic capacitance (Kim et al., 2016b; Kumar et al., 2016).

Adsorption via surface complexation, also related to the ion exchange mechanism, contributes to the adsorption of heavy metals and typically involves the replacement of ions attached to the surface functional groups of melanin with heavy metal ions. Recent studies have demonstrated a strong adsorption affinity of fungal melanin extracted from *E. mesophila* surface groups towards heavy metal cations, where $Cr^{6+} - OH^-$ surface groups can chemically bond with cations through deprotonation ion exchange with H^+ (Fahry et al., 2023). For instance in ink sacs of *Sepia officinalis* melanin, infrared spectrometry analysis examined the bond between Ca(II) and the carboxyl group (COOH). The researchers observed that the stretching vibrations (1700 cm^{-1}) decrease with increasing metal concentration, also decreasing the pH of the solution. The pH effect alleviates proton loss in the presence of metal, indicating that Ca(II) binds to carboxylate groups (Hong and Simon, 2006, 2007). Interestingly, a study in two dark septate endophytes (DSE) *Exophiala pisciphila*, through associated with the mycelia were observed to contain Cd(II) by transmission electron microscopy-energy dispersive X-ray spectroscopy (TEM-EDX). Fourier transform infrared (FTIR) identified that hydroxyl, amine, carboxyl, and phosphate groups were responsible for binding Cd(II) (Zhan et al., 2011). Additionally, the interaction of Pb(II) with fungal melanin from *Armillaria cepistipes* was studied, showing high binding affinity at various sites, including hydroxyl, amine, and carboxyl groups. In contrast, Cd(II), Zn(II), and Ca(II) bind specifically to carboxyl groups (Tran-Ly et al., 2020b). Biosorption assays using *Cladosporium cladosporioides* strains exposed to various heavy metals (Au, Ag, Cu, Cd) suggest differential mechanisms in metal binding. While XPS and FTIR analyses indicate that nitrogen was not involved in the process, hexosamine facilitated non-specific metal binding. Cell-wall polymers also played a role, conferring selectivity (Pethkar et al., 2001). Furthermore, studies indicate that nitrogen groups within proteinaceous material can participate in the binding of copper and iron by fungal phenolic polymers (Fogarty and Tobin, 1996).

FTIR analysis revealed the disappearance of absorption bands corresponding to the vibrational modes of the free heavy metal and changes in the intensity of existing absorption bands during the precipitation or reduction process. Although the aforementioned mechanisms are common for most melanin-based adsorbents, precipitation and reduction of heavy metal ions are not

typically considered as adsorption mechanisms, but rather as chemical processes that sometimes occur alongside adsorption processes under specific conditions. For example, precipitation of heavy metals typically takes place under basic conditions, where the heavy metal ions form hydroxide complex precipitates on the adsorbent surface and separate from the bulk solution. As shown in Figure 2, schematic illustrations of the main adsorption mechanisms of heavy metal ions on melanin-based adsorbents.

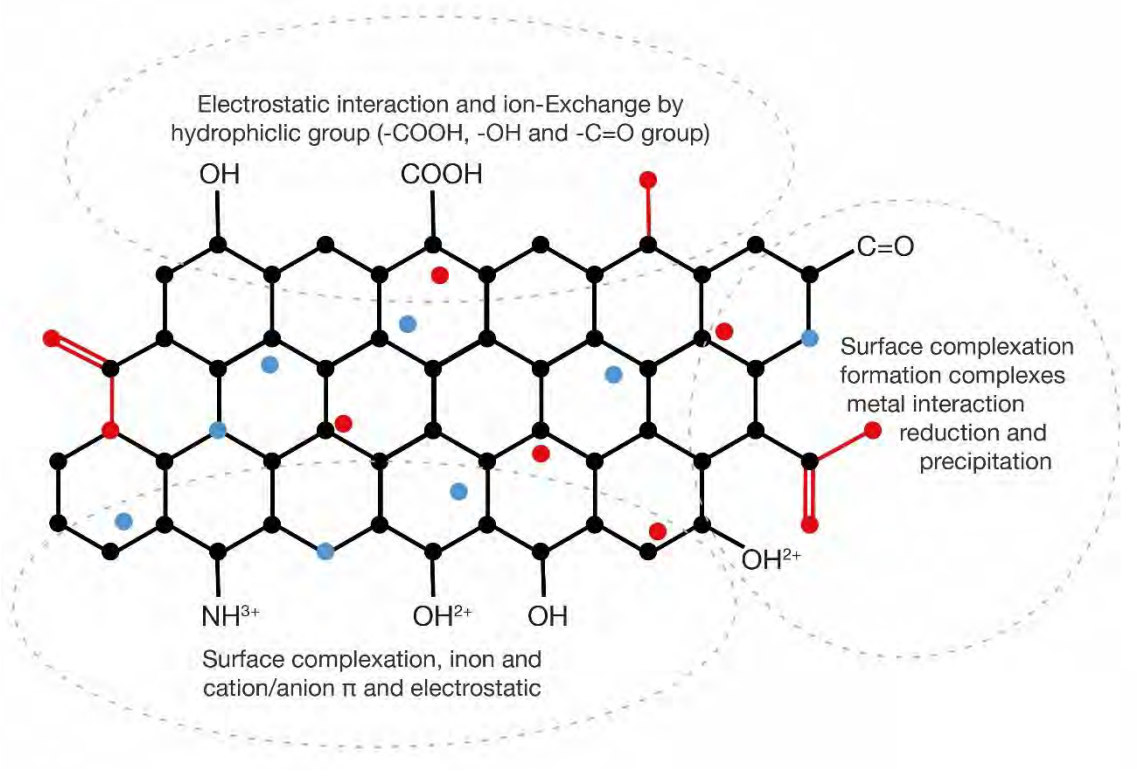

Figure 2. Chemical structure of DHN-melanin polymers and interaction of the melanin's functional groups with heavy metals.

5. Extraction and purification of melanin

In order to utilize melanin in various biotechnological applications, advancements in extraction and purification methods are essential. These tasks can be a challenging due to the fact that most melanin is formed within melanosomes, and organelle that is tightly bound to other cellular components such as lipids, proteins, or minerals (Prota, 1992).

The selection of melanin extraction and purification procedures is highly dependent on the melanin source (fungal, bacterial, human hair), melanin localization (intracellular/extracellular), and the final purpose of the study. Most melanin extractions protocols involve an alkaline treatment of the biomass with 1 M NaOH, 1 M KOH or 0.5 M NH4OH by reflux in water bath or autoclavation (De La Rosa et al., 2017.; Suwannarach et al., 2019; Medina-Armijo et al., 2024). However, the alkaline extraction is not possible for the melanin of human hair and mammalian fur in general, due to the insolubility of eumelanin, the predominant melanin type in this source (Pralea et al., 2019). The destruction of the closely associated proteins and other biological components to melanin can be achieved using boiling acids or bases for several hours, followed

by successive washing steps of the precipitate, this process is very aggressive and the melanin polymeric skeleton suffers chemical alterations, especially through extensive descarboxylation (Pralea et al., 2019) (M et al., 2013). The purification of melanin is then followed by successive washing steps with organic solvents such as chloroform, petroleum ether, acetone or absolute ethanol and centrifugation (Liu and Simon, 2003; Wang and Rhim, 2019).

In recent years, more gentle extraction methods have been developed, such as mechanical separation using ultracentrifugation and proteolytic digestion with specific cell wall-lysing enzymes, guanidine thiocyanate to eliminate residual protein denaturation, and a serine protease for cleavage. Using liquid nitrogen prior to enzymatic digestion can improve tissue grinding and preserve the morphology and properties of melanins. The main advantage of enzymatic extraction methods is that they can retain the melanin structure, even keeping the melanosome intact (Figure 3)

The scaling-up of melanin extraction and purification has received limited attention, primarily due to the difficulty in achieving cost-effective extraction yields. Several yeast and yeast-like species, including *Aureobasidium pullulans*, *Candida albicans*, *Cryptococcus neoformans*, *Hormoconis resinae*, *Spissiomyces endophytica*, *Ochroconis lascauxensis*, and *Kluyveromyces marxianu*s, have been reported for melanin production (Morris-Jones et al., 2005; Hewedy and Ashour, 2009; HC and A, 2012; Zou and Hou, 2017; Camacho et al., 2019). Depending on the isolation method, the extraction efficiency and costs can be very different for industrial applications. For instance, the extraction of melanin from the biomass of the edible fungus *Auricularia auricula* required different steps, including enzymatic digestion, treatment with guanidinium thiocyanate, lipid extraction, and acid hydrolysis. This method resulted in a final yield of the 10% of the initial mushroom biomass in dry matter terms (Prados-Rosales et al., 2015).

In addition to the laborious extraction and purification procedures, the production of fungal melanin requires a relatively long incubation time due to the slow growth rate of fungal cells. For instance, melanin production from *Gliocephalotrichum simplex* supplemented with tyrosine, using acid hydrolysis and flocculants reached approximately 6.60 g L^{-1} in 100 ml culture for 6 days. In another study, *Auricularia auricula* produced 2.22 g L^{-1} in dry weight biomass for 8 days (Jalmi et al., 2012; Sun et al., 2016). Various methods with improved yields were employed for the black fungus *Armillaria cepistipes*. This protocol involved filtration, sterilization via autoclaving at 121°C for 20 minutes, and lyophilization of the liquid phase to obtain 28 g L^{-1} of crude melanin powder. The researchers achieved a yield of 17 g L^{-1} using an acidification procedure, and the maximum yield reached was 99%. (Ribera et al., 2019). In another study, *A. resinae* produced melanin quite rapidly during the autolysis phase of growth, reaching up 4.5 g L^{-1} within 14 days, the method of cell lysis and melanin extraction was carried out with 1M NH3·H2O (Oh et al., 2020). *Hortaea werneckii* strain AS1 was successfully optimized for melanin production via the manipulation of various cultivation media parameters, including salinity, agitation, and nutrient ratios. With a maximum melanin yield of 0.938 g L−*1* on a culture volume of 225 mL, this approach demonstrated the potential of this black fungus as a source of natural melanin (Elsayis et al., 2022).

Despite the progress on fungal melanin production, several challenges remain, such as to improve the relatively low extraction efficiency, and to screen and select suitable strains that have comparatively high growth rates and a low biohazard. Genetic and engineering techniques offer promising avenues for overcoming these challenges. Overexpression of genes encoding enzymes involved in melanin formation, particularly tyrosinases, L-cysteine, tetrahydrophenylacetic or

DHN can significantly improve the productivity of fungal melanin. Additionally, advancements in recombinant melanin production through microorganisms have emerged. One notable example is the modification of *Escherichia coli* to express genes from the actinomycete *Streptomyces antibioticus*, leading to the production of eumelanin from L-tyrosine in agar plates and liquid cultures (Cioppa et al., 1990). Ruan et al. (2004) reported melanin production by *Bacillus thuringiensis* strain 4D11 upon incubation with L-tyrosine at 42°C. This implied the existence of a tyrosinase gene in its genome. However, the absence of the 4D11 genome sequence necessitated a cloning approach based on the expected sequence homology with a known tyrosinase gene from *Bacillus cereus* 10987. This enabled the researchers to devise a strategy for identifying the tyrosinase gene within 4D11. However, it is important to highlight that the biotechnological use of genetically modified organisms is subjeted to regulatory limitations, which vary considerably across different countries.

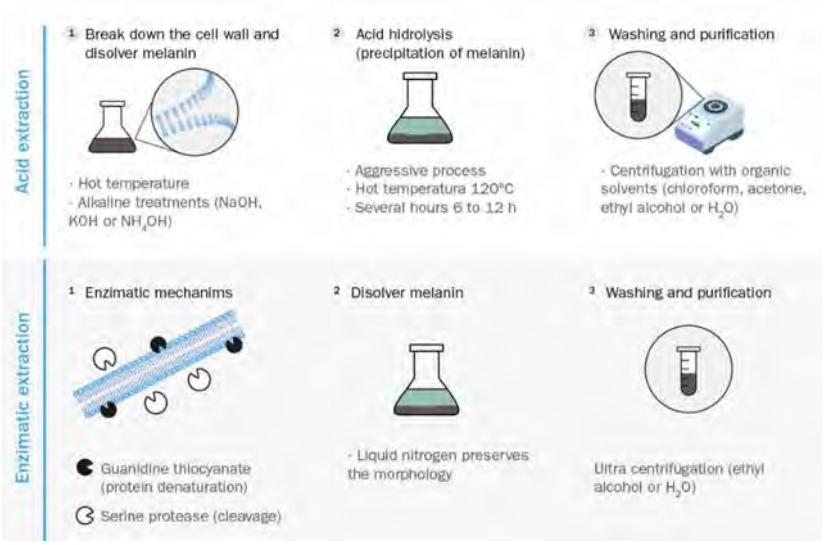

Figure 3. Protocol types and main steps for the extraction of melanin.

6. Application of melanin-based tehniques for the bioremediation of heavy metal pollution

Several approaches have been devised for the remediation of the contamination caused by heavy metals and metalloids (HMM), particularly in the treatment of drinking water. Conventional physicochemical techniques, including chemical oxidation or reduction, ion exchange, reverse osmosis, activated charcoal adsorption, membrane filtration, electrochemical treatment, and evaporative recovery, often struggle to effectively remove HM below 100 mg L^{-1} and contribute to secondary pollution (Mukherjee et al., 2010). Additionally, these techniques are resource-intensive and energy-demanding. Bioremediation processes utilize the activity and/or properties of biomass to transform or capture environmental pollutants, rendering them less harmful. In recent years, the use of novel natural materials with metal-binding capabilities has gained attention. These innovative materials have low production costs, good durability and, when employed in bioremediation systems, do not generate secondary toxic compounds during the decontamination processes.

Melanin and melanin-derived advanced biomaterials have garnered significant attention owing to the versatility of its potential applications (Caldas 2020). Investigations into the removal of

heavy metals using functionalized natural melanin polymers have been conducted with promising results using cuttlefish, bacteria, and fungi. The first biotechnological applications involving melanin for metal sorption studied its immobilization onto various materials, which confers a high versatility and process stability under high temperatures and acidic conditions. Kulkarni et al. (2013) utilized melanin from *Klebsiella* sp. GSK immobilized with sodium alginate to remove Cu(II) and Pb(II). Beads were embedded from two distinct melanin sources (squid ink and commercially extracted plant melanin) with sodium alginate and tested to remove Cr (VI) from aqueous solutions. In this study, the melanin isolated from squid ink exhibited superior sorption capacity of 19.8 mg g^{-1} dry melanin (Cuong et al., 2018).

Additionally, other applications have been explored using functionalized melanin on different supports. The distinct forms of melanin play crucial roles in melanin biochemistry, influencing the supramolecular process of binding to metals. For instance, Sono et al. (2022) employed synthetic L-DOPA melanin and hair melanin on a hydrophobic polyvinylidene fluoride-coated solid support for the adsorption of Pb(II), Zn(II), Cd(II), and Cu(II). As another example, melanin from the herbaceous plant *Amorphophallus campanulatus* was used in the adsorption of uranium, a heavy metal with both radiochemical and toxicological effects. The removal of uranium was relatively fast (equilibrium was reached within 2 hours of contact), and melanin exhibited a significant uptake capacity across a wide pH range, with a maximum loading capacity of 588.24 mg g−1 that was consistent with Lagergren's pseudo-second-order equation (Saini and Melo, 2013).

An interesting study developed an electrospinning technology to integrate fungal melanin from the basidiomycete *Armillaria cepistipes* (Tran-Ly et al., 2020b). Melanin particles were agglomerated into polymeric nanofibrous membranes to create stable and highly porous filtration membranes. This membrane showed distinct affinities for metals (Pb^{2+}>Cr^{3+}>Ni^{2+}>Cd^{2+}>Zn^{2+}>Ca^{2+}). Composed of aggregates of nanosized particles from the black fungus *Amorphotheca resinae* were tested for the adsorption of Cu(II), Pb(II), Cd(II), and Zn(II) using batch tests, with maximum adsorption capacities of 69.18, 103.23, 24.31, and 13.57 mg g^{-1}, respectively. In this work, the complete removal of metals was achieved after 5 cycles of adsorption-desorption (Oh et al., 2021).

Manirethan et al. (2018), functionalized the melanin of *Pseudomona stutzeri* to produce melanin nanoparticles, which were then optimized for heavy metal sorption in remediation applications. The maximum adsorption capacity obtained from Langmuir isotherm was 82.4, 126.9, 147.5 and 167.8 mg g^{-1} for Hg(II), Cr(VI), Pb(II) and Cu(II), respectively (Manirethan et al., 2018). While research on melanin in black fungi remains limited, a recent study by Fahry et al. (2023) demonstrated the potential of melanin extracted from *Aurobasidium pullulant* for removing Cr(VI) from aqueous solutions. Both the fungal biomass and the extracted melanin exhibited remarkable removal capacities, with maximum sorption values reaching 485.747 mg g^{-1} for the biomass and 595.974 mg g^{-1} for the extracted melanin. Table 2 outlines various methodologies for functionalizing melanin to be used for diverse biotechnological applications, including the bioremediation of heavy metal pollution, the development of biosensors, the catalysis of redox reactions, among other applications.

7. Electrochemical properties and applications of melanin

Melanins have been recognized for their unique electrical properties for over four decades. McGinness et al., reported the first experimental evidence of the semiconducting behavior of the eumelanin (Mcginness et al., 1974). They have recently regained attention as promising advanced

functional materials, particularly in the context of bioelectronic interfaces. While fungal melanin possesses promising electrical properties, further research is required to enhance its conductivity. Several studies have investigated the incorporation of eumelanin into polyaniline (PANI) composite materials with higher conductivity (Mihai et al., 2013; Gargiulo et al., 2015; Migliaccio et al., 2019). The extent of electron transfer and the redox properties of the composite depend on the presence and characteristics of the other materials (Mostert et al., 2012). Reverse engineering approaches have demonstrated that natural melanin retains redox activity, enabling rapid and repeated electron donation and acceptance (Kim et al., 2016a). Melanin nanoparticle was also prepared for use in the development of electroconductive film. This matrix was created using 1wt% of dried cuttlefish ink melanin powder and 2wt% of PVA (polyvinyl alcohol). The solutions were sonicated overnight and then slowly dried under ambient conditions to form the film. Composites show electrical conductivities 1.17 ± 0.13 S cm^{-1} (electric semiconductive range), compared to the control (0.24 ± 0.09 S cm^{-1}) and confirmed the biodegradability used ingestion by *Zophobas morios* larvae (Eom et al., 2019). Additionally, studies have shown that natural melanin films can be electrodeposited onto fluorine-doped tin oxide (FTO) glass substrates. The thickness of the deposited films increases with increasing electrochemical deposition time, and the constant potential method exhibits faster film growth compared to cyclic voltammetry (Madkhali et al., 2020).

Based on the accumulating evidence on the chemical and physical properties of melanin, it is evident that the presence of delocalized electrons within the conjugated structure of the polymer plays a crucial role in its electrical conductivity. Migliaccio et al., 2019, revealed that the conductivity of eumelanin is not affected by water content. Thermal annealing in vacuum can rearrange the structure of eumelanin films into conductive layers, significantly increasing the conductivity of up to 318 S cm^{-1} (Migliaccio et al., 2019). In stark contrast, biochar exhibits a conductivity range of 0.002 to 18.51 S/cm (Kane et al., 2021), while the electrical conductivity of Carbon Nanotube (CNT) Fibers asspun is significantly higher, reaching approximately 595.2 S cm^{-1} (Peng et al., 2008). Furthermore, the conductivity can potentially be tuned depending on the polymerization (Jastrzebska et al., 1998; Vahidzadeh et al., 2018). The stacking of polyindole π-systems facilitates the formation of cation-π interactions, a type of non-covalent bonding that occurs between a metal ion (cation) and a π-electron system. These interactions can significantly enhance the electrical conductivity of the material by introducing reversible and dynamic pathways for charge carrier movement (electrons) (Lu et al., 2013.; Hong et al., 2018). Madkhali et al., 2019 showed that metal ions, specifically Fe (0.0179 mS cm^{-1}), Cu (0.778 mS cm^{-1}), and Zn (0.0074 mS cm^{-1}), can favorably alter the electrochemical properties of melanin (0.0027 mS cm^{-1}) (Madkhali et al., 2019).

The electrical conductivity of melanin is influenced by hydration state (Vahidzadeh et al., 2018). This interaction involves a process called comproportionation equilibrium, which occurs between the quinone, hydroquinone, and semiquinone forms of melanin (Sheliakina et al., 2018). As the water content increases, free protons in the form of hydronium ions are created. These ions can migrate through the melanin matrix by a hopping mechanism, thereby enhancing conductivity (Hong et al., 2018). The conductivity can also be controlled by introducing specific π-electron-donor moieties (Lu et al., 2013). A recent study investigated the oxidation states of fungal melanin from *Exophiala mesophila* when exposed to *Geobacter sulfurreducens*, an exoelectrogenic species. Cyclic voltammetry (CV) was employed to monitor the reaction, and the results revealed that melanin can undergo multiple oxidation states, leading to a significant increase in capacitance. CV analysis also revealed a prominent increase in oxidative charge transfer and the emergence of novel electrical peaks (Medina-Armijo et al., 2024).

Moreover, the strength of cation-π interactions is influenced by the solvent polarity and temperature. Polar solvents weaken the electrostatic interaction between the cation and the π-electron system, while nonpolar solvents strengthen it (Xiang et al., 2020). As a result, it has been observed that the interaction of melanin with different polar solvents enhances its capacitance (Madkhali et al., 2020; Medina-Armijo et al., 2024). Temperature also plays a role, as higher temperatures can disrupt the cation-π interactions. This modulation of cation-π interactions provides a mechanism to fine-tune the electrical conductivity of melanin-based materials for various applications.

Table 2. Studies regarding melanin functionalization strategies for biotechnological applications.

Melanin source	Description of methods	Applications	References
Human hair	Synthesis of Polyvinylidene di-fluoride (PVDF) discs coated with Synthetic-Eumelanin using a solution of L-Dopa, tyrosine, and sodium phosphate buffer.	Remove Pb^{2+}	(Sono et al., 2012)
Squid ink sac /sesame seeds	Melanin beads were made with sodium alginato and CaCl2.	Remove Cr^{6+}	(Cuong et al., 2018)
Fungal melanin *Armillaria cepistipes*	Synthesis of melanin membrane-based nanofibrous membranes using two polymers: polycaprolactone (PCL) containing glacial acetic acid, formic acid, and tetraethylammonium bromide (TEAB) and polyurethane (PUR) containing Elastollan C95A55 and dimethylformamide (DMF).	Remove Pb^{2+}, Cd^{2+}, Ni^{2+} and Cr^{3+}	(Tran-Ly et al., 2020a)
Synthetic melanin	Eumelanin nanoparticles were synthesized in a one-pot fast process from a 5,6-diacetoxy indole precursor that is hydrolyzed in situ into dihydroxy indole (DHI). The method allows the possibility of changing the level of sodium ions that ends up in the nanoparticles.	Remove Zn^{2+}, Cd^{2+}, Ni^{2+}, Co^{2+}, Cu^{2+}, Pb^{2+}	(Darwish et al., 2021)
Pseudomonas stutzeri (MTCC)	Melanin nanoparticles were immobilized onto a hydrophobic polyvinylidene fluoride (PVDF) membrane for batch and continuous removal of heavy metals.	Remove Hg^{2+}, Cr^{6+}, Pb^{+2}, Cu^{2+}	(Thaira et al., 2019)
Synthetic melanin-like nanoparticle (MNP)	Synthetic melanin-like nanoparticle-reinforced chitosan nanocomposite films were prepared using	Active food packaging and biomedical packaging	(Roy et al., 2020)

reinforced chitosan nanocomposite films	dopamine hydrochloride and sodium hydroxide, followed by spontaneous oxidation. The prepared nanoparticles exhibited a spherical morphology with an average size of approximately ~100 nm.		
Sepia officinalis inks	Fabrication of multifunctional poly (vinyl alcohol)/melanin nanocomposites by layer-by-layer (LBL) assembly using melanin nanoparticles (MNPs)	Electroceuticals, artificial bionic organs, biosensors, and implantable devices	(Eom et al., 2017)
Squid inks	Conductive melanin composites are prepared using melanin nanoparticles that are tightly clustered in a poly (vinyl alcohol) (PVA) matrix.	Green bioelectronics, biocomposites suggests	(Eom et al., 2019)
Melanin -like polymer	A composite of highly electrically conductive melanin-like polymers (eMLPs) with tunable morphologies was synthesized using an electrochemical method	*in situ* biosensors to implantable bionic interfaces.	(Ozlu and Shim, 2022)
Yarrowia lipolytica NCYC 789	The synthesis of silver nanoparticles (AgNP) using cell associate melanin to preventing bacterial growth and the formation of biofilm.	Antimicrobial	(Apte et al., 2013)
Dopamine	Nanocomposite by mixing melanin nanoparticle with polyvinyl alcohol (PVA)	UV-shielding	(Wang et al., 2017)
Sepia Ink	Nanocomposite with alginate and PVA	Uv blocking, thermal stability	(Yang et al., 2020)

8. Conclusion and future perspectives

Melanin is a polymeric material that has captured the interest of researchers in chemistry, physics, material science and engineering. It has the potential to be part of the next generation biomaterials, which could drive innovation in the new bioeconomy paradigm, under which non-renewable raw materials are to be replaced by high-value resources obtained from biomass. Among the remarkable physical and chemical properties of melanin, the binding to metals ions and the intrinsic electrical conductivity show promising prospects for environmental applications. However, scaling-up production processes can be challenging for industrial use of melanin. In this regard, fungal melanin may be an attractive alternative, as several fungi and yeasts are used as versatile industrial microorganisms in large-scale fermentation processes.

Black fungi are a promising source of melanin owing to the intense and complete melanization of their biomass, as well as because of their metallotolerant nature and metabolic versatility. Future engineering developments could be based on melanin-based nanomaterials so that raw melanin could then be a priced commodity. Processes that functionalize melanin with other advanced materials could significantly improving its metal-binding capacity, prompting the performance and development of efficient environmental solutions to recover polluting heavy metals and metalloids.

On the other hand, the conductive properties of melanin have scarcely been studied despite their promising applications in areas such as bioconductors, photovoltaic cells, and biosensors that are also biodegradable. There is a limited knowledge on the electroconductive properties of melanin while it is still bound to fungal cells. Once released into the open environment, for example in the soil decaying biomas, melanin is a highly recalcitrant organic compound that may play a role in the exoelectrogenic interactions with other microbial species and mediate the nutrient dynamics in the rhizosphere, which in turn can stimulate new biogeochemical processes.

In summary, new biotechnological ideas can be generated from new discoveries about the properties of melanin and black fungi, which could have a significant impact on environmental sustainability and human health. In particular, the relationship between the melanin of black fungi, the adsorption of heavy metals, and its conductive effects in the environment is of great interest. However, the research on the ecophysiology and genetics of the black fungi is still in progress and new knowledge is needed to fully evaluate the potential of this organisms in the development of melanin-based biotechnologies.

9. References

Ametrano, C. G., Muggia, L., and Grube, M. (2019). Extremotolerant black fungi from rocks and lichens. *Fungi Extrem. Environ. Ecol. Role Biotechnol. Significance*, 119–143. doi: 10.1007/978-3-030-19030-9_7.

Apte, M., Girme, G., Bankar, A., Ravikumar, A., and Zinjarde, S. (2013). 3, 4-dihydroxy-L-phenylalanine-derived melanin from *Yarrowia lipolytica* mediates the synthesis of silver and gold nanostructures. doi: 10.1186/1477-3155-11-2.

Ban, Y., Tan, J., Xiong, Y., Mo, X., Li, W., Jia, C., et al. (2023). The responses and detoxification mechanisms of dark septate endophytes (DSE), *Exophiala salmonis*, to CuO nanoparticles. *Environ. Sci. Pollut. Res*. 30, 13773–13787. doi: 10.1007/s11356-022-23099-1.

Bell, A. A., and Wheeler, M. H. (1986). Biosynthesis and functions of fungal Melanins. *Annu. Rev. Phytopathol.* 24, 411–451. doi: 10.1146/annurev.py.24.090186.002211.

Pethkar A. V., Gaikaiwari R. P., and K. M. Paknikar. (2001). Biosorptive removal of contaminating heavy metals from plant extracts of medicinal value. *Current Science Association.* 80, 1216–1219.

Blasi, B., Tafer, H., Kustor, C., Poyntner, C., Lopandic, K., and Sterflinger, K. (2017.). Genomic and transcriptomic analysis of the toluene degrading black yeast *Cladophialophora immunda*. *Scientific reports*. 7: 11436 doi: 10.1038/s41598-017-11807-8.

Butler, M. J., Gardiner, R. B., and Day, A. W. (2005). Fungal melanin detection by the use of copper sulfide-silver. *Mycologia* 97, 312–319. doi: 10.1080/15572536.2006.11832806.

Caesar-Tonthat, T. C., Van Ommen, F., Geesey, G. G., and Henson, J. M. (1995). Melanin production by a filamentous soil fungus in response to copper and localization of copper sulfide by sulfide-silver staining. *Appl. Environ. Microbiol*. 61, 1968–1975. doi: 10.1128/aem.61.5.1968-1975.1995.

Camacho, E., Vij, R., Chrissian, C., Prados-Rosales, R., Gil, D., O'Meally, R. N., et al. (2019). The structural unit of melanin in the cell wall of the fungal pathogen *Cryptococcus neoformans*. *J. Biol. Chem*. 294, 10471–10489. doi: 10.1074/jbc.ra119.008684.

Carmo, J. R. do, Pimenta, C. J., Silva, J. F. da, and Souza, S. M. C. de (2013). Recovery of copper (II) absorbed in biomass of *Cladosporium cladosporioides*. *Sci. Agric*. 70, 147–151. doi: 10.1590/s0103-90162013000300002.

Čertík, M., Breierová, E., and Juršíková, P. (2005). Effect of cadmium on lipid composition of *Aureobasidium pullulans* grown with added extracellular polysaccharides. *Int. Biodeterior. Biodegradation*. 55, 195–202. doi: 10.1016/j.ibiod.2004.11.005.

Cioppa, G. Della, Garger, S. J., Sverlow, G. G., Turpen, T. H., and Grilla, L. K. (1990). Melanin Production in *Escherichia coli* from a Cloned tyrosinase Gene. *Bio/Technology*. 87 8, 634–638. doi: 10.1038/nbt0790-634.

Cox, H. H., Faber, B. W., Heiningen, W. N. Van, Radhoe, H., Doddema, H. J., and Harder, W. (1996). Styrene metabolism in *Exophiala jeanselmei* and involvement of a cytochrome P-450-dependent styrene monooxygenase. *Appl. Environ. Microbiol*. 62, 1471.

Cox, H. H. J., Houtman, J. H. M., Doddema, H. J., and Harder, W. (1993). Enrichment of fungi and degradation of styrene in biofilters. Biotechnol. *Lett.* 1993 157 15, 737–742. doi: 10.1007/bf01080148.

Crippa, R., Horak, V., Prota, G., Svoronos, P., and Wolfram, L. (1990). Chapter 6 Chemistry of Melanins. *Alkaloids Chem. Pharmacol*. 36, 253–323. doi: 10.1016/S0099-9598(08)60085-1.

Cuong, A. M., Le Na, N. T., Thang, P. N., Diep, T. N., Thuy, L. B., Thanh, N. L., et al. (2018). Melanin-embedded materials effectively remove hexavalent chromium (CrVI) from aqueous solution. *Environ. Health Prev. Med*. 23, 1–11. doi: 10.1186/s12199-018-0699-y.

Dadachova, E., Bryan, R. A., Howell, R. C., Schweitzer, A. D., Aisen, P., Nosanchuk, J. D., et al. (2008). The radioprotective properties of fungal melanin are a function of its chemical composition, stable radical presence and spatial arrangement. *Pigment Cell Melanoma Res*. 21, 192–199. doi: 10.1111/j.1755-148X.2007.00430.x.

Dadachova, E., Bryan, R. A., Huang, X., Moadel, T., Schweitzer, A. D., Aisen, P., et al. (2007). Ionizing radiation changes the electronic properties of melanin and enhances the growth of melanized fungi. *PLoS One 2*, e457. doi: 10.1371/journal.pone.0000457.

Darwish, E. R., Kalil, H., Alqahtani, W., Moalla, S. M. N., Hosny, N. M., Amin, A. S., et al. (2021). Fast and reliable synthesis of melanin nanoparticles with fine-tuned metal adsorption capacities for studying heavy metal ions uptake. *Nanotechnol. Sci. Appl*. 14, 101–111. doi: 10.2147/nsa.s296722.

De La Rosa, J. M., Martin-Sanchez, P. M., Sanchez-Cortes, S., Hermosin, B., Knicker, H., and Saiz-Jimenez, C. (2017). Structure of melanins from the fungi *Ochroconis lascauxensis* and *Ochroconis anomala* contaminating rock art in the Lascaux Cave. *Scientific reports.* 7: 13441. doi: 10.1038/s41598-017-13862-7.

de Rome, L., and Gadd, G. M. (1987). Copper adsorption by *Rhizopus arrhizus*, *Cladosporium resinae* and *Penicillium italicum*. *Appl. Microbiol. Biotechnol*. 1987 261 26, 84–90. doi: 10.1007/bf00282153.

Eisenman, H. C., and Casadevall, A. (2012). Synthesis and assembly of fungal melanin. *Appl. Microbiol. Biotechnol*. 93, 931–940. doi: 10.1007/s00253-011-3777-2/figures/2.

Elsayis, A., Hassan, S. W. M., Ghanem, K. M., and Khairy, H. (2022). Optimization of melanin pigment production from the halotolerant black yeast *Hortaea werneckii* AS1 isolated from solar salter in Alexandria. *BMC Microbiol*. 22, 1–16. doi: 10.1186/s12866-022-02505-1.

Enochs, W. S., Nilges, M. J., and Swatz, H. M. (1993). A standardized test for the dentification and Charccterization of melanins using electron paramagnetic resonance (EPR) spectroscopy. *Pigment Cell Res*. 6, 91–99. doi: 10.1111/j.1600-0749.1993.tb00587.x.

Eom, T., Jeon, J., Lee, S., Woo, K., Eun Heo, J., Martin, D. C., et al. (2019). Naturally derived melanin nanoparticle composites with high electrical conductivity and biodegradability. *Part. Part. Syst. Charact*. 36 (10) doi: 10.1002/ppsc.201900166.

Eom, T., Woo, K., Cho, W., Eun Heo, J., Jang, D., In Shin, J., et al. (2017). Nanoarchitecturing of natural melanin nanospheres by layer-by-layer assembly: Macroscale anti-inflammatory conductive coatings with optoelectronic tunability. *Biomacromolecules*. 18, 1908–1917. doi: 10.1021/acs.biomac.7b00336.

Fahry, Kh., Ghoniem, A. A., Al-Otibi, F. O., Helmy, Y. A., El Hersh, M. S., Elattar, K. M., et al. (2023). A Comparative Study of Cr(VI) Sorption by *Aureobasidium pullulans* AKW Biomass and Its Extracellular melanin: complementary modeling with equilibrium isotherms, kinetic studies, and decision tree modeling. *Polymers (Basel)*. 15. doi: 10.3390/polym15183754.

Fan, H., Yang, J. S., Gao, T. G., and Yuan, H. L. (2012). Removal of a low-molecular basic dye (Azure Blue) from aqueous solutions by a native biomass of a newly isolated *Cladosporium* sp.: Kinetics, equilibrium and biosorption simulation. J. Taiwan Inst. Chem. Eng. 43, 386–392. doi: 10.1016/j.jtice.2011.11.001.

Weber. F. J., Hage, K. C., de Bont J. A.. (1995). Growth of the fungus *Cladosporium sphaerospermum* with toluene as the sole carbon and energy source. *Appl. Environ. Microbiol*. 61, 3562–3566. doi: 10.1128/aem.61.10.3562-3566.1995.

Fogarty, R. V., Tobin, J.M., (1996). Fungal melanins and their interactions with metals. *Enzyme Microb. Technol.* 19, 311–317; doi:10.1016/0141-0229(96)00002-6.

Gargiulo, V., Alfè, M., Capua, R. Di, Togna, A. R., Cammisotto, V., Fiorito, S., et al. (2015). Supplementing π-systems: eumelanin and graphene-like integration towards highly conductive materials for the mammalian cell culture bio-interface. *J. Mater. Chem*. B 3, 5070–5079. doi: 10.1039/c5tb00343a.

Ghaedi, M., Brazesh, B., Karimi, F., and Ghezelbash, G. R. (2014). Equilibrium, thermodynamic, and kinetic studies on some metal ions biosorption using black yeast *Aureobasidium pullulans* biomass. *Environ. Prog. Sustain*. Energy 33, 769–776. doi: 10.1002/ep.11807.

Gueidan, C., Ruibal, C., De Hoog, G. S., and Schneider, H. (2011). Rock-inhabiting fungi originated during periods of dry climate in the late Devonian and middle Triassic. *Fungal Biol*. 115, 987–996. doi: 10.1016/j.funbio.2011.04.002.

Harutyunyan, S., Muggia, L., and Grube, M. (2008). Black fungi in lichens from seasonally arid habitats. *Stud. Mycol*. 61, 83. doi: 10.3114/sim.2008.61.08.

HC, E., and A, C. (2012). Synthesis and assembly of fungal melanin. *Appl. Microbiol. Biotechnol*. 93, 931–940. doi: 10.1007/S00253-011-3777-2.

Hewedy, M., and Ashour, S. (2009). Production of a Melanin like Pigment by *Kluyveromyces marxianus* and *Streptomyces chibaensis*. *Aust. J. Basic Appl. Sci*. 3, 920–927. Available at: http://www.ajbasweb.com/ajbas/2009/920-927.pdf.

Hong, L., and Simon, J. D. (2006). Insight into the Binding of Divalent Cations to Sepia Eumelanin from IR Absorption Spectroscopy. *Photochem. Photobiol*. 82, 1265–1269. doi: 10.1562/2006-02-23-ra-809.

Hong, L., and Simon, J. D. (2007). Current understanding of the binding sites, capacity, affinity, and biological significance of metals in melanin. *J. Phys. Chem*. B 111, 7938–7947. doi: 10.1021/jp071439h/asset/images/large/jp071439hf00009.jpeg.

Hong, S., Wang, Y., Park, S. Y., and Lee, H. (2018). Progressive fuzzy cation- assembly of biological catecholamines. *Sci. Adv*. 4, 7457–7464. doi: 10.1126/sciadv.aat7457/suppl_file/aat7457_sm.pdf.

Isola, D., Scano, A., Orrù, G., Prenafeta-Boldú, F. X., and Zucconi, L. (2021). Hydrocarbon-contaminated sites: Is there something more than *exophiala* xenobiotica? new insights into black fungal diversity using the long cold incubation method. *J. Fu*ngi. 7, 817. doi: 10.3390/jof7100817/s1.

Isola, D., Zucconi, L., Onofri, S., Caneva, G., de Hoog, G. S., and Selbmann, L. (2016). Extremotolerant rock inhabiting black fungi from Italian monumental sites. Fungal Divers. 76, 75–96. doi: 10.1007/s13225-015-0342-9.

Jalmi, P., Bodke, P., Wahidullah, S., and Raghukumar, S. (2012). The fungus *Gliocephalotrichum simplex* as a source of abundant, extracellular melanin for biotechnological applications. World *J. Microbiol. Biotechnol*. 28, 505–512. doi: 10.1007/S11274-011-0841-0/figures/7.

Jastrzebska, M. M., Jussila, S., and Isotalo, H. (1998). Dielectric response and a.c. conductivity of synthetic dopa-melanin polymer. *J. Mater. Sci*. 33, 4023–4028. doi: 10.1023/a:1004449631857.

Kim, E., Leverage, W. T., Liu, Y., Panzella, L., Alfieri, M. L., Napolitano, A., et al. (2016). Paraquat-melanin redox-cycling: Evidence from electrochemical reverse engineering. *ACS Chem. Neurosci*. 7, 1057–1067. doi: 10.1021/acschemneuro.6b00007/.

Kogej, T., Stein, M., Volkmann, M., Gorbushina, A. A., Galinski, E. A., and Gunde-Cimerman, N. (2007). Osmotic adaptation of the halophilic fungus *Hortaea werneckii*: Role of osmolytes and melanization. *Microbiology*. 153, 4261–4273. doi: 10.1099/mic.0.2007/010751-0.

Kulkarni, G. B., Nayak, A. S., Mashetty, S. B., and Karegoudar, T. B. (2013). Properties and functions of melanin pigment from *Klebsiella* sp. GSK. *Korean J. Microbiol. Biotechnol*. 41, 60–69. doi: 10.4014/kjmb.1210.10002.

Kumar, P., Di Mauro, E., Zhang, S., Pezzella, A., Soavi, F., Santato, C., et al. (2016). Melanin-based flexible supercapacitors. *J. Mater. Chem*. C 4, 9516–9525. doi: 10.1039/c6tc03739a.

Li, T., Liu, M. J., Zhang, X. T., Zhang, H. B., Sha, T., and Zhao, Z. W. (2011). Improved tolerance of maize (Zea mays L.) to heavy metals by colonization of a dark septate endophyte (DSE) *Exophiala pisciphila*. *Sci. Total Environ*. 409, 1069–1074. doi: 10.1016/j.scitotenv.2010.12.012.

Liu, Y., and Simon, J. D. (2003). The effect of preparation procedures on the morphology of melanin from the ink sac of *Sepia officinalis*. Pigment Cell Res. 16, 72–80. doi: 10.1034/j.1600-0749.2003.00009.x.

Lu, Q., Oh, D. X., Lee, Y., Jho, Y., Soo Hwang, D., and Zeng, H. (2013) Nanomechanics of Cation-p Interactions in Aqueous Solution. *Angewandte Chemie (International ed. in English)*. 52,14. doi: 10.1002/ange.201210365.

M, d'Ischia, K, W., A, N., S, B., JC, G.-B., D, K., et al. (2013). Melanins and melanogenesis: methods, standards, protocols. *Pigment Cell Melanoma Res*. 26, 616–633. doi: 10.1111/pcmr.12121.

Madkhali, N., Alqahtani, H. R., Alterary, S., Albrithen, H. A., Laref, A., and Hassib, A. (2020). Characterization and electrochemical deposition of natural melanin thin films. *Arab. J. Chem*. 13, 4987–4993. doi: 10.1016/j.arabjc.2020.01.021.

Madrid, H.; Gené, J.; Quijada, L.; Cantillo, T.; Gacitúa, R.; Valdés, J.; Sánchez, C.; Prenafeta-Boldú, F.; Wijayawardene, N.; Silva, V.; Godoy, P. *Exophiala atacamensis* sp. nov. and *E. crusticola* from the Atacama Desert, northern Chile. 2023. *Sydowia.* 75, 181–192.

Manirethan, V., Gupta, N., Balakrishnan, R. M., and Raval, K. (2020). Batch and continuous studies on the removal of heavy metals from aqueous solution using biosynthesised melanin coated PVDF membranes. *Environ. Sci. Pollut*. Res. 27, 24723–24737. doi: 10.1007/s11356-019-06310-8/figures/12.

Manirethan, V., Raval, K., Rajan, R., Thaira, H., and Balakrishnan, R. M. (2018). Kinetic and thermodynamic studies on the adsorption of heavy metals from aqueous solution by melanin nanopigment obtained from marine source: *Pseudomonas stutzeri*. J. *Environ. Manage*. 214, 315–324. doi: 10.1016/j.jenvman.2018.02.084.

Mauro, E. Di, Xu, R., Soliveri, G., Santato, C., Physics, E., and Montréal, P. (2017). Natural melanin pigments and their interfaces with metal ions and oxides: emerging concepts and technologies. *MRS Communications*. 7, 141–151. doi: 10.1557/mrc.2017.33.

Mcginness, J., Corry, P., and Proctor, P. (1974). Amorphous semiconductor switching in melanins. *Science*. 183, 853–855. doi: 10.1126/science.183.4127.853.

Medina-Armijo, C., Isola, D., Illa, J., Puerta, A., Viñas, M., and Prenafeta-Boldú, F. X. (2024). The metallotolerance and biosorption of As(V) and Cr(VI) by black fungi. *J. Fungi*. 10, 47 10, 47. doi: 10.3390/jof10010047.

Migliaccio, L., Manini, P., Altamura, D., Giannini, C., Tassini, P., Maglione, M. G., et al. (2019). Evidence of unprecedented high electronic conductivity in mammalian pigment-based eumelanin thin films after thermal annealing in Vacuum. *Front. Chem*. 7, 162. doi: 10.3389/fchem.2019.00162/full.

Mihai, I., Addiégo, F., Del Frari, D., Bour, J. Ô., and Ball, V. (2013). Associating oriented polyaniline and eumelanin in a reactive layer-by-layer manner: Composites with high electrical conductivity. *Colloids Surfaces A Physicochem. Eng. Asp*. 434, 118–125. doi: 10.1016/j.colsurfa.2013.05.028.

Mohsenzadeh, F., Shahrokhi, F. Biological removing of Cadmium from contaminatedmedia by fungal biomass of *Trichoderma* species. *J Environ Health Sci Engineer.* 12, 102. https://doi.org/10.1186/2052-336X-12-102

Moreno, L. F., Mayer, V., Voglmayr, H., Blatrix, R., Benjamin Stielow, J., Teixeira, M. M., et al. (2019). Genomic analysis of ant domatia-associated melanized fungi (*Chaetothyriales*, Ascomycota). *Mycol. Prog*. 18, 541–552. doi: 10.1007/s11557-018-01467-x.

Morris-Jones, R., Gomez, B. L., Diez, S., Uran, M., Morris-Jones, S. D., Casadevall, A., et al. (2005). Synthesis of melanin pigment by *Candida albicans* in vitro and during infection. *Infect. Immun*. 73, 6147–6150. doi: 10.1128/iai.73.9.6147-6150.2005.

Mostert, A. B., Powell, B. J., Pratt, F. L., Hanson, G. R., Sarna, T., Gentle, I. R., et al. (2012). Role of semiconductivity and ion transport in the electrical conduction of melanin. *Proc. Natl. Acad. Sci. U.S.A*. 109, 8943–8947. doi: 10.1073/pnas.1119948109/suppl_file/pnas.1119948109_si.pdf.

Mota, E. A., Felestrino, É. B., Leão, V. A., and Guerra-Sá, R. (2020). Manganese (II) removal from aqueous solutions by *Cladosporium halotolerans* and *Hypocrea jecorina*. *Biotechnol. Reports*. 25, e00431. doi: 10.1016/j.btre.2020.e00431.

Mukherjee, A., Das, D., Kumar Mondal, S., Biswas, R., Kumar Das, T., Boujedaini, N., et al. (2010). Tolerance of arsenate-induced stress in *Aspergillus niger*, a possible candidate for bioremediation. *Ecotoxicol. Environ*. Saf. 73, 172–182. doi: 10.1016/j.ecoenv.2009.09.015.

Oh, J. J., Kim, J. Y., Kwon, S. L., Hwang, D. H., Choi, Y. E., and Kim, G. H. (2020). Production and characterization of melanin pigments derived from *Amorphotheca resinae*. *J. Microbiol*. 58, 648–656. doi: 10.1007/s12275-020-0054-z.

Oh, J., Young, J., Jun, Y., Kim, S., and Kim, G. (2021). Chemosphere Utilization of extracellular fungal melanin as an eco-friendly biosorbent for treatment of metal-contaminated effluents. *Chemosphere*. 272, 129884. doi: 10.1016/j.chemosphere.2021.129884.

Onofri, S., Barreca, D., Selbmann, L., Isola, D., Rabbow, E., Horneck, G., et al. (2008). Resistance of Antarctic black fungi and cryptoendolithic communities to simulated space and Martian conditions. *Stud. Mycol*. 61, 99–109. doi: 10.3114/sim.2008.61.10.

Ozlu, B., and Shim, B. S. (2022). Highly conductive melanin-like polymer composites for nonenzymatic glucose biosensors with a wide detection range. *ACS Appl. Polym. Mater*. 4, 2527–2535. doi: 10.1021/acsapm.1c01818/suppl_file/ap1c01818_si_001.pdf.

Pethkar, A. V., Kulkarni, S. K., and Paknikar, K. M. (2001). Comparative studies on metal biosorption by two strains of *Cladosporium cladosporioides*. *Bioresour. Technol*. 80, 211–215. doi: 10.1016/s0960-8524(01)00080-3.

Polymers, V. (2021). Melanin, the What, the Why and the How: An introductory review for Materials Scientists Interested in Flexible and Versatile Polymers.

Prados-Rosales, R., Toriola, S., Nakouzi, A., Chatterjee, S., Stark, R., Gerfen, G., et al. (2015). Structural characterization of melanin pigments from commercial preparations of the edible mushroom *Auricularia auricula*. *J. Agric. Food Chem*. 63, 7326–7332. doi: 10.1021/acs.jafc.5b02713/asset/images/medium/jf-2015-027132_0006.gif.

Pralea, I. E., Moldovan, R. C., Petrache, A. M., Ilieș, M., Hegheș, S. C., Ielciu, I., et al. (2019). From extraction to advanced analytical methods: The challenges of melanin analysis. *Int. J. Mol. Sci*. 20. doi: 10.3390/ijms20163943.

Prenafeta-Boldú, F. X., Kuhn, A., Luykx, D. M. A. M., Anke, H., Van Groenestijn, J. W., and De Bont, J. A. M. (2001). Isolation and characterisation of fungi growing on volatile aromatic hydrocarbons as their sole carbon and energy source. *Mycol. Res*. 105, 477–484. doi: 10.1017/s0953756201003719.

Prenafeta-Boldú, F. X., Ballerstedt, H., Gerritse, J., and Grotenhuis, J. T. C. (2004). Bioremediation of BTEX hydrocarbons: Effect of soil inoculation with the toluene-growing fungus *Cladophialophora* sp. strain T1. *Biodegradation* 15, 59–65. doi: 10.1023/b:biod.0000009973.53531.96.

Prenafeta-Boldú, F. X., Summerbell, R., and Sybren De Hoog, G. (2006). Fungi growing on aromatic hydrocarbons: Biotechnology's unexpected encounter with biohazard? *FEMS Microbiol. Rev*. 30, 109–130. doi: 10.1111/j.1574-6976.2005.00007.x.

Prenafeta-Boldú, F. X., de Hoog, G. S., and Summerbell, R. C. (2018). "Fungal Communities in Hydrocarbon Degradation," in Microbial Communities Utilizing Hydrocarbons and Lipids: Members, Metagenomics and Ecophysiology (Springer International Publishing), 8-2, 1–36. doi: 10.1007/978-3-319-60063-5_8-2.

Prenafeta-Boldú, F. X., Medina-Armijo, C., and Isola, D. (2022). "Black fungi in the built environment-The good, the bad, and the ugly," in Viruses, Bacteria and Fungi in the Built Environment: Designing Healthy Indoor Environments. *Elsevier*. 65–99. doi: 10.1016/b978-0-323-85206-7.00008-3.

PrKumar, A., Di Mauro, E., Zhang, S., Pezzella, A., Soavi, F., Santato, C., et al. (2016). Melanin-based flexible supercapacitors. *J. Mater. Chem*. C 4, 9516–9525. doi: 10.1039/C6TC03739A.

Prota, G. (1992). Melanins and melanogenesis. *Academic Press. San Diego*, CA, USA, 1992.

Pulschen, A. A., Rodrigues, F., Duarte, R. T. D., Araujo, G. G., Santiago, I. F., Paulino-Lima, I. G., et al. (2015). UV-resistant yeasts isolated from a high-altitude volcanic area on the Atacama Desert as eukaryotic models for astrobiology. *Microbiologyopen*. 4, 574–588. doi: 10.1002/mbo3.262.

Radulovicáradulovicá, M. Đ., Cvetkovicácvetkovicá, O. G., Nikolic´b, S. D., Nikolic´b, N., Đordevicá, D. S. Đ., Jakovljevicá, D. M. J., et al. (2007). Simultaneous production of pullulan and biosorption of metals by *Aureobasidium pullulans* strain CH-1 on peat hydrolysate. Bioresource technology. 14, 6673-7.doi: 10.1016/j.biortech.2007.11.053.

Ribera, J., Panzarasa, G., Stobbe, A., Osypova, A., Rupper, P., Klose, D., et al. (2019). Scalable Biosynthesis of melanin by the Basidiomycete *Armillaria cepistipes*. *J. Agric. Food Chem*. 67, 132–139. doi: 10.1021/acs.jafc.8b05071.

Rome, L. De, and Gadd, G. M. (1987). Copper adsorption by. 1987, 84–90.

Roy, S., Van Hai, L., Kim, H. C., Zhai, L., and Kim, J. (2020). Preparation and characterization of synthetic melanin-like nanoparticles reinforced chitosan nanocomposite films. *Carbohydr. Polym.* 231, 115729. doi: 10.1016/j.carbpol.2019.115729.

Saini, A. S., and Melo, J. S. (2013). Biosorption of uranium by melanin: Kinetic, equilibrium and thermodynamic studies. *Bioresour. Technol*. 149, 155–162. doi: 10.1016/j.biortech.2013.09.034.

Saitoh, Y., Izumitsu, K., Morita, A., and Tanaka, C. (2010). A copper-transporting ATPase BcCCC2 is necessary for pathogenicity of *Botrytis cinerea*. *Mol. Genet. Genomics*. 284, 33–43. doi: 10.1007/S00438-010-0545-4.

Selbmann, L., Egidi, E., Isola, D., Onofri, S., Zucconi, L., de Hoog, G. S., et al. (2013). Biodiversity, evolution and adaptation of fungi in extreme environments. *Plant Biosyst*. 147, 237–246. doi: 10.1080/11263504.2012.753134.

Selbmann, L., Zucconi, L., Isola, D., and Onofri, S. (2015). Rock black fungi: excellence in the extremes, from the Antarctic to space. *Curr. Genet.* 61, 335–345. doi: 10.1007/s00294-014-0457-7.

Selvakumar, P., Rajasekar, S., Periasamy, K., and Raaman, N. (2008). Isolation and characterization of melanin pigment from *Pleurotus cystidiosus* (telomorph of *Antromycopsis macrocarpa*). *World J. Microbiol. Biotechnol*. 24, 2125–2131. doi: 10.1007/s11274-008-9718-2.

Seyedmousavi, S., Badali, H., Chlebicki, A., Zhao, J., Prenafeta-boldú, F. X., and De Hoog, G. S. (2011). *Exophiala sideris*, a novel black yeast isolated from environments polluted with toxic alkyl benzenes and arsenic. *Fungal Biol*. 115, 1030–1037. doi: 10.1016/j.funbio.2011.06.004.

Sheliakina, M., Mostert, A. B., and Meredith, P. (2018). Decoupling Ionic and Electronic Currents in Melanin. *Adv. Funct. Mater*. 28. doi: 10.1002/adfm.201805514.

Shen, M., Zhao, D.-K., Qiao, Q., Liu, L., Wang, J.-L., Cao, G.-H., et al. (2015). Identification of Glutathione S-Transferase (GST) Genes from a Dark Septate Endophytic Fungus (*Exophiala pisciphila*) and Their Expression Patterns under Varied Metals Stress. *PLoS One 10*, 123418. doi: 10.1371/journal.pone.0123418.

Silva, N. M. da, Reis, G. F., Costa, F. de F., Grisolia, M. E., Geraldo, M. R., Lustosa, B. P. R., et al. (2023). Genome sequencing of *Cladophialophora exuberans*, a novel candidate for bioremediation of hydrocarbon and heavy metal polluted habitats. *Fungal Biol*. 127, 1032–1042. doi: 10.1016/j.funbio.2023.03.003.

Sono, K., Lye, D., Moore, C. A., Boyd, W. C., Gorlin, T. A., and Belitsky, J. M. (2012). Melanin-Based Coatings as Lead-Binding Agents. *Bioinorg. Chem. Appl*. 2012. doi: 10.1155/2012/361803.

Steven, cross-linking G., Wang, M.-T., Su, C.-W., Chen, Y.-S., and Hong, M.-Y. (2007). Picogram detection of metal ions by melanin-sensitized piezoelectric sensor. *Biosens. Bioelectron*. 23, 319–325. doi: 10.1016/j.bios.2007.04.011.

Suh, J. H., Yun, J. W., and Kim, D. S. (1999). Effect of pH on Pb^{2+} accumulation in *Saccharomyces cerevisiae* and *Aureobasidium pullulans*. *Bioprocess Eng*. 20, 471–474. doi: 10.1007/pl00009056.

Sun, S., Zhang, X., Chen, W., Zhang, L., and Zhu, H. (2016). Production of natural edible melanin by *Auricularia auricula* and its physicochemical properties. *Food Chem*. 196, 486–492. doi: 10.1016/j.foodchem.2015.09.069.

Suwannarach, N., Kumla, J., Watanabe, B., Matsui, K., and Lumyong, S. (2019). Characterization of melanin and optimal conditions for pigment production by an endophytic fungus, *Spissiomyces endophytica* SDBR-CMU319. *PLoS One*. 14, 1–15. doi: 10.1371/journal.pone.0222187.

Szpoganicz, B., Gidanian, S., Kong, P., and Farmer, P. (2002). Metal binding by melanins: studies of colloidal dihydroxyindole-melanin, and its complexation by Cu(II) and Zn(II) ions. *J. Inorg. Biochem*. 89, 45–53. doi: 10.1016/S0162-0134(01)00406-8.

Teixeira, M. M., Moreno, L. F., Stielow, B. J., Muszewska, A., Hainaut, M., Gonzaga, L., et al. (2017). Exploring the genomic diversity of black yeasts and relatives (*Chaetothyriales*, Ascomycota). *Stud. Mycol*. 86, 1–28. doi: 10.1016/j.simyco.2017.01.001.

Thaira, H., Raval, K., Manirethan, V., and Balakrishnan, R. M. (2019). Melanin nano-pigments for heavy metal remediation from water. *Sep. Sci. Technol*. 54, 265–274. doi: 10.1080/01496395.2018.1443132.

Tran-Ly, A. N., De France, K. J., Rupper, P., Schwarze, F. W. M. R., Reyes, C., Nyström, G., et al. (2021). Melanized-cationic cellulose nanofiber foams for bioinspired removal of cationic dyes. *Biomacromolecules*. 22, 4681–4690. doi: 10.1021/acs.biomac.1c00942.

Tran-Ly, A. N., Reyes, C., Francis, ·, Schwarze, W. M. R., and Ribera, J. (2020a). Microbial production of melanin and its various applications. *World J. Microbiol. Biotechnol*. 36, 170. doi: 10.1007/s11274-020-02941-z.

Tran-Ly, A. N., Ribera, J., Schwarze, F. W. M. R., Brunelli, M., and Fortunato, G. (2020b). Fungal melanin-based electrospun membranes for heavy metal detoxification of water. Sustain. Mater. Technol. 23, e00146. doi: 10.1016/j.susmat.2019.e00146.

Vahidzadeh, E., Kalra, A. P., and Shankar, K. (2018). Melanin-based electronics: From proton conductors to photovoltaics and beyond. *Biosens. Bioelectron*. 122, 127–139. doi: 10.1016/j.bios.2018.09.026.

Visscher, H., Brinkhuis, H., Dilcher, D. L., Elsik, W. C., Eshet, Y., Looy, C. V., et al. (1996). The terminal paleozoic fungal event: Evidence of terrestrial ecosystem destabilization and collapse. *Proc. Natl. Acad. Sci. U.S.A*. 93, 2155–2158. doi: 10.1073/pnas.93.5.2155.

Wang, L. F., and Rhim, J. W. (2019). Isolation and characterization of melanin from black garlic and sepia ink. *LWT*. 99, 17–23. doi: 10.1016/J.LWT.2018.09.033.

Wang, Y., Su, J., Li, T., Ma, P., Bai, H., Xie, Y., et al. (2017). A novel UV-shielding and transparent polymer film: When bioinspired dopamine-melanin hollow nanoparticles. *Join Polymers*. *ACS Appl. Mater. Interfaces*. 9, 36281–36289. doi: 10.1021/acsami.7b08763/asset/images/medium/am-2017-08763a_0013.gif.

Xiang, L., Zhang, J., Wang, W., Gong, L., Zhang, L., Yan, B., et al. (2020). Nanomechanics of π-cation-π interaction with implications for bio-inspired wet adhesion. *Acta Biomater*. 117, 294–301. doi: 10.1016/j.actbio.2020.09.043.

Yang, M., Li, L., Yu, S., Liu, J., and Shi, J. (2020). High performance of alginate/polyvinyl alcohol composite film based on natural original melanin nanoparticles used as food thermal insulating and UV–vis block. *Carbohydr. Polym.* 233, 115884. doi: 10.1016/j.carbpol.2020.115884.

Zhan, F., He, Y., Zu, Y., Li, T., and Zhao, Z. (2011). Characterization of melanin isolated from a dark septate endophyte (DSE), *Exophiala pisciphila*. *World J. Microbiol. Biotechnol*. 27, 2483–2489. doi: 10.1007/s11274-011-0712-8.

Zhang, C., Sirijovski, N., Adler, L., and Ferrari, B. C. (2018). *Exophiala macquariensis* sp. nov., a cold adapted black yeast species recovered from a hydrocarbon contaminated sub-Antarctic soil. doi: 10.1016/j.funbio.2018.11.011.

Zhang, Q., and Wang, C. (2020). Natural and Human Factors Affect the Distribution of Soil Heavy Metal Pollution: a Review. *Water. Air. Soil Pollut*. 231, 1–13. doi: 10.1007/s11270-020-04728-2/figures/3.

Zhang, Y., Zhang, Y., Liu, M., Shi, X., and Zhao, Z. (2008). Dark septate endophyte (DSE) fungi isolated from metal polluted soils: Their taxonomic position, tolerance, and accumulation of heavy metals in Vitro. *J. Microbiol*. 46, 624–632. doi: 10.1007/s12275-008-0163-6.

Zhao, D., Li, T., shen, M., Wang, J., and Zhao, Z. (2015). Diverse strategies conferring extreme cadmium (Cd) tolerance in the dark septate endophyte (DSE), *Exophiala pisciphila*: Evidence from RNA-seq data. *Microbiol. Res*. 170, 27–35. doi: 10.1016/j.micres.2014.09.005.

Zou, Y., and Hou, X. (2017). Optimization of culture medium for production of melanin by *Auricularia auricula*. *Food Sci. Technol*. 37, 153–157. doi: 10.1590/1678-457x.18016.

Zupančič, J., Babič, M. N., Zalar, P., and Gunde-Cimerman, N. (2016). The black yeast *Exophiala dermatitidis* and other selected opportunistic human fungal pathogens spread from dishwashers to kitchens. *PLoS One 11(2): e0148166.*. doi: 10.1371/journal.pone.0148166.

Chapter 2

Research Aims

The general objective of this Thesis is to evaluate the biotechnological potential of fungal melanin as an innovative biomaterial to be used in environmental applications, particularly those related with the binding of toxic metals and metalloids, and as an alternative semiconductive biomaterial that intervenes and impacts, electroactive bacteria and microbial syntrophic interactions that regulate the carbon cycle and methane(i.e CH4 emissions) in flooded soils (e.g. rice paddy fields) . The research approach was based on the use of black fungi as the source of melanin because of their strong melanization and extremophilic nature.

To develop this research project, the general aim has been subdivided into the following specific objectives:

I. To assess the ability of a diverse collection of black fungi isolated from polluted environments to tolerate hexavalent chromium Cr(VI) and pentavalent arsenic As(V), as representatives of environmentally relevant heavy metal and metalloid respectively, to disentangle possible patterns in the metallotolerance of these fungi, and to evaluate the biosorption capacity of selected metallotolerant fungal strains towards Cr(VI) and As(V).

II. To develop and optimize a laboratory protocol for the extraction and purification of fungal melanin and to characterize this biomaterial by means of an array of advanced physicochemical methods, focusing on structure-function relationships for the sorption of heavy metals and metalloids and on its electroconductive behavior and interactions with exoelectrogenic microbes.

III. To identify the biochemical changes that occur when cell cultures of a metallotolerant model black fungus are exposed to toxic concentrations of As(V) and Cr(VI), and correlate these results with an in-depth analysis of the genetic expression profile under such conditions to unravel the fungal molecular response under stress induced by heavy metals.

IV. To explore the potential application of fungal melanin for mitigating methane emissions, compared to other (semi)conductive materials. in anaerobic soil microcosmos simulating postharvest rice paddy soils after rice straw amendment. to gain insights into its effect on the whole microbial community diversity and on interspecies electron transfer (IET) processes that stimulate electroactive microbial populations.

Chapter 3

The metallotolerance and biosorption of As(V) and Cr(VI) by black fungi

Medina-Armijo, C., Isola, D., Illa, J., Puerta, A., Viñas, M., and Prenafeta-Boldú, F. X. (2024). The metallotolerance and biosorption of As(V) and Cr(VI) by black fungi. J. Fungi. 10, 47 10, 47. doi: 10.3390/jof10010047.

Part of this chapter was also presented as an oral communication in Sociedad de Microbiología de Chile (SOMICH) 2023 and Potencial biotecnológico de los hongos melanizados metalotolerantes conference. Article.

Journal of Fungi

MDPI

Article

The Metallotolerance and Biosorption of As(V) and Cr(VI) by Black Fungi

Cristy Medina-Armijo [1,2,*], Daniela Isola [3], Josep Illa [4], Anna Puerta [1], Marc Viñas [1] and Francesc X. Prenafeta-Boldú [1,*]

[1] Program of Sustainability in Biosystems, Institute of Agrifood Research and Technology (IRTA), 08140 Caldes de Montbui, Spain
[2] Faculty of Pharmacy and Food Sciences, University of Barcelona, 08028 Barcelona, Spain
[3] Department of Economics, Engineering, Society and Business Organization (DEIM), University of Tuscia, 01100 Viterbo, Italy
[4] Department of Computing and Industrial Engineering, University of Lleida, 25001 Lleida, Spain
* Correspondence: cristy.medina@irta.cat (C.M.-A.); francesc.prenafeta@irta.cat (F.X.P.-B.)

Abstract: A collection of 34 melanized fungi isolated previously from anthropogenic contaminated sites were assessed for their tolerance to toxic concentrations of As(V) and Cr(VI) anions. Three strains of the species *Cyphellophora olivacea*, *Rhinocladiella similis*, and *Exophiala mesophila* (Chaetothyriales) were identified as hyper-metallotolerant, with estimated IC_{50} values that ranged from 11.2 to 16.9 g L^{-1} for As(V) and from 2.0 to 3.4 g L^{-1} for Cr(VI). *E. mesophila* and *R. similis* were selected for subsequent assays on their biosorption capacity and kinetics under different pH values (4.0 and 6.5) and types of biomass (active and dead cells and melanin extracts). The fungal biosorption of As(V) was relatively ineffective, but significant removal of Cr(VI) was observed from liquid cultures. The Langmuir model with second-order kinetics showed maximum sorption capacities of 39.81 mg Cr^{6+} g^{-1} for *R. similis* and 95.26 mg Cr^{6+} g^{-1} for *E. mesophila* on a dry matter basis, respectively, while the kinetic constant for these two fungi was 1.32×10^{-6} and 1.39×10^{-7} g (mg Cr^{6+} min)$^{-1}$. Similar experiments with melanin extracts of *E. mesophila* showed maximum sorption capacities of 544.84 mg Cr^{6+} g^{-1} and a kinetic constant of 1.67×10^{-6} g (mg Cr^{6+} min)$^{-1}$. These results were compared to bibliographic data, suggesting that metallotolerance in black fungi might be the result of an outer cell-wall barrier to reduce the diffusion of toxic metals into the cytoplasm, as well as the inner cell wall biosorption of leaked metals by melanin.

Keywords: Chaetothyriales; *Exophiala mesophila*; fungal melanin; heavy metal bioremediation; hexavalent chromium tolerance; Langmuir biosorption isotherm; pentavalent arsenic tolerance; second-order kinetic model

check for updates

Citation: Medina-Armijo, C.; Isola, D.; Illa, J.; Puerta, A.; Viñas, M.; Prenafeta-Boldú, F.X. The Metallotolerance and Biosorption of As(V) and Cr(VI) by Black Fungi. *J. Fungi* **2024**, *10*, 47. https://doi.org/10.3390/jof10010047

Academic Editor: Montserrat Sarrà

Received: 24 November 2023
Revised: 28 December 2023
Accepted: 3 January 2024
Published: 5 January 2024

1. Introduction

Heavy metals and metalloids (HMMs) are found naturally in the Earth's crust at relatively diffused amounts, but they might become concentrated as a result of anthropogenic activities such as mining, agriculture, and husbandry, as well as several industrial manufacturing processes. Because of their inherent high toxicity, pollution with HMMs has become a pressing public health issue in many parts of the world [1]. Metal ions persist in the environment due to the bioaccumulation tendency of living organisms and their limited capacity to metabolize them into less toxic forms [2]. Once absorbed into the cell, HMMs bind to vital components, such as structural proteins, enzymes, and nucleic acids, impairing several fundamental metabolic functions [3].

Groundwater contaminated with arsenic is still poisoning millions of people, primarily from developing countries, and has been listed by the WHO as one of the ten chemicals of major public health concern [4,5]. Arsenic exposure to humans can be attributed to

to various sources, including natural deposits, agricultural pesticides, and industrial effluents [5]. Natural geochemical processes can also lead to toxic and subtoxic concentrations of arsenic in groundwater [6]. Arsenic contaminated water typically contains both arsenate and arsenite species, As(V) and As(III). Water pollution with chromium is gaining more consideration because it is globally widespread, and also represents an important public health concern [7,8]. The majority of chromium releases into the environment originate from industrial activities, particularly from the processing and manufacturing of chemicals, minerals, steel, leather tanning, textile dyeing, metallurgical operations, and various other industrial processes [7]. The most stable oxidation states of chromium in water correspond to the hexavalent Cr(VI) and trivalent Cr(III) species, but concerns are primarily related to Cr(VI) owing to its high biotoxicity.

A number of technical approaches for the remediation of HMM pollution and water purification have been proposed [9]. These solutions should rely on technically and economically viable methods, such as the biosorption of HMM into readily available biomass sources. Many reports in the literature describe the capacity of pure cultures of bacteria [10,11], algae [12], aquatic plants [13], and fungi [14,15] to remove HMM ions from aqueous solutions. Such bioremediation alternatives are an interesting option for the decontamination of water and soil, because these processes require few reagents and energy, they generate relatively low amounts of toxic waste products, and because biosorption is highly effective in reducing HMM at relatively low concentrations [1,13]. However, the biotechnological removal of HMM still faces some scalability problems associated to the difficulty to find suitable microorganisms that are able to cope with a highly oligotrophic and toxic environment, while having a high HMM biosoption potential.

In this context, one particular group of ascomycetes known as black fungi (BF) because of their common polymorphism as yeast-like, hyphal and meristematic growth, have been identified recently for their capacity to bind heavy metals to their cell wall [16,17]. These fungi are characterized by a high morphological and metabolic plasticity and poly-extremotolerant traits, which allows them to colonize a high diversity of often divergent and uncommon habitats [18]. The main defining character of BF is a strongly melanized cell wall, which confers them protection against extreme environmental conditions, such as exposure to UV and ionizing radiation, desiccation, cold/hot temperatures, high salinity, and oligotrophic environment [19,20]. This latter trait has also been linked to the ability to use toxic volatile hydrocarbons as the only source of carbon and energy [21,22]. As for their identities, BF primarily fall into two main phylogenetic groups: the Eurotiomycetes (Chaetothyriales) and the Dothideomycetes (Dothideales, Cladosporiales, and a few other related orders in the Mycophaerellales) [18,23].

The structure of fungal melanin is somewhat similar to soil humic acids with respect to volatile compounds released upon pyrolysis and amino acid hydrolysis [24]. In particular, the melanin of BF is composed of short-distance non-hydrolysable strong carbon-carbon bonds based on 1,8-dihydroxynaphthalene (DHN), modified with different functional groups, such as carboxyl, phenolic, hydroxyl, and amino [25,26], which provide many potential binding or biosorption sites for metal ions [27]. Special attention has been given to two main functions attributed to melanin in relation to metal ions: as a reservoir for the temporary storage and release of certain nutrients, and as chelating agents of HMM for protecting the cell against metal toxicity. However, the biodiversity of metallotolerant BF and their HMM bioabsorption potential have seldom been investigated.

In this study we screened a collection of BF species isolated previously from diverse anthropogenic polluted sites for their tolerance to As(V) and Cr(VI), selected respectively as a model heavy metal and metalloid. The biosorption potential was determined on selected metallotolerant strains, using living fungal cultures, dead biomass and melanin extracts. The obtained results could give new insights into the biology of BF and might contribute to the development of biotechnological applications.

2. Materials and Methods

2.1. Biological Material

A culture collection of 34 BF strains confidently identified at the species level were used (Table 1). Most of these strains were isolated during previous studies [21,28] from car fuel dispensers and tanks, stone buildings exposed to pollution and toxic biocides, and washing machines. These strains are currently maintained at the Culture Collection of Fungi from Extreme Environments (CCFEE) at the Tuscia University in Viterbo, the Westerdijk Fungal Biodiversity Center (formerly Centralbureau voor Schimmelcultures – CBS), and the Institute of Agrifood Science and Technology (IRTA).

Table 1. List of melanized fungal strains used in this study.

Species	Phylogenetic group	Isolation source	Strain nr [a]	Accession nr [b]
Aulographina pinorum	Asterinales	Diesel pump	CCFEE 6222	OR660094
A. pinorum	Asterinales	Diesel pump	CCFEE 6230	MZ573423
Aureobasidium melanogenum	Dothideales	Diesel car tank	CCFEE 6213	OR660095
Au. melanogenum	Dothideales	Diesel car tank	CCFEE 6234	OR660096
Au. pullulans	Dothideales	Gasoline car tank	CCFEE 5876	JX681059
Au. pullulans	Dothideales	Gasoline pump	CCFEE 6244	OR660097
Cladosporium herbarum [c]	Cladosporiales	Diesel pump	CCFEE 6193	MZ573426
Cl. herbarum	Cladosporiales	Diesel pump	CCFEE 6192	OR660098
Coniosporium uncinatum	Dothideomycetes i.s. [d]	Gasoline car tank	CCFEE 5820	JX681057
Co. uncinatum	Dothideomycetes i.s.	Gasoline pump	CCFEE 6149	MZ573424
Cyphellophora olivacea	Chaetothyriales	Biocide-treated monument	CCFEE 6619	MT472271
Exophiala angulospora	Chaetothyriales	Biocide-treated monument	CCFEE 6620	MT472272
E. crusticola	Chaetothyriales	Gasoline pump	CCFEE 6188	OR660099
E. equina	Chaetothyriales	Washing machine soap dispenser	CCFEE 5883	JX681045
E. heteromorpha	Chaetothyriales	Gasoline pump	CCFEE 6240	MZ573439
E. heteromorpha	Chaetothyriales	Diesel car tank	CCFEE 6150	OR660100
E. lecanii-corni	Chaetothyriales	Washing machine soap dispenser	CCFEE 5688	OR660101
E. mesophila	Chaetothyriales	Washing machine soap dispenser	CCFEE 5690	JX681043
E. mesophila	Chaetothyriales	Glued ceramics	IRTA M2-F10	OR660102
E. oligosperma	Chaetothyriales	Human patient	CBS 725.88	AY163551
E. oligosperma	Chaetothyriales	Diesel car tank	CCFEE 6139	MZ573441
E. phaeomuriformis	Chaetothyriales	Diesel car tank	CCFEE 6242	MZ573445
E. xenobiotica	Chaetothyriales	Gasoline car tank	CCFEE 5784	OR660103
E. xenobiotica	Chaetothyriales	Bathroom wet cell	CCFEE 5985	JX681024
E. xenobiotica	Chaetothyriales	Diesel car tank	CCFEE 6143	OR660104
E. xenobiotica	Chaetothyriales	Gasoline pump	CCFEE 6142	OR660105
Knufia epidermis	Chaetothyriales	Diesel car tank	CCFEE 6138	MZ573455
K. epidermis	Chaetothyriales	Gasoline car tank	CCFEE 5813	JX681055
K. epidermis	Chaetothyriales	Diesel car tank	CCFEE 6198	OR660106
K. epidermis	Chaetothyriales	Diesel car tank	CCFEE 6366	OR660107
Neohortaea acidophila	Mycospharellales	Lignite	CBS 113389	OL739260
Rhizosphaera kalkholffii	Dothideales	Diesel car tank	CCFEE 6144	OR660108
Rhinocladiella similis	Chaetothyriales	Diesel car tank	CCFEE 6361	MZ573467
Scolecobasidium cft *globale*	Venturiales	Diesel car tank	CCFEE 6363	MZ573464

[a] CCFEE: Culture Collection of Fungi from Extreme Environments, Tuscia University; CBS: Fungal collection of the Westerdijk Fungal Biodiversity Institute; IRTA: Microbial collection of the Laboratory of Environmental Microbiology, Institute of Agrifood Research and Technology. [b] ITS1-5.8S-ITS2 ribosomal DNA sequences deposited in GenBank. [c] The strain reported as *Cladosporium herbarum* should be read as belonging to the corresponding species complex. [d] *Incertae sedis* (uncertain taxonomic placement).

2.2. Metallotolerance Assays

The capacity of the collected fungal strains to grow on the presence of increasing concentrations of As(V) and Cr(VI) was evaluated on solid cultures. Petri dishes (12 cm in diameter) were poured with potato dextrose agar (PDA; Condalab, Spain) supplemented with 2.5, 5.0, 7.5, 10.0, or 12.5 g As^{5+} L^{-1} from sodium arsenate ($Na_2HAsO_4 \cdot 7H_2O$; Thermo Fisher Scientific, Kandel, Germany) and 0.1, 0.5, 1.0, 1.5 and 2.5 g Cr^{6+} L^{-1} from potassium dichromate ($K_2Cr_2O_7$; Scharlab ExpertQ®, Spain). Each BF strain was inoculated six times with an inoculation loop on each agar plate containing a defined concentration of As(V) or Cr(VI). The radial growth of each fungal colony was measured by averaging orthogonal diameters, and this value was then averaged again for all six colonies from every single plate. These measurements were repeated after 7, 15, 30, 45, and 60 days of incubation, which was performed at 25°C under dark conditions. This prolonged timeframe was stablished to account for the potential long-term adaptation of slow growing BF strains. Unamended control plates were also included. The tolerance index (*TI*) was calculated for every strain by dividing the measured growth when exposed to the metal in relation to the control plates.

2.3. Production of Fungal Biomass

Fungal biomass for biosorption experiments on selected BF strains was produced in 0.5 L batch liquid cultures incubated at room temperature under shaking conditions (80 rpm) for 10 days. Yeast extract (4 g L^{-1}) was supplied as the carbon and energy source and macronutrients were added as 4.5 g KH_2PO_4, 0.5 g K_2HPO_4, 2.0 g NH_4Cl, and 0.1 mg $MgSO_4 \cdot 7H_2O$ per litre. Mineral micronutrients were added as 2 mL of a stock solution that contained 120 mg $FeCl_3$, 50 mg H_3BO_3, 10 mg $CuSO_4 \cdot 5H_2O$, 10 mg KI, 45 mg $MnSO_4 \cdot H_2O$, 20 mg $Na_2MoO_4 \cdot H_2O$, 75 mg $ZnSO_4 \cdot H_2O$, 50 mg $CoCl_2 \cdot 6H_2O$, 20 mg $AlK(SO_4)_2 \cdot 12H_2O$, 13.25 g $CaCl_2 \cdot H_2O$, and 10 g NaCl, per litre. Spore suspensions of pure cultures (0.5 mL, > 10^6 CFU mL^{-1}) were used as inoculant. After 10 days of incubation, the fungal biomass was harvested by centrifugation (20 minutes at 4,000 rpm) and washed with milliQ sterilized water. This process was repeated three times before using fungal biomass in batch biosorption assays.

2.4. Extraction and Purification of Melanin

Melanin was extracted from pre-grown BF cultures by adapting an acid hydrolysis method used previously with other fungi [29,30]. Briefly, harvested fungal biomass was homogenized in 100 mL of 1 M NaOH (120 rpm for 10 min), and treated with hot alkali (1M NaOH at 121°C for 20 min). The resulting suspension was centrifuged at 10,000 rpm for 10 min to remove fungal biomass and the brownish liquid fraction was acidified to pH 2.5 with HCl 6N and incubated for 12 h at 100°C. The resulting black precipitate was centrifuged (4,000 rpm for 20 min) and washed with deionized water three times. The precipitate was then lyophilized at a pressure of 0.7 mBar at -50°C for 24 hours, and the obtained melanin powder was kept at -20°C until use.

2.5. Biosorption Assays

The capacity of the fungal biomass to accumulate As(V) and Cr(VI) ions was tested on a oligotrophic liquid medium to minimize growth. Consequently, the number of sorption sites remained consistent. This medium contained a buffer of 35 mM $K_2HPO_4/NaH_2PO_4 \cdot 2H_2O$ (pH 6.5), glucose (0.3 %) and yeast extract (0.01%), along with 20 to 200 mg L^{-1} of As(V) or Cr(VI), added as $Na_2HAsO_4 \cdot 7H_2O$ or $K_2Cr_2O_7$, respectively. Biomass from living and heat-inactivated fungal cultures (in dry matter basis, approx. 50 mg-DM) was resuspended into liquid mineral medium and incubated in serum flasks (30 mL) under sterile conditions on a shaker (80 rpm at 25 °C). Experiments were carried out by triplicate and liquid samples were taken after 2, 5, 7, 14, 21, 30 days of incubation to

measure the concentration of As(V) and Cr(VI). Biosorption experiments were repeated at a pH 4.0 by adding HCl 0.1 M.

The assays for the biosorption of Cr(VI) onto melanin extracts were performed with 0.3 g of powder-melanin resuspended in 50 mL of a solution (pH 6.5; 150 rpm; 25°C). The initial solution Cr(VI) concentration was 30 mg-Cr^{6+} L^{-1} and incubations lasted up to 72 hours. Incubations were carried out by triplicate and liquid samples were taken regularly to measure the time-course evolution of the concentration of Cr(VI).

2.6. Analytical Methods

The content of total arsenic in liquid culture supernatant was determined with a Flame Atomic Absorption Spectroscopy (Model SpectrAA-110, Varian, Mulgrave, Australia). Chromium (VI) in the liquid fraction was determined with a colorimetric method based on the reaction with the complexing agent 1,5-diphenylcabazide (Sigma-Aldrich, USA) that forms a purple-violet colored complex, that was quantified by measuring the absorbance at a wavelength of 540 nm using a spectrophotometer (model EMC-11S UV brand, Germany).

2.7. Numerical Methods and Statistical Analysis

The software GraphPad Prism version 8.0 (GraphPad Software, San Diego, California, USA) was used for performing one-way ANOVA (multiple comparisons Tukey test), and for the calculation of the metal concentration causing a 50% inhibition of fungal growth (IC_{50}). After a given time of incubation, IC_{50} was calculated by fitting the tolerance index (TI) measurements at different HMM concentrations (C_t) to a two-parameter Hill logistic model (IC_{50} and slope factor h; equation 1).

$$TI = \frac{1}{(1+\frac{IC_{50}}{C_t})^h} \quad \text{Eq. 1}$$

As for the biosorption assays, the specific amount of the HMM that is taken up at any given time (q_t) by a defined amount of fungal biomass M_a, when incubated at an initial concentration C_0 in batch incubations of liquid volume V, is a function of the HMM remaining concentration (C_t) as the experimentally measured variable, as described by equation 2.

$$q_t = \frac{V \cdot (C_0 - C_t)}{M_a} \quad \text{Eq. 2}$$

The sorption rate is usually described either as a first or second order kinetics (equation 3), where k_i is the kinetic constant at the considered i^{th} order, and q_e is the adsorbed metal fraction when reaching equilibrium with the concentration C_e of metal in solution. The integration of equation 3, under the hypothesis of constant C_e , by considering second order kinetics gives equation 4, which relates q_t with time. Equation 4 is used to produce a linear plot ($t \cdot q_t^{-1}$) versus t with experimental data that allows the calculation of the two parameters k_2 and q_e from the intercept and slope.

$$\frac{dq_t}{dt} = k_i \cdot (q_e - q_t)^i \quad \text{Eq. 3}$$

$$\frac{t}{q_t} = \frac{1}{k_2 \cdot q_e^2} + \frac{t}{q_e} \quad \text{Eq. 4}$$

When the concentration of metal in solution varies with time the adsorbed fraction at equilibrium q_e is usually modelled as a function of liquid equilibrium concentration C_e by the Langmuir or by the Freundlich isotherms (equations 5 and 6). Both functions have two unknown parameters, q_{max} and K_L in the Langmuir equation, K_F and n in the Freundlich equation.

$$q_e = q_{max} \frac{K_L \cdot C_e}{1 + K_L \cdot C_e} \quad \text{Eq. 5}$$

$$q_e = K_L \cdot C_e^{1/n} \quad \text{Eq. 6}$$

The substitution in equation 3 of q_e by equations 5 or 6, the Langmuir or Freundlich isotherms named here as $q_e(C_t)$, and q_t by equation 2 results in the differential equation 7. This new expression describes the temporal evolution of the concentration in the liquid phase depending on the assumed sorption isotherm model and kinetic order.

$$\frac{dC_t}{dt} = -k_i \cdot \left(\frac{M_a}{V} \cdot q_e(C_t) \cdot (C_0 - C_t)\right)^i \quad \text{Eq. 7}$$

For a given set of the 3 parameters, equation 7 was numerically integrated along time and the goodness of the fit to the measured C_t values evaluated as the sum of square errors. A Matlab (version R2017a) routine was used for this purpose to find the parameter values that produced the best fit.

3. Results and Discussion

3.1. Metallotolerance of Black Fungi

Of the 34 studied BF (Table 1), 29 strains were able to grow on some of the tested concentrations of As(V) and/or Cr(VI) (Table 2). Seventeen strains (50%) displayed measurable growth on agar cultures exposed to As(V) at the maximum tested concentration of 12.5 g-As^{5+} L^{-1}, while 8 strains (23.5%) showed no growth under the minimum tested concentration of 2.5 g-As^{5+} L^{-1} (Table 2). The first group of As(V) tolerant strains primarily belonged to the Chaetothyriales (*Cyphellophora olivacea*, *Exophiala crusticola*, *E. equina*, *E. lecanii-corni*, *E. mesophila*, *E. oligosperma*, *E. phaeomuriformis*, *E. xenobiotica*, and *Rhinocladiella similis*), though some fungi from the Dothidiomycetes were found to be metallotolerant as well (*Aulographina pinorum*, *Aureobasidium melanogenum*, *Coniosporium uncinatum*, and *Neohortaea acidophila*). A few chaetotyrialean species were also found to be low As(V) tolerant (*E. angulospora*, *E. heteromorpha*) but representatives of the order Dothidiomycetes were predominant in this group (*Cladosporium herbarum*, *Knufia epidermis*, *Scolecobasidium globalis*, and *Rhizosphaera kalkhoffii*). As for Cr(VI), only five chaetothyrialean strains (*Rhinocladiella similis*, *Cyphellophora olivacea*, *Exophiala mesophila, E. crusticola* and *E. lecanii-corni*) were able to grow at the highest tested concentration of 2.5 g-Cr^{6+} L^{-1}, while 12 strains showed measurable growth at the lowest tested concentrations of 0.1 g-Cr^{6+} L^{-1} (*Au. pullulans*, *C. uncinatum*, *Cl. herbarum* and *K. epidermis* in the Dothidiomyces, *E. equina* and *E. phaeomuriformis* in the Chaetothyriales).

The tolerance index (TI) of fungi to the tested concentrations of As(V) and Cr(VI), and the estimated 50% inhibitory concentration of these compounds (IC_{50}) after 30 days of incubation are summarized in Table 2. The 30-day incubated period was taken as an intermediate reference between short-term and long-term toxicity. When considering all incubation times, most fungi showed a negative correlation between TI values and exposure time to high HMM concentrations (Supplementary Table S1), which indicates that HMM toxicity tends to manifests after prolonged incubations. A few chaetothyrialean strains stood out from the rest because of their remarkable level of metallotolerance, such as *Exophiala crusticola* CCFEE 6188. This particular strain had the highest tolerance to As(V), with average TI values that after 30 days ranged from 1.00 at 2.5 g-As^{5+} L^{-} to 0.50 at 12.5 g-As^{5+} L^{-1}. The corresponding modelled IC_{50} estimate was 10.0 g-As^{5+} L^{-1}. The number of available strains of *E. crusticola* is relatively small, so that little information is available on the ecophysiology of the species. The type strain was isolated from a biological soil crust sample of the Colorado Plateau and Great Basin desert [31]. More recently, this species has also been reported at the Atacama desert, near Calama in Chile [32], which is among the driest sites in the world and lies close to a large open-pit copper mine. This

environment illustrates the polyextremophilic nature of chaetothyrialean fungi to withstand draught, UV radiation, and exposure to toxic metals.

Table 2. Fungal TI and IC_{50} to As(V) and Cr(VI) after the incubation of agar cultures exposed to the highest and lowest tested concentrations during 30 days. IC_{50} was estimated by fitting the TI data to a logistic model ($r^2 > 0.9$ unless stated otherwise). The strains from Table 1 that are not shown did not display any growth on the tested As(V) and Cr(VI) concentrations.

Species	Strain Nr	TI to As(V)		IC_{50} to As(V)	TI to Cr(VI)		IC_{50} to Cr(VI)
		(2.5 g L^{-1})	(12.5 g L^{-1})	(g As^{5+} L^{-1})	(0.1 g L^{-1})	(2.5 g L^{-1})	(g Cr^{6+} L^{-1})
A. pinorum	CCFEE 6222	0.61	–[a]	3.87 (3.06-4.58)	–	–	–
	CCFEE 6230	0.44	–	1.70 (0.67-2.56)	–	–	–
Au. melanogenum	CCFEE 6213	0.49	–	2.42 (2.15-2.68)	–	–	–
Au. melanogenum	CCFEE 6234	0.66	0.31	4.14 (3.39-4.83)	–	–	–
Au. pullulans	CCFEE 6244	0.28	–	0.96 (0.69-1.21)	0.44	–	0.07 (0.05-0.09)
C. olivacea	CCFEE 6619	0.86	0.48	12.94 (11.53-15.09)	0.47	0.19	0.08 (0.05-0.12)
C. uncinatum	CCFEE 5820	0.36	0.22	0.75 (0.28-1.26)	0.37	–	0.04 (0.02-0.06)
Cl. herbarum	CCFEE 6193	0.56	–	2.61 (2.27-2.90)	–	–	–
	CCFEE 6192	–	–	–	0.24	–	0.00 (0.0002-0.008)
E. crusticola	CCFEE 6188	1.00	0.50	10.04 (8.94-11.61)[b]	0.73	0.32	0.56 (0.36-0.84)[b]
E. equina	CCFEE 5883	0.15	–	0.03 (0.0003-0.15)	0.43	–	0.04[c]
E. lecanii-corni	CCFEE 5688	0.32	–	0.20 (0.001-0.71)	0.65	0.46	1.01 (0.82-1.30)[c]
E. mesophila	CCFEE 5690	0.42	–	1.50 (0.96-1.98)	–	–	–
	IRTA M2-F10	0.81	0.34	6.03 (5.19-6.94)[b]	0.44	0.30	0.05 (0.02-0.09)
E. oligosperma	CBS 725.88	0.49	–	2.49 (1.62-3.20)	–	–	–
	CCFEE 6139	0.19	–	0.16 (0.02-0.44)	–	–	–
E. phaeomuriformis	CCFEE 6242	0.31	–	0.70 (0.32-1.09)	0.32	–	0.01 (0.003-0.03)
E. xenobiotica	CCFEE 5784	0.32	–	0.67 (0.15-1.28)	–	–	–
	CCFEE 5985	0.50	0.24	2.92 (1.59-3.96)[b]	–	–	–
	CCFEE 6142	0.33	–	0.39 (0.04-0.93)	–	–	–
	CCFEE 6143	0.38	–	0.67 (0.16-1.25)	–	–	–
K. epidermis	CCFEE 5813	0.50	0.24	2.92 (1.59-3.96)[b]	–	–	–
	CCFEE 6138	0.14	–	0.01 (~-0.15)	–	–	–
	CCFEE 6198	0.42	–	1.93 (1.54-2.27)	–	–	–
	CCFEE 6366	0.23	–	0.25 (0.06-0.53)	–	–	–
N. acidophila	CBS 113389	0.41	0.52	~	–	–	–
Scolecobasidium	CCFEE 6363	0.26	0.15	~	–	–	–
R. similis	CCFEE 6361	0.65	0.56	48.26 (16.14-~)[b]	0.60	0.40	0.25 (0.18-0.33)

[a] –: No significant growth; [b] $0.80 < r^2 < 0.90$; [c] $r^2 \leq 0.80$

Conversely, the tolerance of *E. crusticola* CCFEE 6188 to Cr(VI) was lower when compared to other fungi, as it had TI of 0.73 at 0.1 g-Cr^{6+} L^{-1} after 30 days of exposure but it grew scarcely at the higher tested concentrations (its IC_{50} was 0.56 g-Cr^{6+} L^{-1}). There were three other strains that displayed a remarkable tolerance to both As(V) and Cr(VI), showing limited inhibition with respect to the control (Figure 1): *R. similis* CCFEE 6361, *C. olivacea* CCFEE 6619, *E. mesophila* IRTA M2-F10. Their TI values were above 0.4 at the tested concentrations of As(V) and Cr(VI), and the IC_{50} ranged 6 – 48 g-As^{5+} L^{-1}, though the latest estimate must be taken with caution as it is well above the highest tested concentration, and 0.05 – 0.25 g-Cr^{6+} L^{-1} after 30 days of exposure (Table 2). These strains were generally characterized by TI values at the highest As(V) and Cr(VI) tested concentrations that tended to increase with longer incubation times, up to 60 days (Supplementary Table S1).

This phenomenon indicates a progressive longer-term adaptation to HMM of these particular strains, in contrast to most of the tested BF collection.

Literature data on the fungal toxicity of HMM is scarce, particularly with melanized fungi despite their polyextremophilic nature and association to toxic chemicals [21]. There are some reports on the fungal toxicity of arsenic oxyanions, but those have often been performed at a rather low milligram per litter range (between 10 to 500 mg L^{-1})[33–37]. A few surveys were carried out at the gram per litter range though. A screening of fungi isolated from an arsenic-polluted soil for As(V) tolerance resulted in the selection of five strains, dubbed as "hyper-tolerant", that had TI values at 10 g-As^{5+} L^{-1} that ranged 0.19 – 0.31 for *Aspergillus* sp., *Neocosmospora* sp., *Rhizopus* sp., and *Penicillium* sp., up to 0.96 for an unidentified sterile fungus [15]. Singh et al. [38] reported nine fungal strains that were tolerant to As(V) up to 10 g-As^{5+} L^{-1}, which belonged to the genera *Trichoderma*, *Aspergillus*, *Rhizopus*, *Microdochium*, *Chaetomium*, *Myrothecium*, *Stachybotrys*, *Rhizomucor*, and *Fusarium*. However, no quantitative tolerance parameters were derived from this study.

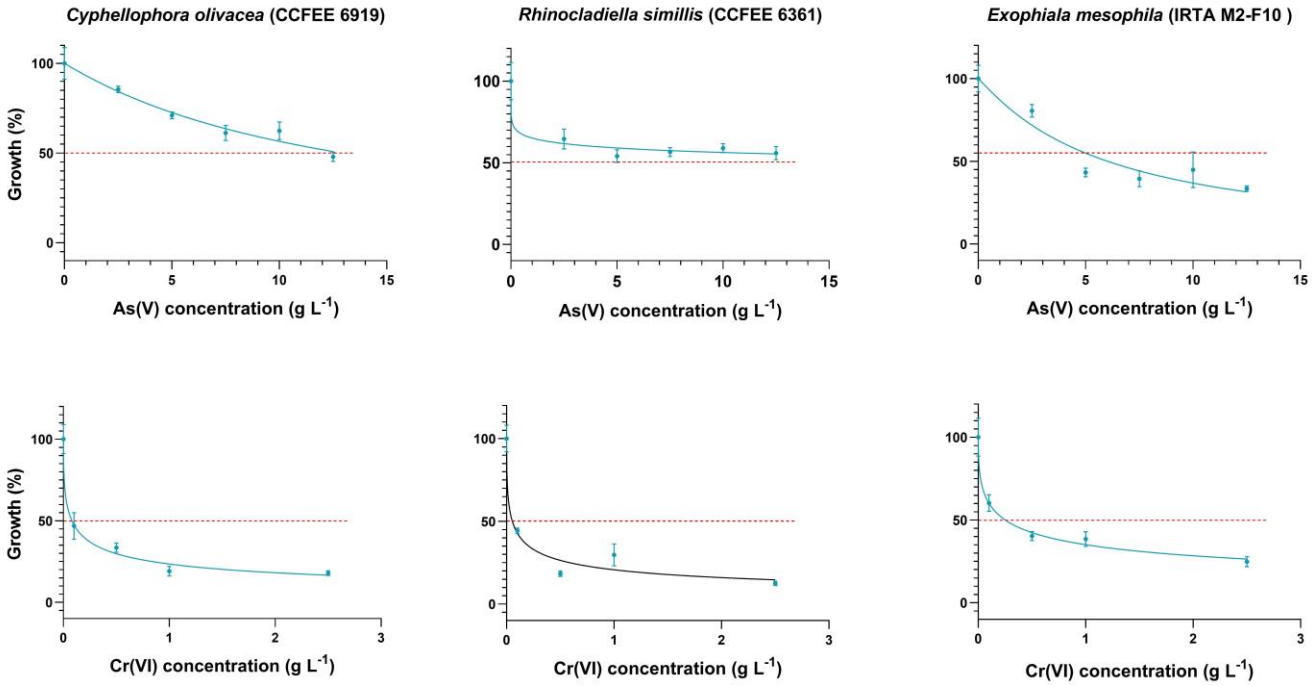

Figure 1. Effect of the concentration of As(V) (top) and Cr(VI) (bottom) on the average and standard deviation (solid bars, n=6) of the tolerance index (TI) of selected metallotolerant fungal strains, measured from the radial growth in agar cultures after 30 days of incubation. Solid lines correspond to a fitted logistic model for the determination of the IC_{50} value.

Chromium has a complex valence layer that produces different oxidation states that interact with specific nutrients, accentuating the toxicity of this metal [3]. Several previous reports have corroborated the severity of Cr(VI) toxicity to fungi, when compared to As(V). In general, Cr(VI) is more toxic than As(V) to fungi because of its higher reactivity and capacity to generate oxygen reactive species (ROS), which can disrupt several metabolic functions [3,8]. For example, out of 14 isolates from tannery effluents contaminated with Cr(VI), only one strain of *Trichoderma viride* (fam. Hypocreaceae), was able to show some growth at 1 g-Cr^{6+} L^{-1} when cultured under laboratory conditions [39]. Other species in this genus have been evaluated for Cr(VI) tolerance, such a *T. harzianum* strain isolated from a HMM polluted mine [40], which displayed a TI at 1 g-Cr^{6+} L^{-1} as low as 0.024. Other *Aspergillus* spp., were also tested in that study (*A. sclerotiorum*, *A. aculeatus*,

and *A. niger*) and yielded higher TI values, between 0.12 and 0.67, depending on the strain and the tested Cr(VI) concentration. Another strain of *T. viride* isolated from tannery wastewaters displayed TI values of 1.15, 0.13, and 0.08, as determined from the biomass production from liquid cultures, after 21 days of incubation with 50, 500, and 1000 mg-Cr^{6+} L^{-1} [39]. A second Cr(VI)-tolerant strain identified as *Penicillium citrinum* showed a similar profile. Interestingly, those fungi seemed to be biostimulated at low concentrations of Cr(VI), both in terms of biomass production and secreted laccase enzymes.

None of the previously mentioned taxa are BF and, in fact, there are few reports quantifying the metallotolerance within this particular group of fungi. The chaetothyrialean *Exophiala pisciphila* has been isolated repeatedly from the roots of plants growing on soils that are polluted with heavy metals, and *in vitro* analyses have shown that this fungus tolerates concentrations of Pb(II), Cd(II) and Zn(II) at an IC_{50} of 0.8, 0.3 and 1.5 g L^{-1}, respectively [41]. Concerning the tolerance to As(V), one study with liquid cultures of different strains of *E. sideris* isolated from HMM-polluted environments reported IC_{50} values between 2.0 and 3.7 g-As^{5+} L^{-1}, depending on the isolate [42]. These latter results are in the As(V) IC_{50} range found in our study for the strains that belong to the *Exophiala* genus. (Table 2). As for specific accounts on the tolerance of BF to Cr(VI), a minimum inhibitory Cr(VI) concentration of 300 mg-Cr^{6+} L^{-1} was determined for the growth a strain identified as *Cladosporium perangustum* (fam. Cladosporiaceae) [43].

Some of the BF included in this study encompassed multiple strains from the same species (i.e. two strains of *Au. pullulans*, *C. uncinatum*, *A. pinorum*, *E. heteromorpha*, *E. mesophila*, and *E. oligosperma*, and four of *E. xenobiotica*, and *K. epidermis*). Comparing growth inhibition patterns among such strains revealed a wide intraspecific variability on their tolerance to HMM (Table 2). Examples on the most disparate cases include *Au. pullulans* and *C. uncinatum*, being one of the two tested strains (CCFEE 6244 and CCFEE 5820) of each species able to grow with the presence of As(V) and Cr(VI) while the other two (CCFEE 5876 and CCFEE 6149) did not show any growth at all. The "hyper-tolerant" *E. mesophila* strain IRTA M2-F10 also differed significantly from the conspecific CCFEE 5690.

This observation deserves further investigation to verify whether the recorded variability in metal tolerance is intrinsic to the species considered or if it is due to the lack of knowledge in the identification of related species. On the one hand, a detailed molecular analysis could be useful in better determining the position occupied by the two strains within the large group of *Au. pullulans*. On the other hand, it could be valuable in defining the close relatives of C. uncinatum, which are currently unknown.

On the contrary, metallotolerance appears to be relatively conserved in the four tested strains of *E. xenobiotica*, which were all able to grow at 12.5 g-As^{5+} L^{-1} and displayed IC_{50} values of 0.7 – 3 g-As^{5+} L^{-1}, but none of them grew on the presence of Cr(VI). The two available strains of *E. oligosperma* displayed a somewhat similar growth pattern on the presence of As(V), with IC_{50} values of 0.2 – 2.5 g-As^{5+} L^{-1}, but they neither grew on any of the tested concentrations of Cr(VI). These strains are very similar to each other when comparing their ITS sequences.

At the intragenus level, significant variability in HMM tolerance is also manifested in *Exophiala* which, along the observed diverse degrees of metallotolerance, also includes species that like *E. heteromorpha* were consistently unable to grow at any tested concentration of As(V) and Cr(VI). The observed intra- and interspecific differences in HMM tolerance might be attributed to diverse degrees of adaptation to HMM-polluted environments, due to specific genetic changes, epigenetic regulation, and phenotypic adaptations to stressful conditions [29]. Melanization is often cited as a feature that confers tolerance to HMM because of its capacity to absorb toxic metals [27,44]. However, all tested strains were conspicuously melanized and were isolated from similar environments exposed to toxic chemicals. Hence, besides melanin production and adaptation to toxic environments, other factors must contribute to the tolerance of HMM

in BF. Earlier studies have proposed an array of multiple mechanisms that enable fungi to cope with HMM [3,45,46], such as reducing the basal energy for metabolism, activating protein protection and DNA repair against oxidative stress, enhancing iron and sulfur acquisition, transforming metal species to less toxic or volatile metabolites, detoxifying free radical, and through homeostasis.

Exposure to As(V) and Cr(VI) caused macroscopic morphological changes on fungal growth that where visible on agar colonies, as shown in Figure 2 for the metallotolerant *R. similis* CCFEE 6361, *C. olivacea* CCFEE 6619 and *E. mesophila* IRTA M2-F10. Fungal biomass tended to display a stronger dark pigmentation upon metal exposure, that might be attributable to an increased level of melanin biosynthesis as a defensive mechanism. A few strains like those of *E. mesophila* also formed colonies that were irregular in shape and displayed coarser edges under stressful conditions, a phenomenon known as meristematic growth. This morphological plasticity has been also observed with *E. oligosperma* CCFEE 6327 when grown at 35°C under laboratory conditions, a temperature close to its upper temperature growth limit [47]. A similar morphology is also manifested in case of opportunistic mammal infections, defined then as muriform cells [48]. The isodiametric growth and the aggregated, compact shape of fungal microcolonies ensures the optimal surface-volume ratio, minimize the direct exposure to external stressors [49]. This type of growth is also expressed as an adaptation in the closely related lithobiontic black fungi (known as rock-inhabiting fungi, RIF) [50].

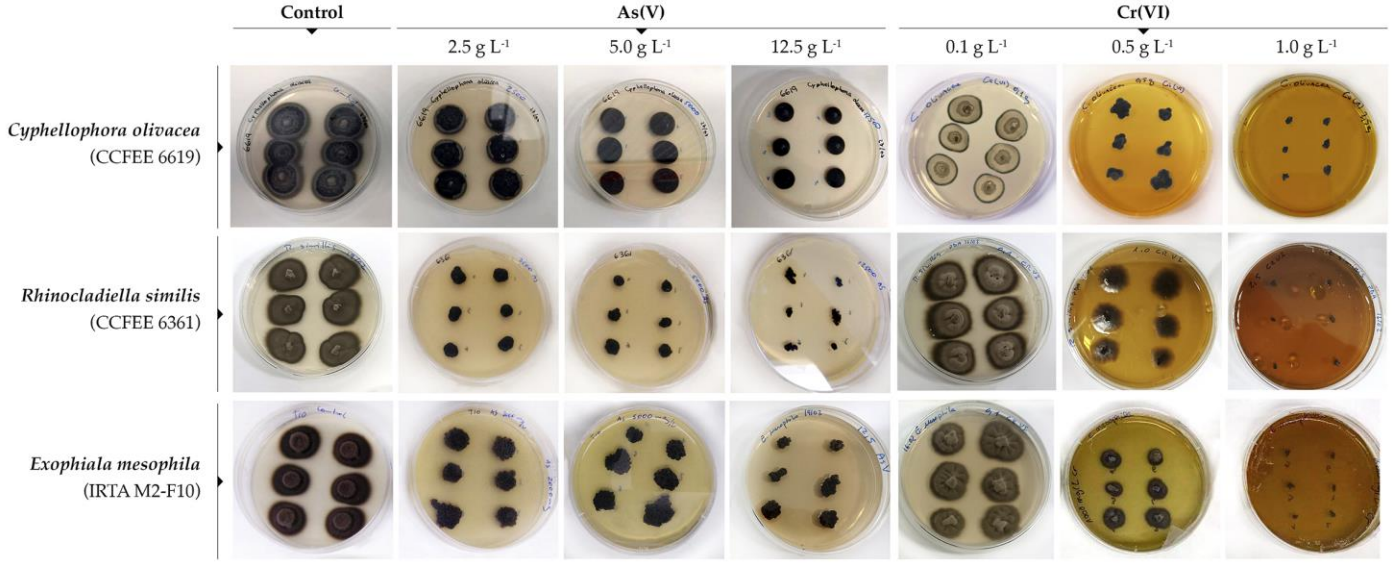

Figure 2. Macromorphological effects of the exposure to increasing concentrations of As(V) and Cr(VI) on fungal agar cultures of the metallotolerant black fungi.

3.2. Biosorption Assays

Two of the strains screened previously for metallotolerance, *R. similis* CCFEE 6361 and *E. mesophila* IRTA M2-F10, were selected for subsequent biosorption experiments because of their intrinsic tolerance to both As(V) and Cr(VI), and for their easy cultivation in liquid media for producing biomass. After 30 days of incubation of pre-grown fungal liquid cultures with As(V) and Cr(VI) (approx. 50 mg-DM L^{-1}; initial HMM concentration of 20 mg L^{-1}), the HMM content remaining in the supernatant was measured (Table 3). From these results it was evident that BF biomass had a comparatively low absorption capacity for As(V) when compared to Cr(VI), as removal efficiencies for the first did not exceed 10% while for the second were higher than 80%, under similar test conditions.

The specific As(V) removal capacity of living cultures of *E. mesophila* than *R. similis* incubated for 30 days at pH 6.5 was 1.07 and 1.34 mg-As^{5+} g-DM^{-1}. The difference between the two fungi was not statistically significant (p>0.05). However, the biosorption of As(V)

by heat-inactivated biomass of *E. mesophila* was significantly lower than that by living cultures of this same fungus. Despite the apparently modest As(V) biosorption results with the tested BF, previous similar studies with this metalloid have yielded even lower numbers. Different fungal species in the genera *Neocosmospora*, *Sordaria*, *Rhizopus*, *Penicillium* displayed biosorption capacities that ranged 0.009–0.016 mg-As^{5+} g-DM^{-1} [15]. Other authors claimed that cultures of fungi belonging to *Aspergillus*, *Fusarium*, *Rhizomucor* and *Emericella* were able to absorb from 0.023 to 0.259 mg-As^{5+} g-DM^{-1} depending on the strain [38]. Those experiments were performed within the pH range of 4–7 used in our study and all used strains correspond to fungi that are not conspicuously melanized. Hence, fungal melanization might indeed improve As(V) biosorption by cultures of BF.

Table 3. Fungal HMM biosorption capacity and removal efficiency. Incubations lasted 30 days and results are expressed as the average and standard deviation of three independent experiments. One-way ANOVA comparisons were performed on the specific removal capacity for every metal and non-significant differences have been indexed (n=3; p<0.05).

Fungus (strain)	Type of biomass	pH	Parameter (units)	As(V)	Cr(VI)
R. similis	Living culture	6.5	Biomass (mg-DM)	48.07 ± 6.05	43.33 ± 2.95
			Final concentration in solution (mg L^{-1})	18.30 ± 0.31	3.48 ± 1.33
			Specific removal capacity (mg g-DM^{-1})	1.07 ± 0.32 ^{AC}	11.50 ± 1.56 ^{A}
			Removal efficiency (%)	8.5	82.6
		4.0	Biomass (mg-DM)	45.28 ± 5.08	49.67±0.01
			Final concentration in solution (mg L^{-1})	19.53 ± 0.31	<0.01
			Specific removal capacity (mg g-DM^{-1})	0.33 ± 0.24 ^{B}	≥12.79
			Removal efficiency (%)	2.3	100
E. mesophila	Living culture	6.5	Biomass (mg-DM)	44.33 ± 1.91	46.90 ± 1.23
			Final concentration in solution (mg L^{-1})	18.04 ± 0.57	1.16 ± 0.25
			Specific removal capacity (mg g-DM^{-1})	1.34 ± 0.42 ^{A}	12.57 ± 3.00 ^{A}
			Removal efficiency (%)	9.8	94.2
		4.0	Biomass (mg-DM)	46.57 ± 6.12	53.57±1.55
			Final concentration in solution (mg L^{-1})	19.67 ± 0.21	<0.01
			Specific removal capacity (mg g-DM^{-1})	0.21 ± 0.12 ^{B}	11.20
			Removal efficiency (%)	1.67	100
	Dead cells	6.5	Biomass (mg-DM) (mg L^{-1})	42.03 ± 0.63	46.40 ± 0.46
			Final concentration in solution	19.41 ± 0.25	5.16 ± 0.66
			Specific removal capacity (mg g-DM^{-1})	0.41 ± 0.17^{BC}	9.59 ± 0.47 ^{A}
			Removal efficiency (%)	2.92	74.2

Fungal biosorption patterns changed completely when Cr(VI) was used. Equivalent incubations with this metal showed that the specific removal capacity after 30 days of incubation was slightly higher for *E. mesophila* (12.57 mg-Cr^{6+} g-DM^{-1}) than by for *R. similis* (11.50 g-Cr^{6+} mg-DM^{-1}). As with As(V), heat inactivation of cultures of *E. mesophila* caused a reduction of the biosorption capacity (9.59 g-Cr^{6+} mg-DM^{-1}). However, differences of the specific Cr(VI) biosorption capacity in all tested fungi and incubation conditions were statistically not significant (p>0.05). Previous reports on the specific Cr(VI) biosorption capacity of fungi correspond primarily to modified biomass, and relatively few records are available with living fungal cultures. Some fungi isolated from samples of sludge and industrial effluents contaminated with heavy metals (*Trichoderma viride*, *T. longibrachiatum*,

Aspergillus niger, and *Phanerochaete chrysosporium*) displayed biosorption capacities that ranged from 0.03 to 0.55 mg Cr^{6+} g-DM^{-1}, when incubated (150 rpm at 28°C) with potato dextrose broth containing 50 mg-Cr^{6+} L^{-1} for 4 days[51]. Lotlikar et al. [52] isolated three strains from the Arabian Sea sediments identified as *Purpureocillium lilacinum*, *Aspergillus sydowii* and *A. terreus*, that were able to grow with 300 mg-Cr^{6+} L^{-1} (pH 5, shaken conditions, and room temperature) and biosorbed 8, 10 and 13 mg Cr^{6+} g-DM^{-1} respectively, after 20 days of incubation. Reports on the Cr(VI) biosorption by BF are very limited; liquid cultures of *Aureobasidium pullulans* growing on the acid hydrolysate of peat containing HMM (200 rpm; 26 °C; pH 6.0) were able to absorb 0.77 mg Cr^{6+} g-DM^{-1} after 160 h of incubation [53].

The sorption of As(V) and Cr(VI) onto organic materials has been described as a pH-dependent phenomenon[54,55]. At acidic conditions, As(V) exists primarily in the form of dihydrogen arsenate ($H_2AsO_4^-$) while Cr(VI) is present as chromate (CrO_4^{2-}). As pH increases $H_2AsO_4^-$ transforms into hydrogen arsenate ($HAsO_4^{2-}$) or arsenate (AsO_4^{3-}), and CrO_4^{2-} into dichromate ($Cr_2O_7^{2-}$), resulting in an increase of the net negative chage. The pH also influences the surface charge of the sorbent, so that the point of zero charge (pzc)—the pH at which the net charge of total absorbent's surface is equal to zero—for fungal biomass is in the range of pH 4.0 – 4.5 [56,57]. Above these pH values the surface becomes negatively charged, exacerbating its electrostatic repulsion towards As(V) and Cr(VI) anions. Interestingly, fungal incubations at pH 4.0 significantly (p<0.05) enhanced the biosorption of Cr(VI), but not that of As(V), compared to analogous experiments at pH 6.5 (Table 3).

The HMM biosorption capacity of heat-inactivated biomass of *E. mesophila* was lower than with equivalent viable cultures (Table 3). Several investigations on the passive adsorption process on the cell surface have been performed using dead fungal biomass [58–60]. It has been claimed that the biosorption of dried biomass increases the contact surface between HMM and the metal binding sites of the fungal cell wall [61]. However, heat-inactivated biomass may still maintain the structures of the fungal cell relatively intact. A comparison between living cultures and dried pulverized biomass of a group of fungi (*Aspergillus foetidus*, *A. niger*, *A. terricola*, *Acremonium strictum*, *Paecilomyces variotii*, *Phanerochaete chrysosporium*, *Aureobasidium pullulans*, and *Cladosporium resinae*) claimed that while Cr(VI) biosorption capacity in the first ranged 0.1–3.0 mg Cr^{6+} g^{-1}-DM, in the second increased up to 11.2 mg Cr^{6+} g^{-1}-DM (pH 3; 100 rpm; 28.1°C) [62]. Literature accounts on the use of inactivated fungal biomass as HMM sorbents often included the addition of specific coadjuvants that mitigate the electrostatic repulsion between sorbent and sorbate. A *Penicillium chrysogenum* was modified with three different surfactants (amines) to increase the removal capacities of modified biomass from 37.85 to 56.07 mg As^{5+} g^{-1} at pH 3 [63].

3.3. Biosorption Isotherms and Kinetics

The differential equation 7 describing the first- and second-order kinetics, integrating the Langmuir and Freundlich isotherms, were fitted to experimental data on the time-course evolution of metal concentration in the supernatant. Changes with As(V) were too subtle to fit any sorption model with enough confidence, but the experimental data on the time-course depletion of Cr(VI) showed that the best fits were obtained with a second-order sorption kinetics and the Langmuir sorption isotherm (Figure 3). Previous similar studies that compared different models to describe the fungal biosorption of metals showed that the Langmuir isotherm and a second-order sorption kinetics displayed the best coefficients of determination [64–66]. The Langmuir isotherm is a theoretical approximation that considers a finite monolayer of available adsorption sites onto a homogeneous surface. This assumption implies that the sorbent has a limited surface-dependent maximum theoretical sorption capacity (q_{max}), and that there is neither interaction nor transmigration of metal ions after monolayer adsorption.

The fitted parameters of Langmuir isotherms and second order kinetics for the biosorption of Cr(VI) with the tested BF are summarized and compared with bibliographic data in Table 4. The 'theoretical' maximum sorption capacity q_{max} of *R. similis* and *E. mesophila* (39.81 and 95.26 mg-Cr^{+6} g-DM^{-1}) are above those seen previously with several other non-melanized fungi in analogous experiments. Most of those assays were performed with inactivated/modified fungal biomass and at a low pH, conditions that might favor biosorption but under which process scaling-up into practical applications is challenging. In what concerns the half saturation concentration (the metal concentration in equilibrium at which the biosorbed metal equals half of q_{max}), which is the reverse of the affinity constant K_L, both tested BF displayed rather similar values of 8.90 and 5.09 mg Cr^{6+} L^{-1}, respectively for *R. similis* and *E. mesophila*. The affinity to Cr(VI) of biomass from hyaline species tested previously is quite low in general when compared to BF (Table 4).

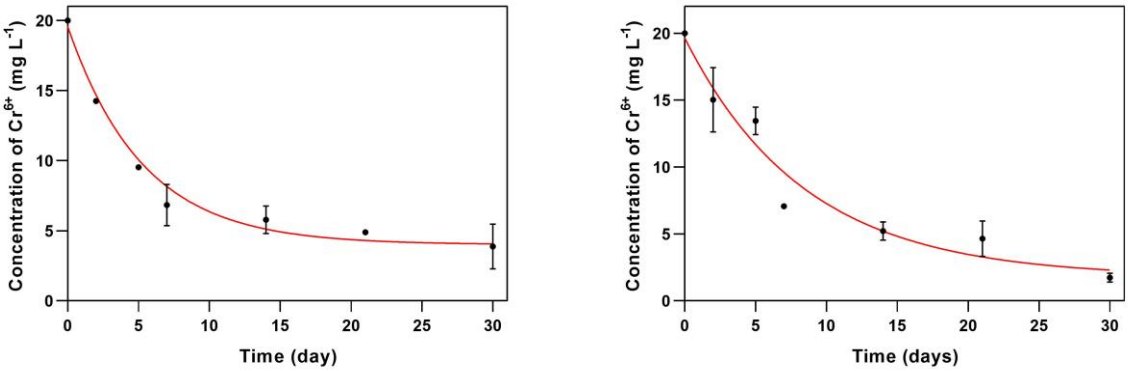

Figure 3. Fits of experimental data of Cr(VI) bioadsorption on living cultures (pH 6.5) of *Rhinocladiella similis* (left) and *Exophiala mesophila* (right) to the second-order kinetics and the Langmuir isotherm model (differential equation 7). Experimental data correspond to the average and standard deviation of three replicates.

The second order kinetic constant k_2, which corresponds to the specific biosorption rate, is one order of magnitude lower for *E. mesophila* when compared to *R. similis*, $1.39 \cdot 10^{-7}$ versus $1.32 \cdot 10^{-6}$ g-DM (mg-Cr^{6+} min)$^{-1}$. The higher q_{max} and lower k_2 of *E. mesophila* when compared to *R. similis* could be related to the higher Cr(VI) tolerance of the former over the latter (Table 2). Several previous accounts on the second order kinetics of Cr(VI) biosorption by non-melanogenic fungi have reported k_2 values above 10^{-2} g-DM (mg-Cr^{6+} min)$^{-1}$ (Table 4). Interestingly, previous studies with melanized fungal structures like lyophilized cells of the BF *Cladosporium cladosporioides* and spores of *Aspergillus niger*, also yielded comparatively low biosorption rates and high substrate affinity.

In order to gain a deeper insight on the role of fungal melanin when exposed to Cr(VI), biosorption experiments were repeated with melanin extracts from *E. mesophila* (Figure 4). The obtained fitted parameter values are between 1 and 2 orders of magnitude higher than those measured with living cultures of the same fungus (q_{max} = 544.84 mg-Cr^{6+} g-DM^{-1}; K_L = 0.0075 L mg^{-1}; and $k_2 = 1.67 \cdot 10^{-6}$ g-DM (mg-Cr^{6+} min)$^{-1}$). Considering that the mass of the extracted melanin corresponded to the 12.5% of the fungal biomass, on a dry matter basis (125 mg g-DM^{-1}), the potential contribution of melanin to the biosorption capacity of whole cells could be as high as the 71.5%. These results confirm that fungal melanin plays a vital role in the biosorption of HMM. Furthermore, the q_{max} of melanin is well above that of several tested Cr(VI) organic absorbants, from raw and modified lignocellulosic materials [67], to advanced carbon nanomaterials [68].

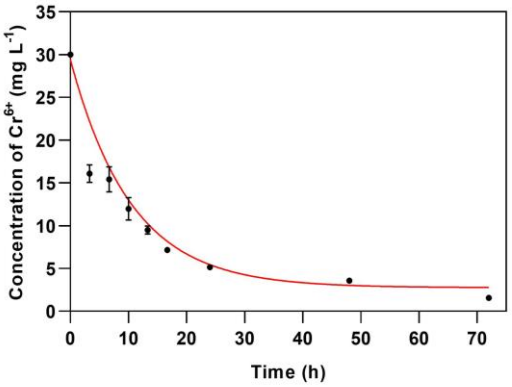

Figure 4. Fit of experimental data of Cr(VI) bioadsorption on melanin extracts of *Exophiala mesophila* to the second-order kinetics and the Langmuir isotherm model (differential equation 7). Experimental data correspond to the average and standard deviation of three replicates.

Table 4. Fitted parameters for modelling the biosorption of Cr(VI) using the second-order kinetic model and/or the Langmuir isotherm by different fungal species.

Fungus [a]	pH	C (mg L^{-1})	Fitted eq.	Model parameters				Source
				k_2 (g (mg min)$^{-1}$)	q_{max} (mg g^{-1})	K_L (L mg^{-1})	r^2	
Rhinocladiella similis (CS)	6.5	25	Eq. 7	$1.32 \cdot 10^{-6}$	39.81	0.1124	0.977	This study
Exophiala mesophila (CS)	6.5	25	Eq. 7	$1.39 \cdot 10^{-7}$	95.26	0.1964	0.924	This study
Exophiala mesophila (ME)	6.5	25	Eq. 7	$1.67 \cdot 10^{-6}$	544.84	0.0075	0.969	This study
Cladosporium cladosporioides (LB)	2.0	25	Eq. 4	$7.50 \cdot 10^{-5}$	28.90	–	0.991	[69]
Aspergillus niger (SS)	2.0	100	Eq. 4	$5.76 \cdot 10^{-4}$	56.15	–	0.994	[70]
			Eq. 5	–	47.33	0.5416	0.999	
Aspergillus niger (DB)	2.0	27	Eq. 4	3.38	6.45	–	0.998	[66]
			Eq. 5	–	71.9	0.031	0.999	
Lentinus sajor-caju (CS)	2.0	30	Eq. 4	$3.39 \cdot 10^{2}$	20.80	–	0.994	[71]
			Eq. 5	–	23.32	0.0133	0.993	
Ustilago maydis (DB)	5.5 – 6.5	25	Eq. 4	$1.37 \cdot 10^{-2}$	1.95	–	ns [b]	[72]
			Eq. 5	–	17.16	0.0090	0.965	
Mucor hiemalis (DB)	2.0	100	Eq. 4	$5.5 \cdot 10^{-1}$	30.5	–	0.993	[73]
			Eq. 5	–	47.4	0.0307	0.999	
Ganoderma applanatum (DB)	2.0	25	Eq. 4	$7.4 \cdot 10^{-1}$	16.13	–	0.999	[74]
			Eq. 5	–	200	0.002	0.999	
Rhizopus sp. (DB)	2.0	25	Eq. 4	$1.13 \cdot 10^{-2}$	5.4509	–	0.986	[64]
			Eq. 5	–	8.0589	0.7730	0.841	

[a] Fungal species and pre-treatment of the biomass: living cell suspension (CS); melanin extracts (ME); lyophilized biomass (LB); spore suspension (SS); dead biomass (DB).
[b] Not determined/not showed.

The results from this study are consistent with the hypothesis that fungal melanin plays an active role in the biosorption of toxic HMM, such as As(V) and Cr(VI). Melanin is an amorphous polymeric structure that concentrates in the fungal cell wall, and offers a great number of heterogeneous binding sites to the sorption of metal ions [27]. Melanin is also a conductive material that mediates electron transport between fungal biomass and the solute, which might contribute to chemisorption by sharing or exchanging electrons

between sorbent and sorbate [75]. A previous study on the binding of copper by melanin extracts, intact cells and albino mutants of the BF *Cladosporium resinae* and *Aureobasidium pullulans*, demonstrated that the metal uptake capacity was higher in melanin extracts, followed by intact cells and, finally, in albino cells [76].

However, other studies have disputed the role of melanin as a metal biosorbent. An early study found no significant differences in the binding of copper by cultures of the melanized plant pathogen *Gaeumannomyces graminis*, either grown at low concentrations of this metal or additionally supplemented with tricyclazole, an inhibitor of DHN-melanin [77]. More recently, it has been proposed that melanin may have a role in binding metals and protecting fungi from toxic metals, but the main mechanisms might not necessarily be related to sorption processes [78,79]. Potisek [79], used different strains of dark septate endophytes of *Cadophora spp.*, with different melanin content, to investigate their tolerance to cadmium. The melanin content was positively correlated to a higher cadmium tolerance but the accumulation of this metal was not. More contentious studies on *Exophiala pisciphila* even claimed that inhibition of melanization in this fungus did not cause any remarkable effect on the tolerance of metal ions [42].

Indeed, the high inter- and intraspecific variability in metallotolerance observed among the studied black fungi (Table 2) suggest that there must be other physiologic mechanisms to cope with the toxic effects of toxic metals and metalloids, rather than lying solely on melanization. In this regard, the comparatively high biosorption capacity of BF to HMM, in combination with low sorption rates could be the result of an evolved strategy to, firstly, minimize the penetration of toxic metals into the cell and, secondly, sequester those that would eventually leak into the cytoplasm.

4. Conclusions

Several published studies have revealed that fungal biomass has a good performance as a biosorbent of heavy metals and metalloids, in comparison to commercial materials such as ion-exchange resins, activated carbon, and metal oxides. Fungal biosorption depends on parameters such as the used fungi and metal species, but also the pH, temperature, biomass pre-treatments, and the presence of various ligands in solution. The fungal cell-wall fraction seems to play an important role in the sorption of heavy metals, though the biosorption mechanisms are understood only to a limited extent. The ability of fungi to tolerate and biosorb specific heavy metals and metalloids has previously been evaluated and reviewed, as is the case for As(V) and Cr(VI), but literature on the metallotolerance of extremophilic black fungi is still comparatively scarce.

To our knowledge, the present work provides the first in-depth survey of metallotolerance of a strain collection of BF isolated previously from polluted sites. The obtained results indicate that there is a broad inter- and intraspecific variability in metallotolerance, using As(V) and Cr(VI) as model HMM. Living cultures of two hyper-metallotolerant strains of *Rhinocladiella similis* and *Exophiala mesophila* displayed a significant biosorption capacity but, conversely, sorption rates were comparatively slow in relation to other non-black fungi. This phenomenon could be explained by the interplay of two protective processes: an outer cell-wall barrier and the inner cell-wall biosorption of leaked metals and metalloids by melanin. These findings might contribute to the development future strategies for the bioremediation of HMM pollution and need to be further investigated. Black fungi could also be valuable bioindicators of HMM in natural and anthropogenic environments.

Author Contributions: Individual contributions to this study are indicated with the authors' initials: Conceptualization, C.M.-A. and F.P.-B.; methodology, C.M.-A. and A.P.; software, C.M.-A. and J.I.; validation, J.I. and F.P.-B..; formal analysis, C.M.-A and F.P.-B.; investigation, C.M.-A. and F.P.-B.; resources, D.I and M.V.; writing—original draft preparation, C.M.-A.; writing—review and editing, F.P.-B., J.I. and D.I.; supervision, F.P.-B. All authors have read and agreed to the published version of the manuscript.

Funding: This research has been partly funded by project AGAUR (Generalitat de Catalunya) through the Consolidated Research Group SOSBIO (ref. 2021 SGR 01568). Cristy Medina-Armijo was the recipient of the grant ANID Chile.

Institutional Review Board Statement: Not applicable.

Informed Consent Statement: Not applicable.
Data Availability Statement: All data of this research are reported in the main text and Supplementary material (pending link).

Acknowledgments: We acknowledge Alexia Douillard, from the University of Angers, and Marta Manyà, from the Autonomous University of Barcelona for laboratory assistance during her undergraduate internship. This research was supported by the CERCA Programme/Generalitat de Catalunya.

Conflicts of Interest: The authors declare no conflict of interest.

References

1. Zhang, Q.; Wang, C. Natural and human factors affect the distribution of soil heavy metal pollution: A Review. Water. *Air. Soil Pollut*. **2020**, *231*, 1–13, DOI: 10.1007/s11270-020-04728-2.
2. Siddiquee, S.; Saallah, S.; Rovina, K.; Al Azad, S.; Naher, L.; Suryani, S.; Chaikaew, P. Heavy metal contaminants removal from wastewater using the potential filamentous fungi biomass: A review. Artic. *J. Microb. Biochem. Technol*. **2015**, *7*, 384–393; DOI:10.4172/1948-5948.1000243.
3. Viti, C.; Marchi, E.; Decorosi, F.; Giovannetti, L. Molecular mechanisms of Cr (VI) resistance in bacteria and fungi. *FEMS Microbiology Reviews*. **2014**, *38*, 633–659; DOI:10.1111/1574-6976.12051.
4. Podgorski, J.; Berg, M. Global threat of arsenic in groundwater. *Science*. **2020**, *368*, 845–850; DOI:10.1126/science.aba1510.
5. Arsenic in drinking-water. (**2019**). Background document for development of WHO guidelines for drinking-water quality. Geneva, World Health Organization. (WHO/SDE/ WSH/03.04/75)
6. Sappa, G.; Ergul, S.; Ferranti, F. Geochemical modeling and multivariate statistical evaluation of trace elements in arsenic contaminated groundwater systems of Viterbo area, (Central Italy). *SpringerPlus*. **2014**, *3*, 237; DOI:10.1186/2193-1801-3-237
7. Tumolo, M.; Ancona, V.; De Paola, D.; Losacco, D.; Campanale, C.; Massarelli, C.; Uricchio, V.F. Chromium pollution in European water, sources, health risk, and remediation strategies: An overview. *Int. J. Environ. Res. Public Health*. **2020**, *17*, 1–25; DOI:10.3390/ijerph17155438.
8. Sun, Q.; Li, Y.; Shi, L.; Hussain, R.; Mehmood, K.; Tang, Z.; Zhang, H. Heavy metals induced mitochondrial dysfunction in animals: Molecular mechanism of toxicity. *Toxicology*. **2022**, *469*, 153136; DOI:10.1016/j.tox.2022.153136.
9. Fu, F.; Wang, Q. Removal of heavy metal ions from wastewaters: A review. *J. Environ. Manage*. **2011**, *92*, 407–418; DOI:10.1016/j.jenvman.2010.11.011.
10. Costa, F.; Tavares, T. Bioremoval of Ni and Cd in the presence of diethylketone by fungi and by bacteria – A comparative study. *Int. Biodeterior. Biodegradation*. **2017**, *120*, 115–123; DOI:10.1016/j.jbiod.2017.02.018.
11. Kang, C.H.; Kwon, Y.J.; So, J.S. Bioremediation of heavy metals by using bacterial mixtures. *Ecol. Eng*. **2016**, *89*, 64–69; DOI:10.1016/j.ecoleng.2016.01.023.
12. Zeraatkar, A.K.; Ahmadzadeh, H.; Talebi, A.F.; Moheimani, N.R.; McHenry, M.P. Potential use of algae for heavy metal bioremediation, a critical review. *J. Environ. Manage*. **2016**, *181*, 817–831; DOI:10.1016/j.jenvman.2016.06.059.
13. Ali, S.; Abbas, Z.; Rizwan, M.; Zaheer, I.E.; Yavas, I.; Ünay, A.; Abdel-Daim, M.M.; Bin-Jumah, M.; Hasanuzzaman, M.; Kalderis, D. Application of floating aquatic plants in phytoremediation of heavy metals polluted water: A review. *Sustain*. **2020**, *12*, 1–33; DOI:10.3390/su12051927.
14. Acosta-Rodríguez, I.; Cardenás-González, J.F.; Pérez, A.S.R.; Oviedo, J.T.; Martínez-Juárez, V.M. Bioremoval of different heavy metals by the resistant fungal strain *Aspergillus niger*. *Bioinorg. Chem. Appl*. **2018**, *2018*, 3457196; DOI:10.1155/2018/3457196.
15. Srivastava, P.K.; Vaish, A.; Dwivedi, S.; Chakrabarty, D.; Singh, N.; Tripathi, R.D. Biological removal of arsenic pollution by soil fungi. *Sci. Total Environ*. **2011**, *409*, 2430–2442; DOI:10.1016/j.scitotenv.2011.03.002.
16. Silva, N.M. da; Reis, G.F.; Costa, F. de F.; Grisolia, M.E.; Geraldo, M.R.; Lustosa, B.P.R.; Lima, B.J.F. de S.; Weiss, V.A.; de Souza, E.M.; Li, R.; et al. Genome sequencing of *Cladophialophora exuberans*, a novel candidate for bioremediation of hydrocarbon and heavy metal polluted habitats. *Fungal Biol*. **2023**, *127*, 1032–1042; DOI:10.1016/j.funbio.2023.03.003.
17. Oh, J.J.; Kim, J.Y.; Kim, Y.J.; Kim, S.; Kim, G.H. Utilization of extracellular fungal melanin as an eco-friendly biosorbent for treatment of metal-contaminated effluents. *Chemosphere*. **2021**, *272*, 129884; DOI:10.1016/j.chemosphere.2021.129884.
18. Teixeira, M.M.; Moreno, L.F.; Stielow, B.J.; Muszewska, A.; Hainaut, M.; Gonzaga, L.; Abouelleil, A.; Patané, J.S.L.; Priest, M.; Souza, R.; et al. Exploring the genomic diversity of black yeasts and relatives (Chaetothyriales, Ascomycota). *Stud. Mycol*. **2017**, *86*, 1–28; DOI:10.1016/j.simyco.2017.01.001.
19. Selbmann, L.; Egidi, E.; Isola, D.; Onofri, S.; Zucconi, L.; de Hoog, G.S.; Chinaglia, S.; Testa, L.; Tosi, S.; Balestrazzi, A.; et al. Biodiversity, evolution and adaptation of fungi in extreme environments. *Plant Biosyst*. **2013**, *147*, 237–246; DOI:10.1080/11263504.2012.753134.

20. Selbmann, L.; Isola, D.; Fenice, M.; Zucconi, L.; Sterflinger, K.; Onofri, S. Potential extinction of antarctic endemic fungal species as a consequence of global warming. *Sci. Total Environ*. **2012**, *438*, 127–134; DOI:10.1016/j.scitotenv.2012.08.027.
21. Isola, D.; Selbmann, L.; de Hoog, G.S.; Fenice, M.; Onofri, S.; Prenafeta-Boldú, F.X.; Zucconi, L. Isolation and screening of black fungi as degraders of volatile aromatic hydrocarbons. *Mycopathologia*. **2013**, *175*, 369–379; DOI:10.1007/s11046-013-9635-2.
22. Prenafeta-Boldú, F.X.; de Hoog, G.S.; Summerbell, R.C. Fungal communities in hydrocarbon degradation. In: McGenity, T. (eds) Microbial communities utilizing hydrocarbons and lipids: Members, metagenomics and ecophysiology. Handbook of hydrocarbon and lipid microbiology. *Springer*, **2019**; pp. 1–36.
23. Abdollahzadeh, J.; Groenewald, J.Z.; Coetzee, M.P.A.; Wingfield, M.J.; Crous, P.W. Evolution of lifestyles in Capnodiales. *Stud. Mycol*. **2020**, *95*, 381; DOI:10.1016/j.simyco.2020.02.004.
24. Butler, M.J.; Gardiner, R.B.; Day, A.W. Fungal melanin detection by the use of copper sulfide-silver. *Mycologia*. **2005**, *97*, 312–319; DOI:10.1080/15572536.2006.11832806.
25. Prota, G. Melanins and Melanogenesis. *Academic Press*. San Diego, CA, USA, **1992**.
26. Kumar, C.G.; Mongolla, P.; Pombala, S.; Kamle, A.; Joseph, J. Physicochemical characterization and antioxidant activity of melanin from a novel strain of *Aspergillus bridgeri* ICTF-201. *Lett. Appl. Microbiol*. **2011**, *53*, 350–358; DOI:10.1111/j.1472-765X.2011.03116.x.
27. Fogarty, R. V.; Tobin, J.M. Fungal melanins and their interactions with metals. *Enzyme Microb. Technol*. **1996**, *19*, 311–317; DOI:10.1016/0141-0229(96)00002-6.
28. Isola, D.; Scano, A.; Orrù, G.; Prenafeta-Boldú, F.X.; Zucconi, L. Hydrocarbon-Contaminated sites: Is there something more than *Exophiala xenobiotica*? New insights into black fungal diversity using the long cold incubation method. *J. Fungi*. **2021**, *7*, 817; DOI:10.3390/jof7100817.
29. Selvakumar, P.; Rajasekar, S.; Periasamy, K.; Raaman, N. Isolation and characterization of melanin pigment from *Pleurotus cystidiosus* (telomorph of antromycopsis macrocarpa). *World J. Microbiol. Biotechnol*. **2008**, *24*, 2125–2131; DOI:10.1007/S11274-008-9718-2.
30. Suwannarach, N.; Kumla, J.; Watanabe, B.; Matsui, K.; Lumyong, S. Characterization of melanin and optimal conditions for pigment production by an endophytic fungus, *Spissiomyces endophytica* SDBR-CMU319. *PLoS One*. **2019**, *14*, e0222187; DOI:10.1371/journal.pone.0222187.
31. Bates, S.T.; Reddy3, G.S.N.; Garcia-Pichel, F. *Exophiala crusticola* Anam. Nov. (affinity Herpotrichiellaceae), a novel black yeast from biological soil crusts in the western United States. *Int. J. Syst*. **2006**, *56*, 2697–702; DOI:10.1099/ijs.0.64332-0.
32. Madrid, H.; Gené, J.; Quijada, L.; Cantillo, T.; Gacitúa, R.; Valdés, J.; Sánchez, C.; Prenafeta-Boldú, F.; Wijayawardene, N.; Silva, V.; Godoy, P. *Exophiala atacamensis* sp. nov. and *E. crusticola* from the Atacama desert, northern Chile. **2023**. *Sydowia* vol. 75, pp 181–192.
33. Vala, A.K. Tolerance and removal of arsenic by a facultative marine fungus *Aspergillus candidus*. *Bioresour. Technol*. **2010**, *101*, 2565–2567; DOI:10.1016/j.biortech.2009.11.084.
34. Mukherjee, A.; Das, D.; Kumar Mondal, S.; Biswas, R.; Kumar Das, T.; Boujedaini, N.; R. Khuda-Bukhsh, A. Tolerance of arsenate-induced stress in *Aspergillus niger*, a possible candidate for bioremediation. *Ecotoxicol. Environ. Saf*. **2010**, *73*, 172–182; DOI:10.1016/j.ecoenv.2009.09.015.
35. Nam, I.H.; Murugesan, K.; Ryu, J.; Kim, J.H. Arsenic (As) removal using *Talaromyces* Sp. KM-31 isolated from As-contaminated mine soil. *Miner*. **2019**, *9*, 568; DOI:10.3390/min9100568.
36. Ceci, A.; Spinelli, V.; Massimi, L.; Canepari, S.; Persiani, A.M. Fungi and arsenic: Tolerance and bioaccumulation by soil saprotrophic species. *Appl. Sci*. **2020**, *10*, 3218; DOI:10.3390/app10093218.
37. Oladipo, O.G.; Awotoye, O.O.; Olayinka, A.; Bezuidenhout, C.C.; Maboeta, M.S. Heavy metal tolerance traits of filamentous fungi isolated from gold and gemstone mining sites. *Brazilian J. Microbiol*. **2018**, *49*, 29–37, DOI:10.1016/j.bjm.2017.06.003.
38. Singh, M.; Srivastava, P.K.; Verma, P.C.; Kharwar, R.N.; Singh, N.; Tripathi, R.D. Soil fungi for mycoremediation of arsenic pollution in agriculture soils. *J. Appl. Microbiol*. **2015**, *119*, 1278–1290; DOI:10.1111/jam.12948.
39. Zapana-Huarache, S. V.; Romero-Sánchez, C.K.; Gonza, A.P.D.; Torres-Huaco, F.D.; Rivera, A.M.L. Chromium (VI) Bioremediation potential of filamentous fungi isolated from Peruvian Tannery industry effluents. *Brazilian J. Microbiol*. **2020**, *51*, 271–278; DOI:10.1007/s42770-019-00209-9.
40. Liaquat, F.; Munis, M.F.H.; Haroon, U.; Arif, S.; Saqib, S.; Zaman, W.; Khan, A.R.; Shi, J.; Che, S.; Liu, Q. Evaluation of metal tolerance of fungal strains isolated from contaminated mining soil of Nanjing, China. *Biology (Basel)*. **2020**, *9*, 1–12; DOI:10.3390/biology9120469.
41. Zhang, Y.; Zhang, Y.; Liu, M.; Shi, X.; Zhao, Z. Dark septate endophyte (DSE) fungi isolated from metal polluted soils: Their taxonomic position, tolerance, and accumulation of heavy metals *in vitro*. *J. Microbiol*. **2008**, *46*, 624–632; DOI:10.1007/s12275-008-0163-6.
42. Seyedmousavi, S.; Badali, H.; Chlebicki, A.; Zhao, J.; Prenafeta-boldú, F.X.; De Hoog, G.S. *Exophiala sideris*, a novel black yeast isolated from environments polluted with toxic alkyl benzenes and arsenic. *Fungal Biol*. **2011**, *115*, 1030–1037; DOI:10.1016/j.funbio.2011.06.004.
43. Sharma, S.; Malaviya, P. Bioremediation of Tannery wastewater by chromium resistant novel fungal consortium. *Ecol. Eng*. **2016**, *91*, 419–425; DOI:10.1016/j.ecoleng.2016.03.005.
44. Fomina, M.; Gadd, G.M. Metal sorption by biomass of melanin-producing fungi grown in clay-containing medium. *J. Chem. Technol. Biotechnol*. **2003**, *78*, 23–34; DOI:10.1002/jctb.736.

45. Liu, S.; Chen, M.; Cao, X.; Li, G.; Zhang, D.; Li, M.; Meng, N.; Yin, J.; Yan, B. Chromium (VI) removal from water using cetylpyridinium chloride (CPC)-modified montmorillonite. *Sep. Purif. Technol*. **2020**, *241*, 116732; DOI:10.1016/j.seppur.2020.116732.
46. Acevedo-Aguilar, F.J.; Espino-Saldaña, A.E.; Leon-Rodriguez, I.L.; Rivera-Cano, M.E.; Avila-Rodriguez, M.; Wrobel, K.; Wrobel, K.; Lappe, P.; Ulloa, M.; Gutiérrez-Corona, J.F. Hexavalent chromium removal *in vitro* and from industrial wastes, using chromate-resistant strains of filamentous fungi indigenous to contaminated wastes. *Can J Microbiol*. **2006**, *52*, 809–15; DOI:10.1139/W06-037.
47. Isola, D.; Bartoli, F.; Meloni, P.; Caneva, G.; Zucconi, L. Black fungi and stone heritage conservation: Ecological and metabolic assays for evaluating colonization potential and responses to traditional biocides. *Appl. Sci*. **2022**, *12*, 2038; DOI:10.3390/app12042038.
48. Seyedmousavi, S.; Netea, M.G.; Mouton, J.W.; Melchers, W.J.G.; Verweij, P.E.; de Hoog, G.S. Black yeasts and their filamentous relatives: Principles of pathogenesis and host defense. *Clin. Microbiol. Rev*. **2014**, *27*, 527–542; DOI:10.1128/cmr.00093-13.
49. Harutyunyan, S.; Muggia, L.; Grube, M. Black fungi in lichens from seasonally arid habitats. *Stud. Mycol*. **2008**, *61*, 83; DOI:10.3114/SIM.2008.61.08.
50. Sterflinger, K.; De Hoog, G.S.; Haase, G. Phylogeny and ecology of meristematic Ascomycetes. *Stud. Mycol*. **1999**, 1*999*, 5–22.
51. Joshi, P.K.; Swarup, A.; Maheshwari, S.; Kumar, R.; Singh, N. Bioremediation of heavy metals in liquid media through fungi isolated from contaminated sources. *Indian J Microbiol*. **2011**, *4*, 482–7; DOI:10.1007/s12088-011-0110-9.
52. Lotlikar, N.P.;; Damare, S.R.; Meena, R.M.; Linsy, P.; Mascarenhas, B. Potential of marine-derived fungi to remove hexavalent chromium pollutant from culture broth. *Indian J Microbiol*. **2018**, *2*, 182–192; DOI:10.1007/s12088-018-0719-z.
53. Radulović, M. D.; Cvetković, O. G.; Nikolić, S. D.; Dordević, D. S.; Jakovljević, D. M.; Vrvić, M. M. Simultaneous production of pullulan and biosorption of metals by *Aureobasidium pullulans* strain CH-1 on peat hydrolysate. *Bioresour technol*. **2008**, *14*, 6673–6677; DOI:10.1016/j.biortech.2007.11.053.
54. Unceta, N.; Séby, F.; Malherbe, J.; Donard, O.F.X. Chromium speciation in solid matrices and regulation: A review. *Anal. Bioanal. Chem*. **2010**, *397*, 1097–1111; DOI:10.1007/S00216-009-3417-1.
55. Chiban, M.; Zerbet, M.; Carja, G.; Sinan, F. Application of low-cost adsorbents for arsenic removal: A Review. *J. Environ. Chem. Ecotoxicol*. **2012**, *4*, 91–102; DOI:10.5897/jece11.013.
56. Mohamed, L.A.; Aniagor, C.O.; Taha, G.M.; Abou-Okeil, A.; Hashem, A. Mechanistic investigation of the mass transfer stages involved during the adsorption of aqueous lead onto *Scopulariopsis brevicompactum* fungal biomass. *Environ. Challenges*. **2021**, *5*, 100373; DOI:10.1016/j.envc.2021.100373.
57. Long, D.-D.; Wang, Q.; Han, J.-R. Biosorption of copper (II) from aqueous solutions by sclerotiogenic *Aspergillus oryzae* G15. *Water Environ. Res*. **2017**, *89*, 703–713; DOI:10.2175/106143017X14839994523749.
58. Benila Smily, J.R.M.; Sumithra, P.A. Optimization of chromium biosorption by fungal adsorbent, *Trichoderma* sp. BSCR02 and its desorption studies. *Hayati J. Biosci*. **2017**, *24*, 65–71; DOI:10.1016/j.hjb.2017.08.005.
59. Velmurugan, P.; Shim, J.; You, Y.; Choi, S.; Kamala-Kannan, S.; Lee, K.J.; Kim, H.J.; Oh, B.T. Removal of zinc by live, dead, and dried biomass of *Fusarium* spp. Isolated from the abandoned-metal mine in South Korea and its perspective of producing nanocrystals. *J. Hazard. Mater*. **2010**, *182*, 317–324; DOI:10.1016/j.jhazmat.2010.06.032.
60. Shroff, K.A.; Vaidya, V.K. Kinetics and equilibrium studies on biosorption of nickel from aqueous solution by dead fungal biomass of *Mucor hiemalis*. *Chem. Eng. J*. **2011**, *171*, 1234–1245; DOI:10.1016/j.cej.2011.05.034.
61. Ayele, A.; Haile, S.; Alemu, D.; Kamaraj, M. Comparative utilization of dead and live fungal biomass for the removal of heavy metal: A concise review. *Sci. World J*. **2021**, *2021*; DOI:10.1155/2021/5588111.
62. Ahluwalia, S.S.; Goyal, D. Removal of Cr(VI) from aqueous solution by fungal biomass. *Eng. Life Sci*. **2010**, *10*, 480–485; DOI:10.1002/ELSC.200900111.
63. Loukidou, M.X.; Matis, K.A.; Zouboulis, A.I.; Liakopoulou-Kyriakidou, M. Removal of As(V) from wastewaters by chemically modified fungal biomass. *Water Res*. **2003**, *37*, 4544–4552; DOI:10.1016/S0043-1354(03)00415-9.
64. Espinoza-Sánchez, M.A.; Arévalo-Niño, K.; Quintero-Zapata, I.; Castro-González, I.; Almaguer-Cantú, V. Cr(VI) Adsorption from aqueous solution by fungal bioremediation based using *Rhizopus* sp. *J. Environ. Manage*. **2019**, *251*, 109595; DOI: 10.1016/j.jenvman.2019.109595.
65. Subbaiah, M.V.; Kalyani, S.; Reddy, G.S.; Boddu, V.M.; Krishnaiah, A. Biosorption of Cr(VI) from aqueous solutions using *Trametes versicolor polyporus* Fungi. *J. Chem*. **2008**, *5*, 499–510; DOI:10.1155/2008/618375.
66. Samuel S, M.; Abigail M, E.A.; Chidambaram, R. Isotherm modelling, kinetic study and optimization of batch parameters using response surface methodology for effective removal of Cr(VI) using fungal biomass. *PLoS One*. **2015**, *10*, e0116884; DOI: 10.1371/journal.pone.0116884.
67. Miretzky, P.; Cirelli, A.F. Cr(VI) and Cr(III) Removal from aqueous solution by raw and modified lignocellulosic materials: A review. *J. Hazard. Mater*. **2010**, *180*, 1–19; DOI:10.1016/j.jhazmat.2010.04.060.
68. Aigbe, U.O.; Osibote, O.A. A review of hexavalent chromium removal from aqueous solutions by sorption technique using nanomaterials. *J. Environ. Chem. Eng*. **2020**, *8*, 104503; DOI:10.1016/j.jece.2020.104503.
69. Garza-González, M.T.; Ramírez-Vázquez, J.E.; García-Hernández, M. de los Á.; Cantú-Cárdenas, M.E.; Liñan-Montes, A.; Villarreal-Chiu, J.F. Reduction of chromium (VI) from aqueous solution by biomass of *Cladosporium cladosporioides*. *Water Sci. Technol*. **2017**, *76*, 2494–2502; DOI:10.2166/wst.2017.427.

70. Ren, B.; Zhang, Q.; Zhang, X.; Zhao, L.; Li, H. Biosorption of Cr(VI) from aqueous solution using dormant spores of *Aspergillus niger*. *RSC Adv*. **2018**, *8*, 38157–38165; DOI:10.1039/c8ra07084a.
71. Arica, M.Y.; Bayramoğlu, G. Cr(VI) Biosorption from aqueous solutions using free and immobilized biomass of *Lentinus sajor-caju*: Preparation and kinetic characterization. *Colloids Surfaces. A Physicochem. Eng. Asp*. **2005**, *253*, 203–211; DOI:10.1016/j.colsurfa.2004.11.012.
72. Serrano-Gómez, J.; Olguín, M T. Separation of Cr(VI) from aqueous solutions by adsorption on the microfungus *Ustilago maydis*. *Int. J. Environ. Sci. Technol*. **2015**, *12*, 2559–2566; DOI:10.1007/s13762-014-0665-1.
73. Tewari, N.; Vasudevan, P.; Guha, B.K. Study on biosorption of Cr(VI) by *Mucor hiemalis*. *Biochem. Eng. J*. **2005**, *23*, 185–192; DOI:10.1016/j.bej.2005.01.011.
74. Pourkarim, S.; Ostovar, F.; Mahdavianpour, M.; Moslemzadeh, M. Adsorption of chromium(VI) from aqueous solution by artist's bracket fungi. *Separation Science and Technology*. **2017**, *52*, 1733–1741; DOI:10.1080/01496395.2017.1299179.
75. Thaira, H.; Raval, K.; Manirethan, V.; Balakrishnan, R.M. Melanin nano-pigments for heavy metal remediation from water. *Sep. Sci. Technol*. **2019**, *54*, 265–274; DOI:10.1080/01496395.2018.1443132.
76. Gadd, G.M.; de Rome, L. Biosorption of copper by fungal melanin. *Appl. Microbiol. Biotechnol*. **1988**, *29*, 610–617; DOI:10.1007/BF00260993
77. Caesar-Tonthat, T.C.; Van Ommen, F.; Geesey, G.G.; Henson, J.M. Melanin production by a filamentous soil fungus in response to copper and localization of copper sulfide by sulfide-silver staining. *Appl. Environ. Microbiol*. **1995**, *61*, 1968–1975; DOI:10.1128/aem.61.5.1968-1975.1995.
78. Zhan, F.; He, Y.; Yang, Y.; Li, Y.; Li, T.; Zhao, Z. Effects of tricyclazole on cadmium tolerance and accumulation characteristics of a dark septate endophyte (DSE), *Exophiala pisciphila*. *Bull. Environ. Contam. Toxicol*. **2016**, *96*, 235–241; DOI:10.1007/s00128-015-1676-4.
79. Potisek, M.; Likar, M.; Vogel-Mikuš, K.; Arčon, I.; Grdadolnik, J.; Regvar, M. 1,8-Dihydroxy naphthalene (DHN)-melanin confers tolerance to cadmium in isolates of melanised dark septate endophytes. *Ecotoxicol. Environ. Saf*. 2021, *222*; DOI:10.1016/j.ecoenv.2021.112493.

Chapter 4

Characterization of melanin from Exophiala mesophila with the prospect of potential biotechnological applications

Medina-Armijo, C., Yousef, I., Berna, A., Puerta, A., Esteve-Núñez, A., Viñas, M. and Prenafeta-Boldú, F.X. (2024). Characterization of melanin from *Exophiala mesophila* with the prospect of potential biotechnological applications. Frontiers in Fungal Biology. 5, 1390724. doi: 10.3389/ffunb.2024.1390724.

Part of this chapter was presented as an oral communication in Sociedad de Microbiología de Chile (SOMICH) 2023 and XXVIII International Symposium on Bioelectrochemistry and Bioenergetics (BES 2024) in Alcalá de Henares, Spain.

frontiers | Frontiers in Fungal Biology

TYPE Original Research
PUBLISHED xx xx 2024
DOI 10.3389/ffunb.2024.1390724

OPEN ACCESS

EDITED BY
Claudia Coleine,
University of Tuscia, Italy

REVIEWED BY
Macit Ilkit,
C, ukurova University, Türkiye
Jing Si,
Beijing Forestry University, China

*CORRESPONDENCE
Cristy Medina-Armijo
cristy.medina@irta.cat
Francesc X. Prenafeta-Boldu´
francesc.prenafeta@irta.cat

RECEIVED 23 February 2024
ACCEPTED 25 April 2024
PUBLISHED xx xx 2024

CITATION
Medina-Armijo C, Yousef I, Berna´ A, Puerta A, Esteve-Nu´ ñez A, Viñas M and Prenafeta- Boldu´ FX (2024) Characterization of melanin from *Exophiala mesophila* with the prospect of potential biotechnological applications. *Front. Fungal Biol.* 5:1390724. doi: 10.3389/ffunb.2024.1390724

Characterization of melanin from *Exophiala mesophila* with the prospect of potential biotechnological applications

Cristy Medina-Armijo[1,2]*, Ibraheem Yousef[3], Antonio Berná[4], Anna Puerta[1], Abraham Esteve-Núñez[4], Marc Viñas[1] and Francesc X. Prenafeta-Boldú[1]*

[1]Program of Sustainability in Biosystems, Institute of Agrifood Research and Technology (IRTA), Caldes de Montbui, Catalonia, Spain, [2]Faculty of Pharmacy and Food Sciences, University of Barcelona, Catalonia, Spain, [3]ALBA Synchrotron Light Source, Cerdanyola del Valle´s, Catalonia, Spain, [4]University of Alcala´ de Henares, Alcala´ de Henares, Madrid, Spain

Fungal melanin is an underexplored natural biomaterial of great biotechnological interest in different areas. This study investigated the physical, chemical, electrochemical, and metal-binding properties of melanin extracted from the metallotolerant black fungus *Exophiala mesophila* IRTA-M2-F10. Specific inhibitory studies with the tricyclazole and biochemical profiling of whole cells by synchrotron radiation-based Fourier-transform infrared spectral microscopy (SR-FTIRM) have indicated that 1,8-dihydroxynaphthalene might be the main precursor molecule of fungal melanin (DHN-melanin). An optimized extraction protocol was also implemented, and fungal melanin was characterized using an array of spectrophotometric techniques (UV-Vis, FTIR, and EPR) and by cyclic voltammetry (CV) experiments. The obtained results were benchmarked against those from two melanins comprising the precursor molecule L-3,4-dihydroxiphenylalanine (DOPA-melanin): extracts from the ink of the cephalopod *Sepia officinalis* and DOPA-melanin synthesized in the laboratory. The CV results of melanin extracts incubated with and without cell suspensions of the electroconductive bacterium *Geobacter sulfurreducens* are indicative of novel semiquinone/hydroquinone redox transformations specific for each melanin type. These interactions may play an important role in cation exchange for the adsorption of metals and in microbial interspecies electron transfer processes. The obtained results provide further evidence for the DHN-nature of *E. mesophila* melanin. The FTIR profiling of melanin extracts exposed to Cr(VI) as a model heavy metal, compared to unexposed melanin, resulted in useful information on the distinct surface-binding properties of fungal melanin. The Langmuir and Freundlicht adsorption isotherms of Cr(VI) onto fungal melanin were also determined and compared to bibliographic data. Altogether, the inherent properties of fungal melanin suggest its promising potential as a biomaterial for environmental applications.

10.3389/ffunb.2024.1390724

KEYWORDS

bioelectroconductivity, dihydroxynaphthalene, extremophilic black fungi, FTIR chemical profiling, fungal melanin, metal biosorption, natural biomaterials

1 Introduction

Recent advances in biotechnology have paved the way in finding alternative materials with well-characterized structures that can be engineered, and are biocompatible, biodegradable, and harmless to public health and the environment. Certain natural biomaterials are of great interest to engineers and materials scientists because they offer a wide range of exceptional physical and chemical properties that can be exploited for a variety of applications, including bioremediation, bioelectronics, pharmaceuticals, cosmetics, packaging and food (Roy and Rhim, 2021). Among these novel extractable biomaterials, melanin is emerging as a promising substance with diverse potential applications (Tran-Ly et al., 2020a; Roy and Rhim, 2021).

Melanin comprises a group of ancestral and functionally analogous dark polymeric pigments that have evolved across a high diversity of organisms, including bacteria, fungi, plants and animals (Eisenman and Casadevall, 2012). According to a broadly accepted classification based on the chemical structure of precursor molecules and macroscopic characteristics (Pralea et al., 2019), there are three major types of melanin: i) Brown-black eumelanin is biosynthesized from L-tyrosine, which is converted into L-3,4-dihydroxiphenylalanine (DOPA-melanin); these precursors are oxidized further to 5,6-dihydroxyindole and 5,6-dihydroxyindole-2-carboxylic acid as the building blocks of eumelanin. ii) Brown-red phaeomelanin is also produced from the precursor molecule L-tyrosine, but its biochemical pathway involves the addition of cysteine to form benzothiazine intermediates. iii) Allomelanin is a very heterogeneous group of nitrogen-free polymers that include pyomelanin (a red pigment found in bacteria and some fungi), which is obtained through the catabolic pathway of L-tyrosine. The biodegradation of L-tyrosine generates p-hydroxyphenylpyruvate, which is oxidized to homogentisic acid as the main building block of pheomelanin. Moreover, within this last group of allomelanins, most ascomycetes synthetize melanin through the polyketide pathway, using 1,8-dihydroxynaphthalene (DHN-melanin) as precursor. Instead, basidiomycetes generally produce eumelanin (DOPA-melanin) in a pathway resembling that of animal melanin biosynthesis. All melanin types are generally characterized by cross-like amorphous polymeric aromatic structures that contain different functional groups (carboxyl, phenolic, hydroxyl, and amine), depending on the chemical nature of precursor molecules, which are interlinked by short-distance non-hydrolyzable and strong carbon–carbon bonds (Prota, 1992).

The secondary structure of melanin is contributed by its polyelectrolyte nature due to the stacking of aromatic oligomers by bond p–p interaction (D1́æ et al., 2005). This extended p-conjugation of melanin allows for some degree of delocalized electron movement within the melanin network, contributing to limited intrinsic semiconductivity across the molecule. This delocalization of electron density plays a fundamental role in stabilizing metal–ion complexes that enhance the chelation capacity of melanin (Panzella et al., 2013). This phenomenon might also promote redox interactions with the surrounding environment, such as the direct participation of melanin in interspecies electron transfer pathways, whereby electrons are exchanged between different syntrophic microorganisms (Chen et al., 2014).

In fungi, melanization is particularly conspicuous in the so-called black fungi, which are predominantly clustered in the orders Dothideales and Chaetothyriales (Ascomycota). Melanin from black fungi has primarily been ascribed to the DHN-melanin type (Eisenman and Casadevall, 2012). Fungal melanization occurs at the cell wall, but, in black fungi, melanin accumulates within membrane-bounded organelles (rounded/elongated shape up to 500 nm in diameter) referred to as melanosomes, analogous to those found in animal cells (D'Alba and Shawkey, 2019). While melanin is not essential for fungal growth and development, it provides protection against a variety of stressors, including UV and ionizing radiation (Dadachova et al., 2008), the presence of heavy metals (Medina-Armijo et al., 2024), and toxic organic compounds (Prenafeta-Boldúet al., 2019a). Melanin also acts as an antioxidant, neutralizing reactive oxygen species (ROS) that are produced in some of the above-mentioned stress conditions (Jacobson and Tinnell, 1993).

The use of black fungi has already been proposed for a variety of biotechnological applications, such as the biosorption of heavy metals (Medina-Armijo et al., 2024) and volatile aromatic hydrocarbons (Prenafeta-Boldúet al., 2019b). Melanin seems to play a fundamental role in binding and metabolizing these toxic molecules, as well as the secondary reactive products that might result from their metabolism. Hence, fungal melanin is a particularly attractive biomaterial due to its sustainable and scalable production, as well its relatively easy extraction and purification, when compared to that of plants and animals. It is also a low-cost and high-performance alternative to synthetic analogues. However, and in contrast to the existing literature on bacterial (Pavan et al., 2019) and animal melanins (D'Alba and Shawkey, 2019), the melanin of black fungi has yet to be studied in detail.

In a previous paper (Medina-Armijo et al., 2024), we verified the biosorption capacity and kinetics of hexavalent Chromium Cr (VI) by whole cells and melanin extracts from the metallotolerant black fungus *Exophiala mesophila* strain IRTA-M2-F10. The aim in this study is to gain a deeper understanding of the properties of

melanin from black fungi, specifically regarding its electrochemical properties and the binding of metals. To this end, we implemented an array of advanced analytical techniques for the characterization of the physicochemical and electrochemical characteristics of melanin extracts from *E. mesophila*. These results were then benchmarked against DOPA-melanins from natural (ink of the cephalopod *Sepia officinalis*) and synthetic origins. Understanding the specific properties of melanin from black fungi might be of interest for developing new environmental biotechnologies.

2 Materials and methods

2.1 Strains and growth condition

The black fungus *Exophiala mesophila* strain IRTA-M2-F10 (culture collection at the Institute of Agrifood Research and Technology, Spain) isolated previously from biodeteriorated glued ceramics was selected the source of fungal melanin because of its tolerance to heavy metals and easy cultivation under laboratory conditions (Medina-Armijo et al., 2024). Active cultures of this fungus were routinely maintained on potato dextrose agar (PDA; Condalab, Spain) incubated at 25°C in the darkness. Ten agar pre-grown fungal colonies of 5 to 7 mm in diameter (after about three weeks of incubation) were transferred into 250 mL of liquid medium that contained macronutrients (4.5 g KH_2PO_4, 0.5 g K_2HPO_4, 2.0 g NH_4Cl, and 0.1 mg $MgSO_4$ $7H_2O$ per liter), 2 mL of a stock solution of micronutrients (120 mg $FeCl_3$, 50 mg H_3BO_3, 10 mg $CuSO_4$ $5H_2O$, 10 mg KI, 45 mg $MnSO_4 \cdot H_2O$, 20 mg Na_2MoO_4 H_2O, 75 mg $ZnSO_4$ H_2O, 50 mg $CoCl_2$ $6H_2O$, 20 mg $AlK(SO_4)_2$ $12H_2O$, 13.25 g $CaCl_2$ H_2O, and 10 g NaCl, per liter), and yeast extract (4 g L^{-1}) as the carbon and energy source. The incubation of this liquid culture was performed under dark conditions at 25°C on a horizontal shaker (80 rpm) and was maintained for three weeks. Fungal biomass was then harvested by centrifugation (18 g for 20 min) and used immediately for melanin extraction.

2.2 Inhibition of fungal melanin biosynthesis

Tricyclazole (5-methyl-1,2,4-triazolo[3,4-b] benzothiazole) (abcr GmbH, Karlsruhe, Germany) was employed as a selective inhibitor of the DHN-melanin biosynthesis pathway, resulting in visible changes in the fungal biomass dematiaceous pigmentation. This approach builds upon previous studies (Butler et al., 2009; Suwannarach et al., 2019) with some modifications. Notably, tricyclazole treatment allows for the specific accumulation of the biochemical precursor to fungal melanin, known as 1,8-dihydroxynaphthalene (DHN). This approach offers a valuable tool for comparing the precursors of fungal melanin with those of other melanin types, such as DOPA-melanin. Inhibition assays were performed with liquid cultures of *E. mesophila*, incubated in batches of 250 mL, as described in the previous section. After autoclaving the culture medium, a solution of tricyclazole in absolute ethanol was added to the liquid medium up to a final concentration of 50 mg mL^{-1}, according to Kumar et al. (2015) with some modifications. Culture batches were then inoculated with colony plugs from cultures of *E. mesophila* growing on PDA, and incubated in the dark under shaking conditions at 25°C. The same procedure was repeated on batches without tricyclazole and three independent replicates were performed for each treatment/control condition. After three weeks of incubation, fungal cells were harvested by centrifugation (10000 rpm, equivalent to 9391 g, for 5 min at 4°C). The pellet was rinsed with Millipore water and resuspended with 1% formalin (Sigma Aldrich, Saint Louis, USA) as the fixing agent, and the cells were kept at 4°C for a maximum of 7 days.

Synchrotron-based Fourier transform infrared microscopy (SR-FTIRM) measurements on fixed cells of *E. mesophila* exposed to tricyclazole were performed at the infrared beamline MIRAS of the ALBA-CELLS synchrotron light source, using a Hyperion 3000 microscope coupled to a Vertex 70 spectrometer (Bruker, Germany). The SR-FTIRM was operated with a 36× Schwarzschild magnification objective (NA=0.65). The microscope was equipped with a mercury cadmium telluride (MCT) detector of 50 mm. All spectra were obtained using a single masking aperture size 15 × 15 mm, covering the full cell size. Single point maps of individual cells were collected in the 4000-900 cm^{-1} mid infrared range at 4 cm^{-1} spectral resolution with 256 co-adds scans per spectrum. A control measurement with the same parameters was performed with unexposed fungal cells. A background on the CaF_2 slides without cells, with 10 measurements repeated, was also included. The absorbance spectrum for tricyclazole-exposed and unexposed fungal cells was obtained by subtracting the background spectrum. The subtraction was done directly (automatically) by means of the OPUS 7.5 software (Bruker, Germany), according to (Martıńez-Rovira et al., 2019). This program was also used to perform multivariate principal component analysis (PCA) and Savitzky–Golay second derivative of the averaged absorbance spectra on FTIR profiles.

2.3 Extraction and purification of melanin

Melanin extraction from pre-grown fungal biomass of *Exophiala mesophila* IRTA M2-F10 was performed by adapting previously described methods based on acid hydrolysis (Selvakumar et al., 2008; Suwannarach et al., 2019). The fungal biomass was first resuspended with 1M NaOH (1:1.5 w/v biomass/NaOH) and then autoclaved for 20 min at 120 ± 1°C. The resulting suspension was centrifuged at 3220 g (4000 rpm) for 20 min, and the supernatant was collected and acidified with 6N HCL final concentration (1:1 v/v NaOH–melanin/HCl) to pH 2.5 for 12 h at 100°C, in order to induce the precipitation of melanin. Centrifugation at 3220 g for 20 min was then performed to collect the melanin precipitate, which was then washed three times with deionized water and centrifuged again at 3220 g for 15 min. The final melanin pellet was lyophilized at a pressure of 0.7 mBar at -50°C for 24 hours, resulting in a black powder that was kept at -20°C for further studies. In order to compare and characterize the fungal melanin extract, melanin was also extracted from the ink of sepia (*Sepia officinalis*), following the

same protocol with a few differences in the washing steps. Sepia melanin was firstly washed once with chloroform and centrifuged at 3220 g for 15 min, to remove oily and protein substances, and then twice with deionized water, and centrifuged at 3220 g for 15 min each time. In addition, synthetic melanin from the polymerization of L-3,4-dihydroxyphenylalanine (DOPA-melanin, Sigma-Aldrich, United Kingdom) was also used for comparative purposes.

2.4 Physicochemical characterization of melanin

The morphology and particle size of melanin precipitates obtained from *E. mesophila* were observed using a scanning electron microscope (SEM) model JEOL JSM-5610 (brand, Japan). A sample of the melanin powdery extract was coated with a gold layer using a vacuum sputterer to increase the conductivity of the samples. The physical and chemical properties of melanin extracts were determined by following similar protocols to those described in previous studies (Selvakumar et al., 2008; Suwannarach et al., 2019). Melanin solubilization tests on organic solvents were performed with 99.9% methanol, absolute ethanol, 96% acetone, 99.9% acetonitrile, 99.8% benzene, 99.9% 1-butanol, and 99.5% 2-propanol. Precipitation tests were conducted under acid conditions using 3M of HCl and 1% $FeCl_3$. Decolorization assays were performed with 30% H_2O_2 and 10% NaOCl. These experiments were also performed with sepia melanin extracts and synthetic DOPA melanin, using 0.1 mg of melanin in 5 mL of solution. All used reagents were of analytical grade.

Fungal and non-fungal melanin samples were subjected to an array of spectroscopic analyses, similar to the methods described in previous studies (Selvakumar et al., 2008, Selvakumar et al., 2012; Gonçalves et al., 2012). Melanin (0.5 mg) was dissolved in 10 mL of 0.01 M NaOH in a quartz cube and loaded onto a UV-Vis spectrophotometer (model EMC-11S UV brand, Germany). The UV−visible absorption spectrum of the melanin samples was scanned in the wavelength range of 200−750 nm, and the 0.01M NaOH solution was used as a reference blank. Electron paramagnetic resonance (EPR) spectra of powdery melanin samples were obtained with an X-Band (9.7 GHz) Bruker ELEXSYS E500 spectrometer equipped with an ST8911 microwave cavity and a variable temperature unit, a field frequency lock system ER 033 M and an NMR Gaussmeter ER 035 M (Bruker, Germany). The instrumental parameters of EPR analysis were set at 100 kHz modulation frequency, 1.0 G modulation amplitude, 0.498 mW microwave power, 9.872 GHz and 20.48 ms scan time.

FTIR spectroscopy is a well-established technique for characterizing complex melanin polymeric matrices by detecting specific functional groups and chemical bonds present in their structure (Pacelli et al., 2020; Elsayis et al., 2022). The analysis of fungal melanin was performed using a Hyperion 3000 microscope coupled to a Vertex 70 spectrometer (Bruker, Germany). Samples of melanin extracts (1 mg) were mixed with KBr dried powder (1:100) in an agate mortar and ground for a few minutes to break up melanin and KBr lumps. The transmittance spectrum was obtained with melanin samples exposed to Cr(VI) and using non-exposed samples as control. The spectra of Cr(VI)-exposed melanin were acquired by subtracting the reference spectra from non-exposed raw melanin (4000-600 cm^{-1}) according to the method of Karimi et al. (2021). The subtraction was done directly (automatically) using the OPUS 7.5 software (Bruker, Germany).

2.5 Electrochemical characterization of melanin

The electrochemical properties of fungal melanin were compared to those of cephalopod melanin extracts and synthetic DOPA-melanin, in solutions prepared by adding 15 mL of NaOH (1M) to 0.1 g melanin powder upon sonication for 2 hours at 37°C. The resulting solution was diluted with deionized water (resistivity 18.0 MΩ·cm) until reaching a final concentration of 5g L^{-1} with a pH of 7.0 ± 0.05. Then, 80 µL suspensions of the studied melanin types were used to coat screen-printed electrodes (SPE) using gold working electrodes and a Ag/AgCl reference electrode (DRP-220AT, DropSens, Asturias, Spain). Electrochemical assays were then performed immediately using a PC-controlled potentiostat (NEV4, Nanoelectra S.L., Alcaláde Henares, Spain) by adapting the methodology from González et al. (2011) and Estevez-Canales et al. (2015). To gain a deeper understanding of melanin's redox properties and potential interactions with electroactive bacteria, cultures of *Geobacter sulfurreducens* (GS), strain ATCC 51573, were mixed with melanin and deposited onto gold SPEs. Cyclic voltammetry (CV) experiments were conducted at three different scan rates, 0.005, 0.01and 0.05 V s^{-1}, and two potential windows were explored: from -1.00 V up to 0.50 V in the absence of GS, and from −0.80 up to 0.50 V in presence of GS. Anaerobic conditions were maintained, as elsewhere described (Estevez-Canales et al., 2015). GS was grown at 30°C in a freshwater medium containing the following mineral salts (per liter): 2.5 g $NaHCO_3$, 0.25 g NH_4Cl, 0.06 g $NaH_2PO_4{\cdot}H_2O$, and 0.1 g KCl. Additionally, the medium contained 0.024 g $C_6H_5FeO_7$ (ferric citrate), 10 mL of a vitamins mix, and 10 mL of a trace mineral mix (Lovley and Phillips, 1988). Anaerobic conditions were kept by purging the culture medium with a gas mixture N_2:CO_2 (80:20) to remove oxygen and maintain the pH of the bicarbonate buffer at 7.0.

2.6 Heavy metal sorption experiment

Melanin extracts were resuspended in 50 mL Erlenmeyer flasks containing Cr(VI), added as potassium dichromate ($K_2Cr_2O_7$; Scharlab ExpertQ®, Sentmenat, Spain), in concentrations ranging from 20 to 200 mg Cr^{6+} L^{-1}, and incubated at 25°C on a shaker at 150 rpm for various times (4 to 72 hours). These experiments were performed using 0.3 g of melanin powder at pH 6.5. Each condition was assayed in triplicate. At the end of incubation, the suspensions were centrifuged (3220 g for 10 min) and filtered with a 0.45 µm filter before the Cr(VI) concentration was determined. The collected samples were acidified with sulfuric acid for the solubilization of Cr(VI), which then reacted with 0.05% of 1,5-

diphenylcabazide (Sigma-Aldrich, St. Louis, MI, USA) (0.5 ml) to form a purple-violet complex. The concentration of Cr(VI) was measured using a spectrophotometer (model EMC-11S UV brand, Germany). Absorbance was measured at a wavelength (l) of 540 nm. The sorption capacity (q_e, in mg Cr(VI) per g of melanin in dry weight) and sorption efficiency (H, in %) were respectively calculated through the following equations:

$$q_e = [C_o - C_e] \cdot \frac{V}{m} \quad (1)$$

$$H = \frac{C_o - C_e}{C_o} \cdot 100\,\% \quad (2)$$

where C_0 is the initial concentration of chromium, C_e is the concentration at equilibrium (mg L^{-1}), V is the volume of the incubations (L), and m is the dry weight of the fungal melanin powder added as a sorbent (g-DW). The experimental data on the melanin uptake of Cr(VI) were fitted to the Langmuir and Freundlich isotherm models. The Langmuir isotherm assumes that adsorption occurs at a monolayer of specific and homogeneous sites, and, once an adsorbate unit occupies a site, no further adsorption can occur on that particular site, according to the following formula:

$$q_e = q_{max} \frac{K_L \cdot C_e}{1 + K_L \cdot C_e} \quad (3)$$

The K_L value is a constant related to the energy of sorption, q_e (mg g^{-1}) is the equilibrium biosorption capacity, q_{max} (mg g^{-1}) is the maximum adsorption capacity, and C_e (mg L^{-1}) is the final concentration in a certain interval time. The Freundlich adsorption isotherm is an empirical model of the equilibrium between the adsorbate uptakes per mass unit of the adsorbent:

$$q_e = K_F \cdot C_e^{1/n} \quad (4)$$

where n is a constant related to the efficiency of sorption and sorption energy, K_F is a constant measuring adsorption capacity, q_e is the amount of adsorbate removed per mass unit of melanin, and C_e is the equilibrium concentration of the adsorbate in solution. Isotherm model fitting to experimental data was performed with the linearized versions of the Langmuir and Freundlich equations.

2.7 Software and statistical methods

Experiments on Cr(VI) removal capacity by fungal melanin were repeated thrice, and the results are presented as the average with standard deviation (± SD). The software OriginPro v9.3 (OriginLab Corporation, Northampton, MA, USA) was employed for the fitting of Equations (3) and (4) to experimental data, by minimizing the sum of squared errors (SSE). The same software was used for the visualization of cyclic voltammetry (CV) curves, and for the extraction of relevant peak values.

3 Results and discussion

3.1 Melanization inhibitory studies

Tricyclazole is a fungicide that is widely used in agriculture and other applications, as it has multiple modes of action, mainly by disrupting mitochondrial function and acting as a specific inhibitor of DHN-melanin biosynthetic pathway (Kong et al., 2018). An effective disruption of melanization was observed after exposing cultures of *E. mesophila* to tricyclazole for five days, both on plates (Figure 1) and in liquid media (not shown). The color of fungal cells shifted from black to reddish brown, and the agar medium was also tinged with a reddish color. This phenomenon has previously been attributed to the accumulation and excretion of the intermediates flaviolin and 2-hydroxy juglone, which are formed by the auto-oxidation of aromatic substrates when DHN-melanin biosynthesis is inhibited (Bárcena et al., 2015).

SR-FTIRM was also employed to examine the intracellular response of *E. mesophila* to tricyclazole. Principal component analysis (PCA) was applied to identify clustering patterns in the biochemical profiles of fungal cells that were inhibited with tricyclazole (T) in comparison to non-exposed cells as control (C). Figure 2 shows the PCA score loading plots and average FTIR spectra in the fingerprint and protein regions (1800-1000 cm^{-1}), and in the high region (3000-2800 cm^{-1}) dominated mainly by lipids. The changes induced by tricyclazole are clearly visible in both regions, and the PCA score plot shows that T and C FTIR profiles are well resolved. Clustering occurs mostly along the first axis, which explains 74% of the variance in the fingerprint region and 68% of the variance in the lipid region.

The second derivative of the FTIR spectra for T and C, along with the distribution of relative intensities for several spectral bands, was also performed (Figure 2). Notably, exposure to tricyclazole (T) triggered alterations in protein conformational structures associated with the amide I band at 1660 cm^{-1} (which corresponds to C=O stretching vibrations), the amide I band at 1638 cm^{-1} (N–H bending vibrations), and the amide II band at 1547 cm^{-1} (N–H bending and C–N stretching vibrations). These findings imply a shift in protein conformational structures from a-helix to b-sheet, as evidenced by the vibrational patterns (C=O, C–N, and N–H) associated with protein secondary structures (Martínez-Rovira et al., 2019). In addition, the PO^{2-} asymmetric band at 1242 cm^{-1} and the PO^{2-} symmetric band at 1087 cm^{-1}, which are primarily derived from nucleic acids and the contribution of phospholipids, exhibit several alterations in intensity and peak position. This suggests that a range of variations in DNA organization occurred stemming from tricyclazole exposure on the cell. The spectra at 1120 and 1050 cm^{-1} were attributed to the symmetric C–C stretching of a-glucan and asymmetric C–O–C and P–O–C b-glucan complexes, respectively. These modifications in polysaccharide vibrations can be ascribed to changes in the cell wall. The distinct response of glucan could potentially impact the cell wall's permeability, enhancing fungal metallotolerance. The lipid spectral region (3100–2800 cm^{-1}) reveals alterations in the intensity of CH_2 and CH_3 symmetric and asymmetric stretching

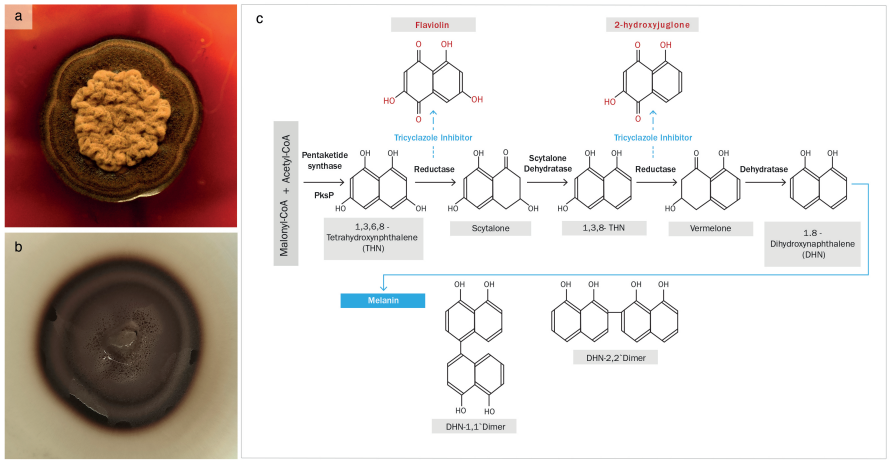

FIGURE 1
(A) *Exophiala mesophila* growing on PDA supplemented with 50 μg L^{-1} of tricyclazole, and (B) an analogous culture without tricyclazole; (C) proposed pathway for the biosynthesis of DHN-melanin, highlighting the tricyclazole inhibition of reductases that leads to the accumulation of the intermediates flaviolin and 2-hydroxyjuglone (Adapted from Lee et al., 2003).

modes, which could be associated with the state of hydrocarbons and lipids unique to the cell wall. Hence, besides the inhibition of melanization, tricyclazole also affects the cell wall structure, potentially causing the trans-chains to become more rigid, perhaps as a protective mechanism against environmental stresses. This could, for instance, influence the transport of ions, water, and nutrients into the cell.

The impact of tricyclazole on melanin structure can also be inferred from the SR-FTIRM spectra (Figure 2). Peaks between 1670 and 1600 cm^{-1} correspond to conjugated double bonds C=C and C=O in the aromatic ring and C=O in secondary amine features of typical quinoid structures, like those found in melanins. The second derivative illustrates the reduction of these bands in cells exposed to tricyclazole. In other words, tricyclazole induced evident changes in the decreased intensity of peaks between 1670 and 1600 cm^{-1}. This effect is attributed to tricyclazole's inhibition of the polymerization of DHN, affecting the amount of melanin that accumulates in the cell.

Our research demonstrates the detrimental effects of tricyclazole on fungal growth, beyond the inhibition of

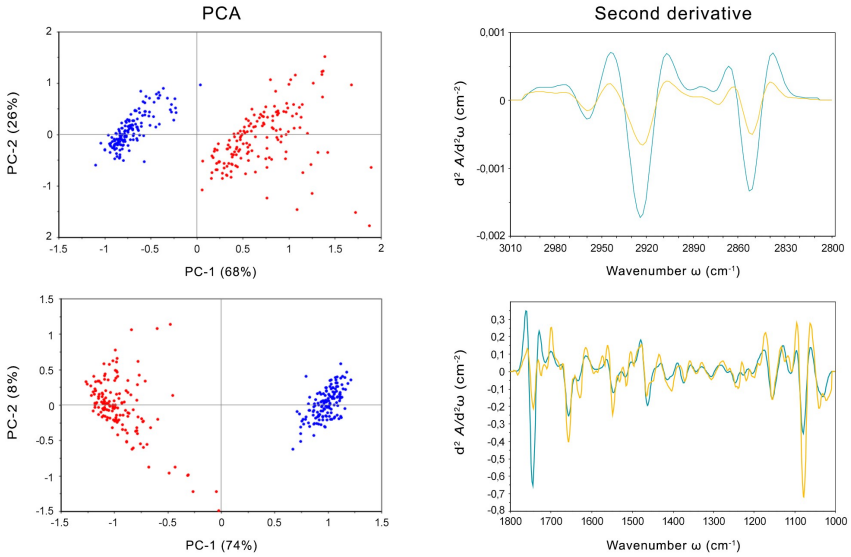

FIGURE 2
Left: PCA scores and loading plots of cells of *Exophiala mesophila* exposed to tricyclazole (T, red dots) and uninhibited cells (C, blue dots). Right: Savitzky-Golay second derivative of the averaged absorbance spectra in fungal cells exposed to tricyclazole (yellow lines) and uninhibited cells (blue lines). Up: results corresponding to the lipids' (3000–2800 cm^{-1}) spectral region. Down: results corresponding to the fingerprint (1800–1000 cm^{-1}) spectral region.

melanization. This compound additionally alters the lipid composition of fungal cells, potentially leading to an increase in reactive oxygen species (ROS) levels through the peroxidation of lipid molecules, particularly those with methyl groups (Kumar et al., 2015). While tricyclazole at low doses may not be detrimental to cell survival, it can elevate ROS levels within cells, potentially affecting the integrity of various biochemical metabolic pathways. Hence, melanin inhibition may lead to DNA, lipid, and amide damage, among other potentially deleterious effects. Previous studies have emphasized melanin's role in alleviating oxidative stress and neutralizing free radicals (Smith and Casadevall, 2019), and shown that the tricyclazole-mediated inhibition of melanin synthesis alters fungal growth and physiological processes (Bárcena et al., 2015). Tricyclazole inhibits enzymes that reduce 1,3,6,8-tetrahydroxynaphthalene to scytalone and 1,3,8-trihydroxynaphthalene to vermalone (Figure 1; Lee et al., 2003). This enzyme repression induces DNA transcription and methylation, which may be the main cause of the changes in the protein and DNA of melanin intermediates observed in this study, themselves related to the process of autoxidation (Zhan et al., 2016).

The FTIR profiling confirms the disruptive effect of tricyclazole on the biosynthesis of DHN-melanin in black fungi and, more specifically, the predominance of this melanin type in *Exophiala mesophila*. However, further research is warranted to elucidate the precise interplay between melanin production and tricyclazole's mechanism of action. Additionally, investigations into the potential alterations of key physicochemical properties of the fungus in response to tricyclazole treatment are necessary.

3.2 Physicochemical characterization of fungal melanin

The protocols implemented for the extraction and purification of melanin from the fungus *Exophiala mesophila* yielded 155.05 ± 25.64 mg (n = 4) of melanin extract per gram fungal biomass, both expressed on a dry weight basis. This extract had the macroscopic appearance of a powdery dark brown pigment (Figure 3). A more detailed morphological characterization through scanning electron microscopy showed that fungal melanin extracts consisted of an array of opaque and amorphous black granules of 10 to 200 µm in size (Figure 3E).

The results of the solubilization, precipitation, and oxidation tests are similar for the fungal and cephalopodal melanin extracts, as well as for the synthetic DOPA-melanin, and are also consistent with previous research (Gonçalves et al., 2012; Suwannarach et al., 2019). All three melanins were insoluble in distilled water, but were soluble in 1 M NaOH and 1 M KOH. They were also largely insoluble in most of the tested organic solvents (methanol, absolute ethanol, acetone, acetonitrile, benzene and chloroform), with the exception of methanol and absolute ethanol, in which they were slightly soluble. The precipitation test was positive with 2N HCl and 1% $FeCl_3$ solutions, where a brown precipitate was clearly observed. All three melanins were also effectively decolorized with 30% H_2O_2 and 10% NaOCl solutions.

Melanin's insolubility in most common solvents hinders its detailed chemical characterization. However, several analytical techniques offer rapid and informative results for melanin analysis, including ultraviolet−visible (UV-Vis) spectroscopy, electron paramagnetic resonance (EPR), and Fourier-transform infrared (FTIR) spectroscopy (Gonçalves et al., 2012; Suwannarach et al., 2019; Pacelli et al., 2020; Mostert, 2021). The spectral properties of three different melanin types were investigated using these techniques (Figure 4). The UV-Vis absorption spectra reveal similar maximum absorbance peaks for the natural fungal and cephalopodal melanin extracts, as well as the synthetic DOPA-melanin (wavelengths of 225, 236 and 224 nm, respectively), and sharp decreases in absorbance in the visible region. Similar profiles have been reported previously with melanin from various fungi, in which the maximum absorbance was observed in the UV range of 200−300 nm, swiftly decreasing toward the visible region (Suryanarayanan et al., 2004; Selvakumar et al., 2008; Eisenman and Casadevall, 2012; Gonçalves et al., 2012). The overall absorption profile of melanin has previously been modeled as multiple overlapping distinct chromophores (Di Mauro et al., 2017; Mostert, 2021), and high absorbance in the UV region generally reflects the abundance of aromatic rings containing conjugated double bonds (Kumar et al., 2011).

The log absorbance of melanin (Figure 4) against wavelength in the visible region (Dlog A/l) has a typically linear correlation with a negative slope, which might be specific for every melanin type (Selvakumar et al., 2008; Pal et al., 2014; Suwannarach et al., 2019). Fungal and cephalopodal melanin extracts had very similar Dlog A/l slopes of −0.0025 and −0.0028, respectively, but the synthetic DOPA-melanin showed a steeper slope of −0.0060. Previously reported Dlog A/l slope values for the melanin of black fungi range from −0.0015 for *Phyllosticta capitalensis* (Suryanarayanan et al., 2004) to −0.0030 for *Exophiala pisciphila* (Zhan et al., 2011). The UV-Vis absorbance profile of melanin has been attributed to potential electronic transitions within individual chromophore components present in its aromatic polymeric structure (Meredith et al., 2006). Tran et al. (2006) suggested that the inherent chemical heterogeneity of melanin contributes to this phenomenon. The negative Dlog A/l slope emphasizes the role of melanin's chromophoric absorption at shorter wavelengths, with light scattering playing a minimal role, especially in this region of the spectrum (Di Mauro et al., 2017). These findings highlight the excellent photoprotective properties of melanin against UV and visible radiation and have paved the way for the development of novel applications in various fields, including UV-resistant textiles, UV exposure sensors, and biomedicine (Tran-Ly et al., 2020a).

Electron paramagnetic resonance (EPR) spectroscopy, a well-established technique for identifying free radicals in melanin (Enochs et al., 1993), offers insights into various aspects of its redox and magnetic properties. The g-value, a parameter derived from EPR spectra that reflects the ratio of magnetic moment to angular momentum in a magnetic field, provides valuable information for the identification of melanin. Analyses of fungal and cephalopodal melanin extracts and synthetic DOPA-melanin revealed similar g-values (2.0030, 2.0028, and 2.0033, respectively). Additionally, the EPR spectra exhibited peaks at a magnetic field

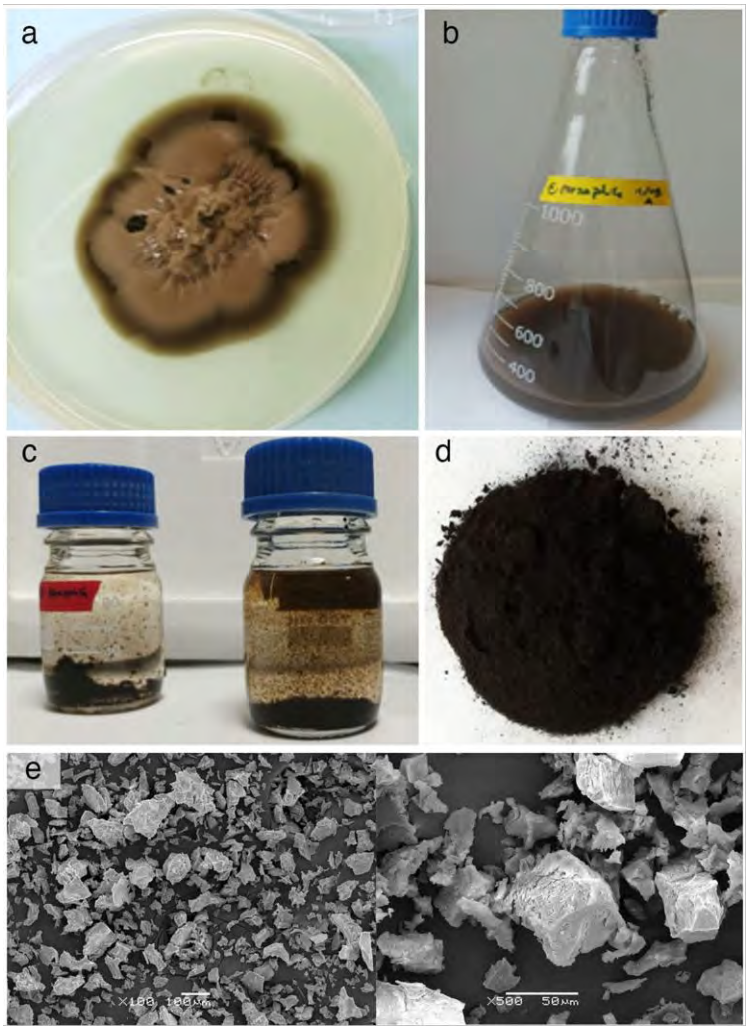

FIGURE 3
(A) PDA agar culture used as inoculum and (B) nutrient-rich liquid culture used to obtain larger amounts of biomass of *Exophiala mesophila*; (C) acid hydrolysis of fungal melanin after 12 hours at 100°C and precipitation of melanin in HCl at 6N; (D) lyophilized fungal melanin powder; (E) SEM microscopic images at different magnifications of melanin extracts.

strength of 3524 G (Figure 4), confirming the presence of free radicals, a hallmark characteristic of melanin (Zhan et al., 2011; Gonçalves et al., 2012; Suwannarach et al., 2019). EPR spectroscopy reveals a characteristic single line in the spectrum with slight asymmetry (Figure 4), which corresponds to a semiquinone radical formed by the coupling of a free electron with the aromatic rings within melanin. The EPR signal can be influenced by redox processes, particularly by changes in pH (Szpoganicz et al., 2002). Some studies suggest that redox reactions involving heavy metals modulate the EPR signal, possibly due to physical and magnetic interactions between the metals and melanin (Żądło and Sarna, 2019). However, discrepancies exist regarding the

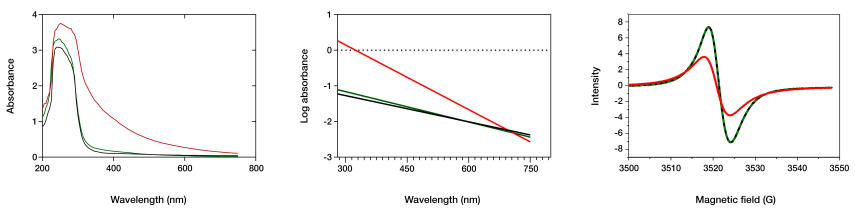

FIGURE 4
Spectral analysis of fungal (black line) and cephalopodal (green) melanin extracts, and of synthetic DOPA-melanin (red). Left: UV and visible absorbance raw spectra. Center: log plot of the negative linear slope absorbance region against the wavelength. Right: EPR spectral analysis.

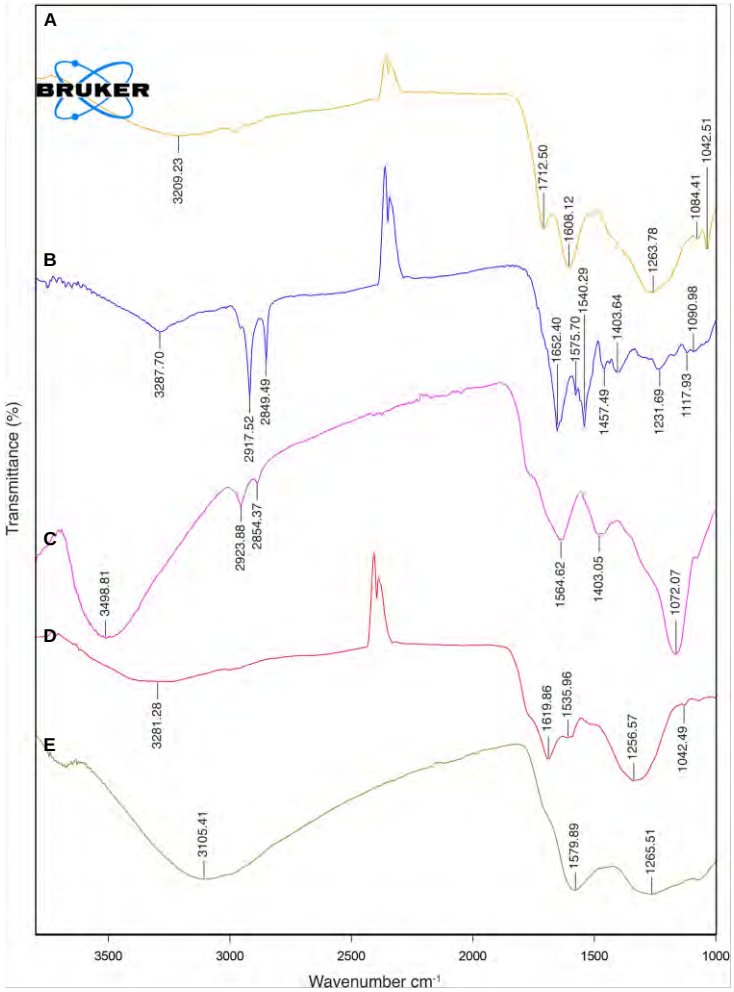

FIGURE 5
FTIR spectra: (A) synthetic DOPA-melanin, (B) natural fungal melanin, (C) natural fungal melanin/Cr(VI), (D) natural cephalopodal melanin and (E) natural cephalopodal melanin/Cr(VI).

mechanisms of free radical production at varying redox potentials (Szpoganicz et al., 2002). Notably, at high pH, some studies report a potential depletion of quinones, which are precursors for semiquinone formation (Meredith et al., 2006).

The FTIR spectra of natural melanin extracts (both fungal and cephalopodal) and of synthetic DOPA-melanin are coherent with the different melanin types they are assigned to (Figure 5). This analysis showed a broad adsorption peak at 3300–3000 cm^{-1}, which has been attributed to the stretching vibrations of the OH, NH, COO^- and phenolic groups that are characteristic of melanins in general (Barretto and Vootla, 2020). These broad bands peaked at 3288, 3281 and 3209 cm^{-1} for melanin extracts of *E. mesophila*, *S. officinalis*, and synthetic DOPA melanin, respectively. However, due to the peak overlap in this region, it is not possible to determine the exact contribution of each functional group. Interestingly, two high-intensity absorption bands at 2918–2849 cm^{-1} were observed exclusively with fungal melanin, which could be attributed to the vibration of aliphatic C–H stretching. Similar studies agree with these specificities of the FTIR profiling of fungal DHN-melanin (Pacelli et al., 2020; Elsayis et al., 2022) when compared to DOPA-melanin. In fact, the relatively lower abundance of aliphatic chains in DOPA-melanin, compared to DHN-melanin, could be a key distinction between these two melanin types.

The aromatic skeletal C=C ring stretching of amide I C=O and COO- groups was assigned at 1652–1620 cm^{-1} in fungal and cephalopodal melanins, while in synthetic DOPA-melanin, these functional groups were detected at 1608–1713 cm^{-1}, as seen previously (Watt et al., 2009; Zhan et al., 2011). The aromatic/pyrrole stretching vibration and indole ring vibration were observed at 1540 cm^{-1} and 1536 cm^{-1} in the fungal and cephalopodal melanin, respectively. However, synthetic DOPA-melanin did not show vibrations in these functional groups, which finding is consistent with previous reports, in that synthetic melanins do not exhibit indole ring bands (Watt et al., 2009; Zhan et al., 2011). Phenol groups' C–O or OH deformation of alcohol groups were characterized by peaks at 1232, 1257 and 1264 cm^{-1} in all melanin types. The presence of peaks near 1250 cm^{-1} has been reported in previous studies on melanin (Mbonyiryivuze et al., 2015;

Suwannarach et al., 2019). The FTIR spectrum of *E. mesophila* melanin is similar to that of melanin extracted from other black fungi such as *Hortaea werneckii* (Elsayis et al., 2022) and *Spissiomyces endophytica* (Suwannarach et al., 2019). Overall, the observed FTIR features demonstrate a strong resemblance of the analyzed samples to the typical spectral profiles of the melanin types they are associated to, concerning OH or NH, and C=O stretching or the phenolic group (Pralea et al., 2019). The high abundance of functional groups in the melanin structure contributes to the interesting properties and potential applications of this biomaterial.

In Table 1, the main physicochemical characteristics of the melanin types analyzed in this study have been summarized and compared with similar data from previous studies. While natural melanins extracted from *E. mesophila* and *S. officinalis* display a very similar spectrophotometric behavior when analyzed with UV-Vis and EPR techniques (Figure 4), they are clearly distinct in their origin and chemical structure, as shown by the FTIR profiling (Figure 5). Synthetic DOPA-melanin, on the other hand, is also quite different from sepia melanin, despite sharing the same precursor molecule. Synthetic melanins are usually purer and, depending on the manufacturing method, have a more uniform but generally less complex structure than their natural counterpart. These results suggest that similar environmental pressures might have caused the development of independent origins of melanin throughout evolution, but caused a convergence on similar functions, such as protection against UV or the adsorption of toxic metals. Whether or not melanins have evolved independently multiple times, or share a common ancestry with subsequent diversification and convergence driven by environmental pressures, is a matter that deserves further research.

3.3 Electrochemical characterization of melanin

The electrochemical characterization of fungal and cephalopodal melanin extracts using cyclic voltammetry (CV) revealed their redox properties within a potential interval from -1.00 to +0.50 V *vs.* Ag/AgCl and at a scanning rate of 10 mV s^{-1} on a gold SPE electrode. The comparison of CV responses on gold electrodes and in the absence/presence of both natural melanins revealed the existence of electrochemical interactions. The presence of melanin completely modified the interface of the electrode/solution, blocking the characteristic electrochemical fingerprint response originating from the adsorption/desorption of hydroxide anions (Hamelin et al., 1990). The voltametric response of melanin-covered gold electrodes resembled the CV obtained by González et al. (2011). Anodic and cathodic peaks appeared at different

TABLE 1 Summary of the main physicochemical properties of different types of melanins.

Melanin type	Source/ Species	λ max (nm)	Dlog A/l	EPR g-value	FTIR main peaks (cm^{-1})	Solubility	Reference
Fungal (DHN)	Biomass/ *Exophiala mesophila*	225	-0,0025	2.003	3288 2918 1652 1232	Insoluble: water, organic solvents Partly soluble: strong alkali, borate buffer	This study
	Biomass/ *Cryomyces antarcticus*	~215	-0.0027	2.004	2917 2843 1621 1024	Insoluble: water, organic solvents Soluble: strong alkali	Pacelli et al. (2020)
	Biomass/ *Hortaea werneckii*	240	n/a	n/a	3438 2927 1637 1240	Insoluble: water, most organic solvents Soluble: strong alkali, ethanol, methanol, dimethyl sulfoxide (upon vigorous mixing)	Elsayis et al. (2022)
Cephadophodal (DOPA)	Ink/ *Sepia officialis*	236	-0,0028	2.003	3281 1620 1536 1257	Insoluble: water, organic solvents Soluble: strong alkali, borate buffer	This study
		280	n/a	n/a	3100–3300 2920 1650 1200	n/a	Wang and Rhim (2019)
Bacterial (Untypified)	Biomass/ *Rhizobium radiobacter*	222	−0,0030	2.005	3277 2933 1514 1227	Insoluble: water, organic solvents, strong acids Soluble: strong alkali	Zajdo and Sarna (2019)
Synthetic (DOPA)	Commercial	~215	n/a	2.004	3360–3000 1621	Insoluble: water, organic solvents Soluble: strong alkali	Pacelli et al. (2020)

λ max, frequency of the maximum UV-VIS absorbance; Dlog A/l, log absorbance–wavelength slope; n/a, not available.

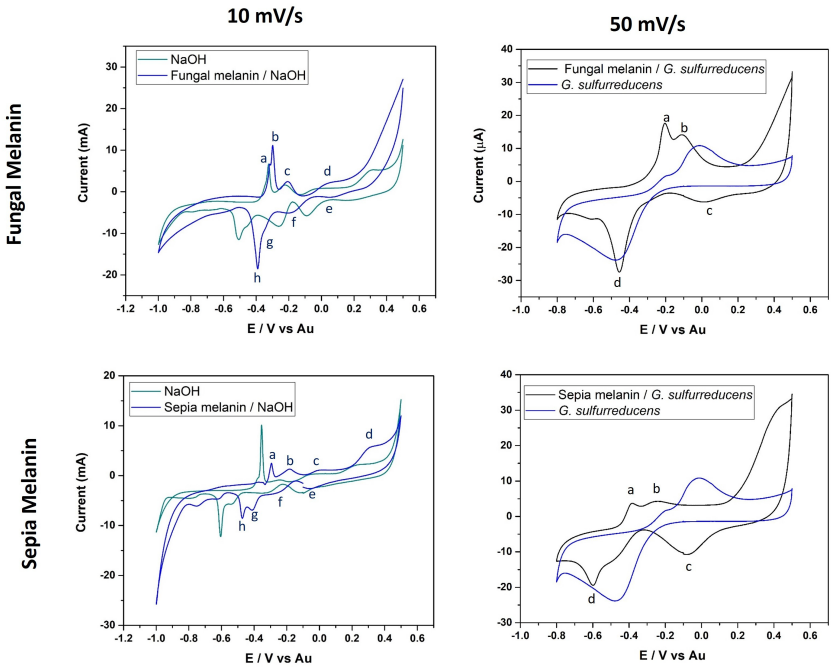

FIGURE 6
Cyclic voltammograms of fungal and cephalopodal melanin extracts, at a scan rate of 10 mV s^{-1} with 0.1 M NaOH, and a voltage range from −1.0 to +0.5 The scan rate 50 mV s^{-1} corresponds to natural fungal and cephalopodal melanin in contact with *fi. sulfurreducens*, with a voltage range from −0.8 to 0.5 V.

potentials, mainly due to the different electrode materials (highly oriented pyrolytic graphite (HOPG) instead Au) and reference electrode (SPE instead of Ag) used.

Regarding the electrochemical properties of the studied melanins, the synthetic DOPA-melanin exhibited a rather simple CV profile, with two redox couples observed at −0.28 V (cathodic) and -0.40 V (anodic), and a reversible couple at -0.18 V (results not shown). Instead, the fungal and cephalopodal melanins (Figure 6) revealed a complex CV with four redox couples appearing at 0.06 V (peaks d/e), −0.20 V (peaks c/f), −0.30 V (anodic) and −0.35 V (cathodic) (peaks b/g), and −0.32 V (anodic) and −0.39 V (cathodic) (peaks a/h). Notably, two redox couples (d/e and c/f) exhibited a reversible behavior at a relatively strong positive potential. In contrast, the other two couples (a/h and b/g) displayed a non-reversible behavior at slight positive potentials. The reversible redox couples can be assigned to oxidation/reduction processes involving quinone groups, which are typically present in melanin (Kumar et al., 2016), while the other two redox couples may correspond to processes related to the uptake of cations by melanin (González et al., 2011). It must be noted that the specific nature of both processes is highlighted by the different shapes of the voltametric peaks for each redox couple. The peaks associated with the oxidation/reduction of quinone groups are very broad, probably due to the different chemical environments surrounding these groups. In the case of the redox couples related to cation uptake, voltametric peaks are very sharp and narrow. There are slight differences between the CVs of fungal and cephalopodal melanin extracts, regarding the peak currents (Figure 6). The redox couple b/g of fungal melanin shows higher peak currents compared to the redox couple a/h. In the case of sepia melanin, the peak current of the redox couple a/h is comparable to that of the redox couple b/g, probably revealing a different mechanism for cation uptake. This singular behavior opens the door to exploring the sensitivity of each melanin type to different cations in the uptake process.

To provide more compelling evidence for redox cycling and potential interactions of natural melanins, melanin extracts of both *E. mesophila* and *S. officinalis* ink were combined with viable cells of the electroactive bacterium *Geobacter sulfurreducens* (GS) on a gold SPE electrode. The recorded voltametric currents were larger for the combination of natural melanin plus GS than with GS alone (at 50 mV s^{-1}), which points to the enhancement of extracellular electron transfer processes involving different compounds, such as quinones, catalyzed by the functional groups of melanins (Kumar et al., 2016). According to the CV of Figure 6, a broad anodic peak (b) appeared at −0.10 V in both melanin extracts, overlapping the potential at which the oxidation of quinone groups occurs. In the cathodic scans, broad peaks (d) were observed at −0.45 V and −0.6 V for fungal and cephalopodal melanins, which could be assigned to reduction processes. Tentatively, those peaks could be assigned to cation uptake processes because they appear in the same potential range in the absence of melanin. Nevertheless, the shape of the reduction wave points towards a reduction process involving hydroquinone, semiquinone, and quinone chemical structures identified previously in both melanins by EPR at 3524 G

(Figure 5_right). These oxidative species, especially semiquinone, can act as a sink for unpaired electrons, explaining the quenching activity of melanin on free radicals (Dadachova et al., 2008; Eom et al., 2019). It is interesting to note that, in the absence of melanin, the voltametric peaks for redox couples of quinone groups exhibited a very reversible behavior, in contrast with what is observed in the case of melanin/GS-coated electrodes. The explanation for this abnormal behavior can be found in the electroactive behavior of GS. At a potential of about −0.3V, GS can use electrodes as electron acceptors in its metabolism (Estevez-Canales et al., 2015). If quinones are involved in facilitating the extracellular electron transfer processes of GS, a reduction in quinones could be prevented when using GS as the electrode in an electron acceptor. Only when GS interacts with the electrode as an electron donor can the reduction in quinones be observed. Consequently, this process could explain the origin of the non-reversible behavior of the oxidation/reduction of quinone groups.

These results demonstrate that both types of melanins (fungal allomelanin and animal eumelanin) enhanced the bioelectroactivity of *Geobacter sulfurreducens*, despite their inherent chemical-structural differences. This phenomenon is likely due to the ability of melanin to act as a semiconductor, facilitating electron transfer between the organism and the electrode. The semiconducting nature of melanin holds promise for biotechnological applications, particularly in interspecies electron transfer and bioelectrode development (Kim et al., 2020).

3.4 Melanin–metal adsorption mechanisms

Samples of fungal and cephalopodal melanin extracts exposed to Cr(VI) were also analyzed by FTIR spectrometry (Figure 5). From the FTIR profiling of Cr(VI)-bound melanin extracts, it can be inferred that this phenomenon is governed by multiple processes, as illustrated in Figure 7. The obtained FTIR spectral profiles reveal enhanced vibrations in fungal melanin at 3499 and 1072. cm^{-1}, suggesting the involvement of aromatic, COO^-, and OH groups in Cr(VI) adsorption (Figure 5). Hydrogen bonding plays a primary role in the polarization of Cr(VI) ions, so theses peaks might be attributed to the attachment of Cr(VI) to OH groups (Kulkarni et al., 2013). The peak shift towards higher wavenumbers indicates the chemisorption of heavy metals onto the functional groups of melanin (Manirethan et al., 2018, 2020). The reduced intensity of the peaks at 2924 and 2854 cm^{-1} suggests a significant weakening of C−H vibrations due to the interaction between melanin and adsorbed Cr(VI).

The FTIR spectroscopic analysis of Cr(VI)-exposed melanin unveils intriguing alterations in its spectral profile. Specifically, the disappearance of absorption bands near 1650 cm^{-1}, previously attributed to the quinone C=O stretching of carboxylic groups (COOH) resulting from oxidation, signifies a significant change upon exposure to Cr(VI). Notably, fungal melanin exhibits a discernible decrease in C=O transmittance alongside the emergence of a distinct peak around 1550 cm^{-1} upon Cr(VI) exposure. This shift towards lower wavenumbers likely stems from the augmented electron density induced by Cr(VI) binding to adjacent functional groups within the melanin structure. This observed phenomenon resonates with established findings (Larsson, 1993; Manirethan et al., 2020). Furthermore, in contrast to treatments devoid of metal exposure, where various bands manifest in this region, the singular presence of this peak in Cr (VI) treatments suggests a complexation with the C=O functional group. The observed peak shift concurs with the notion of heightened electron density attributable to metal binding. This observation could also be attributed to precipitation and reduction processes occurring during the Cr(VI)−melanin interaction, as stated by Yang et al. (2023). The C=O stretching band serves as a dual indicator: firstly, for inferring the strength of the p bond within the carbonyl group, and secondly, for monitoring the Cr(VI) uptake process involving this functional group. These data suggest that Cr(VI) binding amplifies the electrostatic capacitance of melanin, a property that has been confirmed

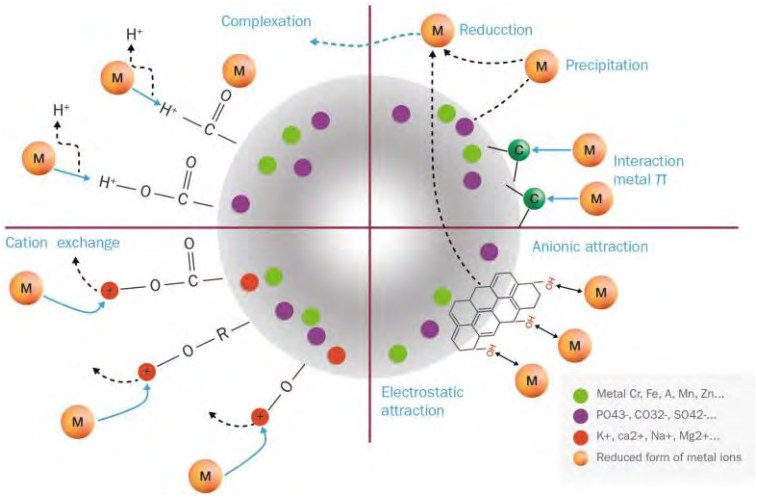

FIGURE 7
Proposed binding mechanisms of free Cr(VI) ions on an idealized melanin particle.

earlier through electrochemical characterization (Eom et al., 2019). This unique capacitance allows melanin to act as a semiconductor-like reservoir, facilitating the capture of unpaired electrons, as illustrated in Figure 7.

As for the sepia melanin (Figure 5), the shift of the OH absorption peak from 3105 cm^{-1} suggests the involvement of the carboxylic/phenolic hydroxyl group in the adsorption of Cr(VI). Alterations in the region 1240−1200 cm^{-1} further point to the role of the amine group in the adsorption process with this type of melanin. This observation aligns with previous reports (Liu et al., 2004; Liu and Simon, 2005; Di Mauro et al., 2017), in which sepia melanin is identified as a DOPA-melanin that contains nitrogenated functional groups (NH), in contrast to the nitrogen-free DHN-melanin, which seems to be the predominant type in *E. mesophila*.

3.5 Adsorption of hexavalent chromium onto fungal melanin

The Langmuir isotherm model (Figure 8) provides a more accurate description of Cr(VI) adsorption by melanin extracts of *Exophiala mesophila* (R^2 = 0.904) than the Freundlich isotherm (R^2 = 0.670). Table 1 summarizes the corresponding model parameters, in comparison with those from other similar studies. The Langmuir affinity constant seen here (K_L = 0.193 L mg^{-1}) was practically identical to the value we obtained previously by fitting experimental time-course adsorption data to a three-parameter model that integrated the Langmuir isotherm and second-order adsorption kinetics (Medina-Armijo et al., 2024). However, the modeled theoretical maximum Cr(VI) adsorption capacity obtained in this study (q_{max} = 19.37 mg g^{-1}) is lower than that which we obtained previously through dynamic experiments (q_{max} = 95.26 mg g^{-1}). Since equilibrium isotherms and kinetic models address different aspects of the adsorption process, the q_{max} values they estimate might not necessarily be the same, as seen previously by other authors (Fahry et al., 2023). The higher correlation of experimental adsorption data to the Langmuir isotherm, compared to the Freundlich isotherm, suggests that fungal melanin extracts present a monolayer with a finite distribution of active sites on the surface for the adsorption of Cr(VI) ions. In similar previous studies (Table 2), values for the q_{max} of melanin extracts ranged from 6.53 mg g^{-1} for sepia ink embedded in sodium alginate to 595.97 mg g^{-1} for crude melanin extracts of the black fungus

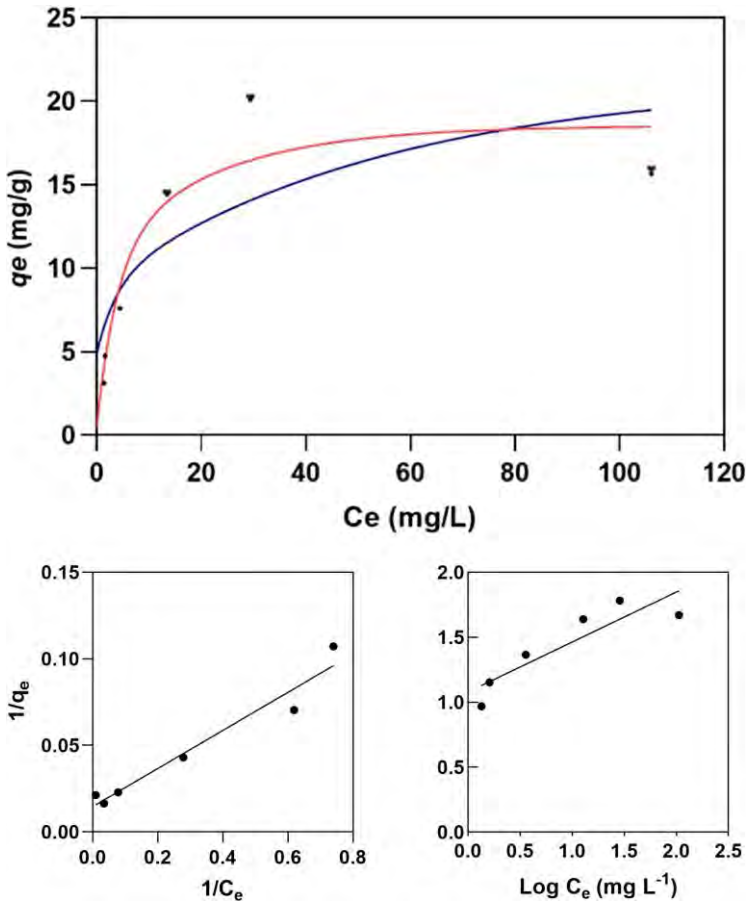

FIGURE 8
Langmuir (red line) and Freundlich (blue line) isotherm models for the adsorption of Cr(VI) on melanin (top graph) fitted to the experimental data (dots). Experimental conditions: initial Cr(VI) concentration 30 mg L^{-1}, melanin content 6 g L^{-1}, pH 6.5, temperature 25 °C.

Aureobasidium pullulans. However, these results must be analyzed and compared with caution, as the experimental conditions in which these assays have been conducted vary significantly, especially as regards the melanin content and extraction/functionalization procedure, as well as the pH, which both have a great impact on the adsorption process.

The parameter constants of the Freundlich isotherm K_F and n also provide useful information for a better understanding of the adsorption behavior. K_F corresponds to the Freundlich adsorption capacity, which reflects a combination of adsorption capacity and affinity, while the dimensionless n characterizes the heterogeneity of the system. For a viable adsorption process, the parameter n is usually greater than the unity, but the larger the n value is, the more heterogeneous the system is. When comparing this study with the limited literature on the melanin adsorption of Cr(VI) (Table 2), we find that the obtained K_F = 5.96 mg g^{-1} and n = 3.94 indicate that melanin extracted from the black fungus *E. mesophila* has a relatively high adsorption potential, despite being a comparatively heterogeneous adsorbent as well.

In summary, melanin's unique physicochemical properties—metal sorption capacity, resistance to acidic pH, and high-temperature stability—make it an attractive biomaterial for various environmental applications. Novel melanin-based nanoparticles have shown significant improvements in metal removal rates from polluted waters, compared to conventional methods (Tran-Ly et al., 2020b). Besides heavy metals, previous studies have shown melanin's capacity to bind diverse pollutants, including organic compounds and synthetic dyes (Lino et al., 2022). Such specific sorption capacity presents a promising avenue for the development of highly sensitive and selective sensors for heavy metals and other environmental contaminants (Steven et al., 2007). Melanin's electrochemical interactions with metal ions and other charged molecules offer new options for modulating electron transfer processes within microbial syntrophic communities that govern important bioprocesses such as methanogenesis (Sriphirom et al., 2021). The large-scale production of melanin and its regeneration after metal sorption are crucial for the economic viability and long-term sustainability of melanin-based treatments (Lino et al., 2022; Michael et al., 2023). Black fungi like *Exophiala mesophila* can easily be cultivated by common fermentation techniques, offering a new scalable source of melanin. However, the production of melanin for industrial applications also requires the optimization of melanin extraction techniques (Choi, 2021). While this study provides a preliminary insight into the characteristics and potential application of melanin from black fungi, further research efforts are warranted to develop efficient and cost-effective strategies for large-scale melanin production.

4 Conclusion

This study describes a detailed physicochemical characterization of melanin extracted from the metallotolerant black fungus *Exophiala mesophila* (Chaetothyriales). Based on inhibitory studies using the fungicide tricyclazole in relation to whole cells, as well as FTIR spectrometric analyses performed on melanin extracts in comparison to natural and synthetic DOPA-melanin, we conclude that this fungus produces melanin primarily via the DHN pathway. The electrochemical characterization of melanin extracts also demonstrated that this biomaterial exhibits semiconductor-like properties that may lead to interesting interactions between fungal melanin and other electroactive microorganisms. Based on these results and using Cr(VI) as a model heavy metal, we also conclude that the melanin–metal binding process primarily occurs through electrostatic interactions and cation exchange mechanisms. These findings pave the way for the development of novel biotechnological applications utilizing fungal melanin. Potential areas of exploration include the bioremediation of environmental pollutants, sensor development, nanoparticle synthesis, and bioelectrochemical processes.

TABLE 2 The absorption of Cr(VI) onto the fungal melanin powder used here, based on Langmuir and Freundlich parameters, and comparison with the results of previous studies.

Source	Matrix	Langmuir isotherm			Freundlich Isotherm			pH	Dosage (g L^{-1})	Reference
		q_{max} (mg g^{-1})	K_L (L mg^{-1})	R^2	K_F (mg g^{-1})	n	R^2			
Fungal biomass (*Exophiala mesophila*)	Melanin extracts	19.37	0.19	0.904	5.96	3.94	0.670	6.5	6.0	This study
Fungal biomass (*Exophiala mesophila*)	Melanin extracts	95.26	0.20	0.924	-	-	-	6.5	6.0	Medina-Armijo et al. (2024)
Fungal biomass (*Aureobasidium pullulans*)	Melanin extracts	595.97	0.04	0.986	1.91	1.55	0.959	5.0	0.1	Fahry et al. (2023)
Cephalopodous ink (*Sepia officinalis*)	Melanin embedded in sodium alginate	6.53	0.11	0.955	0.79	2.04	0.989	2.0	20	Cuong et al. (2018)
Bacterial biomass (*Peudomonas stutzeri*)	Melanin extracts	126.90	0.30	0.99	28.93	1.69	0.97	3.0	0.2	Manirethan et al. (2018)

Data availability statement

The raw data supporting the conclusions of this article will be made available by the authors, without undue reservation.

Author contributions

CM-A: Conceptualization, Data curation, Formal Analysis, Investigation, Methodology, Software, Writing – original draft, Writing – review & editing. IY: Methodology, Validation, Project administration, Writing – review & editing. AB: Methodology, Validation, Writing – review & editing. AP: Methodology, Validation, Writing – review & editing. AE-N: Methodology, Validation, Writing – review & editing. MV: Funding acquisition, Methodology, Project administration, Validation, Writing – review & editing. FP-B: Conceptualization, Project administration, Supervision, Writing – review & editing.

Funding

The author(s) declare that financial support was received for the research, authorship, and/or publication of this article. This research was funded by the Spanish Agencia Estatal de Investigación for funding (PID2019-111572RB-I00/AEI/10.13039/501100011033, MIC-RICE project), and the Consolidated Research Group SOSBIO (ref. 2021 SGR 01568) Generalitat de Catalunya).

Cristy Medina-Armijo was a recipient of the fellowship Agencia Nacional de investigación y Desarrollo (ANID) from Chile.

Acknowledgments

The FTIR experiments were performed at MIRAS beamline at ALBA Synchrotron with the collaboration of ALBA staff. The support of the CERCA Programme/Generalitat de Catalunya is also acknowledged.

Conflict of interest

The authors declare that the research was conducted in the absence of any commercial or financial relationships that could be construed as a potential conflict of interest.

Publisher's note

All claims expressed in this article are solely those of the authors and do not necessarily represent those of their affiliated organizations, or those of the publisher, the editors and the reviewers. Any product that may be evaluated in this article, or claim that may be made by its manufacturer, is not guaranteed or endorsed by the publisher.

References

Zado, A. C., and Sarna, T. (2019). Interaction of iron ions with melanin. *Acta Biochim. Pol.* 66, 459–462. doi: 10.18388/abp.2019_2889

Bárcena, A., Petroselli, G., Velasquez, S. M., Estévez, J. M., Erra-Balsells, R., Balatti, P. A., et al. (2015). Response of the fungus *Pseudocercospora griseola f. mesoamericana* to Tricyclazole. *Mycol. Prog.* 14. doi: 10.1007/s11557-015-1102-7

Barretto, D. A., and Vootla, S. K. (2020). Biological activities of melanin pigment extracted from Bombyx mori gut-associated yeast *Cryptococcus rajasthanensis* KY627764. *World J. Microbiol. Biotechnol.* 36, 1–17. doi: 10.1007/S11274-020-02924-0/metrics

Butler, M. J., Gardiner, R. B., and Day, A. W. (2009). Melanin synthesis by Sclerotinia sclerotiorum. *Mycologia* 101, 296–304. doi: 10.3852/08-120

Chen, S., Rotaru, A.-E., Shrestha, M., Malvankar, N. S., Liu, F., Fan, W., et al. (2014). Promoting interspecies electron transfer with biochar. *Sci Rep.* 4, 5019 doi: 10.1038/srep05019

Choi, K. Y. (2021). Bioprocess of microbial melanin production and isolation. *Front. Bioeng. Biotechnol.* 9. doi: 10.3389/fbioe.2021.765110

Cuong, A. M., Le, N. N. T., Thang, P. N., Diep, T. N., Thuy, L. B., Thanh, N. L., et al. (2018). Melanin-embedded materials effectively remove hexavalent chromium (CrVI) from aqueous solution. *Environ. Health Prev. Med.* 23, 1–11. doi: 10.1186/s12199-018-0699-y

Dadachova, E., Bryan, R. A., Howell, R. C., Schweitzer, A. D., Aisen, P., Nosanchuk, J. D., et al. (2008). The radioprotective properties of fungal melanin are a function of its chemical composition, stable radical presence and spatial arrangement. *Pigment Cell Melanoma Res.* 21, 192–199. doi: 10.1111/j.1755-148x.2007.00430.x

D'Alba, L., and Shawkey, M. D. (2019). Melanosomes: Biogenesis, properties, and evolution of an ancient organelle. *Physiol. Rev.* 99, 1–19. doi: 10.1152/physrev.00059.2017

Díaz, P., Gimeno, Y., Carro, P., González, S., Schilardi, P. L., Benítez, G., et al. (2005). Electrochemical self-assembly of melanin films on gold. *Langmuir* 21, 5924–5930. doi: 10.1021/la0469755

Di Mauro, E., Xu, R., Soliveri, G., Santato, C., Physics, E., and Montréal, P. (2017). Natural melanin pigments and their interfaces with metal ions and oxides: emerging concepts and technologies. *MRS Commun.* 7, 141–151. doi: 10.1557/mrc.2017.33

Eisenman, H. C., and Casadevall, A. (2012). Synthesis and assembly of fungal melanin. *Appl. Microbiol. Biotechnol.* 93, 931–940. doi: 10.1007/S00253-011-3777-2/figures/2

Elsayis, A., Hassan, S. W. M., Ghanem, K. M., and Khairy, H. (2022). Optimization of melanin pigment production from the halotolerant black yeast *Hortaea werneckii* AS1 isolated from solar salter in Alexandria. *BMC Microbiol.* 22, 1–16. doi: 10.1186/s12866-022-02505-1

Enochs, W. S., Nilges, M. J., and Swatz, H. M. (1993). A standardized test for the identification and characterization of melanins using electron paramagnetic resonance (EPR) Spectroscopy. *Pigment Cell Res.* 6, 91–99. doi: 10.1111/j.1600-0749.1993.tb00587.x

Eom, T., Jeon, J., Lee, S., Woo, K., Eun Heo, J., Martin, D. C., et al. (2019). Naturally derived melanin nanoparticle composites with high electrical conductivity and biodegradability. *Part. Part. Syst. Charact.* 2019, 36, 1900166. doi: 10.1002/ppsc.201900166

Estevez-Canales, M., Berná, A., Borjas, Z., Esteve-Núñez, A., and Sato, C. (2015). Screen-printed electrodes: New tools for developing microbial electrochemistry at microscale level. *Energies.* 8, 13211–13221. doi: 10.3390/en81112366

Fahry, Kh., Ghoniem, A. A., Al-Otibi, F. O., Helmy, Y. A., El Hersh, M. S., Elattar, K. M., et al. (2023). A comparative study of Cr(VI) sorption by *Aureobasidium pullulans* AKW biomass and its extracellular melanin: Complementary modeling with equilibrium isotherms, kinetic studies, and decision tree modeling. *Polymers (Basel).* 15, 3754. doi: 10.3390/polym15183754

Gonçalves, R. C. R., Lisboa, H. C. F., and Pombeiro-Sponchiado, S. R. (2012). Characterization of melanin pigment produced by *Aspergillus nidulans*. *World J. Microbiol. Biotechnol.* 28, 1467–1474. doi: 10.1007/s11274-011-0948-3

González, O. A., Grumelli, D., Vericat, C., Ramallo-López, J. C., Giovanetti, L., Benitez, G., et al. (2011). Naked gold nanoparticles supported on HOPG: melanin functionalization and catalytic activity. *Nanoscale* 3, 1708–1716.

Hamelin, A., Sottomayor, M. J., Silva, F., Chang, S. C., and Weaver, M. J. (1990). Cyclic voltammetric characterization of oriented monocrystalline gold surfaces in aqueous alkaline solution. *J. Electroanal. Chem. Interfacial Electrochem.* 295, 291–300. doi: 10.1016/0022-0728(90)85023-X

Jacobson, E. S., and Tinnell, S. B. (1993). Antioxidant function of fungal melanin. *J. Bacteriol.* 175, 7102–7104. doi: 10.1128/jb.175.21.7102-7104.1993

Karimi, F., Shaabani, E., Martıńez-Rovira, I., Yousef, I., Ghahremani, M. H., and Kharrazi, S. (2021). Infrared microspectroscopy studies on the protective effect of curcumin coated gold nanoparticles against H_2O_2-induced oxidative stress in human neuroblastoma SK-N-SH cells. *Analyst.* 146, 6902–6916. doi: 10.1039/dian01379c

Kim, E., Panzella, L., Napolitano, A., and Payne, G. F. (2020). Redox activities of melanins investigated by electrochemical reverse engineering: implications for their roles in oxidative stress. *J. Invest. Dermatol.* 140, 537–543. doi: 10.1016/j.jid.2019.09.010

Kong, Q., Yu, X., Song, D., and Ren, X. (2018). Effect of tricyclazole on morphology, virulence and gene expression of Aspergillus aculeatus for management of soft rot disease in peach. *J Appl Microbiol.* 125, 1827–1835 doi: 10.1111/jam.14076

Kulkarni, G. B., Nayak, A. S., Mashetty, S. B., and Karegoudar, T. B. (2013). Properties and functions of melanin pigment from *klebsiella* sp. GSK. *Korean J. Microbiol. Biotechnol.* 41, 60–69. doi: 10.4014/kjmb.1210.10002

Kumar, M., Chand, R., Dubey, R. S., and Shah, K. (2015). Effect of Tricyclazole on morphology, virulence and enzymatic alterations in pathogenic fungi Bipolaris sorokiniana for management of spot blotch disease in barley. *World J. Microbiol. Biotechnol.* 31, 23–35. doi: 10.1007/s11274-014-1756-3

Kumar, P., Di Mauro, E., Zhang, S., Pezzella, A., Soavi, F., Santato, C., et al. (2016). Melanin-based flexible supercapacitors. *J. Mater. Chem. C* 4, 9516–9525. doi: 10.1039/C6TC03739A

Kumar, C. G., Mongolla, P., Pombala, S., Kamle, A., and Joseph, J. (2011). Physicochemical characterization and antioxidant activity of melanin from a novel strain of *Aspergillus bridgeri* ICTF-201. *Lett. Appl. Microbiol.* 53, 350–358. doi: 10.1111/j.1472-765X.2011.03116.x

Larsson, B. S. (1993). Interaction between chemicals and melanin. *Pigment Cell Res.* 6, 127–133. doi: 10.1111/j.1600-0749.1993.tb00591.x

Lee, J. K., Jung, H. M., and Kim, S. Y. (2003). 1,8-Dihydroxynaphthalene (DHN)-melanin biosynthesis inhibitors increase erythritol production in *Torula corallina*, and DHN-melanin inhibits erythrose reductase. *Appl. Environ. Microbiol.* 69, 3427–3434. doi: 10.1128/aem.69.6.3427-3434.2003

Lino, V., Castaldo, R., Gentile, G., and Manini, P. (2022). Reusable melanin-based biosorbents for efficient methylene blue removal: the new frontier of fungi-inspired allomelanin coatings for sustainable water remediation processes. *MTS.* 21, 2589–2347. doi: 10.1016/j.mtsust.2022.100283

Liu, Y., and Simon, J. D. (2005). Metal–ion interactions and the structural organization of Sepia eumelanin. *Pigment Cell Res.* 18, 42–48. doi: 10.1111/j.1600-0749.2004.00197.x

Lovley, D. R., and Phillips, E. J. P. (1988). Novel mode of microbial energy metabolism: organic carbon oxidation coupled to dissimilatory reduction of iron or manganese. *Appl. Environ. Microbiol.* 54, 1472–1480. doi: 10.1128/aem.54.6.1472-1480.1988

Manirethan, V., Gupta, N., Balakrishnan, R. M., and Raval, K. (2020). Batch and continuous studies on the removal of heavy metals from aqueous solution using biosynthesised melanin-coated PVDF membranes. *Environ. Sci. pollut. Res.* 27, 24723–24737. doi: 10.1007/S11356-019-06310-8/figures/12

Manirethan, V., Raval, K., Rajan, R., Thaira, H., and Balakrishnan, R. M (2018). Kinetic and thermodynamic studies on the adsorption of heavy metals from aqueous solution by melanin nanopigment obtained from marine source: *Pseudomonas stutzeri*. *J. Environ. Manage.* 214, 315–324. doi: 10.1016/j.jenvman.2018.02.084

Martıńez-Rovira, I., Seksek, O., Puxeu, J., Gómez, J., Kreuzer, M., Dučić, T., et al. (2019). Synchrotron-based infrared microspectroscopy study on the radiosensitization effects of Gd nanoparticles at megavoltage radiation energies. *Analyst* 144, 5511–5520. doi: 10.1039/c9an00792j

Mbonyiryivuze, A., Mwakikunga, B., Dhlamini, S. M., and Maaza, M. (2015). Fourier transform infrared spectroscopy for sepia melanin. *Phys. Mater. Chem.* 3, 25–29. doi: 10.12691/pmc-3-2-2

Medina-Armijo, C., Isola, D., Illa, J., Puerta, A., Viñas, M., and Prenafeta-Boldú, F. X. (2024). The metallotolerance and biosorption of As(V) and Cr(VI) by black fungi. *J. Fungi.* 10, 47. doi: 10.3390/jof10010047

Meredith, P., Powell, B. J., Riesz, J., Nighswander-Rempel, S. P., Pederson, M. R., and Moore, E. G. (2006). Towards structure–property–function relationships for eumelanin. *Soft Matter.* 2, 37–44. doi: 10.1039/B511922G

Michael, H. S. R., Subiramanian, S. R., Thyagarajan, D., Mohammed, N. B., Saravanakumar, V. K., Govindaraj, M., et al. (2023). Melanin biopolymers from microbial world with future perspectives—a review. *Arch. Microbiol.* 205, 1–24. doi: 10.1007/s00203-023-03642-5

Mostert, A. B. (2021). Melanin, the what, the why and the how: an introductory review for materials scientists interested in flexible and versatile polymers. *Polymers (Basel).* 13, 1670. doi: 10.3390/polym13101670

Pacelli, C., Cassaro, A., Maturilli, A., Timperio, A. M., Gevi, F., Cavalazzi, B., et al. (2020). Multidisciplinary characterization of melanin pigments from the black fungus *Cryomyces antarcticus*. *Appl. Microbiol. Biotechnol.* 104, 6385–6395. doi: 10.1007/S00253-020-10666-0/metrics

Pal, A. K., Gajjar, D. U., and Vasavada, A. R. (2014). DOPA and DHN pathway orchestrate melanin synthesis in Aspergillus species. *Med. Mycol.* 52, 10–18. doi: 10.3109/13693786.2013.826879

Panzella, L., Gentile, G., D'Errico, G., Della Vecchia, N. F., Errico, M. E., Napolitano, A., et al. (2013). Atypical structural and p-electron features of a melanin polymer that lead to superior free-radical-scavenging properties. *Angew. Chemie Int. Ed.* 52, 12684–12687. doi: 10.1002/anie.201305747

Pavan, M. E., López, N. I., and Pettinari, M. J. (2019). Melanin biosynthesis in bacteria, regulation and production perspectives. *Appl. Microbiol. Biotechnol.* 104, 1357–1370. doi: 10.1007/S00253-019-10245-Y

Pralea, I. E., Moldovan, R. C., Petrache, A. M., Ilieș, M., Heghеș, S. C., Ielciu, I., et al. (2019). From extraction to advanced analytical methods: the challenges of melanin analysis. *Int. J. Mol. Sci.* 20. doi: 10.3390/ijms20163943

Prenafeta-Boldú, F. X., de Hoog, G. S., and Summerbell, R. C. (2019a). "Fungal communities in hydrocarbon degradation," in *Microbial communities utilizing hydrocarbons and lipids: members, metagenomics and ecophysiology* (Springer International Publishing), 1–36. doi: 10.1007/978-3-319-60063-5_8-2

Prenafeta-Boldú, F. X., Roca, N., Villatoro, C., Vera, L., and de Hoog, G. S. (2019b). Prospective application of melanized fungi for the biofiltration of indoor air in closed bioregenerative systems. *J. Haz. Mat* 361, 1–9. doi: 10.1016/j.jhazmat.2018.08.059

Prota, G. (1992). *Melanins and melanogenesis* (San Diego, CA, USA: Academic Press).

Roy, S., and Rhim, J.-W. (2021). New insight into melanin for food packaging and biotechnology applications. *Crit. Rev. Food Sci. Nutr.* 62, 4629–4655. doi: 10.1080/10408398.2021.1878097

Selvakumar, P., Rajasekar, S., Periasamy, K., and Raaman, N. (2008). Isolation and characterization of melanin pigment from *Pleurotus cystidiosus* (telomorph of *Antromycopsis macrocarpa*). *World J. Microbiol. Biotechnol.* 24, 2125–2131. doi: 10.1007/s11274-008-9718-2

Smith, D. F. Q., and Casadevall, A. (2019). The role of melanin in fungal pathogenesis for animal hosts. *Curr. Top. Microbiol. Immunol.* 422, 1–30. doi: 10.1007/82_2019_173

Sriphirom, P., Chidthaisong, A., Yagi, K., Tripetchkul, S., Boonapatcharoen, N., and Towprayoon, S. (2021). Effects of biochar on methane emission, grain yield, and soil in rice cultivation in Thailand. *Carbon Manage.* 12, 109–121. doi: 10.1080/17583004.2021.1885257

Steven, G., Wang, M.-T., Su, C.-W., Chen, Y.-S., and Hong, M.-Y. (2007). Picogram detection of metal ions by melanin-sensitized piezoelectric sensor. *Biosens. Bioelectron.* 23, 319–325. doi: 10.1016/j.bios.2007.04.011

Suryanarayanan, T. S., Ravishankar, J. P., Venkatesan, G., and Murali, T. S. (2004). Characterization of the melanin pigment of a cosmopolitan fungal endophyte. *Mycol. Res.* 108, 974–978. doi: 10.1017/S0953756204000619

Suwannarach, N., Kumla, J., Watanabe, B., Matsui, K., and Lumyong, S. (2019). Characterization of melanin and optimal conditions for pigment production by an endophytic fungus, *Spissiomyces endophytica* SDBR-CMU319. *PloS One* 14. doi: 10.1371/journal.pone.0222187

Szpoganicz, B., Gidanian, S., Kong, P., and Farmer, P. (2002). Metal binding by melanins: studies of colloidal dihydroxyindole-melanin, and its complexation by Cu(II) and Zn(II) ions. *J. Inorg. Biochem.* 89, 45–53. doi: 10.1016/S0162-0134(01)00406-8

Tran, M. L., Powell, B. J., and Meredith, P. (2006). Chemical and structural disorder in eumelanins: A possible explanation for broadband absorbance. *Biophys. J.* 90, 743–752. doi: 10.1529/biophysj.105.069096

Tran-Ly, A. N., Reyes, C., Francis,, Schwarze, W. M. R., and Ribera, J. (2020a). Microbial production of melanin and its various applications. *World J. Microbiol. Biotechnol.* 36, 170. doi: 10.1007/s11274-020-02941-z

Tran-Ly, A. N., Ribera, J., Schwarze, F. W. M. R., Brunelli, M., and Fortunato, G. (2020b). Fungal melanin-based electrospun membranes for heavy metal detoxification of water. *Sustain. Mater. Technol.* 23, e00146. doi: 10.1016/j.susmat.2019.e00146

Wang, L. F., and Rhim, J. W. (2019). Isolation and characterization of melanin from black garlic and sepia ink. *LWT* 99, 17–23. doi: 10.1016/J.LWT.2018.09.033

Watt, A. A. R., Bothma, J. P., and Meredith, P. (2009). The supramolecular structure of melanin. *Soft Matter* 5, 3754–3760. doi: 10.1039/b902507c

Yang, H., Kim, N., and Park, D. (2023). Superior removal of toxic cr(VI) from wastewaters by natural pine bark. *Sep.* 10, 430. doi: 10.3390/separations10080430

Zhan, F., He, Y., Yang, Y., Li, Y., Li, T., and Zhao, Z. (2016). Effects of tricyclazole on cadmium tolerance and accumulation characteristics of a dark septate endophyte (DSE), *exophiala pisciphila*. *Bull. Environ. Contam. Toxicol.* 96, 235–241. doi: 10.1007/s00128-015-1676-4

Zhan, F., He, Y., Zu, Y., Li, T., and Zhao, Z. (2011). Characterization of melanin isolated from a dark septate endophyte (DSE), *Exophiala pisciphila*. *World J. Microbiol. Biotechnol.* 27, 2483–2489. doi: 10.1007/s11274-011-0712-8

Chapter 5

Biochemical and transcriptomic response of the metallotolerant black fungus *Exophiala mesophila* upon exposure to toxic concentrations of As(V) and Cr(VI)

Part of this chapter was presented as an oral contribution in the Sociedad de Microbiología de Chile (SOMICH) 2023 conference.

Biochemical and transcriptomic response of the metallotolerant black fungus *Exophiala mesophila* upon exposure to toxic concentrations of As(V) and Cr(VI)

Cristy Medina-Armijo[1], Ibraheem Yousef[2], Francesc X. Prenafeta-Boldú[1].

[1]Program of Sustainability in Biosystems, Institute of Agrifood Research and Technology (IRTA), Caldes de Montbui, Catalonia, Spain.

[2] ALBA Synchrotron Light Source, Cerdanyola del Vallés, Catalonia, Spain.

Abstract

Exophiala mesophila is a filamentous black fungus in the Chaetothyriales order that exhibits remarkable biochemical and metabolic adaptability to toxic chemicals. This fungus displays exceptional tolerance to high concentrations of heavy metals and metalloids (HMMs) like arsenic As(V) and chromium Cr(VI). This study investigated the overall biochemical and transcriptomic response of *E. mesophila* to HMM stress. A combined approach using SR-FTIR spectroscopy (analyzing functional group intensity) and RNA-sequencing (RNA-seq) was employed. RNA-seq was performed on *E. mesophila* cultures grown under As/Cr)-free and (As/Cr)-stressed conditions. The analysis identified 572 differentially expressed genes (DEGs) upon HMM exposure. Approximately 40% (228 unigenes) were associated with 10 established HMM tolerance pathways. These pathways included metal ion handling, organic acid metabolism, ROS scavenging, and DNA repair, all crucial for *E. mesophila's* extreme As/Cr tolerance. Biochemical analyses revealed changes in protein, lipid, and DNA in HMM-exposed cells, supporting the RNA-seq data. These findings suggest a coordinated strategy involving both extracellular and intracellular mechanisms for enhanced HMM tolerance. Furthermore, using tricyclazole, a DHN-melanin inhibitor, alongside HMM exposure resulted in significant changes in phosphodiester and protein molecules. This indicates an oxidative stress response with ROS generation and potential membrane disruptions, ultimately leading to cell lysis in melanin-deficient cells exposed to HMMs. This study is the first to explore the *E. mesophila* transcriptome under As/Cr stress. The findings provide valuable insights for future molecular studies on HMM tolerance mechanisms in fungi.

Keywords: *Exophiala mesophila*, fungal melanin, tricyclazole, supramolecular structure, transcriptomics, metallotolerance, genomics, proteomics, SR-FTIR

1. Introduction

The genus *Exophiala* is a polyphyletic group within the family Herpotrichiellaceae (order Chaetothyriales) that exhibits a remarkable ecophysiological adaptability. *Exophiala* species are often dimorphic, transitioning between yeast-like budding cells and filamentous hyphae depending on the growth conditions. This morphological flexibility allows them to thrive in diverse environments, as evidenced by the isolation of clinical specimens (Woo et al., 2013; Usuda et al., 2021), from plant and animal tissue (de Hoog et al., 2011; Zhan et al., 2011), and from a wide variety of habitats that are characterized by extreme temperature, pressure, radiation, salinity, or pH level (ref). An increasing number of *Exophiala* strains have also been isolated from sites that are polluted with heavy metals and metalloids, such as creosoted wood and arsenic mine tailings (Seyedmousavi et al., 2011), from roots of plants (dark septate endophytes) that grow on soils from a lead-zinc mine smelting site (Zhang et al., 2008), and . Several *Exophiala* species have been found to grow and alkylbenzenic hydrocarbons as the sole source of carbon and energy (Prenafeta-Boldu, et al., 2006)

Recently, we screened a collection of black fungi isolated from hydrocarbon-rich environments, which comprised several *Exophiala* species, for their tolerance to pentavalent arsenic (As(V)) and hexavalent chromium (Cr(VI)) (Medina-Armijo et al., 2024). The *Exophiala mesophila* strain IRTA M2-F10 isolated from glued ceramics was found to have a remarkable metalotolerance, with an IC50 values of 6.03 g As^{5+} L^{-1} and 0.05 g Cr^{6+} L^{-1}. The type of strain of *E. mesophila* was isolated from silicone seals in the shower room of a hospital ward, and described by Listemann and Freiesleben (1996). Additional strains belonging to this species have been isolated from a variety of synthetic materials and environments often exposed to toxic chemicals, such as dental unit waterlines treated with chemical biocides (Porteous et al., 2003) domestic wet cells and swimming pools (Blasi et al. 2015). This latter study also verified the capacity of a *E. mesophila* strain isolated from a human host to assimilate toluene as the sole source of carbon and energy. Such hydrocarbonoclastic-opportunistic dual ecology is characteristic from several species in the genus *Exophiala* (Isola et al., 2021). However, the inability of *E. mesophila* to grow at 37 °C impairs its potential virulence so that this fungus is currently classified under the biosafety 1 level (de Hoog et al., 2003).

A subsequent physicochemical characterization of the melanin from *E. mesophila* suggested that this biopolymer may play a relevant role in conferring metalotolerance, either by the direct biosorption of the toxic metals and/or of secondary stress metabolites such as reactive oxygen species (Medina-Armijo et al., 2024b). This later study concluded that the melanin of *E. mesophila* was synthesized from 1,8-dihydroxynaphthalene as the primary building block (DHN-melanin), and that the mechanisms of melanin-metal biosorption involve a complex interplay of functional groups (OH, COOH, C=O) cross-linked into a rigid structure within the melanin amorphous scaffold. Furthermore, the extended aromatic chains of melanin act as chromophores and exhibit a high capacity for electromagnetic interactions due to the formation of π-bonds (Díaz et al., 2005). These attributes have garnered significant interest in black fungi like *Exophiala* spp. due to their potential applications in bioremediation processes (Tran-Ly et al., 2020)(Medina-Armijo et al., 2024a). Despite the well-established protective role of melanin in black fungi, the underlying mechanisms of their remarkable tolerance to high levels of heavy metal and metalloid contamination remain an intriguing area of scientific inquiry. The high intra and interspecific variability seen previously in the metalotolerance of a collection of *Exophiala* spp., displaying similar apparent levels of melanization, suggest that other mechanisms that contribute to the tolerance of toxic metals, may also be expressed (Medina-Armijo et al., 2024b) These additional

mechanisms likely encompass the expression of novel proteins, and a coordinated metabolic response that can trigger host-regulating processes, transport mechanisms, DNA repair, and other stress-response pathways.

In this study, we implemented a combined analysis approach to comprehensively investigate the biochemical profile of whole cells using synchrotron radiation-based Fourier-transform infrared spectroscopy (SR-FTIR) and gene expression changes in *E. mesophila* upon exposure to high concentrations of As(V) and Cr(VI). To elucidate the specific role of melanin in metalotolerance mechanisms, this study also incorporated the inhibition of DHN-melanin biosynthesis by using tricyclazole alongside exposure to toxic metalloids. This approach allows for a biochemical analysis of *E. mesophila* with suppressed melanin production.

2. Material and methods

2.1 Fungi strain and cultivation conditions

The fungus *Exophiala mesophila* strain IRTA M2-F10 isolated previously (Medina-Armijo et al., 2024), was used for the metal exposure experiments and the inhibiton DHN-melanin using tricyclazole. Agar plugs of fungal colonies growing on PDA agar (Condalab, Spain) at 25°C were used as inocula for the production of fungal biomass in 100 mL of sterilized liquid medium: yeast extract (4 g L^{-1}) was supplied as the carbon and energy source, and macronutrients were added as 4.5 g KH_2PO_4, 0.5 g K_2HPO_4, 2.0 g NH_4Cl, and 0.1 mg $MgSO_4 \cdot 7H_2O$, per litre. Mineral micronutrients were added as 2 mL of a stock solution that contained 120 mg $FeCl_3$, 50 mg H_3BO_3, 10 mg $CuSO_4 \cdot 5H_2O$, 10 mg KI, 45 mg $MnSO_4 \cdot H_2O$, 20 mg $Na_2MoO_4 \cdot H_2O$, 75 mg $ZnSO_4 \cdot H_2O$, 50 mg $CoCl_2 \cdot 6H_2O$, 20 mg $AlK(SO_4)_2 \cdot 12H_2O$, 13.25 g $CaCl_2 \cdot H_2O$, and 10 g NaCl, per litre. Incubations were performed in the dark at 25 °C under shaking at 120 rpm for two weeks. Fungal biomass was then harvested from 1.5 mL of the cultures in exponential phase (10^6 CFU mL^{-1}) by centrifugation at 9391 g for 5 min. The pellet was washed with ultrapure sterilized water and used for the metal/melanin inhibitor exposure assays.

2.2 In-vitro metal exposure assays of fungal cells

Fungal cell suspensions of E. mesophila were incubated with 5 g L−1 of As(V) and 1 g L−1 of Cr(VI), supplied as HAsNa2O4+7H2O (Thermo Fisher Scientific, Kandel, Germany) and K2Cr2O (Scharlab ExpertQ®, Spain), respectively. These concentrations correspond to the As(V) and Cr(VI) IC50 values determined previously for *E. mesophila* (Medina-Armijo et al., 2024b), and so they are expected to cause significant alterations of the normal fungal metabolism. Fungal incubation were perfomed in serum flasks filled (10 mL final volume) with a buffered (35 mM $K_2HPO_4/NaH_2PO_4+2H_2O$, pH 7) mineral medium amended with glucose (0.3 %) and yeast extract (0.01 %), similar to what has previously been described (Medina-Armijo et al., 2024). A second set of fungal incubation batches also contained tricyclazole (chemical name, provider), in addition to equivalent conentrations of As(V) and Cr(VI). Tricyclazole was supplied as an ethanol solution (50 μg L−1 final concentration) to liquid fungal cells suspensions, as previously described (Medina-armijo, n.d.). In summary, four fungal incubation conditions were prepared and each of them was carried out in triplicate: unexposed melanized control cells (C1), hyaline (tricyclazole-inhibited) control cells (C2), melanized cells exposed to As(V) (T1) and Cr(VI) (T2), and hyaline (tricyclazole-inhibited) cells exposed to As(V) (T3) and Cr(VI) (T4). After 6 days of incubation at

25°C at 120 rpm, the cell suspensions were immediately fixed for interrupting fungal growth (details on the fixation medium). For the SR-FTIRM profiling of the fungal cells, the fixed medium was removed by centrifugation at 9391 g for 5 min at 4°C, rinsing the pellets with water and by resuspend them with 1% formalin (Sigma Aldrich, Saint Louis, USA). The final cell suspensions were kept at 4°C until use. All used chemical and reagents were of analytical grade.

2.3 R-FTIRM measurements and data analysis

Stored cell suspensions were centrifuged at 9391 g for 5 min at 4°C and the pellet was washed three times in sterile water. The resulting cell suspension was deposited on infrared transparent calcium fluoride (CaF_2) cover glasses. SR-FTIRM measurements were performed at the infrared beamline MIRAS of the ALBA-CELLS synchrotron light source using a Hyperion 3000 microscope coupled to a Vertex 70 spectrometer (Bruker, Germany). The microscopy opening was equipped with a 36x Schwarzschild magnification objective (NA=0.65) and a cadmium telluride 50 μm MCT detector. All spectra were obtained using a single masking aperture size 15 x 15 μm, covering the full cell size. Single point maps of individual cells were collected in the 4000-900 cm−1 mid-infrared range at 4 cm−1 spectral resolution with 256 co-added scans per spectrum. A background measurement was performed on the CaF_2 slides without cells, with 10 repeated measurements. The absorbance spectrum was obtained by subtracting the reference spectrum from the raw cells. The subtraction data and was done directly (automatically) using the OPUS 7.5 software (Bruker, Germany), according to (Medina-Armijo,et al., 2024a.; Martínez-Rovira et al., 2019).

The SR-FTIR spectral features were evaluated by Principal Component Analysis (PCA) using the Unscrambler X program (CAMO Software AS, Norway). PCA was performed on vector normalized second derivative spectra (Savitzky–Golay algorithm; 3rd polynomial order). The normalization (standard normal variate SNV) and PCA were applied separately in the 3100–2800 cm−1 and 1800–1000 cm−1 spectral regions. Raw spectra were corrected following the rubber band method (32 baseline points) using the OPUS 7.5 software. The following bans/regions were evaluated: methyl asymmetric stretching: 2980–2945 cm−1 (CH_3); methylene asymmetric stretching: 2945–2900 cm−1 (CH_2); amide I: 1710–1598 cm−1 (AI); amide II: 1590–1483 cm−1 (AII); phosphate I: 1270–1186 cm−1 (PhI); phosphate II: 1146–1004 cm−1 (PhII). The total area under the spectra (except for the 2800–1800 cm−1 region) was associated with the total cell biomass (Cell) following previous studies (Yousef et al., 2016; H. Valido et al., 2020).

2.4 Transcriptomic analysis

Fixed cell suspensions of *Exophiala mesophila* for each of the treatments were centrifuged at 4 °C and 9391 g for 10 min, and the pellets were stored at -80 °C. The total RNA of each pellet was extracted using the Trizol reagent (Invitrogen, USA), followed by the treatment of total RNA with Rnase-free Dnase I (Merck KgaA, Darmstadt, Germany) with prior homogenization (30 s 30Hzgx2). The quality of the extracted RNA was verified by using a 2100 Bioanalyzer (Agilent, CA, USA), by checking the UV absorbance ratios at the wavelengths (nm) 260/280 ≥ 1.8 and 260/230 ≥ 1.6. At least, 1 mg of RNA from each sample was used for RNA-Seq. The construction of sequencing libraries from their respective total mRNA were sequenced using an Illumina NextSeq (150x2 bp). Quality control of raw demultiplexed forward and reverse reads was performed using multiple tools. Briefly, descriptive stats of read-quality were calculated using FastQC v0.11.8 (Andrews., 2012) and summarised with MultiQC v1.0 (Ewels et al. 2016), and

adapters in 5′ ends were removed using Trimmomatic v0.39 (Bolger et al., 2014). Paired reads were mapped against *Exophiala mesophila* strain CBS 40295 reference genome using STAR v2.7.10.a (Dobin et al., 2013). Qualimap v.2.2.2 (García-Alcalde et al., 2012) was used to perform the quality control of the mapping and transcript quantification was estimated using feature Counts v1.6.4 (Liao et al., 2014). The subsequent analyses fo the obtained libraries were conducted with the assistance of Microomics Systems S.L. (Barcelona, Spain).

2.5 Enrichment analysis of diferentially expressed genes

The clean reads for each sample library were aligned back to the constructed transcriptome assembly using Ensembl Fungi browser 111 (Benson et al., 2018, Benson et al., 2013). The script align_and_estimate_abundance.pl in DESeq2 v1.36.0 (in R) program was used to identify the differentially expressed genes (DEGs) given an adjusted p-value < 0.05 and a log2fold change > 1 as a threshold for 6ignificant diferential expression (Love et al., 2014). All assembled transcripts and unigenes were searched against the Gene Ontology (GO), which covers molecular functions, cellular components and biological processes and the Kyoto Encyclopedia of Genes and Genomes (KEGG), which covers metabolic pathways. In the case of the GO enrichment analysis, it was obtained using AnnotationForge v.1.38.1 (Carlson and Pagès, 2022) and clusterProfiler v.4.7.1.0003 (Yu et al., 2012), while KEGG enrichment analysis was calculated using KofamScan (Aramaki, 2020) and a custom script.

3. Results

3.1 Biochemical effects of heavy metal exposure on fungal cells

The exposure of *E. mesophila* to As(V) and Cr(VI) resulted in visible changes in the SR-FTIR profiles, when compared to unexposed cells. Figures 1 and 2 depict the averaged absorbance and the corresponding principal component analysis (PCA) for three regions: 1) the fingerprint region (1,800-1,000 cm^{-1}), 2) the amide I and II regions (1,700-1,500 cm^{-1}), associated with protein structure modifications, and 3) the DNA region (1,350-1,000 cm^{-1}), corresponding to the phosphodiester group primarily found in nucleic acids. PCA score analysis revealed distinct spectral variations in several regions, particularly concerning melanin content, when comparing Ar(V)-exposed cells (T1) to the unexposed control (C1). Within the fingerprint region, PCA also displayed a clear distinction between melanized cells, either exposed or not to As(V) (T1 and C1), and those where melanin biosynthesis was inhibited with tricyclazole (T3 and C2). This distinction was primarily driven by PC1, explaining 70% of the total variance observed. In the lipid region, the PC1 accounted for 68% of the variance and showed a greater variation for the tricyclazole treated cells C2 and T3. This suggests a stronger influence of both melanin inhibition and arsenate exposure on the lipid profile.

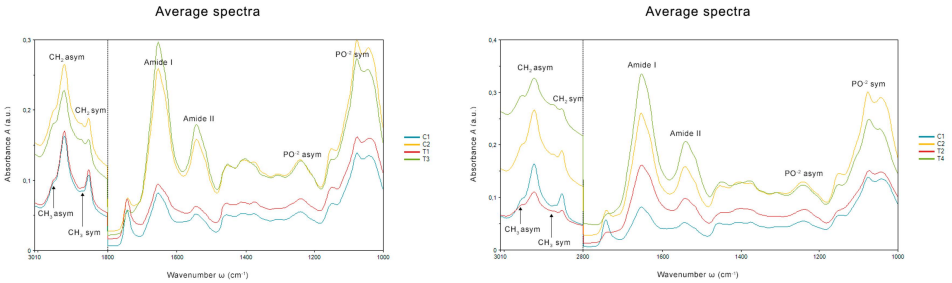

Figure 1. Averaged absorbance spectra from controls and treatments (unit vector normalized). The different averaged absorbance spectra have been shifted along the absorbance axis. Non-exposed cells: intact cells (C1) and cells treated with the melanin inhibitor tryciclazole (C2). (rigth) Cells exposed to arsenate (5 g L^{-1}): Intact cells exposed to As(V) (T1); and tricyclazole-induced cells exposed to As(V) (T3). (left) Chromium exposure treatment (1 g L^{-1}) of intact cells (T2) and albino-induced cells by means of tryciclazole (T4). For the sake of clarity, the different averaged absorbance spectra have been shifted along the absorbance axis.

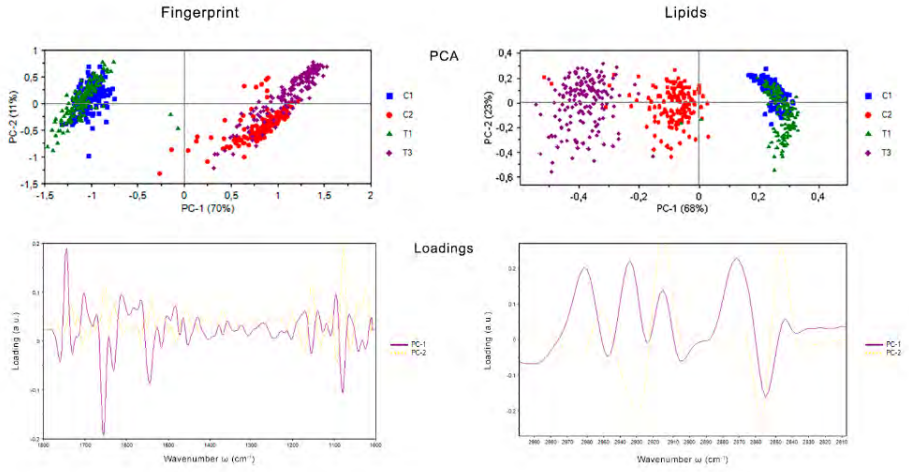

Figure 2. PCA score at the fingerprint region (1,800-1,000 cm^{-1} left) and the lipid region (3,100-2,800 cm^{-1}, right). C1: intact cells and, C2: tricyclazole -induced cells; T1: intact cells exposed to Arsenic; T3: tricyclazole-induced cells exposed to Arsenic.

Further analysis using second-derivative spectra from averaged absorbance data (Figure 3) also reveal alterations in the position and intensity of peaks corresponding to amide I and II bands, particularly in cells exposed to As(V) and lacking melanin (T3). Amide I (1,700^{-1} - 1,600 cm^{-1}) is associated with the C=O stretching in proteins, and amide II (1,600^{-1} - 480 cm^{-1}) has been assigned to N-H bending and C-N stretching vibrations in proteins. Hence, bands in this region are indicators of protein secondary structures and the observed spectral shifts in T3 cells suggest a more pronounced β-type structure compared to melanized cells. Additionally, the fingerprint region spectra (Figure 3) show significant variance in the amide I and II bands for the T3 cells. The spectral region between 1,350 and 1,000 cm^{-1} corresponds to asymmetric stretching of PO_2 groups in nucleic acids and phospholipids, while sugars exhibit strong bands due to C-O-C and

P-O-C vibrations. Compared to the control C1 (non-exposed melanized cells), Figure 3 displays several changes in intensity and position of peaks in the C2 (non-exposd hyaline cells) and the As(V) exposed T1 (melanized) and T3 (hyaline) cells. Peaks in the region between 1,120 and 1,050 cm^{-1} are assigned to symmetric C-C stretching in α-glucans and asymmetric stretching in C-O-C, P-O-C β-glucan complexes, respectively. These spectral shifts suggest changes in cell wall polysaccharides. In the lipid region (3,100-2,800 cm^{-1}), changes in the intensity of CH_2 and CH_3 symmetric and asymmetric modes were observed. These alterations could be related to the state of hydrocarbons and lipids specific to cell walls and membranes. Notably, a significant perturbation was observed in hyaline cells (C2 and T3; inhibition of melanin biosynthesis by tricyclazole) compared to non-inhibited melanized ones (C1 and T2).

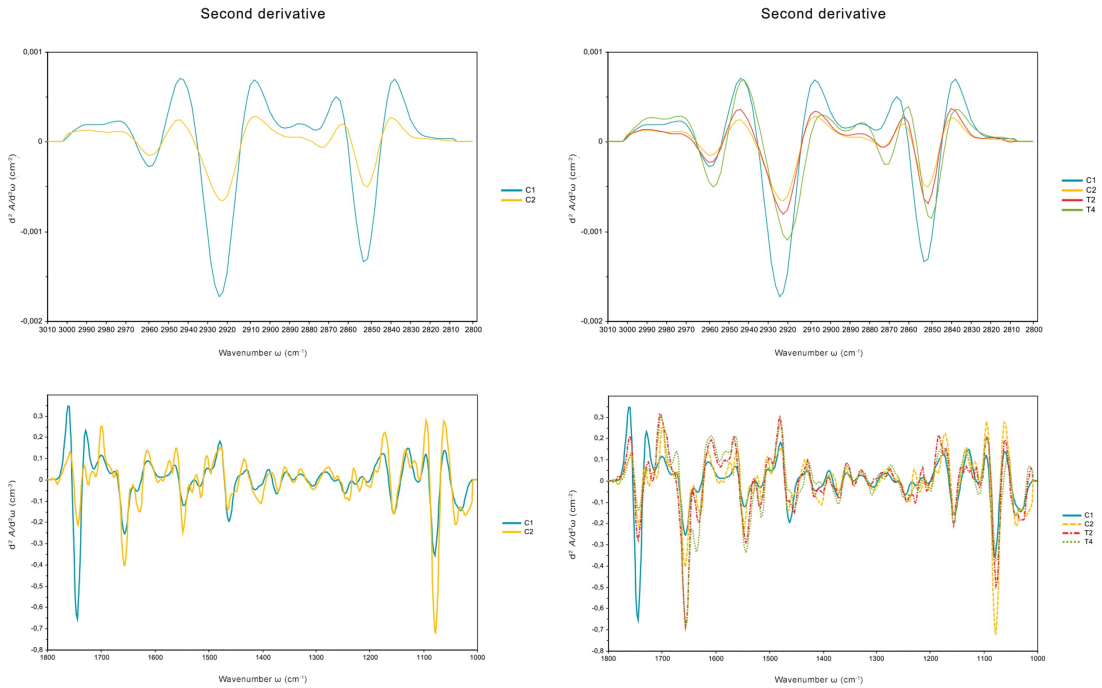

Figure 3. The Savitzky-Golay second derivative spectra is shown for the two controls and the treatment exposed to arsenic (rigth) and chromium (left). Fingerprint region (1,800-1,000 cm^{-1}left) and the lipid region (3,100-2,800 cm^{-1}, right).

Exposure to Cr(VI) revealed a stronger influence on spectral changes compared to As(V), likely due to the severe toxicity of this metal. Figures 2 and 4 depict the average spectra and corresponding PCA plots of the FTIR spectral profiling. The results demonstrate that there is a clear discrimination between exposed and un-exposed cells to Cr(VI), primarily along PC1 which explains 46% of the variance in the fingerprint region (1,800 – 1,000 cm^{-1}). In the fingerprint region, non-exposed melanized cells (C1) clearly separated from those exposed to Cr(VI), alone (T2) or in combination with tricyclazole (T4). This observation is distinct from the response to arsenic, where exposure to the melanin inhibitor tricyclazole was the main factor driving the separation of samples into two main clusters (Figure 12). PCA loading plots highlight a high contribution from the lipid region, which PC1 explains 83% of the variance in the fingerprint region (3,000-2,800 cm^{-1}). Figure 4, shows a strong change in the total lipid content for the T4 treatment (hyaline cells exposed to Cr(VI)). This observation is supported by a slight increase in the absorbance of

CH_2 and CH_3 stretching modes in the spectra, particularly for T4. These changes might be indicative of either lipid peroxidation or altered lipid metabolism associated with early stages of cell death processes.

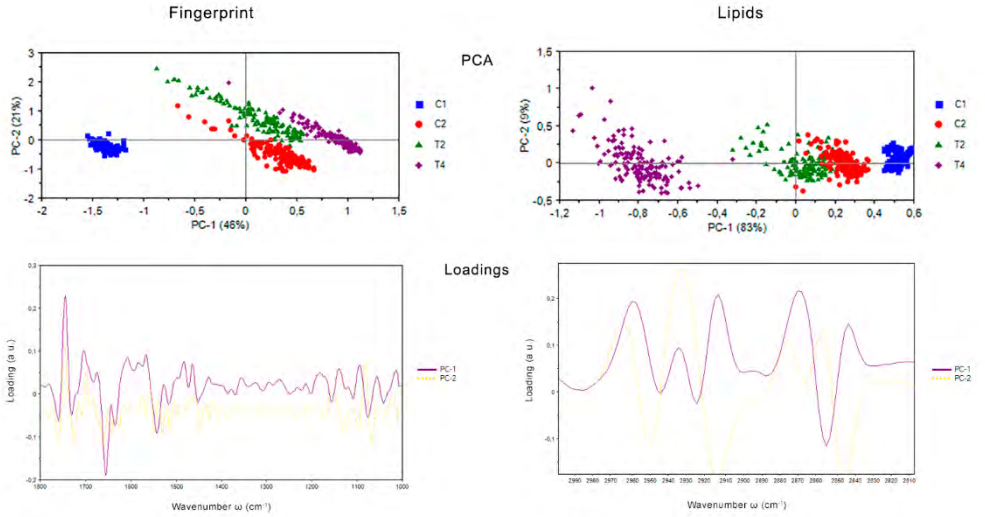

Figure 4. PCA score at the fingerprint region (1,800-1,000 cm^{-1} left) and the lipid region (3,100-2,800 cm^{-1}, right) are represented: non-exposed intact cells (C1) and tricyclazole-induced cells (C2); and exposed intact cells (T2) and tricyclazole-induced cells (T4).

Figure 3 depicts the second derivative spectra of several key bands, including phosphate (Ph I, II), amide I, and amide II, revealing their relative intensity distribution. The spectra show an increase in amide I and II band vibrations in Cr(VI)-exposed cells and those lacking melanin (C2, T2, T4). Chromium exposure correlated with peaks at 1,660 cm^{-1} and 1,638 cm^{-1}, corresponding to the β-sheet and α-helix conformations of the amide I band, respectively. These observations suggest potential alterations in protein secondary structure. Additionally, changes in DNA organization were observed upon metal exposure and melanin deficiency. Shifts in wavenumbers between 1,350-1,000 cm^{-1} and 1,242-1,082 cm^{-1} were attributed to asymmetric and symmetric stretching of PO^{2-} groups, particularly significant in the T2 and T4 cells. These shifts suggest alterations in DNA organization.

Finally, the lipid spectral region (3,100-2,800 cm^{-1}) revealed changes in the intensity of symmetric and asymmetric CH_2 and CH_3 stretching modes. Notably, C2, T2, and T3 cells subjected to the stress caused by Cr(VI) exposure and/melanin inhibition due to tricyclazole, displayed more prominent changes compared to As(V) exposure. This observation is particularly relevant for the T2 cells, and suggests that the toxic nature of Cr(VI) might significantly affect fungal membrane permeability, similar to the effects observed in treatments where melanin synthesis was suppressed.

3.2 De novo assembly of a Exophiala mesophila reference transcriptome

A total of 22,033,333 (C1 cells); 35,700,000 (T1 cells) and 31,666,667 (T2 cells) raw reads were generated from the unexposed control and As(V) and Cr(VI)-exposed cultures of *E. mesophila*.

After cleaning and quality checks, 21,300,330 and 34,666,667 and 31,100,000 clean reads were obtained, which had a GC content that ranged between 50 to 53%. More than 96.88% of bases in raw reads had a Q value ≥ 20 (and error probability of 0.95%) and more than 98.80% of bases in clean reads had a Q value ≥ 20 (and error probability of 0.94%). Transcriptome sequencing revealed a total of 9,056 expressed genes in both the control and exposed cells. PCA was employed to evaluate the transcriptome sequencing data and assess the similarity between biological replicates, and between the control and exposed cells. Significant differences were observed in this respect, especially with Cr(V) exposition, being the transcriptome of As(V)-exposed cells more similar to that of control cells (Figure 5).

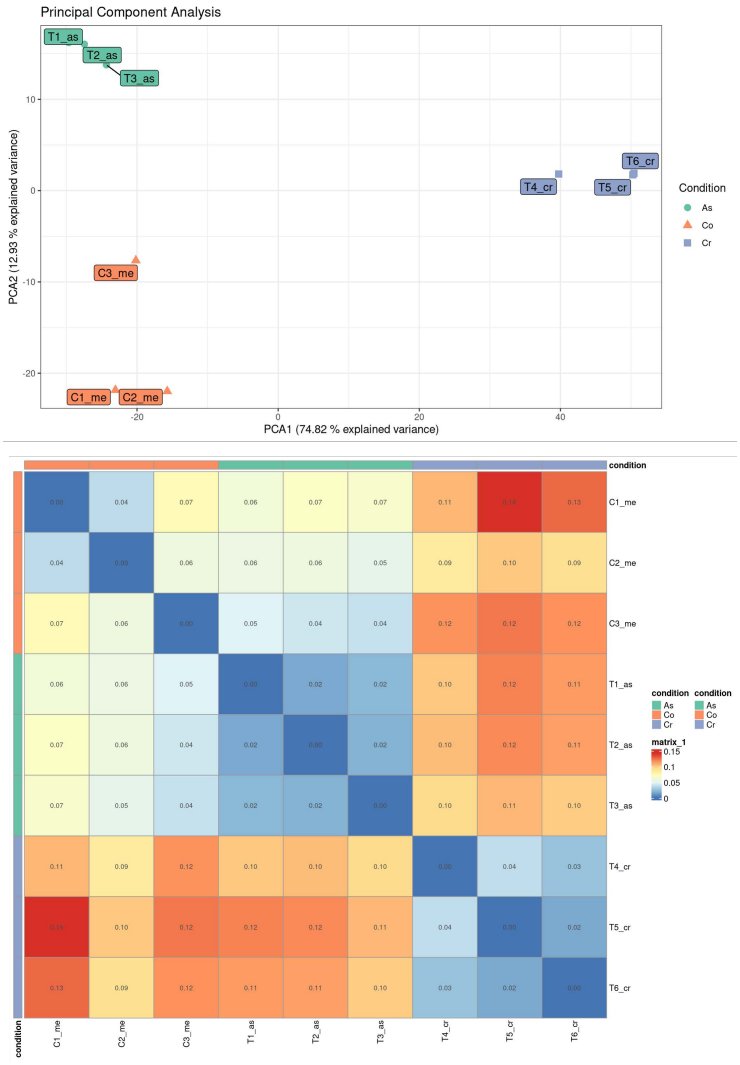

Figure 5. Up, principal component analysis of the trancriptome secuencing of *Exophiala mesophila*. Down hetmap correlation of DEG between control without metal and the treatments As(V)/Cr(VI).

As expected, the gene expression profile in response to distinct culture conditions exhibited clear separation along the first two principal components (Figure 5). Differential gene expression (DEG) analysis between culture conditions identified distinct patterns. When comparing the expression profile under As(V) exposure (C1 versus T1), 1,134 genes were positively expressed (increased expression), while 7,922 were negatively expressed (decreased expression). Further analysis revealed 572 underexpressed and 562 overexpressed genes within the positively expressed group. The Cr(VI) expression profile (C1 vs. T2) showed that 3,773 genes were positively expressed, and 5,283 were negatively expressed. Among the positively expressed genes, 1,652 were underexpressed, and 2,121 were overexpressed. When comparing T1 and T2, 4,168 genes were positively expressed, and 4,888 were negatively expressed. Within the positively expressed group, 1,968 were underexpressed, and 2,200 were overexpressed (Figure 6).

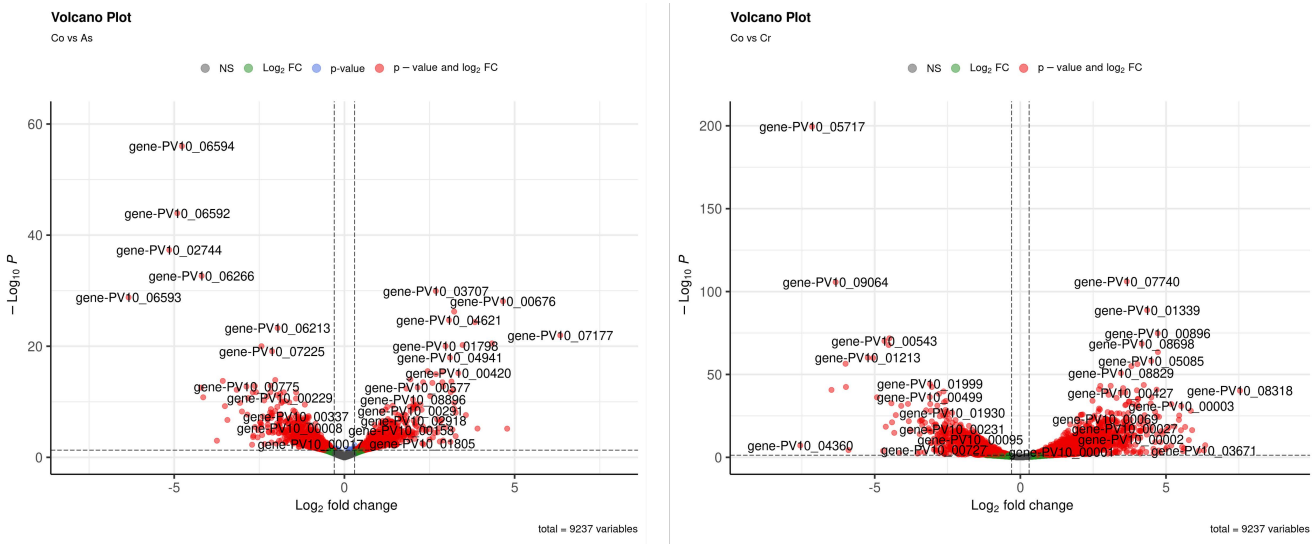

Figure 6. Volcano plot demonstrating the *E. mesophila* genes displaying high expression profile (large fold change values) and high statistical significance (as evidenced by the p-values) in (As/Cr)-free vs. (As/Cr)-stressed conditions. The data for all detected transcripts were plotted as $\log_2$ fold change (x-axis), versus the $-\log_{10}$ of the adjusted p-value (y-axis). Genes significantly upregulated or downregulated (at least 4-fold at $p < 0.05$)

3.3 GO and KEGG Pathway Enrichment Analysis of Differentially Expressed Genes

During GO classification, each of the unigenes were classified based on three functional categories: molecular functions, biological processes and cellular components (p-value ≤ 0.01 and FDR ≤ 0.1), which were clustered into 15, 10 and 0 classifications, respectively in As(V)-exposure conditions, and into 22, 21 and 16 classifications for Cr(VI) exposure (Figure 7). KEGG pathway analysis was performed to identify metabolic routes associated with the DEGs. The DEGs were mapped into 126 and 356 enriched pathways for As(V) and Cr(VI). Eight significant enrichment pathways were identified (p-value < 0.05 and FDR ≤ 0.1) and listed in Table 1. During the analysis, pathways associated with human diseases were deliberately excluded.

Table 1. The 10 most significant pathways and number DEGs in Gene Ontology (GO)

	Term	GO	Description	GeneRatio	BgRatio	pvalue	p.adjust	qvalue
As(VI)	GO:0006520	Biological proccess	cellular amino acid metabolic process	40/370	190/3125	0.00013	0.06533	0.06515
	GO:0019752		carboxylic acid metabolic process	49/370	277/3125	0.00175	0.23823	0.23755
	GO:0044281		small molecule metabolic process	77/370	483/3125	0.00206	0.23823	0.23755
	GO:1901566		organonitrogen compound biosynthetic process	76/370	478/3125	0.00239	0.23823	0.23755
	GO:0043436		oxoacid metabolic process	49/370	283/3125	0.0028	0.23823	0.23755
	GO:0022804	Molecular Function	active transmembrane transporter activity	23/591	96/4821	0.001	0.24119	0.235
	GO:0015291		secondary active transmembrane transporter activity	9/591	27/4821	0.00357	0.375	0.36538
	GO:0015318		inorganic molecular entity transmembrane transporter activity	26/591	133/4821	0.00971	0.375	0.36538
	GO:0015085		calcium ion transmembrane transporter activity	5/591	12/4821	0.0103	0.375	0.36538
	GO:0008289		lipid binding	12/591	48/4821	0.01107	0.375	0.36538
Cr(VI)	GO:0051258	Biological proccess	protein polymerization	13/1341	14/3125	0.00014	0.07728	0.07199
	GO:0006950		response to stress	98/1341	177/3125	0.0004	0.10245	0.09544

GO:0030163		protein catabolic process	49/1341	80/3125	0.00063	0.10245	0.09544
GO:0006281		DNA repair	69/1341	120/3125	0.00074	0.10245	0.09544
GO:0006974		cellular response to DNA damage stimulus	71/1341	125/3125	0.001	0.10245	0.09544
GO:0051179		localization	205/1341	410/3125	0.00116	0.10245	0.09544
GO:0009056		catabolic process	151/1341	295/3125	0.00163	0.11491	0.10704
GO:0033554		cellular response to stress	84/1341	154/3125	0.00191	0.11688	0.10887
GO:0051234		establishment of localization	195/1341	395/3125	0.00337	0.16936	0.15776
GO:0006810		transport	191/1341	387/3125	0.00378	0.16936	0.15776
GO:0005543		phospholipid binding	22/2019	29/4821	0.00021	0.05625	0.05337
GO:0035091		phosphatidylinositol binding	18/2019	24/4821	0.00101	0.08212	0.07792
GO:0017056	Molecular process	structural constituent of nuclear pore	oct-19	nov-21	0.00112	0.08212	0.07792
GO:0008289		lipid binding	31/2019	48/4821	0.0012	0.08212	0.07792
GO:0003684		damaged DNA binding	nov-19	13/4821	0.00204	0.08726	0.08281
GO:0005198		structural molecule activity	80/2019	149/4821	0.00209	0.08726	0.08281

GO:0140097		catalytic activity. acting on DNA	49/2019	85/4821	0.00225	0.08726	0.08281
GO:0051539		4 iron. 4 sulfur cluster binding	19/2019	27/4821	0.00255	0.08726	0.08281
GO:0015075		ion transmembrane transporter activity	75/2019	140/4821	0.00307	0.0935	0.08873
GO:0008233		peptidase activity	81/2019	155/4821	0.00518	0.142	0.13474
GO:0000502		proteasome complex	27/1627	34/3748	0.00002	0.0028	0.00258
GO:1905368		peptidase complex	35/1627	49/3748	0.00006	0.00408	0.00376
GO:1905369		endopeptidase complex	29/1627	39/3748	0.00008	0.00408	0.00376
GO:0005839		proteasome core complex	12/1627	14/3748	0.00144	0.05442	0.05008
GO:0005643	Cellular component	nuclear pore	14/1627	18/3748	0.00321	0.07855	0.07228
GO:0005856		cytoskeleton	50/1627	86/3748	0.00385	0.07855	0.07228
GO:0015629		actin cytoskeleton	19/1627	27/3748	0.00415	0.07855	0.07228
GO:0090575		RNA polymerase II transcription regulator complex	15/1627	20/3748	0.00416	0.07855	0.07228
GO:0071944		cell periphery	64/1627	115/3748	0.0049	0.08228	0.07571
GO:0005635		nuclear envelope	18/1627	27/3748	0.01236	0.17238	0.15862

3.4 Fungal metallotolerance mechanisms

Gene Ontology (GO) analysis revealed a significant enrichment of terms related to small molecule metabolism (biological process). Specifically, enriched terms included carboxylic acid metabolic process, organic acid metabolic process, and oxoacid metabolic process (Figure 7 a-b). Furthermore, enriched terms within the molecular function category highlighted processes associated with energy metabolism and transport. These included ATP hydrolysis activity, transmembrane transporter activity, and active transmembrane transporter activity. Importantly, GO terms associated with cellular process were not significantly enriched. Among the differentially expressed genes (DEGs), a cluster of 90 genes was identified that were associated with functions relevant to heavy metal tolerance. These functions included ATP-binding cassette (ABC) transporter activity, cation (Na^+, K^+, Ca^{2+}) binding, vacuolar localization, and hemerythrin HHE cation binding.

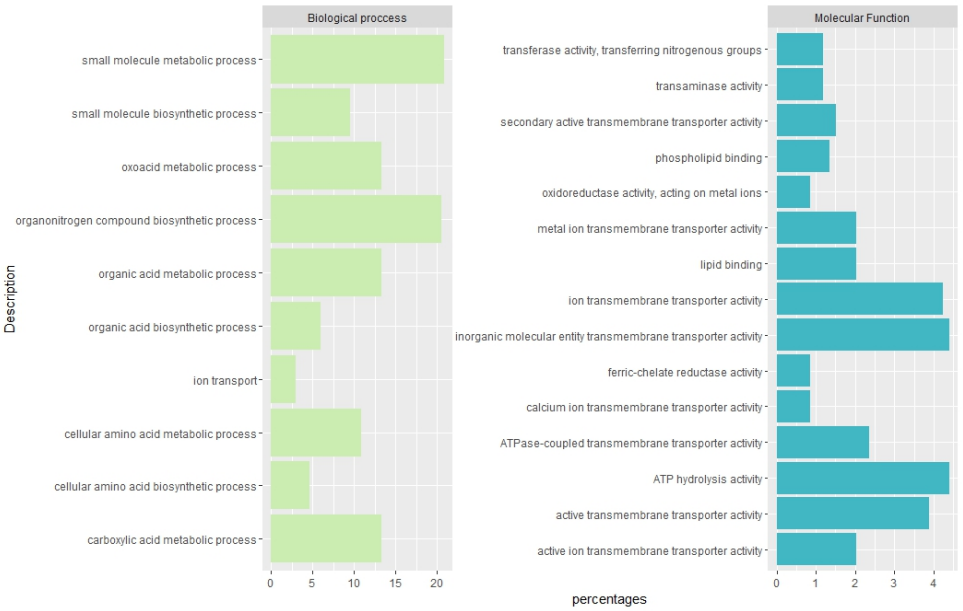
Biological proccess
small molecule metabolic process
small molecule biosynthetic process
oxoacid metabolic process
organonitrogen compound biosynthetic process
organic acid metabolic process
organic acid biosynthetic process
ion transport
cellular amino acid metabolic process
cellular amino acid biosynthetic process
carboxylic acid metabolic process
Description
0 5 10 15 20
Molecular Function
transferase activity, transferring nitrogenous groups
transaminase activity
secondary active transmembrane transporter activity
phospholipid binding
oxidoreductase activity, acting on metal ions
metal ion transmembrane transporter activity
lipid binding
ion transmembrane transporter activity
inorganic molecular entity transmembrane transporter activity
ferric-chelate reductase activity
calcium ion transmembrane transporter activity
ATPase-coupled transmembrane transporter activity
ATP hydrolysis activity
active transmembrane transporter activity
active ion transmembrane transporter activity
0 1 2 3 4
percentages

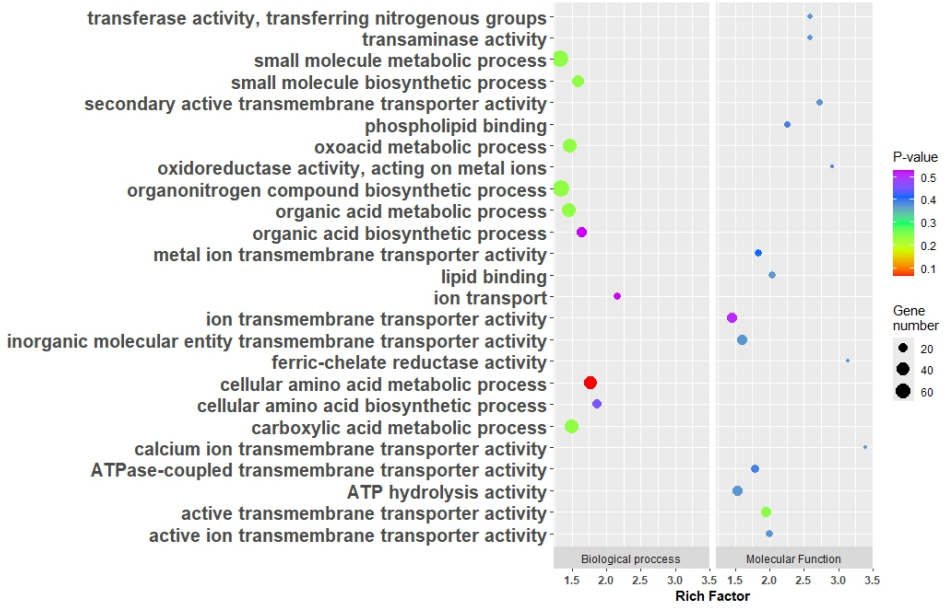
transferase activity, transferring nitrogenous groups
transaminase activity
small molecule metabolic process
small molecule biosynthetic process
secondary active transmembrane transporter activity
phospholipid binding
oxoacid metabolic process
oxidoreductase activity, acting on metal ions
organonitrogen compound biosynthetic process
organic acid metabolic process
organic acid biosynthetic process
metal ion transmembrane transporter activity
lipid binding
ion transport
ion transmembrane transporter activity
inorganic molecular entity transmembrane transporter activity
ferric-chelate reductase activity
cellular amino acid metabolic process
cellular amino acid biosynthetic process
carboxylic acid metabolic process
calcium ion transmembrane transporter activity
ATPase-coupled transmembrane transporter activity
ATP hydrolysis activity
active transmembrane transporter activity
active ion transmembrane transporter activity
Biological proccess
Molecular Function
1.5 2.0 2.5 3.0 3.5 1.5 2.0 2.5 3.0 3.5
Rich Factor
P-value
0.5
0.4
0.3
0.2
0.1
Gene number
20
40
60

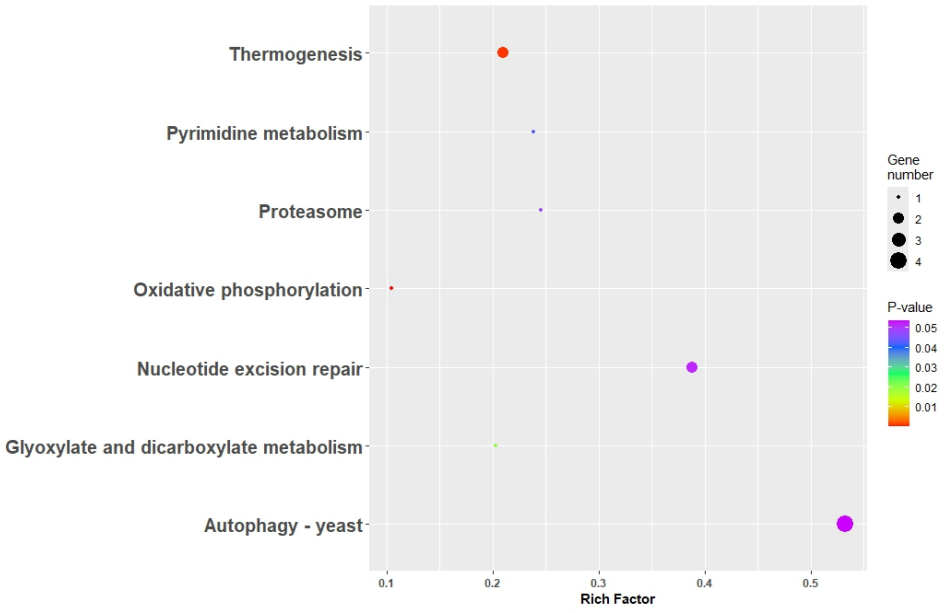
Thermogenesis
Pyrimidine metabolism
Proteasome
Oxidative phosphorylation
Nucleotide excision repair
Glyoxylate and dicarboxylate metabolism
Autophagy - yeast
0.1 0.2 0.3 0.4 0.5
Rich Factor
Gene number
1
2
3
4
P-value
0.05
0.04
0.03
0.02
0.01

Figure 7. The enriched biological process, cellular component and molecular function GO terms of DEGs in *Exophiala mesophila* under As-free and As-stressed exposure. (Up) indicates the percentage of DEGs (center) gene numbers vs. P-values gene numbers in each GO term, and (down) KEGG metabolic pathways analysis of *E. mesophila* transcripts (numerous unigenes were classified into more than one metabolic class). Gene transcripts of a specific class in number of total 1231 annotated unigenes.

KEGG pathway analysis (Figure 7c), identified several significantly enriched pathways, including thermogenesis, pyrimidine metabolism, proteasome, oxidative phosphorylation, nucleotide excision repair, glyoxylate metabolism, dicarboxylate metabolism, and autophagy (yeast) (Figure X). However, these enriched pathways were associated with a relatively low number of expressed genes. To further investigate the As(V) resistance mechanism, a detailed analysis of genes related to heavy metal tolerance was conducted. These genes included those involved in metal binding and transport, transferase activity (nitrogenous group transfer), ferric-chelate reductase activity, methylation, DNA repair, superperoxide dismutate, and cell wall metabolic processes (listed in Table).

Gene Ontology (GO) enrichment analysis of differentially expressed genes (DEGs) in Cr(VI)-exposed *E. mesophila* revealed associations with diverse genetic functions categorized under cellular component, molecular function, and biological processes (Figure 8 a-b). Positively regulated DEGs across all treatments were significantly enriched in biological processes primarily involving localization, transport, catabolic process, response to stress, and cellular response to DNA damage stimulus. Enriched molecular functions included ion transmembrane transporter activity, peptidase activity, structural molecule activity, and ATP hydrolysis activity. At the cellular component level, enriched terms encompassed cell periphery, cytoskeleton, peptidase complex, proteasome complex, and supramolecular polymer.

Unigenes associated with the induction of tolerance and detoxification of inorganic compounds were identified in the expression of genes encoding proteins involved in transport (NAPH2-quinone reductase, ferric quinone reductase, peroxisomal catalase (CAT), mitochondrial distribution and morphology protein), DNA repair oxidoreductase complex (DNA repair protein rda, and structural maintenance of chromosomes protein).

KEGG analysis (Figure 8c) of fungal DEGs identified pathways involved in metal stress response, categorized primarily into eleven physiological categories, including carbohydrate metabolism, energy metabolism, and cofactor and vitamin metabolism (Table 1). Positively regulated DEGs were significantly enriched in valine, leucine, and isoleucine degradation, tyrosine and tryptophan metabolism, the thermogenesis pathway, oxidative phosphorylation, and alanine, aspartate, and glutamate metabolism, suggesting their essential role in metal stress response. Pentose and glucuronate interconversions, RNA polymerase, the pentose phosphate pathway, and pyrimidine and purine metabolism were primarily enriched in downregulated DEGs.

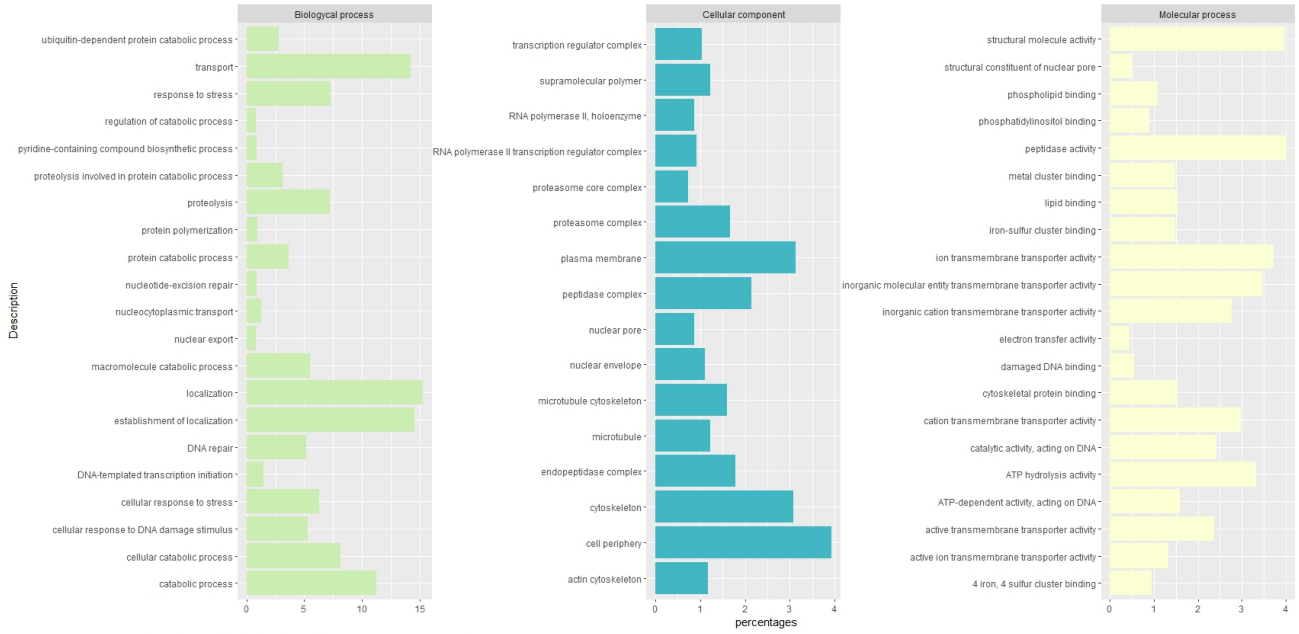
Biologycal process
Cellular component
Molecular process
Description
ubiquitin-dependent protein catabolic process
transport
response to stress
regulation of catabolic process
pyridine-containing compound biosynthetic process
proteolysis involved in protein catabolic process
proteolysis
protein polymerization
protein catabolic process
nucleotide-excision repair
nucleocytoplasmic transport
nuclear export
macromolecule catabolic process
localization
establishment of localization
DNA repair
DNA-templated transcription initiation
cellular response to stress
cellular response to DNA damage stimulus
cellular catabolic process
catabolic process
transcription regulator complex
supramolecular polymer
RNA polymerase II, holoenzyme
RNA polymerase II transcription regulator complex
proteasome core complex
proteasome complex
plasma membrane
peptidase complex
nuclear pore
nuclear envelope
microtubule cytoskeleton
microtubule
endopeptidase complex
cytoskeleton
cell periphery
actin cytoskeleton
structural molecule activity
structural constituent of nuclear pore
phospholipid binding
phosphatidylinositol binding
peptidase activity
metal cluster binding
lipid binding
iron-sulfur cluster binding
ion transmembrane transporter activity
inorganic molecular entity transmembrane transporter activity
inorganic cation transmembrane transporter activity
electron transfer activity
damaged DNA binding
cytoskeletal protein binding
cation transmembrane transporter activity
catalytic activity, acting on DNA
ATP hydrolysis activity
ATP-dependent activity, acting on DNA
active transmembrane transporter activity
active ion transmembrane transporter activity
4 iron, 4 sulfur cluster binding
percentages

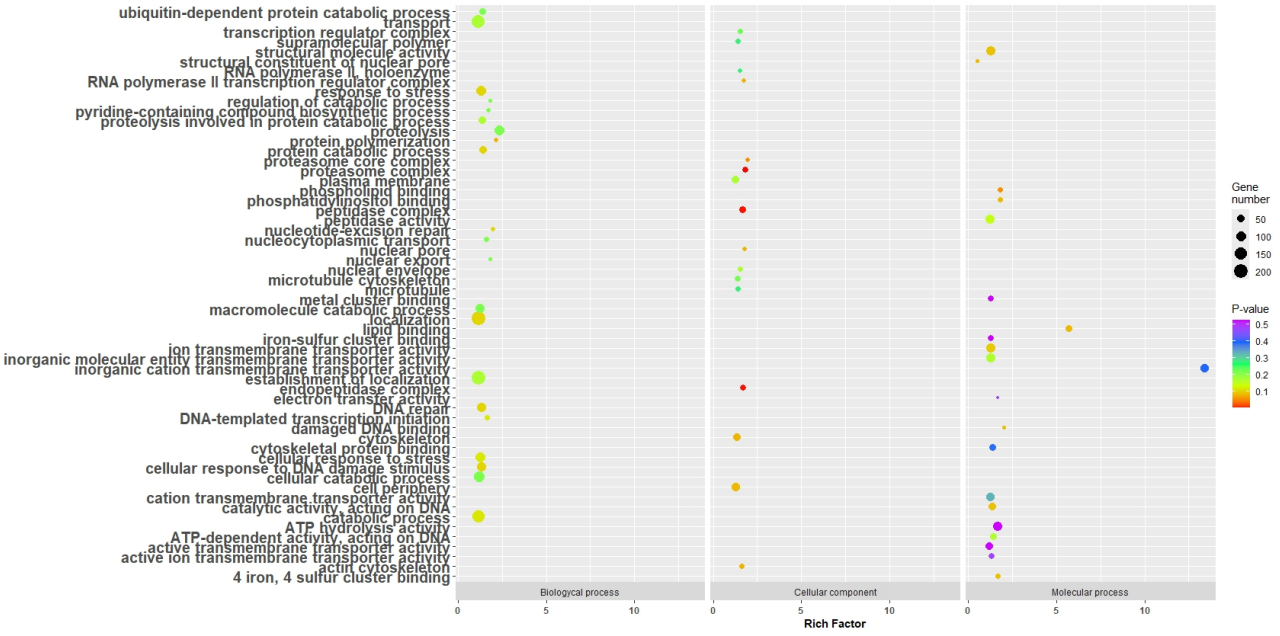
ubiquitin-dependent protein catabolic process
transport
transcription regulator complex
supramolecular polymer
structural molecule activity
structural constituent of nuclear pore
RNA polymerase II, holoenzyme
RNA polymerase II transcription regulator complex
response to stress
regulation of catabolic process
pyridine-containing compound biosynthetic process
proteolysis involved in protein catabolic process
proteolysis
protein polymerization
protein catabolic process
proteasome core complex
proteasome complex
plasma membrane
phospholipid binding
phosphatidylinositol binding
peptidase complex
peptidase activity
nucleotide-excision repair
nucleocytoplasmic transport
nuclear pore
nuclear export
nuclear envelope
microtubule cytoskeleton
microtubule
metal cluster binding
macromolecule catabolic process
localization
lipid binding
iron-sulfur cluster binding
ion transmembrane transporter activity
inorganic molecular entity transmembrane transporter activity
inorganic cation transmembrane transporter activity
establishment of localization
endopeptidase complex
electron transfer activity
DNA repair
DNA-templated transcription initiation
damaged DNA binding
cytoskeleton
cytoskeletal protein binding
cellular response to stress
cellular response to DNA damage stimulus
cellular catabolic process
cell periphery
cation transmembrane transporter activity
catalytic activity, acting on DNA
catabolic process
ATP hydrolysis activity
ATP-dependent activity, acting on DNA
active transmembrane transporter activity
active ion transmembrane transporter activity
actin cytoskeleton
4 iron, 4 sulfur cluster binding
Biologycal process
Cellular component
Molecular process
Rich Factor
Gene number
50
100
150
200
P-value
0.5
0.4
0.3
0.2
0.1

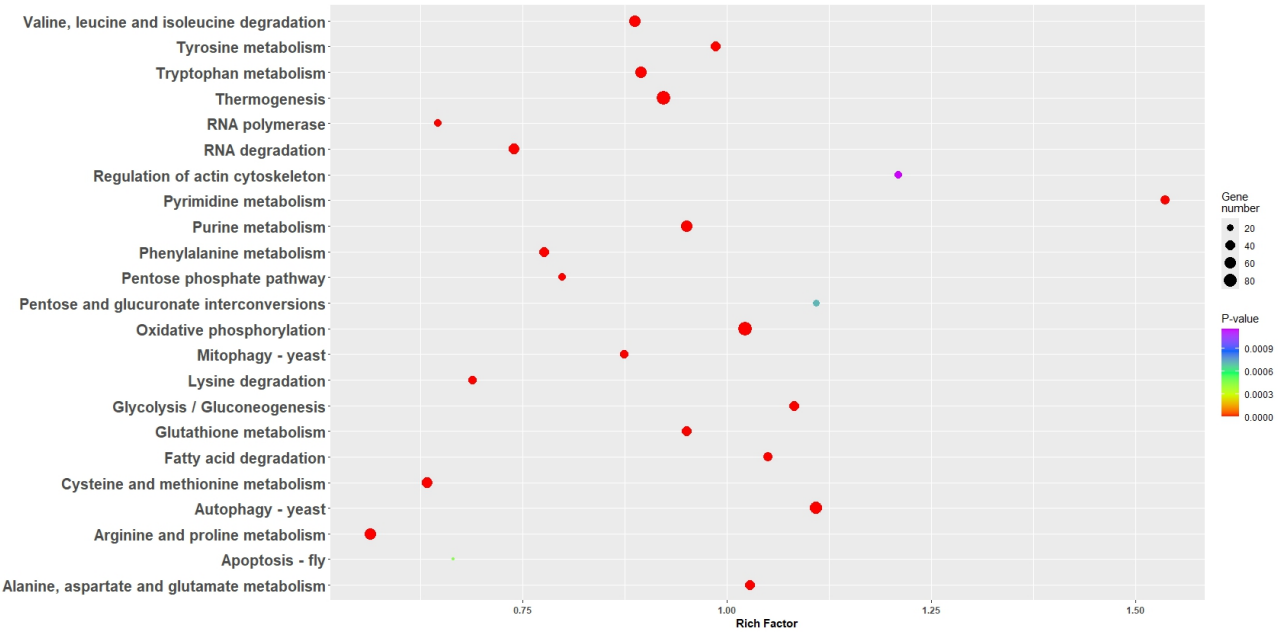
Valine, leucine and isoleucine degradation
Tyrosine metabolism
Tryptophan metabolism
Thermogenesis
RNA polymerase
RNA degradation
Regulation of actin cytoskeleton
Pyrimidine metabolism
Purine metabolism
Phenylalanine metabolism
Pentose phosphate pathway
Pentose and glucuronate interconversions
Oxidative phosphorylation
Mitophagy - yeast
Lysine degradation
Glycolysis / Gluconeogenesis
Glutathione metabolism
Fatty acid degradation
Cysteine and methionine metabolism
Autophagy - yeast
Arginine and proline metabolism
Apoptosis - fly
Alanine, aspartate and glutamate metabolism
Rich Factor
Gene number
20
40
60
80
P-value
0.0009
0.0006
0.0003
0.0000

Figure 8. GO enrichment analysis of all DEGs. The enriched biological process, cellular component and molecular function GO terms of DEGs in *E. mesophila* under Cr-free and Cr-stressed exposure. (Up) indicates the percentage of DEGs (center) gene numbers vs. P-values gene numbers in each GO term, and (down) KEGG metabolic pathways analysis of *E. mesophila* transcripts (numerous unigenes were classified into more than one metabolic class). Gene transcripts of a specific class in number of total 1231 annotated unigenes.

4. Discussion

4.1 Melanin rol in metalotolerance HHM

Our analysis of SR-FTIR revealed alterations in the DNA fingerprint region, particularly within the phosphodiester group bands, upon exposure to As(V) and Cr(VI). These changes suggest potential modifications in DNA structure, such as pyrimidine dimers or DNA-DNA/protein-DNA cross-links. Notably, these alterations were predominantly observed in the vibrations of the phosphodiester group (asymmetric PO_2 and symmetric PO_2), primarily in melanin-deficient cells exposed As(V)/Cr(VI). This suggests a heightened susceptibility to DNA organization or conformation changes under these conditions.

Overall, our investigation highlights a more pronounced biochemical response in the absence of melanin during As(V)/Cr(VI) exposure. The significant variance in the asymmetric and symmetric PO_2 bands, along with the initial changes in protein secondary structure, could be attributed to ROS generation through contact with toxic ions. This ROS generation can induce oxidative damage a wide range of molecules, including nucleic acids, proteins and lipids, potentially leading to the observed conformational changes, consistent with previous studies (Perrone et al., 2008; Zhan et al., 2016). Additionally, the changes in the phosphodiester group of proteins point towards a cascade of events involving extensive metabolic reorganization, encompassing transport, cellular homeostasis, DNA repair, and DNA/RNA synthesis.

The dramatic changes observed in As(V)/Cr(VI)-exposed and melanin-inhibited cells could be attributed to the initial apoptotic response triggered by ROS generation. In *Saccharomyces cerevisiae*, a direct link between endoplasmic reticulum (ER) stress induction, elevated mitochondrial matrix Ca(II) levels, ROS accumulation, and apoptosis promotion has yet to be established (Perrone et al., 2008). These findings suggest that melanin inhibition potentiates ROS generation within the cells, surpassing the levels observed in non-inhibited cells upon exposure to As(V)/Cr(VI). This elevated oxidative stress likely exerts a direct impact on mitochondria, cytochrome c, and the ER, prompting the cell to self-destruct through apoptosis.

Furthermore, Cr(VI)-exposure exhibited the most pronounced effects across all investigated biochemical groups. In addition to the significant changes observed in DNA and proteins, we also identified a slight increase in the absorbance of the CH_2 and CH_3 stretching modes in the SR-FTIR spectra of lipids from exposed cells. This observation suggests potential alterations in lipid metabolism or increased lipid peroxidation, which is a hallmark of oxidative stress (Kumar et al., n.d.). Chromium-mediated lipid damage could disrupt the cell membrane of E. mesophile, ultimately leading to cell lysis. Furthermore, these peroxidation reactions could contribute to the generation of additional ROS, exacerbating the oxidative stress response.

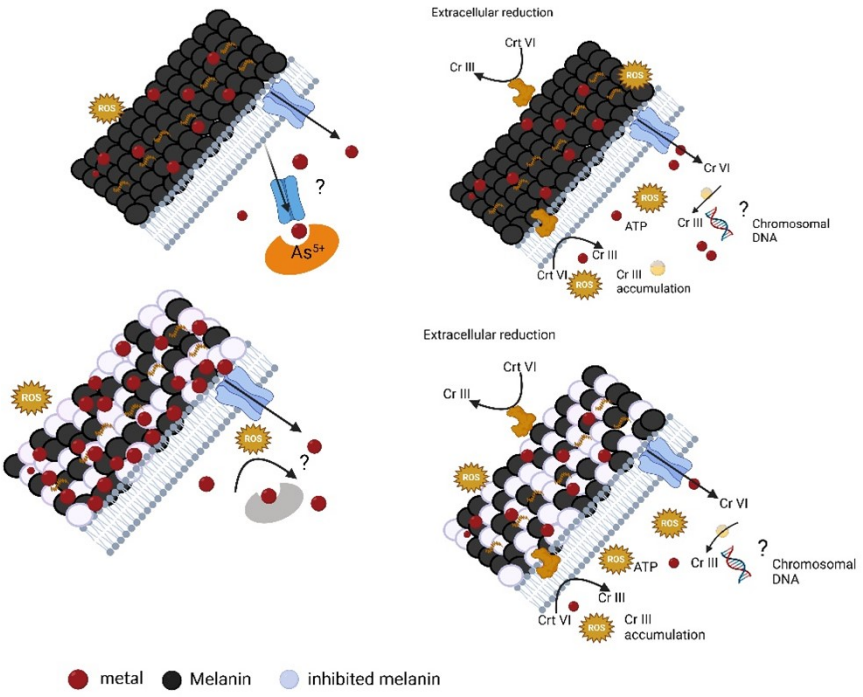

Figure 9. Disruption of Melanin Synthesis and Effects of Exposure to As(V) and Cr(VI)

4.2 *Arsenic Metallotolerance Mechanisms*

The SR-FTIR analysis also revealed potential alterations in protein secondary structure in *Exophiala mesophila* following arsenic exposure. These changes are likely attributed to the generation of reactive oxygen species (ROS) and subsequent oxidative damage. This finding aligns with the observed upregulation of superoxide dismutase (SOD) genes in *E. mesophila* through gene expression analysis. This is a well-documented phenomenon, suggesting a cellular defense mechanism against the increased ROS generated by arsenic stress.

Previous studies have established the metal-chelating properties of melanin due to its abundant carboxyl, phenolic, hydroxyl, and amine groups (Fogarty and Tobin, 1996). These functional groups act as potential binding sites for metal ions. Interestingly, our SR-FTIR analysis of arsenic-exposed *E. mesophila* cells with melanin revealed significant changes in wavenumbers associated with cell wall and membrane hydrocarbons and lipids. However, no alterations were observed in the aromatic structures corresponding to melanin or chitin. This observation suggests that direct binding of arsenic to cell wall melanin via electrostatic attraction is less likely. The negatively charged cell wall and arsenate could lead to repulsion. Consequently, complexation with other cations like Fe(III) or Ca(II) might mediate arsenic association with melanin. Supporting this notion, we observed the overexpression of ferri-chelate reductase (FRO2) genes. This suggests the formation of a complex between As(V) and Fe(III), potentially facilitating arsenic binding to melanin. Additionally, iron reduction can generate ROS, further contributing to oxidative stress in the cell wall. Melanin's ability to quench and detoxify superoxide ions might be crucial for maintaining cellular stability, potentially creating a functional overlap with metal binding. Melanin and the antioxidant enzyme SOD could act synergistically during arsenic stress.

Extracellular melanin could initially buffer oxidative bursts, while intracellular SOD provides further protection. SR-FTIR analysis with melanin inhibition revealed alterations in functional groups associated with potential metal binding, including prominent protein modifications. This suggests excess ROS production, potentially due to reduced cell wall melanin. However, further research is necessary to fully elucidate the intricate interaction between melanin, ROS, and their combined protective roles.

In the cytosol, potential protective mechanism involves Hemerythrin/HHE (Hr) proteins. Traditionally known for their iron Fe(III) and oxygen binding capabilities, Hr proteins in *E. mesophila* might be upregulated to sequester arsenic or other displaced cations, shielding cellular components from their toxic effects. In *Cryptococcus neoformans*, Hr cation-binding domains have been implicated in the response to nitric oxide (Chow et al., 2007), suggesting potential alternative ligand interactions. However, research on the role of fungal Hr proteins in metal detoxification, including intracellular sequestration, metal compartmentalization in vacuoles, and ROS management in conjunction with antioxidant enzymes like superoxide dismutase (SOD) and catalase (CAT), is scarce (Bellini et al., 1583).

Transcriptomic analysis revealed a significant upregulation of genes encoding transporter proteins in *Exophiala mesophila* following arsenic exposure. These upregulated transporters included ATP-binding cassette (ABC) transporters, Na^+/K^+ transporters, Fe^{2+} transporters, and Ca^{2+} transporters (Yor1). This robust transcriptional response suggests a potential mechanism for *E. mesophila* to adapt to arsenic stress. Interestingly, biochemical analyses did not detect dramatic changes in metabolite profiles between control and arsenic-treated samples. This suggests that the upregulated transporter genes likely contribute to maintaining cellular integrity by facilitating the controlled influx and efflux of various ions (Na^+, K^+, Ca^{2+}, Fe^{2+}) across the cell membrane. This regulated transport system could act to counteract the disruptive effects of arsenic on cellular ion homeostasis. Similar observations of upregulated transporter gene expression in response to arsenic stress have been reported in other fungi, such as *Aspergillus oryzae* (Liang et al., 2021). Additionally, *Cladophialophora exuberans* exhibits upregulated transporter regulation in response to copper stress (Silva et al., 2023). These findings support the hypothesis that transporter regulation plays a crucial role in fungal adaptation to various metal exposures. The observed downregulation of some putative arsenic transporters may represent another facet of *E. mesophila's* resistance strategy. By downregulating these transporters, the fungus might limit arsenic influx. However, the upregulation of transporters like the vacuolar calcium ion transporter (VCX) suggests a more complex regulatory network. This specific transporter might facilitate the movement of arsenic ions into the vacuole, potentially sequestering them away from sensitive cellular components. Similar roles for vacuoles in heavy metal detoxification have been described in other organisms (Lenassi et al., 2013; Zhao et al., 2015; Silva et al., 2023).

A remarkable alignment between biochemical and gene expression analyses highlights the complex mechanisms underlying arsenic tolerance in *Exophiala mesophila*. SR-FTIR analysis revealed alterations in protein secondary structure and downregulation of molecular functions in Gene Ontology (GO) analysis. These findings are consistent with the functional genomics data, suggesting a prominent role for transport mechanisms in arsenic resistance. This notion is further supported by the lack of dramatic changes in biochemical parameters between control and arsenic-treated samples. This suggests that the regulated transport system effectively buffers cells against arsenic-induced perturbations.

Beyond transport regulation, KEGG pathway analysis unveils additional adaptation strategies employed by *E. mesophila*. Alterations in pyrimidine metabolism suggest a prioritization of RNA synthesis, potentially for the production of new proteins or enzymes essential for stress response and adaptation. Additionally, the upregulation of genes associated with oxidative phosphorylation implies an effort to maintain energy production despite the stress induced by arsenic. Notably, the overexpression of proteins potentially acting as arsenic transporters to mitochondria (COX1) was observed. This finding aligns with the observed upregulation of the proteasome, specifically the protein Putative Proteasome Subunit Beta 7 (PSMB7). Proteasome metabolism in Golgi complex play a crucial role in eliminating misfolded or damaged proteins resulting from arsenic exposure (Sigler et al., 1999; Poljsak et al., 2010).

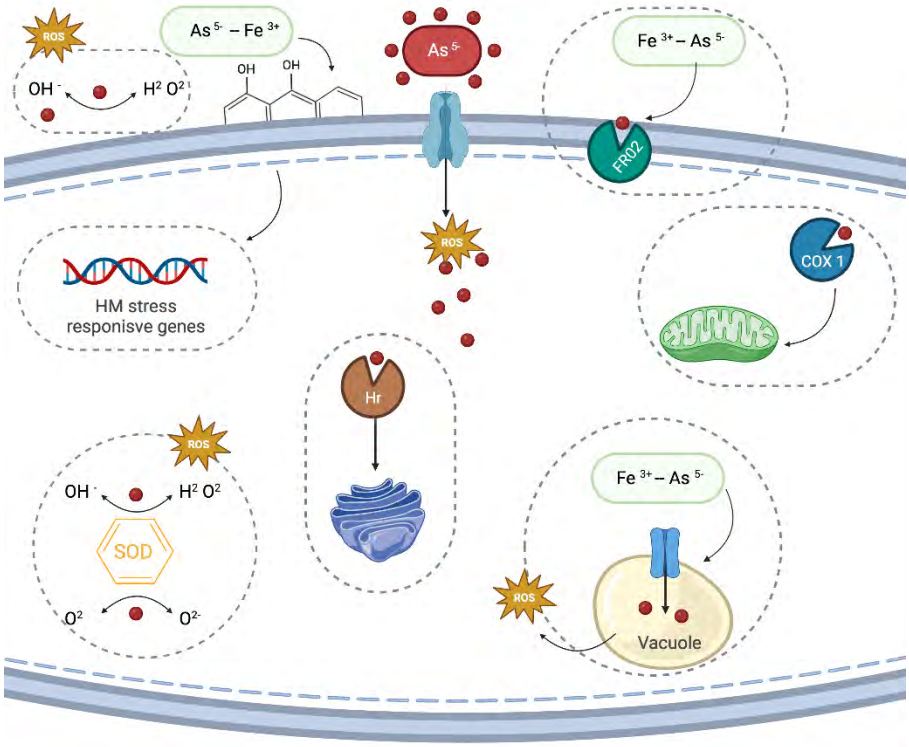

Figure 10. Schematic representation of possible genetic pathways associated to influx and efflux of As(V) in *Exophiala mesophila* (As(V)- is the Red spheric). YOR1 - Putative ABC transporter permease protein; FRO2 - Ferric/chelate reductase; HR - Hemerithrin; SOD - Superoxide dismutase; PMC1 - Calcium Transport Protein in vacuole; COX - Cytochrome c oxidase; PIC2 - Mitochondrial phosphate carrier protein 2; CRM1 - Chromosome region maintenance protein 1; PSMB7 - Putative Proteasome Subunit Beta 7.

4.3 Chromium Metallotolerance Mechanisms

Chromium exposure exerts its toxic effects on *E. mesophila* at the cellular level, causing significant damage to the cell wall, proteins, DNA, polysaccharides, and overall cellular integrity. This is in contrast to arsenic exposure, where the primary response involves altered transport mechanisms. SR-FTIR analysis revealed that chromium exposure affects the biochemistry of *E. mesophila* regardless of melanin inhibition, which suggests a high likelihood of cell lysis.

Metal exposure has been linked to the increased biosynthesis of glutathione (GSH), a low-molecular-weight chelator molecule that protects essential metabolic proteins from binding to heavy metals (Perrone et al., 2008). Furthermore, chromium exposure can induce apoptosis through oxidative stress, due increased formation of reactive oxygen species (ROS) and mitochondrial damage. This process involves cytochrome c release, DNA fragmentation, phosphatidylserine exposure, and metacaspase activation (Majumder et al., 2017). Mitochondria play a crucial role in cell cycle regulation and differentiation, and their membrane permeability is critical during apoptosis.

Exposure to chromium triggers rapid changes in gene expression in *E. mesophila*, contrasting with the significant supramolecular changes observed through SR-FTIR analysis. Notably, there is upregulation of genes associated with cellular detoxification, including those encoding NDH-quinone: NADPH dehydrogenase quinone (YCP4) and peroxisomal catalase (CAT). This finding suggests the activation of defense mechanisms against chromium-induced stress. Intriguingly, overexpression of NDH-quinone is observed. This is consistent with the reduction of chromium Cr(VI) to Cr(III) under aerobic conditions, a process typically associated with soluble chromate reductases that utilize NADH or NADPH as cofactors (Viti et al., 2014). However, it is important to note that this NADPH-dependent reduction of Cr(VI) to Cr(III) generates reactive oxygen species (ROS) intermediates. The upregulation of catalase (CAT) suggests a potential mechanism for controlling these ROS intermediates. Additionally, quinols produced by the quinone reductase activity of NDH-quinone confer tolerance to ROS (Gonzalez et al., 2005). Therefore, it is possible that the ROS generated by NDH-quinone during Cr(VI) reduction are neutralized by the quinols formed by the same enzyme. This creates a potential self-regulating system for managing ROS production during chromium detoxification.

Exposure to chromium triggers diverse responses in *E. mesophila*, including the upregulation of genes associated with various transport mechanisms. Gene Ontology (GO) analysis revealed significant changes in biological processes and molecular functions related to transport. Among the highly expressed genes, those encoding transporter proteins stand out, including K/Na efflux P-type ATPase (fungal type) (ENA1), copper-translocating P-type ATPase (ctpA), electron carrier (ETC), and F-actin-capping protein alpha subunit (CAP1). This suggests a multifaceted adaptation for chromium transport into the cytosol. These transport mechanisms may also facilitate the reduction of Cr(VI) and the release of reduced chromium compounds, such as $CrO4^{2-}$ and $SO4^{2-}$. GO analysis indicates involvement in iron-sulfur cluster binding, potentially implicating the electron transport chain (ETC) of complex I. This ETC could utilize S(0) or Fe(0) as inorganic electron donors for biological Cr(VI) reduction.

The oxygen-containing functional groups of melanin (C–O, CO–OH, C–OH, and C–O–R) could also serve as electron donors (π electrons) for Cr(VI) reduction. SR-FTIR analysis revealed a decrease in the C=O stretch ratio in chromium- and melanin-exposed samples compared to the control. This observation suggests that during the interaction between Cr(VI) and fungal biomass, some C–O groups may be oxidized to C=O, leading to the reduction of Cr(VI) to Cr(III). Similar observations have been reported by other researchers, suggesting that fungi can bind Cr(VI) to available carboxyl groups on their mycelia, converting Cr(IV) to non-toxic Cr(III) (Vieira et al., 2010; Majumder et al., 2017). Furthermore, SR-FTIR analysis detected changes in frequencies between C-O streching in the chromium-exposure treatments. These changes may represent the formation of Cr(III)-phosphate complex moieties. Majumder et al. (2017) reported the oxidation of C–O groups to C=O under Cr(VI) exposure and also found the involvement of phosphate and sulfonyl groups in chromate ion coordination. Additionally, they observed shifts in peaks from

1,029 cm^{-1} to 1,033 cm^{-1} and 531 cm^{-1} to 576 cm^{-1}, potentially indicating the formation of Cr(III)-phosphate compounds (Majumder et al., 2017). Overall, the findings highlight the complex interplay between reduction mechanisms of Cr(VI), and melanin-mediated redox reactions in the chromium of *E. mesophila*.

Exposure to chromium has a profound impact on various metabolic pathways in *E. mesophila*, as revealed by KEGG pathway analysis. Notably, purine and pyrimidine metabolism, which provide building blocks for DNA and RNA synthesis, are significantly affected. These combined effects highlight the widespread cellular disruption caused by chromium exposure (Poljsak et al., 2010). To counteract chromium-induced DNA damage, two types of proteins involved in DNA repair processes were overexpressed, as indicated by Gene Ontology (GO) analysis: DNA protein rad2 (RAD2) and ATP-dependent DNA helicase II (ku70).

The disruption of DNA integrity and the subsequent repair mechanisms are accompanied by alterations in energy regulation through oxidative phosphorylation. This suggests that cells attempt to maintain energy production despite the stress induced by chromium exposure. In addition to autophagy-related metabolic pathways, the upregulation of autophagy genes reveals another adaptive mechanism employed by *E. mesophila* to cope with chromium-induced stress. Autophagy is an essential cellular process that involves the recycling of damaged or unnecessary cytoplasmic components through lysosomal degradation (Chiarelli and Roccheri, 2012). Fatty acid degradation may also highlight a crucial role for melanin as an electron acceptor in lipid degradation reactions. This electron-accepting capacity of melanin could potentially reduce the generation of reactive oxygen species (ROS) during lipid metabolism. Consequently, melanin might act as a protective mechanism against chromium-induced oxidative stress.

Intriguingly, chromium exposure appears to induce the metabolic activity of tyrosine, tryptophan, and phenylalanine, potentially leading to melanin production via the dopa-melanin pathway. This finding contrasts with the previously observed tricyclazole-induced inhibition of DHN-melanin synthesis in *E. mesophila*. This suggests a remarkable ability for *E. mesophila* to produce melanin through distinct pathways depending on the specific environmental stress encountered. However, increased tyrosine metabolism does not solely confirm melanin synthesis. It could contribute to protein synthesis for fungal growth, or alternatively, tyrosine degradation could serve as an energy source during limited nutrients. Notably, previous studies reported similar observations: overexpression of tyrosine metabolism in *Exophiala pisciphila* (Zhao et al., 2015), but without a connection to dopa-melanin production. Additionally, another study documented enhanced melatonin synthesis enzymes in *E. pisciphila* driven by tryptophan hydroxylase activity (Yu et al., 2021). These findings highlight the diverse metabolic pathways *Exophiala* species can utilize for melanin production depending on the specific environmental stressor.

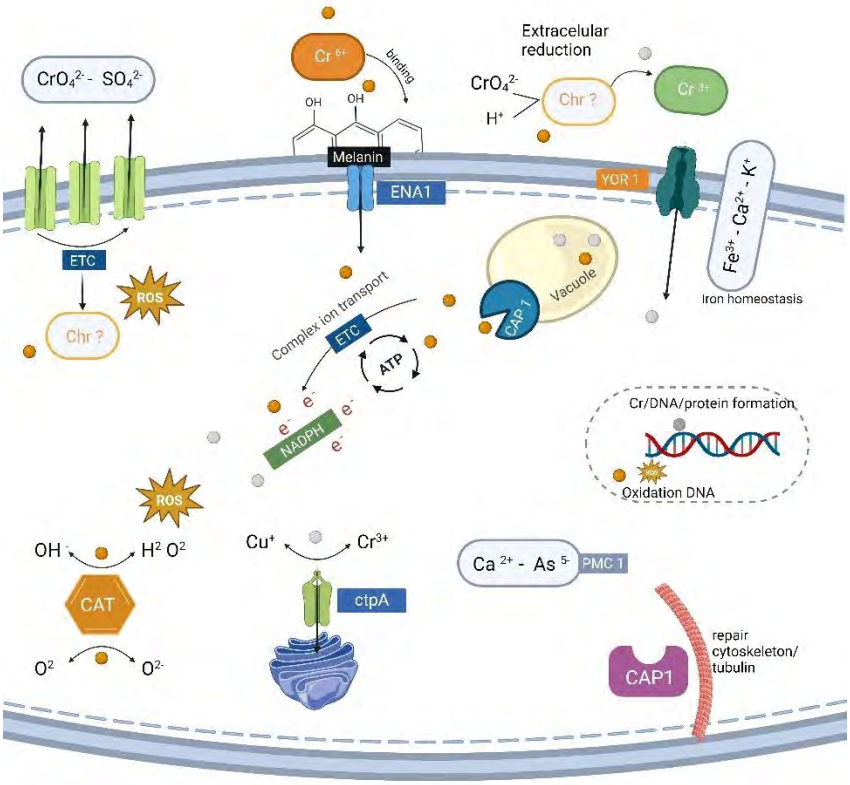

Figure 11. Schematic representation of possible genetic pathways associated to influx and efflux of Cr(VI) in *Exophiala mesophila* Cr(VI)- is the yellow spheric). YOR1 - Putative ABC transporter permease protein; ENA1 - K/Na efflux P-type ATPase (fungal type); CAP1 - F-actin-capping protein alpha subunit; CAT - Catalase; ETC - Calcium Transport; ctpA - copper-translocating P-type ATPase.

5. Conclusión

In conclusion, the combined analysis of the *Exophiala mesophila* genome assembly and annotation with SR-FTIR biochemical profiling of fungal cells exposed to heavy metals and metalloids provides valuable insights into the mechanisms employed by this fungus to tolerate extreme environments and potentially adapt to them. This comprehensive approach goes beyond establishing *E. mesophila*'s potential for hydrocarbon bioremediation by identifying it as a promising candidate for heavy metal bioremediation. Transcriptome analysis revealed genes associated with transport mechanisms potentially responsible for arsenic uptake and homeostasis within the fungal cell. While chromium exhibits greater cellular toxicity, the combined action of Cr(VI) reduction mechanisms, repair processes, and catalase activity likely allows this fungus to tolerate high chromium concentrations. However, due to the limited genomic information available for black fungi, further studies are needed to validate the function and expression of identified genes in the presence of the tested heavy metals. This validation will solidify *E. mesophila*'s potential as a bioremediation agent.

Author Contributions: CM-A: conceptualization, data curation, formal analysis, investigation, writing—original draft. IY: analytical work, interpretation (FTIR characterization). CM-A: laboratory experiments and bioinformatics work. FP-B: project administration, supervision, writing—review and editing. All the authors made critical contributions to the whole manuscript.

Funding: This research was funded by the Spanish Agencia Estatal de Investigación for funding (PID2019-111572RB-I00/AEI/10.13039/501100011033, MIC-RICE project), and the Consolidated Research Group SOSBIO (ref. 2021 SGR 01568) Generalitat de Catalunya). Cristy Medina-Armijo was a recipient of the fellowship Agencia Nacional de investigación y Desarrollo (ANID) from Chile.

Acknowledgments: This research was supported by the CERCA Programme/Generalitat de Catalunya. The FTIR experiments were performed at MIRAS beamline at ALBA Synchrotron with the collaboration of ALBA staff. The support of the CERCA Programme/Generalitat de Catalunya is also acknowledged.

Conflicts of Interest: The authors declare no conflict of interest.

6. References

Andrews, S. 2012. "FastQC: a quality control tool for high throughput sequence data." http://www.bioinformatics.babraham.ac.uk/projects/fastqc.

Aramaki, Takuya. 2020. "KofamScan." GitHub Repository. https://github.com/takaram/kofam_scan.

Benson, Dennis A et al. (2018). "GenBank." *Nucleic acids research.* 46, D41-D47. doi:10.1093/nar/gkx1094Benson DA, Cavanaugh M, Clark K, Karsch-Mizrachi I, Lipman DJ, Ostell J, Sayers EW. (2013). GenBank. *Nucleic Acids Res*. 41,D36-42. doi: 10.1093/nar/gks1195.

Bellini, E., Maresca, V., Betti, C., Castiglione, M. R., Fontanini, D., Capocchi, A., et al. (2020). The Moss Leptodictyum riparium Counteracts Severe Cadmium Stress by Activation of Glutathione Transferase and Phytochelatin Synthase, but Slightly by Phytochelatins. Int. J. Mol. Sci. Artic. Int. J. Mol. Sci 2020, 1583. doi: 10.3390/ijms21051583.

Blasi, B., Poyntner, C., Rudavsky, T., Prenafeta-Boldú, F.X., Hoog, S.D., Tafer, H. and Sterflinger, K. (2016) Pathogenic yet environmentally friendly? Black fungal candidates for bioremediation of pollutants. *Geomicrobiology Journal.* 33(3-4), 308-317.

Bolger, A. M., Lohse, M., and Usadel, B. (2014). Trimmomatic: a flexible trimmer for Illumina sequence data. *Bioinformatics.* 30, 2114–2120. doi: 10.1093/bioinformatics/btu170.

Chiarelli, R., and Roccheri, M. C. (2012). Heavy Metals and Metalloids as Autophagy Inducing Agents: Focus on Cadmium and Arsenic. *Cells*. 1, 597. doi: 10.3390/cells1030597.

Chow, E. D., Liu, O. W., O'Brien, S., and Madhani, H. D. (2007). Exploration of whole-genome responses of the human AIDS-associated yeast pathogen *Cryptococcus neoformans* var grubii: Nitric oxide stress and body temperature. *Curr. Genet*. 52, 137–148. doi: 10.1007/S00294-007-0147-9/figures/6.

de Hoog, G. S., Vicente, V. A., Najafzadeh, M. J., Harrak, M. J., Badali, H., and Seyedmousavi, S. (2011). Waterborne *Exophiala* species causing disease in cold-blooded animals. *Persoonia Mol. Phylogeny Evol. Fungi.* 27, 46–72. doi: 10.3767/003158511x614258.

de Hoog, G S et al. "Species diversity and polymorphism in the *Exophiala spinifera* clade containing opportunistic black yeast-like fungi. *Journal of clinical microbiology.* 41, 4767-78. doi:10.1128/jcm.41.10.4767-4778.2003

Díaz, P., Gimeno, Y., Carro, P., González, S., Schilardi, P. L., Benítez, G., et al. (2005). Electrochemical self-assembly of melanin films on gold. *Langmuir*. 21, 5924–5930. doi: 10.1021/la0469755.

Dobin, A., Davis, C. A., Schlesinger, F., Drenkow, J., Zaleski, C., Jha, S., et al. (2013). STAR: ultrafast universal RNA-seq aligner. *Bioinformatics*. 29, 15–21. doi: 10.1093/bioinformatics/bts635.

Ewels, P., Magnusson, M., Lundin, S., and Käller, M. (2016). MultiQC: summarize analysis results for multiple tools and samples in a single report. *Bioinformatics*. 32, 3047–3048. doi: 10.1093/bioinformatics/btw354.

Feng, L., Song, Q., Jiang, Q., and Li, Z. (2021). The horizontal and vertical distribution of deep-sea sediments fungal community in the south China sea. *Front. Mar. Sci*. 8, 592784. doi: 10.3389/fmars.2021.592784/bibtex.

Fogarty, R. V., and Tobin, J. M. (1996). Fungal melanins and their interactions with metals. *Enzyme Microb. Technol.* 19, 311–317. doi: 10.1016/0141-0229(96)00002-6.

García-Alcalde, F., Okonechnikov, K., Carbonell, J., Cruz, L. M., Götz, S., Tarazona, S., et al. (2012). Qualimap: evaluating next-generation sequencing alignment data. *Bioinformatics*. 28, 2678–2679. doi: 10.1093/bioinformatics/bts503.

Gonzalez, C. F., Aekerley, D. F., Lynch, S. V., and Matin, A. (2005). ChrR, a soluble quinone reductase of *Pseudomonas putida* that defends against H_2O_2. *J. Biol. Chem*. 280, 22590–22595. doi: 10.1074/jbc.M501654200.

Isola, D., Scano, A., Orrù, G., Prenafeta-Boldú, F. X., Zucconi, L. Hydrocarbon-Contaminated Sites: Is there something more than *Exophiala xenobiotica*? New insights into black fungal diversity using the long cold incubation method. *J. Fungi.* 7, 817. doi: 10.3390/jof7100817

Kirchhoff, L., Olsowski, M., Rath, P. M., and Steinmann, J. (2019). *Exophiala dermatitidis*: Key issues of an opportunistic fungal pathogen. *Virulence.* 10, 984–998. doi: 10.1080/21505594.2019.1596504.

Lenassi, M., Gostinčar, C., Jackman, S., Turk, M., Sadowski, I., Nislow, C., et al. (2013). Whole genome duplication and enrichment of metal cation transporters revealed by de novo genome sequencing of extremely halotolerant black yeast *Hortaea werneckii*. *PLoS One 8*. e71328. doi: 10.1371/journal.pone.0071328.

Liang, J., Liu, J., Cheng, T. Q., and Song, W. (2021). Comparative transcriptome analysis providing resistance mechanism of *Aspergillus oryzae* under arsenate stress. *Geomicrobiol. J.* 38, 426–435. doi: 10.1080/01490451.2021.1877854.

Liao, Y., Smyth, G. K., and Shi, W. (2014). Feature Counts: an efficient general purpose program for assigning sequence reads to genomic features. *Bioinformatics*. 30, 923–930. doi: 10.1093/bioinformatics/btt656.

Listemann, H. and Freiesleben, H. (1996) *Exophiala mesophila* spec. nov. *Mycoses* 39(1-2), 1-3.

Love, M. I., Huber, W., and Anders, S. (2014). Moderated estimation of fold change and dispersion for RNA-seq data with DESeq2. *Genome Biol*. 15, 1–21. doi: 10.1186/S13059-014-0550-8/figures/9.

Majumder, R., Sheikh, L., Naskar, A., Vineeta, Mukherjee, M., and Tripathy, S. (2017). Depletion of Cr(VI) from aqueous solution by heat dried biomass of a newly isolated fungus *Arthrinium malaysianum*: A mechanistic approach. *Sci. Rep. 7*. doi: 10.1038/s41598-017-10160-0.

Martínez-Rovira, I., Seksek, O., Puxeu, J., Gómez, J., Kreuzer, M., Dučić, T., et al. (2019). Synchrotron-based infrared microspectroscopy study on the radiosensitization effects of Gd nanoparticles at megavoltage radiation energies. *Analyst*. 144, 5511–5520. doi: 10.1039/c9an00792j.

Medina-Armijo, C., Yousef, I., Berna, A., Puerta, A., Esteve-Núñez, A., Viñas, M., et al. (2024a). Characterization of melanin from Exophiala mesophila with the prospect of potential biotechnological applications. *Front. Fungal Biol*. 5, 1390724. doi: 10.3389/ffunb.2024.1390724.Medina-Armijo, C., Isola, D., Illa, J., Puerta, A., Viñas, M., and Prenafeta-Boldú, F. X. (2024b). The metallotolerance and biosorption of As(V) and Cr(VI) by Black Fungi. *J. Fungi*. 10, 47 . doi: 10.3390/jof10010047.

Ng, C. Y., de Hoog, S., Li, H. E., Lee, Y. Y., Chen, C. B., and Sun, P. L. (2017). Cutaneous *Exophiala oligosperma* infection in a patient with bullous pemphigoid with a review of the Literature. *Mycopathologia.* 182, 539–547. doi: 10.1007/s11046-016-0104-6/tables/3.

Perrone, G. G., Tan, S. X., and Dawes, I. W. (2008). Reactive oxygen species and yeast apoptosis. *Biochim. Biophys. Acta - Mol. Cell Res*. 1783, 1354–1368. doi: 10.1016/j.bbamcr.2008.01.023.

Prenafeta-Boldú, F.X., Summerbell, R. and de Hoog, G.S. (2006) Fungi growing on aromatic hydrocarbons: biotechnology's unexpected encounter with biohazard? *FEMS Microbiology Reviews.* 30, 109-130.

Prota, G. (1992). Melanins and melanogenesis. *Academic Press. San Diego*, CA, USA, 1992.

Porteous, N.B., Grooters, A.M., Redding, S.W., Thompson, E.H., Rinaldi, M.G., Hoog, G.S.d. and Sutton, D.A. (2003) Identification of *Exophiala mesophila* isolated from treated dental unit waterlines. *Journal of Clinical Microbiology.* 41, 3885-3889.

Seyedmousavi, S., Badali, H., Chlebicki, A., Zhao, J., Prenafeta-boldú, F. X., and De Hoog, G. S. (2011). *Exophiala sideris*, a novel black yeast isolated from environments polluted with toxic alkyl benzenes and arsenic. *Fungal Biol*. 115, 1030–1037. doi: 10.1016/j.funbio.2011.06.004.

Silva, N. M. da, Reis, G. F., Costa, F. de F., Grisolia, M. E., Geraldo, M. R., Lustosa, B. P. R., et al. (2023). Genome sequencing of *Cladophialophora exuberans*, a novel candidate for bioremediation of hydrocarbon and heavy metal polluted habitats. *Fungal Biol*. 127, 1032–1042. doi: 10.1016/j.funbio.2023.03.003.

Tran-Ly, A. N., Reyes, C., Francis, ·, Schwarze, W. M. R., and Ribera, · Javier (2020). Microbial production of melanin and its various applications. *World J. Microbiol. Biotechnol*. 36, 170. doi: 10.1007/s11274-020-02941-z.

Usuda, D., Higashikawa, T., Hotchi, Y., Usami, K., Shimozawa, S., Tokunaga, S., et al. (2021). *Exophiala dermatitidis. World J. Clin. Cases.* 9, 7963. doi: 10.12998/wjcc.v9.i27.7963.

Valido, H. I., Resina-Gallego, M., Yousef, I., Luque-Gálvez, M. P., Valiente, M., and López-Mesas, M. (2020). Calcium oxalate kidney stones, where is the organic matter?: A synchrotron based infrared microspectroscopy study. *J. Biophotonics*. 13, 1–8. doi: 10.1002/jbio.202000303.

Vieira, R. S., Lisa Oliveira, M. M., Guibal, E., Rodríguez-Castellón, E., and Beppu, M. M. (2010). Copper, mercury and chromium adsorption on natural and crosslinked chitosan films: An XPS investigation of mechanism. *Physicochem. Eng. Asp*. 374, 108–114. doi: 10.1016/j.colsurfa.2010.11.022.

Viti, C., Marchi, E., Decorosi, F., and Giovannetti, L. (2014). Molecular mechanisms of Cr (VI) resistance in bacteria and fungi. 38, 633–659. doi: 10.1111/1574-6976.12051.

Woo, P. C. Y., Ngan, A. H. Y., Tsang, C. C. C., Ling, I. W. H., Chan, J. F. W., Leung, S. Y., et al. (2013). Clinical spectrum of *Exophiala* infections and a novel *Exophiala* species, *Exophiala hongkongensis*. *J. Clin. Microbiol*. 51, 260–267. doi: 10.1128/jcm.02336

Yousef, I., Seksek, O., Sulé-Suso, J., Gil, S., Prezado, Y., and Martinez-Rovira, I. (2016). FTIR Study of the biochemical effects induced by X-Ray irradiations combined with GD nanoparticles in F98 glioma cells. *Biophys. J.* 110, 475a. doi: 10.1016/j.bpj.2015.11.2543.

Yu, G., Wang, L. G., Han, Y., and He, Q. Y. (2012). ClusterProfiler: An R package for comparing biological themes among gene clusters. Omi. *A J. Integr. Biol*. 16, 284–287. doi: 10.1089/omi.2011.0118/asset/images/large/figure1.jpeg.

Yu Y, Teng Z, Mou Z, et al. (2021). Melatonin confers heavy metal-induced tolerance by alleviating oxidative stress and reducing the heavy metal accumulation in *Exophiala pisciphila*, a dark septate endophyte (DSE). *BMC Microbiol*. 21(1):40. doi:10.1186/s12866-021-02098-1

Zhang, Y., Zhang, Y., Liu, M., Shi, X. and Zhao, Z. (2008) Dark septate endophyte (DSE) fungi isolated from metal polluted soils: Their taxonomic position, tolerance, and accumulation of heavy metals In Vitro. *The Journal of Microbiology.* 46, 624-632.

Zhan, F., He, Y., Yang, Y., Li, Y., Li, T., and Zhao, Z. (2016). Effects of tricyclazole on cadmium tolerance and accumulation characteristics of a dark septate endophyte (DSE), *Exophiala pisciphila*. *Bull. Environ. Contam. Toxicol*. 96, 235–241. doi: 10.1007/s00128-015-1676-4.

Zhan, F., He, Y., Zu, Y., Li, T., and Zhao, Z. (2011). Characterization of melanin isolated from a dark septate endophyte (DSE), *Exophiala pisciphila*. World *J. Microbiol*. *Biotechnol*. 27, 2483–2489. doi: 10.1007/s11274-011-0712-8.

Zhao, D., Li, T., Shen, M., Wang, J., and Zhao, Z. (2015). Diverse strategies conferring extreme cadmium (Cd) tolerance in the dark septate endophyte (DSE), *Exophiala pisciphila*: Evidence from RNA-seq data. *Microbiol. Res*. 170, 27–35. doi: 10.1016/j.micres.2014.09.005.

Chapter 6

Utilizing conductive materials to mitigate methane emissions in postharvest paddy rice soil microcosms

In preparation (to be submitted to Science of the Total Environment)

Part of this chapter was presented as an oral communication in AQUACONSOIL 2023 Congress Prague, Czech Republic and Red Remedia 2023 Congress, Bilbao, Spain.

Red Remedia 2023 Congress, Cordova Spain. Poster presentation.

Utilizing conductive materials for reducing methane emissions in postharvest paddy rice soil microcosms

Cristy Medina-Armijo[1*], Belén Fernández[1], Yolanda Lucas[1], Massimo Marchesi[2], Maite Martinez-Eixarch[3], Carles Alcaraz[3], Miriam Guivernau[1], Francesc X. Prenafeta-Boldú[1], Marc Viñas[1*].

[1]Program of Sustainability in Biosystems, Institute of Agrifood Research and Technology (IRTA), Caldes de Montbui, Barcelona, Spain.

Abstract

Paddy fields are a major anthropogenic source of global methane (CH_4) emissions, a powerful greenhouse gas (GHG). This study aimed at gaining insights of different organic and inorganic conductive materials (CMs) – biochar, fungal melanin, and magnetite – to mitigate CH_4 emissions, and on their influence on key microbial populations, mimicking the postharvest season throughout the degradation of rice straw in microcosms under anaerobic conditions encompassing postharvest paddy rice soils from the Ebro Delta, Spain. Results showed that fungal melanin was the most effective CM, significantly reducing CH_4 emissions by 29%, while biochar amendment also reduced emissions by 10%. Magnetite increased CH_4 production (3%), but non-significantly in the microcosms under anaerobic conditions. All treatments (with and without CM) followed an acetoclastic methanogenesis pathway according to isotopic signature of $\delta^{13}C$-CH_4, $\delta^{13}C$-CO_2 and δ_2H-CH_4. The archaea composition *Methanobacteria*, *Methanosarcina*, and *Bathyarchaeia*, showed major abundance in the presence of CMs. Furthermore, linear discriminant analysis effect size (*LefSe*) revealed specific positive linkage between fungal melanin and electroactive bacteria like *Geobacter*, and biochar with *Clostridia* and Magnetite with *Thiobacillus* differed, being specifically related with specific archaea, particularly *Bathyarchaeia*. Furthermore, CMs potentially promote the rapid degradation of volatile fatty acids (VFAs), leading to a shortened lag phase for CH_4 production but with lower rates in the case of biochar and melanine. The results suggest that CMs might facilitate specific potential direct interspecies electron transfer (DIET) between syntrophic electroactive bacteria (i.e *Geobacter*, *Clostridia*) and electroactive methanogens such as *Methanosarcina* and *Methanobacteria.* Magnetite differed fom other CMs being specifically related with certain archaea from *Bathyarchaeia*.

Keywords: Paddy rice fields, methane mitigation, postharvest season, biochar, fungal melanin, magnetite, electroactive bacteria, direct interspecies electron transfer (DIET), methanogens.

1. Introduction

Methane, a potent greenhouse gas (GHG) found in the atmosphere, is a significant contributor to global climate change. Its global warming potential is 28 times greater than carbon dioxide over a 100-year period, and its concentration has increased by a remarkable 2.5 times since pre-industrial time (IPCC 2023). Paddy rice fields are one of the major sources of agricultural methane emissions globally, responsible for 6–11% of the global methane (CH_4) emissions from anthropogenic sources (Smith et al., 2021).

A significant portion of methane (CH_4) emissions from rice cultivation stems from post-harvest agricultural practices that involve incorporating rice straw into the soil (Ma et al., 2008; Martinez-Eizarch et al., 2018). Anaerobic decomposition of straw produces volatile fatty acids (VFAs) and hydrogen gas (H_2) as end fermentation products, which serve as energy sources for methanogenic archaea. Martínez-Eixarch et al., 2018, identified the rice postharvest season, after the incorporation of rice straw, as the major contributor to CH_4 emissions in crops in the Ebro Delta, Spain, accounting for 60-70% of total annual cumulative CH_4 emissions (Martínez-Eixarch et al., 2018). Although, different agronomic management practices offer a range of mitigation strategies for GHG emissions (i.e. water management, rice cultivation techniques, organic matter addition, and fertilization), sometimes they do not disrupt or outcompete the intricate microbial pathways involved in methane production (Duc Phung et al., n.d.; Gu et al., 2022). Therefore, it is crucial to better understand the behavior of bacterial and archaeal communities in flooded soils under different conditions and with both organic and inorganic amendmentse. In this context, the effectiveness of methanogenesis depends on the symbiotic interactions between these soil bacteria and methanogens, as their metabolic processes mutually support one another. (Cavalcante et al., 2021; Xiao et al., 2021). In addition, interspecies electron transfer seems to be an important syntrophic process occurring through two main mechanisms: (1) transfer of small electron carriers like hydrogen or formate (Stams and Plugge, 2009) and (2) direct interspecies electron transfer (DIET) (Wang et al., 2016). In the first mechanism, termed interspecies hydrogen/formate transfer, hydrogen and formate act as electron shuttles between bacteria and methanogens. Alternatively, DIET allows for direct extracellular electron transfer between electroactive bacteria and methanogens, facilitated by electrically conductive *pili* (*e-pili*), specific proteins, (semi)conductive minerals, and organic material (Kato et al., 2012; Liu et al., 2012; Rotaru et al., 2013, 2014; Chen et al., 2014; Lovley, 2017).

Conductive materials (CMs) can modify the electron acceptor proportion and availability under anaerobic conditions during methanogenesis by acting both as electron acceptors and donors (Xiao et al., 2021). This stimulates electron transfer between CMs and electroactive microorganisms, which provide a pathway for electron flow, reducing and oxidizing available releasing electrons and creating an energy field. Redox activity fluctuations can influence metabolic competition based on energy yields (Thauer et al., 2008). In recent years, there has been a growing interest in the use of natural materials, such as biochar or activated carbon, for methane mitigation (Han et al., 2016; Yin et al., 2020a). These materials are relatively biodegradable and have the dual benefit of carbon sequestration and improvement of soil physicochemical properties. Biochar, a carbon-rich material produced by pyrolyzing biomass such as wood, crop residues, and manure, has been shown to effectively mitigate GHG emissions, particularly methane emissions from paddy soil (Lu et al., 2022). The exploration of novel materials with comparable characteristics can enhance biotechnological processes and elucidate the impacts on microbial communities exposed to CMs. Fungal melanin, an intriguing new natural material, is a

pigment found in the cell walls of less-investigated black fungi categorized as ascomycetes (Butler et al., 2005). Melanin shares similar properties with biochar, promising to mitigate methane emissions in rice paddy soils (e.g., aromatic structure, conductive properties, π-bond, functional group abundance, or recalcitrant compound) (Medina-Armijo et al., 2024). Further, melanin production necessitates the large-scale cultivation of black fungi, and extraction and purification can be developed using acid hydrolysis, offering economic and energy production advantages (Choi, 2021). An alternative approach leverages the melanin-producing capabilities of melanized fungi. These fungi can be directly inoculated onto substrates, bypassing the need for a separate melanin extraction step, which can be expensive.

This investigation explored and compared the effects of biochar, fungal melanin, and inorganic magnetite, as organic and inorganic CM on the CH_4 accumulation and on the microbial community in paddy rice soil microcosms from the Ebro Delta (Spain), under rice straw amendment, mimicking the postharvest season of rice fields. The soil was incubated under anaerobic conditions in microcosms. The study aimed to: 1) evaluate the influence of CMs on CH_4 accumulation during anaerobic cultivation; 2) determine the succession dynamics of methanogenic archaeal and bacterial populations, and their association with key environmental factors, including compound specific isotope analysis of accumulated biogas (CSIA) of $\delta^{13}C\text{-}CH_4$, $\delta^{13}C\text{-}CO_2$ and $\delta^{2}H\text{-}CH_4$ to disentangle methanogenic pathways that occurred in rice paddy field under CM presence.

2. Materials and methods

2.1 Conductor material

Biochar was obtained by pyrolyzing pine biomass at 700 °C for 1 hour inside a Kon Tiki oven a particle size of 500 μm, was obtained from Carbón Vivo, Barcelona, Spain. Magnetite in FeO_3 (95%) was purchased from (Sigma Aldrich, Saint Louis, USA). Fungal melanin was extracted and purified according to the method described by Medina-Armijo et al., (2024). Extensive cultivation of the black fungus *Exophiala mesophila* was used to extract the pigments. The biomass was autoclaved to 120 °C for 20 minutes using NaOH (1 biomass: 1.5 NaOH). The biomass was then separated by centrifugation (4000 rpm) and the liquid portion was acidified with 6N HCl (1 NaOH-melanin: 1 HCl) to pH 2.5. The mixture was heated to 100 °C for 12 hours, causing the melanin to precipitate. The melanin precipitate was collected by centrifugation (4000 rpm) and washed three times with Milli-Q water. The melanin powder was then lyophilized at a pressure of 0.7 mBar at -50 °C for 24 hours, resulting in a black powder that was stored at -20 °C for further studies.

2.2 Soil sampling and incubation Soil

Soil samples were collected during the post-harvest in rice paddy fields from Ebro Delta of Spain (40º42’28.3’’N 0º37’58.6’’E) before the incorporation of rice straw into the soil. The sample were used to prepare a slurry with a (1dw: 1.75w) soil(dw)-to-water ratio, correspondig at 18 g soil and 19.5 ml of milliQ water. The slurry was then distributed into 120 mL screw capped serum flasks and supplemented with a nutrient solution containing macro and micronutrients to enhance methanogenic activity. The macronutrient composition was: 17 g NH_4Cl; 3.70g K_2HPO_4; 0.56g $MgSO_4$; 0.8g $CaCl_2.2H_2O$; 2.0g $FeCl2.4H_2O$; 0.05mg H_3BO_3; 0.07mg $ZnSO_4.H_2O$; 0.04mg

$CuCl_2.2H_2O$; 0.05mg $MnCl_2.4H_2O$; micronutrients compositions: 0.05mg $(NH_4)6Mo_7O_2.4H_2O$; 0.05mg $CoCl_2.6H_2O$; 0.09 mg $NiCl_2.6H_2O$; 0.5mg EDTA; 1 ml HCl 36%; 0.07mg Na_2SeO_3, 0.6% v/v salinity (NaCl) final concentration and bicarbonate at 0.1g L^{-1}. To mimic postharvest season and to promote microbial activity, rice straw was added at a rate of 3% (w/soil dw) and CMs (Biochar, fungal melanin and magnetite) were separately added at 1% (w/soil dw) To provide a baseline of CH_4 production for comparison, two controls were prepared: i) without straw and CMs at initial and final time (C1T0 and C1TF) and ii) with straw and without CMs at initial and final time (C2T0 and C2TF). These controls were used to quantify net methane production and evaluate changes in microbial community composition. All treatments with CMs (melanin ME; biochar BIO; magnetite MAG) and controls were performed in four replicates. To establish anaerobic conditions, all microcosms were purged with nitrogen gas for 20 minutes in the headspace. The samples were then incubated at room temperature for 130 days.

2.3 Measurement of Methane

Concentration of CH_4 and CO_2 in the serum bottle were measured with gas chromatography (detector TCD, model 8860 GC System de Agilent Technology, USA). Gas samples (200 mL) were taken from the headspace with a N_2-flushing syringe. Gas measurements were taken for 5 or 10 days up to 130 days of incubation. H2S was not detected in the headspace gas in microcosms by means TCD detector.

The kinetics of methane emission were determined by fitting the mean values of net methane to a first-order kinetic model or a modified Gompertz model (Eq.1) (Li et al., 2018). This model divided methane production into two phases, as observed in the experimental data.

$$BMP_t = A\exp(-\exp(\frac{\mu m1}{A}(\lambda 1 - t) + 1) \quad \textbf{eq 1}$$

Where: BMP: biochemical potential of methane at time t (mL CH_4 g^{-1} COD); A: maximum yield in methane production (mL CH_4 g^{-1} COD); μm: maximum rate of methane production (mL CH_4^{-1} g COD · day) and λ : delay time or lag phase (days).

2.4 Compound Specific Isotope Analysis of biogas from microcosms.

The isotopic composition of methane (CH_4) and carbon dioxide (CO_2) was analyzed at the Isotope Trace Institute in Milan, Italy, using a ThermoFisher GC-Isolink II (IRMS) system coupled with a Trace 1310, Cnflow4 – IRMS Delta V Plus. The Gas Chromatography (GC) was coupled to the Isotope Ratio Mass Spectrometer (IRMS) for stable isotope analysis. Isotope ratios were reported relative to Vienna Pee Dee Belemnite (V-PDB) for $\delta^{13}C$ and Vienna Standard Mean Ocean Water (V-SMOW) for δ^2H. The analytical precision for carbon isotope analysis was greater than ± 0.5 ‰ for hydrocarbons, ± 0.2 ‰ for CO_2, and ± 2‰ for δ^2H of CH_4. The carbon isotope ratios were all expressed in delta notation (‰) relative to the VPDB standard. This notation indicates parts per thousand (‰) difference between the sample and the standard. We then determined the apparent fractionation factor (αC) following the method described by (Conrad et al., 2009). Alpha (αC) values between 1.040 and 1.055 suggest a process dominated by acetotrophic/methylotrophic

anaerobic digestion (AD), whereas values between 1.055 and 1.080 are indicative of a primarily hydrogenotrophic AD process (Penning and Conrad, 2007).

2.5 Physicochemical análisis

Microcosm samples of soil collected at the beginning and end of the experiment were frozen at −20ºC for subsequent analysis. pH, total chemical oxygen demand (COD), Kjeldahl total nitrogen (N), ammonia, and sulfates, all parameters were determined following standard methods (Standard Methods for the Examination of Water and Wastewater, 2005). Samples of the liquid fraction (liquid supernatant after centrifuging aliquots of soil slurry (1 ml) from each microcosm were taken every 10 days for 55 days to measure volatile fatty acids (VFA) using GC-FID (model 8860 GC System de Agilent Technology, USA).

2.6 DNA extraction and gene quantification

Soil samples gathered from the bottles were preserved at − 80°C for molecular analysis. Samples collected on day 0 (T0) (incubated for 3 hours) and 130 days (TF) were chosen for the evaluation of gene copies and 16S metabarcoding in bacteria, archaea (16S rRNA), and fungi (ITS2).

DNA extraction was performed using the DNeasy® PowerSoil® kit (ref. 47,016, Qiagen, Germany) according to the manufacturer's instructions. The microbial communities were quantified based on the bacterial *16S rRNA* gene, methanogenic archaea *mcrA* gene, and dissimilatory sulfate-reducing bacteria *Apra* gene. Quantitative polymerase chain reaction (qPCR) was employed for DNA-based assessment using an Mx3000P instrument (Stratagene, Bellingham, WA, USA).

2.7 16S rRNA Amplicon Sequence high-throughput sequencing (16S rRNA-metabarcoding)

Library generation was performed following the 16S rRNA Metagenomic Sequencing Library Preparation guide (Illumina, 2013). Amplification was performed separately for bacteria in V4-V5 region of bacterial 16S rRNA gene with 515f (5'-GTGCCAGCMGCCGCGGTAA-3') and 907r (5'-CCGTCAATTCCTTTGAGTTT-3') primers; and for archaea 16S rRNA with 519f (5'-CAGCCGCCGCGGTAA-3') and 915r (5'-GTGCTCCCCCGCCAATTCCT-3') primers (Klindworth et al., 2013); and Fungi ITS2 region with ITS3-2024f (5'-GCATCGATGAAGAACGCAGC-3') and ITS4-2409r (5'-TCCTCCGCTTATTGATATGC-3') primers pairs (Toju et al., 2012) . After amplification and purification, PCR amplicons were pooled equimolarly and sequenced on an Illumina MiSeq platform at Novogene. Co., Ltd. Data analysis was conducted in house by using a workflow based on the R package DADA2 (v138.1) (Callahan et al., 2016). The SILVA database (v138.1) and UNITE database served as a reference library for bacterial and fungal taxonomy classification of amplicon sequence variants (ASVs), with ASVs exhibiting bootstrapping confidence <80% classified as unassigned. The number of reads per sample was rarefied to the minimum sample depth using the R package vegan (V2.6–4) and normalized using total sum scaling (McKnight et al., 2019). Information about the samples metadata and the classification of the sequences taxonomy generated for each database and amplicon sequence variants (ASVs) were merged into a single phyloseq object for each sequencing run using the phyloseq package (version 1.46.0) (McMurdie and Holmes, 2013). To enable comparisons between databases, the individual phyloseq objects from each database across the three runs were then combined using

the merge_phyloseq function. After discarding chimeras, singletons, chloroplasts, and kingdom selection and rarefying data by the minimum number of reads, overall rarefied clean reads and ASVs were 6045, 361 and 738 for bacteria, archaea and ITS, respectively.

2.8 Statistical analyses

To assess the significance of differences between groups, all samples were evaluated for normality (Shapiro-Wilk test) and homoscedasticity (Levene's test). Where normality was met, a student's t-test was employed to identify significant differences ($P < 0.05$). To analyze alpha diversity, which was represented by ACE, Simpson, and Shannon index (Kim et al., 2017), ANOVA followed by a post hoc Tukey's HSD test (honestly significant difference) was performed ($P < 0.05$). For non-parametric data, a Kruskal-Wallis test ($P < 0.05$) accompanied by a post hoc Wilcoxon test was employed using the R packages phyloseq, microbiome, and ggpubr. Beta diversity was visualized using principal coordinate analysis (PCoA) based on Bray-Curtis distance matrices, incorporating 999 permutations of amplicon variant sequence (ASVs) (Bray and Curtis, 1957). A permutational multivariate analysis of variance (PERMANOVA) was conducted to determine significant differences in beta diversity ($P < 0.001$) between treatments. The R package Vegan and pairwise Adonis function were utilized for this analysis.

Differential abundances between treatments at the phylum and family levels with a relative abundance of ≥ 1.0% prevalence of abundance were determined using the methods Ampvis, using the R package ampvis2. The linear discriminant analysis effect size (LEfSe) was applied to reveal the potential microbial taxa biomarkers. LEfSe is obtained from an algorithm to find significant differences in taxonomic abundance between treatments and control, using a nonparametric Kruskal-Wallis test. Subsequently, LDA is applied to the significantly abundant taxa and the effect sizes of the taxa are provided by the analyses. Those taxa bestowed higher log LDA scores than 2.0 are chosen for subsequent plotting. LEfSe analyses were conducted by means of microbiomeMarke package (Yang Cao et al., 2022)

The influence of environmental parameters on the beta diversity of bacteria and archaea at ASV level between treatments was assessed by using a partial Redundancy Analysis (RDA) with Hellinger-transformed between soil microbial communities and environmental factors (pH, ammonia (NH_3), chemical oxygen demand (COD), total nitrogen (N), sulfate (SO_4), methane (CH_4), and carbon dioxide (CO_2), using the R package "microeco." (Liu et al., 2021) All statistical analyses and R packages were performed and run in RStudio version 4.1.2.

3. Results

3.1 CH4 and VFA

Significant reductions in methane (CH_4) emissions were observed after 130 days of incubation in the Biochar treatment (10.3 %) compared to the control without CM; 209 ± 4.5 mLCH_4 g^{-1} COD_straw, P <0.05) and the melanin treatment (29.2% of depletion compared with control without CM; 165 ± 3.0 mL CH_4 g^{-1} COD_straw, P <0.0001) treatments (Figure 1). The magnetite treatment showed an increase of methane compared to the control at the end of the experiment (3% of increment, 240 ± mL CH_4 g^{-1} COD_straw), which was not significantly different from the control C2TF (Tukey HSD) test, P > 0.05). The maximum VFA accumulation occurred after 15 days, reaching concentrations of 0.014 ± 0.005 mmol VFA L^{-1}, 0.016 ± 0.07 mmol L^{-1}, 0.010 ± 0.005 mmol L^{-1} and 0.016 ± 0.0009 mmol VFA L^{-1} in the C2TF, ME, BIO, and MAG treatments, respectively (Figure 1). A decline in VFA levels was observed between 25 and 55 days, coinciding with the initiation of exponential methane accumulation in the microcosms. Table S1 summarizes the observed relationship between methane (CH_4) and carbon dioxide (CO_2), accumulation.

The cumulative CH_4 yield data obtained from the microcosms was fitted using Gompertz kinetic models. Kinetic parameters, such as *lag phase* and biogas production yield, were determined for control and treatment experiments as detailed in Table S3. The Gompertz model exhibited a good fit, with a high coefficient of determination (R^2) ranging from 0.97 to 0.99 for all experiments. Based on the regression analysis, the highest CH_4 production rates (mL $CH_4 \cdot g\ COD^{-1} \cdot d^{-1}$) were observed in control (5.427), biochar (5.348), magnetite (4.282), and melanin (4.167). Additionally, the lag phase (λ) time was calculated to assess the effect of the carrier material on CH_4 yield (Table and Figure S1). The shortest *lag phases* were observed in biochar and magnetite (7 and 6 days, respectively), indicating faster initiation of methane production compared to the control (9 days) and melanin (11 days). Melanin exhibited a delayed onset of methane production compared to the control and other treatments (Table S1).

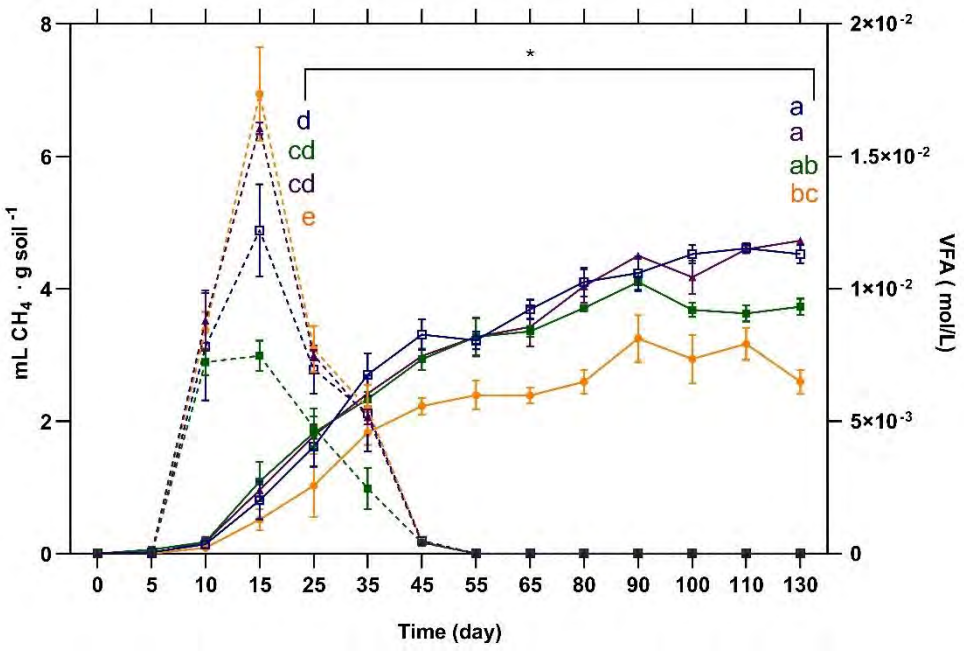

Figure 1. Cumulative methane production and volatile fatty acid (VFA) production yields. Data are presented as mean ± standard deviation (N = 4). Statistical analysis was performed using the

Kruskal-Wallis test to compare multiple treatments across 25 and 130 days time points (* denotes significant differences, $P < 0.05$, Krukal-Wallis test). Additionally, Tukey's HSD test was used to identify significant differences in methane production between specific treatments at 25 and 130 days of incubation. Different letters after 25 and 130 days of incubation in CH_4 cumulative curves, denotes statistical significance ($P<0.05$, Tukey's HSD test). The color orange: melanin; green: biochar; purple: magnetite and blue: control without conductive material (CM).

Regarding CSIA of biogas, the $\delta^{13}C\text{-}CH_4$ and $\delta^{13}C\text{-}CO_2$ isotopic signatures of CH_4 in samples collected after 25 days of incubation ranged from ⁻50 to −60‰ and −18 to −21‰, respectively (Figure 2b). These values indicate that the CH_4 was originated from microbial production, most likely via acetate fermentation, but potentially also mixed with CH_4 derived from hydrogenotrophic methanogenesis as previously suggested (Lamarche-Gagnon et al., 2019) for all treatments, including controls. The methane carbon and hydrogen isotopic signature (−50 to -60‰ $\delta^{13}C\text{-}CH_4$ and -360‰ $\delta^{2}H\text{-}CH_4$) further supports acetoclastic-methylotrophic, instead hydrogenotrophic methanogenesis, as described by Whiticar, (1999). Additionally, the apparent fractionation factor (α CO_2,CH_4 for all treatments (Table S2) suggests a value of 1.0361 ± 0.0028 (*N*=20) on average, which is indicative of predominantly acetotrophic-methylotrophic methanogenesis in all treatments (αCO_2, CH_4 <1.055; with $\delta^{13}C\text{-}CH_4$ in the range−62.8 and −50.6 ‰, $\delta^{13}C\text{-}CO_2$ in the range −17.1 and −21.1 ‰, and $\delta^{2}H\text{-}CH_4$ in the range of −353 and −370 ‰) a common isotopic signature described within the zone for aceticlastic/methylotrophic methanogenesis ($\delta^{13}C\text{-}CH_4$ from −50 to −70 and $\delta^{13}C\text{-}CO_2$ from −5 to −25 ‰ as described in Whiticar (1999) and Ruff et al., (2023).

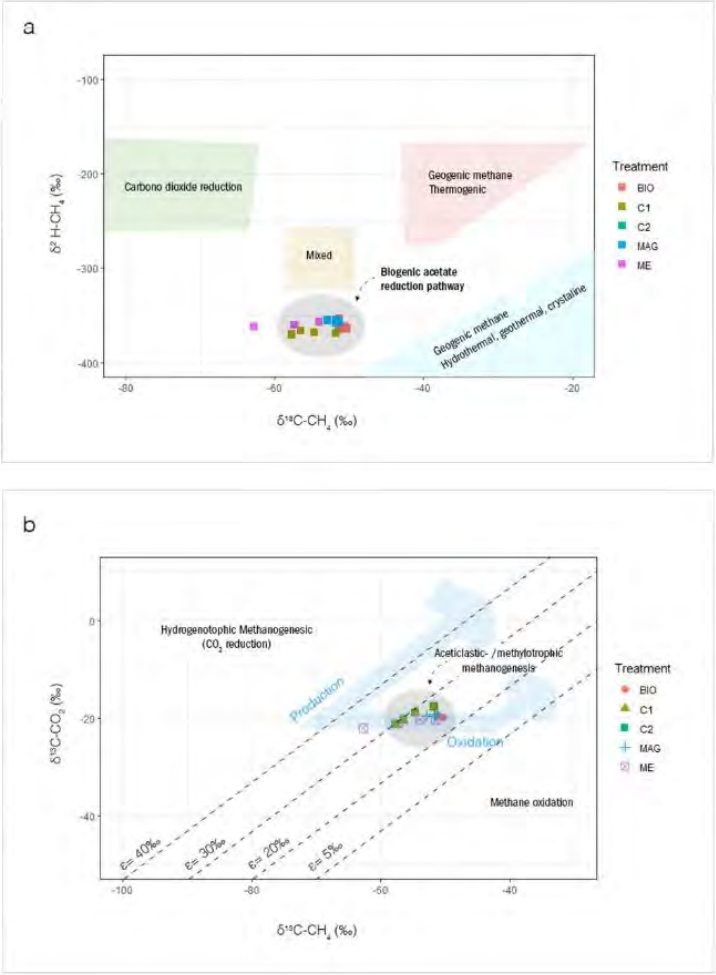

Figure 2. a) The carbon and hydrogen isotopic composition of methane (δ^{13} C-CH_4 vs δ^{2} H-CH^4) and b) and the carbon isotopic composition of methane and carbon dioxide (δ^{13} C-CH_4 vs δ^{13} C-CO_2), in anaerobic microcosms after 25 days of incubation. The isotopic composition of methane and CO_2 from microcosms fit the methylotrophic/aceticlastic zone as described in Ruff et al., (2023). Zone boundaries for biogenic methane are from (Whiticar et al., 1986), and oxidation trends in are from (Coleman et al., 1981)

3.2 Abundance of methanogens and sulfatorreduction in rice paddy soil

Table S3 summarizes the qPCR analysis, including gene copy numbers, ratios, and statistical significance tests. qPCR revealed changes in the abundance of methanogenic archaea (mcrA), sulfate-reducing bacteria (aprA), and total bacteria (16S rRNA) in the treatments (C1TF: without straw; C2TF: with straw, fungal melanin + straw, biochar + straw, and magnetite + straw). Straw addition significantly increased the total bacterial community (16S rRNA) C2TF (64.4% ± 21.2, representing 3.88 x 10^8 ± 1.47 x 108 copies·g-1) at day 130 compared to the control without straw (CM) C1TF (28.5% ± 16.1) and ($P < 0.05$) (Table S2 showed figure with gene copy and significant difference). In contrast, the aprA (sulfate reducer) and mcrA (methanogen) genes showed significant differences between treatments and compared to the control. Gene copy numbers for these functional groups decreased in treatments with melanin (4.23% ± 2.9), biochar (2.72% ± 2.7),

and magnetite (7.37% ± 2.8 for aprA) and melanin (28.5% ± 19.20), biochar (25.27% ± 20.35), and magnetite (43.60% ± 44.16 for mcrA) compared to the control ($p < 0.05$).

3.3 Effects of Different Types of conductor material (CM) on Paddy Soil Microbial Communities

The microbial community of paddy soils was analyzed using 16S rRNA gene-based metataxonomy for both bacteria and archaea. The ecological indices are summarized in Table S4. CM did not significantly affect the alpha diversity of the bacterial community in paddy soils during the anaerobic cultivation period (Figure 3). After optimization, a total of 23666 high-quality reads were obtained, in a total of 6045 amplicon sequence variants (ASVs) at a similarity cutoff of 95%. Magnetite treatments showed lower richness (ACE), diversity (Shannon), and relative dominance index (Simpson) compared to the controls, biochar, and fungal melanin (p-value < 0.05). In contrast, the species richness (ACE) of archaea (after optimization 6935 and high-quality reads 231 ASVs) increased with time of incubation when straw was added (C2TF) (Figure 3) whereas Simpson index declined with time of incubation. The addition of magnetite significantly increased ACE in comparison with the presence of biochar, melanin and the absence of conductive materials (i.e. control treatments with and without straw addition). Shannon diversity index analysis did not differed across the treatments whereas the Simpson dominance index significantly declined with the presence of conductive materials, with the exception of biochar, in relation to control treatments without straw and controls with straw at T0. Notably, the highest dominance was observed in the controls at the initial incubation time.

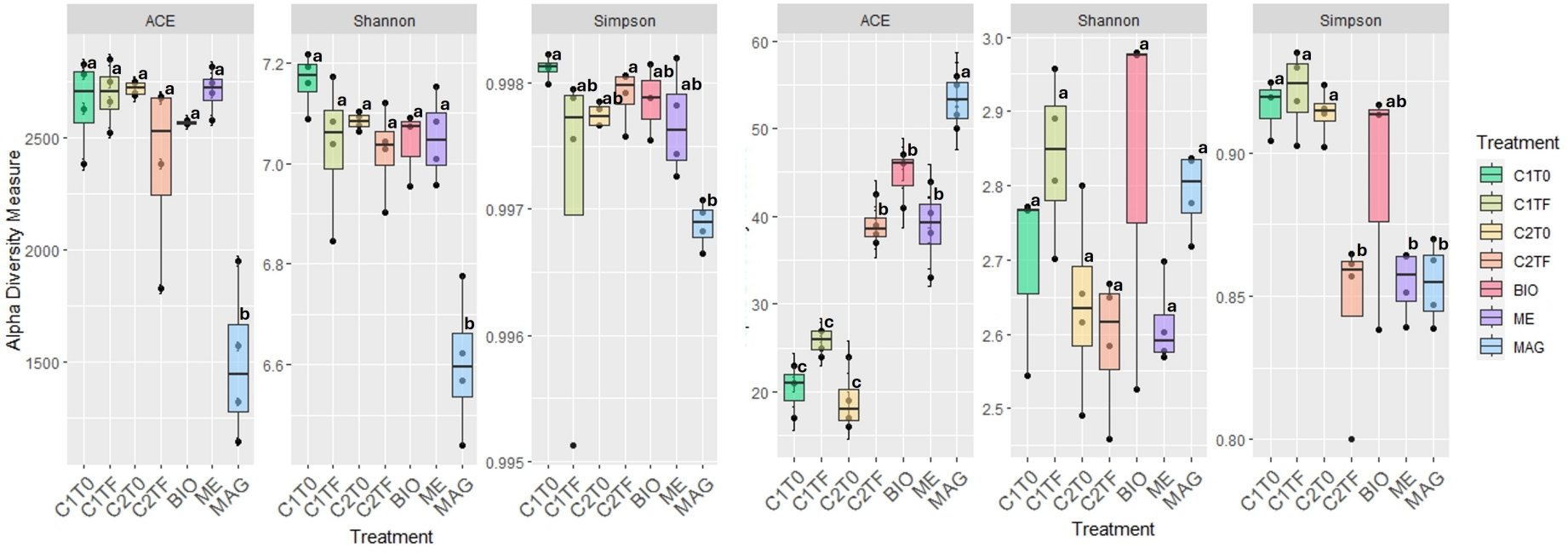

Figure 3. Bacteria (left) and Archaea (right) community metrics: richness (Chao1), diversity (Shannon), and relative dominance index (Simpson). Significance p-value $p < 0.05$, letter indicate statistical differences according to Tukey HSD test between the CM treatments (BIO: biochar; ME: fungal melanin MAG: magnetite); Control: C2T0 (time 0 incubation) and C2TF (final time) both without CM and with straw.

Notably, both the bacterial and archaeal communities in the control without straw displayed similar distribution patterns at the beginning and end of the incubation period, suggesting a stable microbial response to the absence of straw fertilization. The PCoA analysis (Figure 4) revealed six distinct clusters for the bacterial community and three clusters for the archaeal community. While variations were observed between incubation times and rice straw treatments, the overall structure of both communities remained distinct. Within the bacterial communities, the C2TF control (with straw) exhibited the greatest difference compared to the magnetite treatments (PERMANOVA $F_{:16.261}$; P: 0.027), and different between treatment also were observed MAG/BIO (PERMANOVA $F_{:10.361}$, P: 0.034) and MAG/MEL (PERMANOVA $F_{:28.344}$, P: 0.037). A similar pattern was observed in archaea, where the magnetite treatment showed significant differentiation from the C2TF control (PERMANOVA $F_{:13.121}$; P: 0.031). In contrast, no statistically significant differences were detected among the conductive materials (biochar, melanin, and magnetite). Additionally, a lower differentiation rate was observed between the melanin/C2TF and biochar/C2TF treatments. Table S5 summarizing the PERMANOVA analysis for all pairwise comparisons between controls and treatments are available in the supplementary material.

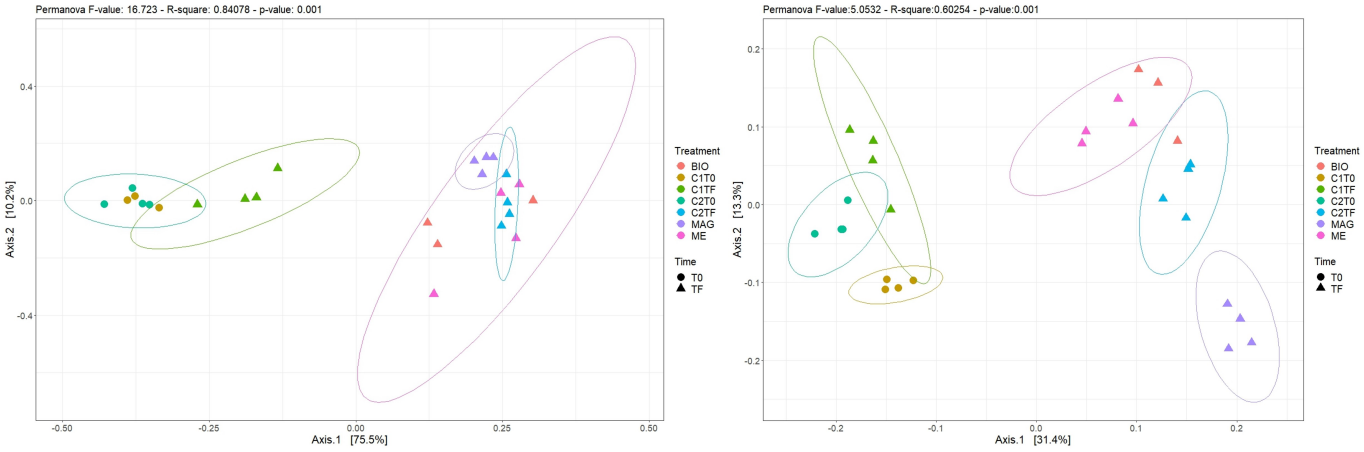

Figure 4. Principal coordinate analysis (PCoA) plots based on Bray-Curtis dissimilarities, illustrating the beta-diversity of bacterial (left panel) and archaeal (right panel) communities. PERMANOVA test results are displayed in the corresponding headers.

3.4 Composition and Diversity of Fungal Communities (ITS) in Rice Soil

Fungal community diversity in the rice soil was also analyzed (Table S6). The results indicated no significant differences in the ACE, Shannon, and Simpson diversity indices between the C2T0, C2TF, and CM (biochar, melanin, and magnetite) treatments compared to the C1T0 control group. However, the ACE and Shannon indices were significantly higher in the C1T0 control group compared to the C2T0 treatment, suggesting that straw addition to reduce the overall fungal diversity in the soil.

Principal coordinate analysis (PCoA) of fungal communities revealed significant differences in overall composition between the C2T0 treatment (control with straw at initial time) and all other treatments (Table S6). Principal component 1 (PC1) explained 52.6% of the variation, while PC2 explained 18.6%. Interestingly, the fungal communities in the C2TF control (with straw at final time) and other treatment groups (biochar, melanin, magnetite, and controls C1TF) exhibited no significant difference from each other. This suggests that straw addition itself may not be the main driver of fungal community composition after 130 days of incubation. Instead, the anoxic environment likely selects for specific fungal taxa that can tolerate anoxic conditions and potentially form dormant structures for survival.

Fungal community composition analysis at the taxonomic level (Table S6) further supported these observations. The fungal communities in the control groups, C1T0 (no straw) and C2T0 (straw), were significantly different, especially regarding the *Ascomycota* phylum. The relative abundance (RA) of the *Cladosporium* genus in C1T0 was just 0.6%, whereas it increased to 36% in C2T0. This dramatic increase suggests that Cladosporium, likely abundant in the initial rice straw material used in treatment C2T0, thrives in aerobic conditions and is significantly reduced by anoxic environments. Similar trends were observed for *Chytridiomycota_cls_Incertae_sedis*, which was significantly more abundant in C1T0 (27% RA) compared to C2T0 (7.8%). Notably, *Chytridiomycota_cls_Incertae_sedis* was the dominant group in most treatments at the end of anoxic incubation (25-38% RA) except for C2T0. Additionally, treatments with conductive materials (CM) and straw in the C2TF control also displayed enrichment of *Pseudeurotiaceae* populations (17-30% RA) compared to the initial control (C1T0). Overall, the relative abundances of various fungal taxa fluctuated between the initial controls and final treatments, with both increases and decreases observed. However, there were no significant differences among the final treatments (including the C2TF control) in the 130-day anaerobic microcosms. This aligns with the observations from the *alpha* and *beta* diversity analyses of the rice fungal communities. Supplementary Table S6 provides comprehensive statistical analyses and illustrative fungal ITS images.

3.5 Response of microbial structure to conductor material (CM)

Anaerobic cultivation and the amendment of straw significantly altered the bacterial community composition over time. CM treatments significantly impacted the relative abundance of various phyla, particularly *Proteobacteria* (especially *Gammaproteobacteria* and *Alphaproteobacteria*), *Chloroflexi*, *Actinobacteria*, *Firmicutes*, *Desulfobacterota*, and *Bacteroidetes*, with these changes being evident between the initial (T0) and final (TF) incubation times. Notably, *Thiobacillus*, *Marmoricola*, *Anaeroliea*, *Treponema*, UTCFX1, *Desulfobacca*, *Gaiella*, *Clostriudium sensu stricto 1*, *Mycobacterium*, and the *Cytophaga xylanolitica* group were the most abundant genera across most samples in the bulk environment (Figure 5 depicts the top 10 phyla using a heatmap dendrogram and average relative abundance). Table S7 summarize the statistical analysis of bacterial phyla abundance changes and the accompanying bar plot analysis of the relative abundances. Interestingly, the heatmap of ASV-specific genus taxa (Tabla S7) reveals that biochar enrichment was associated with a higher abundance of *Clostridium* sensu stricto 1 (ASV1035), while fungal melanin enrichment was linked to the *Cytophaga xylanolytica* group (ASV901). Similarly, magnetite enrichment was associated with a higher abundance of *Thiobacillus denitrificans* (ASV5910), similar as a DIET interaction non-related with methanogenis described previously with *Geobacter* and *T. denitrificans* with magnetite nanoparticles (Kato et al., 2012).

Initially, the archaeal community primarily consisted of *Bathyarchaeia* and *Nitrososphaeria* classes (C1T0 without straw and C2T0 with straw). However, a significant shift occurred after 130 days of incubation under anaerobic conditions, with *Methanobacteria* and *Methanosarcinia* becoming the dominant classes, as shown in Table S4 summarizing the statistical analysis of archaeal phyla. While *Thermoplasmata*, *Methanocellales*, and other *Methanomicrobia* remained present, their abundances decreased, as evidenced by the heatmap dendrogram (Figure 5). Notably, specific ASV genera within *g_Methanobacterium* (ASV51, ASV61, ASV56) and *c_Bathyarchaia* (ASV34, ASV60, ASV48) showed a strong response to the magnetite treatment. Conversely, the relative abundances of *g_Methanobacterium* and *g_Methanosarcina* were more dispersed in the biochar, melanin, and control (C2TF) treatments (see Table S7, heatmap ASV).

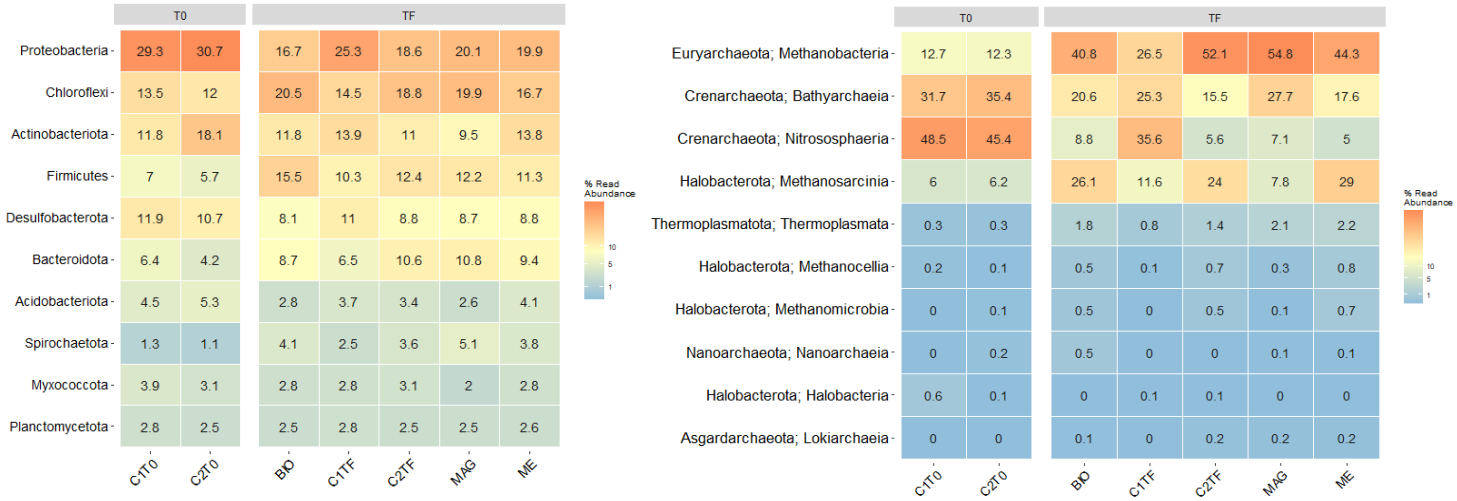

Figure 5. Heatmap average relative abundance (RA) of bacterial phyla (left) and archae phyla-family (right) in different sample types (control initial (C1T0/C2T0); control 130 days of incubation (C1TF/C2TF); and treatments 130 days of incubation (biochar: BIO, melanin: ME, magnetita: MAG).

To identify persistent differences in bacterial and archaeal communities between control soils (initial/final time and straw-amended) and soils amended with conductive materials (CMs), we employed linear discriminant effect size (LEfSe) and Kruskal-Wallis test, p-value < 0.05 analysis. Figure 6 and 7, highlights bacterial and archaeal taxa significantly enriched in each treatment group (LDA > 3).

LEfSe analysis revealed enrichment significant differences in bacterial phyla between the initial time (C1T0 withaout straw) and control (C2TF with straw). C1T0 showed higher abundance of *Proteobacteria*, *Desulfobacteriota*, *Acidobacterota*, and *Myxococcota*, while C2TF exhibited enrichment of *Firmicutes*, *Chloroflexi*, *Bacteroidetes*, and *Spirochaetes* (detailed in Table SS).

To explore the impact of specific CMs on bacterial and archaeal communities, we compared the unamended control (C2TF) with biochar (BIO), magnetite (MAG), and fungal melanin (ME) treatments (Figure 6-7). Table S9 provides specific LEfSe statistics for differentiating genera between C2TF and CM treatments. Key differentiating taxa include BIO vs C2TF

(*Proteinivoracales_f_g*, *Alkaphilus*), ME vs C2TF (*Geobacteraceae_g*, *Marmoricola*), and MAGvs C2TF (*Thiobacillus*, *Treponema*). Among these, biochar and fungal melanin enriched distinct electroactive bacteria. The *Clostridium* class (including *Clostridium sensu stricto* 1, *Alkaliphilus g*, *Christensenellaceae* R-7 group, *Proteinivoracales_f_g*, *Paraclostridium*) served as the primary differentiating marker for biochar. *Geobacteraceae_g*, with minor presence of *Pseudopelobacter*, exhibited increased abundance in response to fungal melanin. Magnetite amendment displayed a particular enrichment of *Thiobacillus*, *Treponema*, and *Anaerolinea* which could be also potential electroactive bacteria (i.e Thiobacillus, as described in Kato et al., 2012)

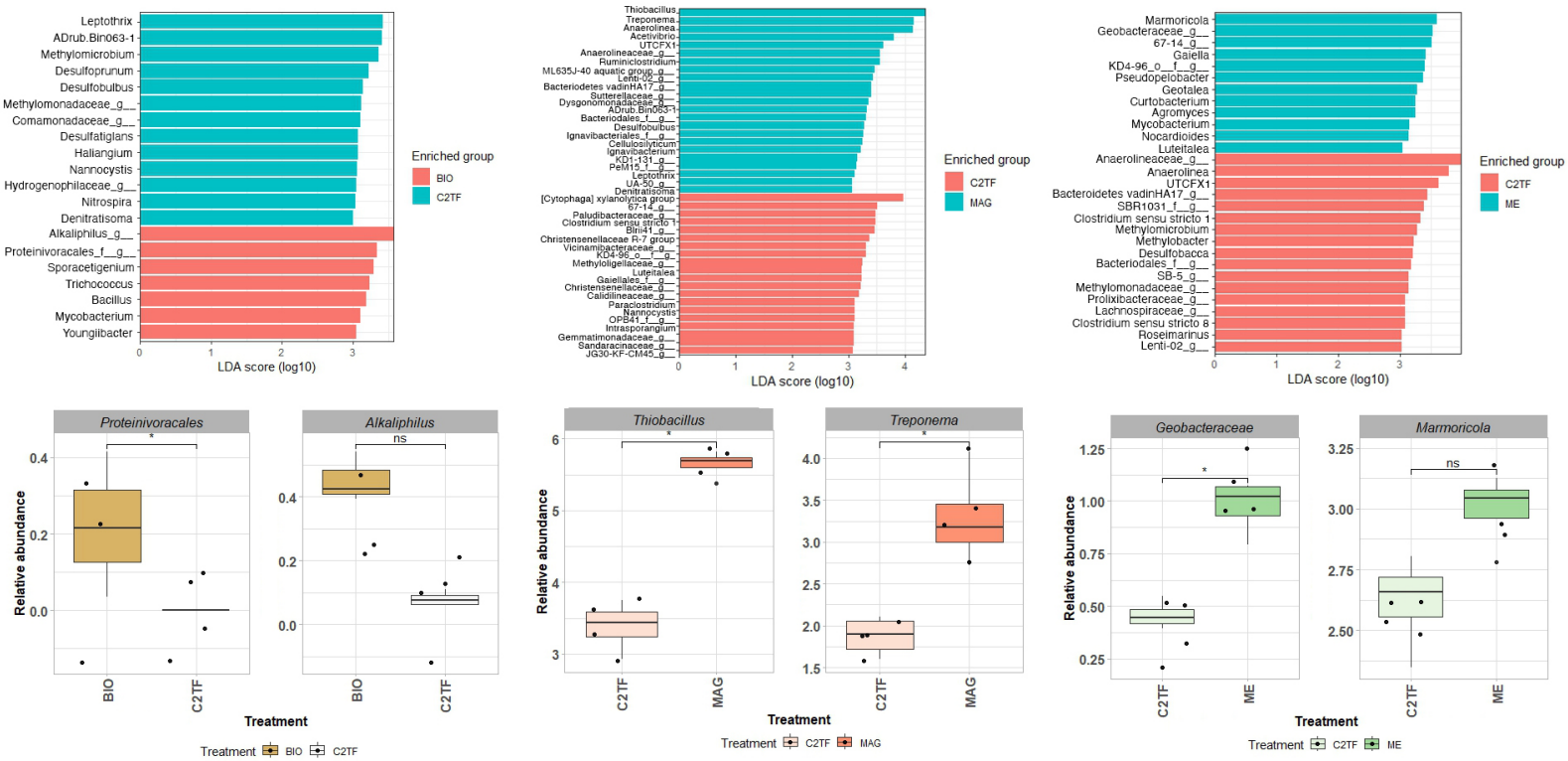

Figure 6. Differential abundance of Bacteria communities between two controls and treatments. Differently abundant taxa detected with Kruskal Wallis test p <0.05 value of linear discriminant analysis (LDA) score >3.0. Differently abundant taxa detected between the C2TF and treatment by separate, (LDA) score, and the boxplot shows the quartiles above and below the median with dark line at center of the box denoting median, black dots showing the outlier. The respective p value for each family group is reported using Wilcoxon rank sum test. Significance p-value codes (*** $P < 0.001$, ** $P < 0.01$; * $P < 0.05$) indicate statistical differences according to Wilcox test.

LEfSe analysis of archaea revealed distinct differences between C2TF/MAG and ME/MAG treatments, particularly within *Bathyarchaeia*, *Methanomicrobia*, *Methanosarcinia*, and *Methanocellia*. Interestingly, a marker of significant difference emerged between C1T0 and C2TF (initial and final incubation times). Specifically, the relative abundance of *Nitrososphaeria*, *Bathyarchaeia*, and *Halobacteria* notably decreased at 130 days of incubation, even with the addition of electron mediator (CM). Furthermore, the magnetite treatment displayed a higher relative abundance within the *Bathyarchaeia* group at 130 days of incubation (Figure 7).

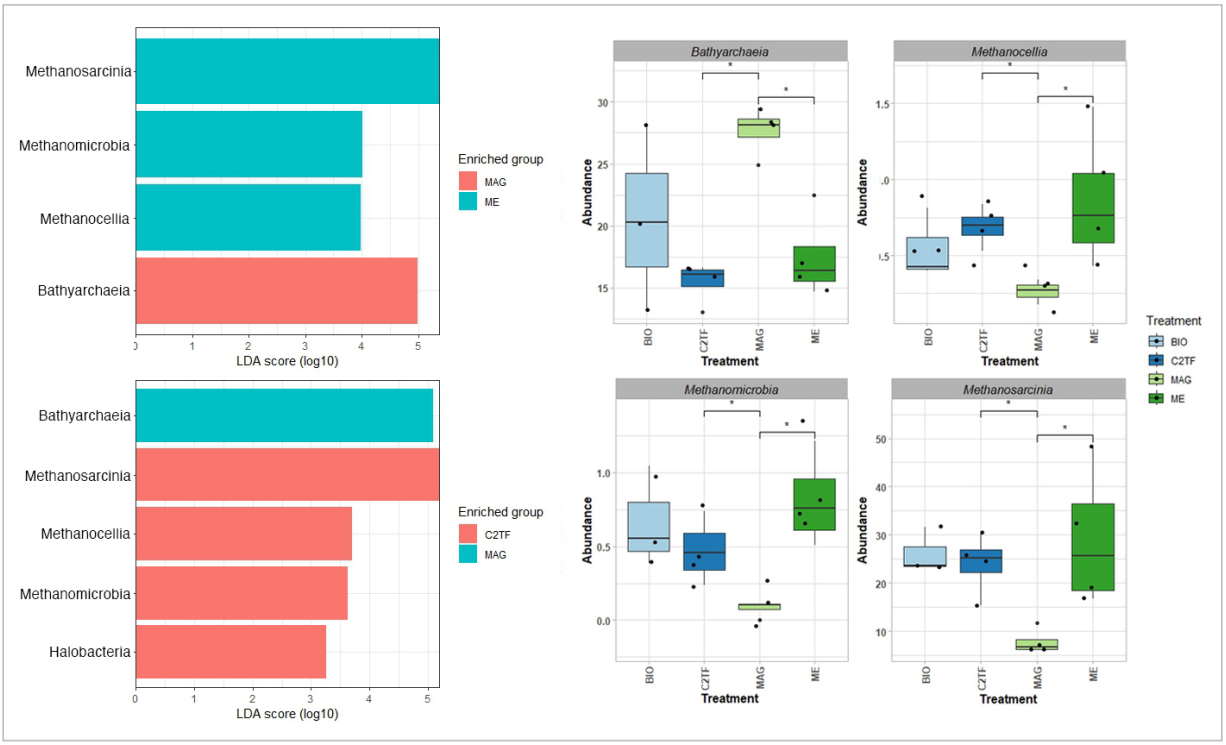

Figure 7. Differential abundance analysis of archaeal communities between CM vs control (C2TF) and vs the other CMs. Differently abundant taxa detected with Kruskal Wallis test $P < 0.05$ value of linear discriminant analysis (LDA) score > 3.0. a) The heatmap shows the differential abundance of (LDA) score > 3.0, transform in log 10p, between the treatments and control to final time (C2TF), c) Differently abundant taxa detected archaea C2TF and magnetite and melanin with magnetite, (LDA) score, biochar noy showed marked, a) The boxplot shows the quartiles above and below the median with dark line at center of the box denoting median, black dots showing the outlier. The respective p value for each family group is reported using Wilcoxon rank sum test. The boxplot shows the quartiles, between the principal taxa marker in the LDA analysis. Significance p-value codes (*** $P < 0.001$, ** $P < 0.01$; * $P < 0.05$) indicate statistical differences according to Wilcoxon test.

3.6 Effects of environmental factors on the microbial community

Changes in soil chemical properties in response to different CMs amendments at the rice soil are shown in Table S10. The pH was decreased at more neutral conditions in CMs compared to C1T0 /C1TF/C2T0 represent alkaline conditions, with significant differences in pH of the tested soils

were observed between the biochar, melanin and magnetite and C1TF ($p>0.05$). Besides, there were significant differences in EC between melanin with C1T0 /C1TF/C2T0/C2TF non-CM amendment. Soil available NH_3 gradually decreased during the whole incubaton period with significant difference among CMs with C1TF, special difference in magnetite treatments respect to C2TF. The N-nitrate concentrations was specialy significan different in the magnetite treatments with an increment (704.25±18.84 mg N/Kg, $p<0.05$), compared to all treatments and control. Furthermore, the available COD show an increased in biochar treatment (28391.75±2985.01 mg O_2/Kg) compared to C1T0/C1TF 1517.75±962.48 - 13659.25±642.56 mg O_2/Kg, respectively. SO_4 an importat increased in the CMs treatment respect to C2TF significant difference was observed ($p< 0.05$).

To explore the connection between environmental factors and the changes in the microbial community and the presence of different conductive materials (CM) in rice soil, we performed a Redundancy Analysis (RDA) by comparing both physicochemical parameters and bacterial diversity at ASV level (Figure 8). The RDA revealed that environmental factors, including pH, ammonia (NH_3), chemical oxygen demand (COD), total nitrogen (N), sulfate (SO_4), methane (CH_4), and carbon dioxide (CO_2), explained 50.26% of the variation in CM performance and 28.55% of the variation in bacterial communities.

For bacterial communities, total nitrogen ($F = 4.36$, $P = 0.01$), CH_4 ($F = 3.23$, $P = 0.05$), and pH ($F = 1.96$, $P = 0.1$) were the most significant factors influencing their overall variation. Notably, the bacterial communities in the magnetite treatment formed a distinct cluster, likely due to total nitrogen. Additionally, the C2TF treatment displayed a separate grouping compared to both the CM and C1TF treatments, which could be attributed to CH_4. Finally, the analysis suggests a positive correlation between COD and SO_4 content with the development trajectory of the microbial community, this is contrasted with the analyzes observed in table S10, where an increase in the concentrations of these two parameters is observed. Among archaeal communities, methane (CH_4) concentration ($F = 8.20$, $P < 0.001$), total nitrogen (N-total) ($F = 3.52$, $P < 0.05$), and carbon dioxide (CO_2) concentration ($F = 3.25$, $P < 0.05$) were the most significant factors in explaining the total variation. Specifically, the archaeal communities associated with the C2TF treatment formed a distinct group. This separation likely resulted from higher CH_4 and CO_2 concentrations, and conversely, lower N-total in the C2TF treatment. Interestingly, mirroring the pattern observed in bacterial communities, the magnetite treatment separated from the BIO and ME treatments, again influenced by total nitrogen.

Correlation analysis was performed comparing the abundant bacterial genera (50% prevalence) and their relationships with these physicochemical factors 130days of incubation, are shown in Figure 8 (Spearman Correlation Heatmap). Interestingly, methane accumulation showed no significant correlation with most bacterial genera, except for negative associations with *Chloroflexi* and positive ones with *Cyanobacteria* (both $P < 0.001$). Similarly, sulfate levels were negatively correlated with *Acidobacteria*, *Actinobacteria*, and *Campylobacterota* ($P < 0.001$). In contrast, total nitrogen, pH, ammonia, and chemical oxygen demand displayed positive correlations with these same bacterial groups. Among archaea, the dominant *Methanocellaceae* and *Methanomicrobiaceae* showed negative correlations with methane ($P < 0.001$), while *Methanobacteriaceae*, exhibited positive correlations with factors CH_4 ($P < 0.001$), which is contrasted with the abundance analyses, where it is the group of methanogenic archaea with the greatest representativeness. Additionally, *Nitrososphaeraceae* positively correlated with NH_3 and chemical oxygen demand.

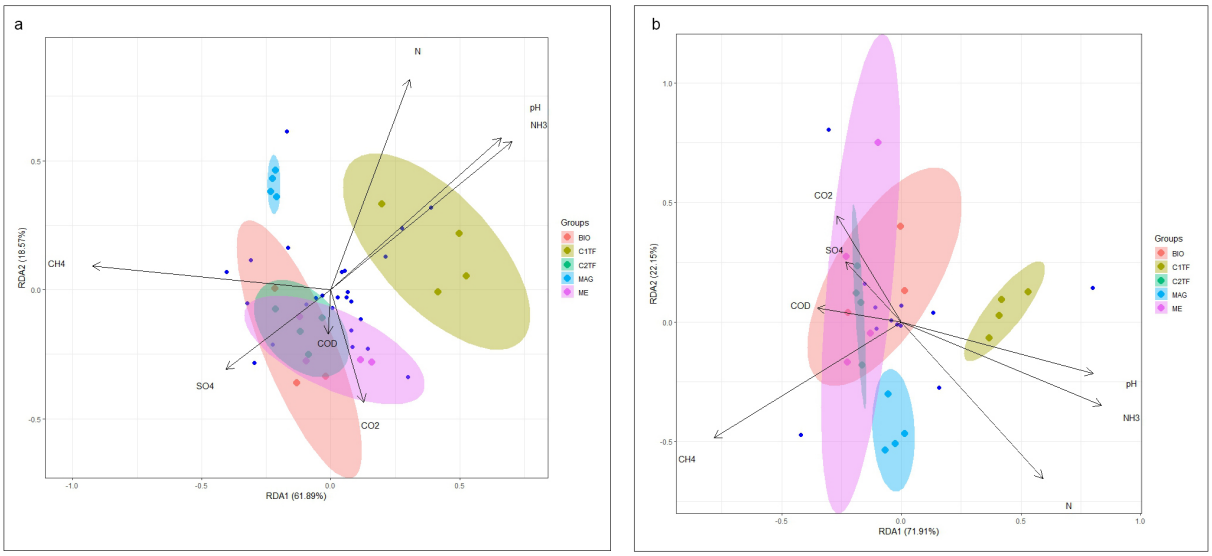

Figure 8. Redundancy analysis (RDA) of treatment (BIO: biochar, ME: melanin, MAG: magnetite) and Contro (C1TF: withot/Straw/EM and C2TF: with/Straw and without/EM) of the relative abundance of microbial community composition among samples and environmental variables that were significantly associated with community composition including pH, ammonia (NH_3), chemical oxygen demand (COD), total nitrogen (N), sulfate (SO_4), methane (CH_4), and carbon dioxide (CO_2).

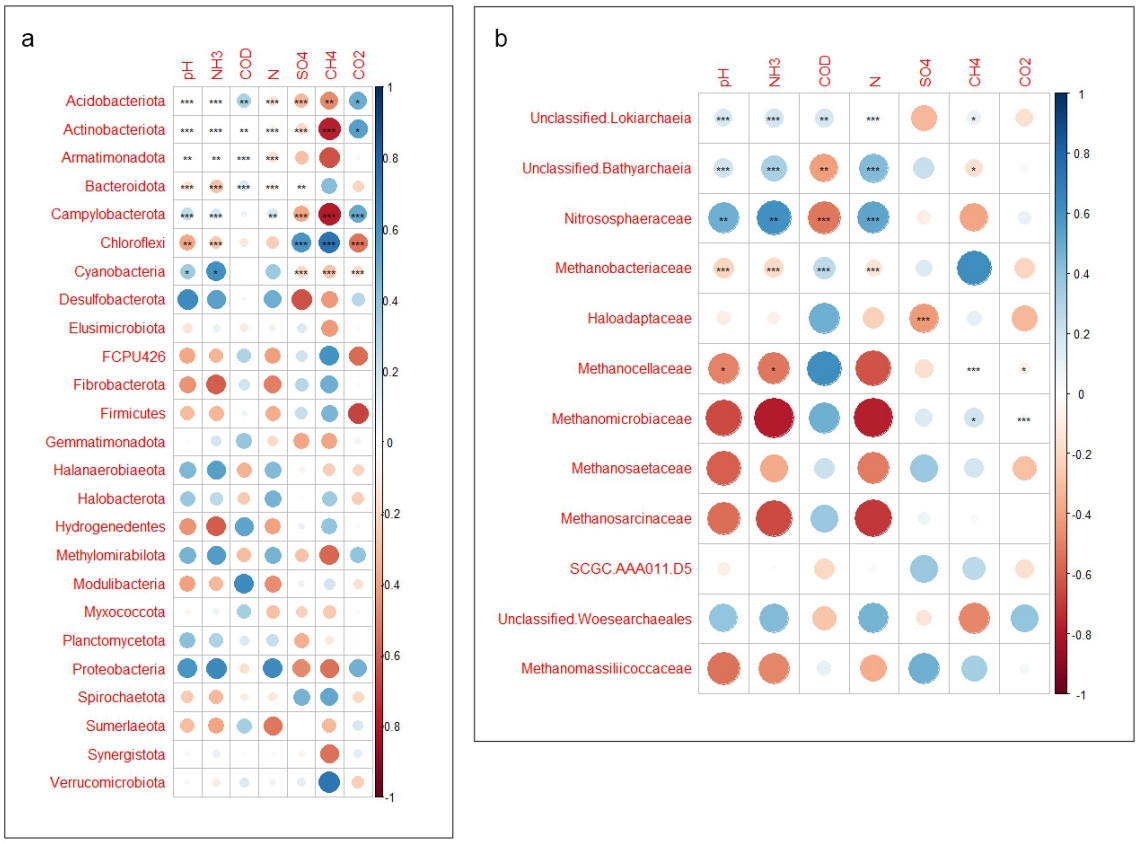

Figure 9. Spearman's correlation analysis between environmental factors (pH, ammonia (NH_3), chemical oxygen demand (COD), total nitrogen (N), sulfate (SO_4), methane (CH_4), and carbon dioxide (CO_2), and relative abundance of bacteria and archaea respectively. Significance level: *: $P < 0.05$; **: $P < 0.01$; ***: $P < 0.001$. CH_4 total: expressed in mL g^{-1} of CH_4 per microcosm.

4. Discussion

4.1 Effect of rice-straw in methane production on complex microbial communities.

The incorporation of rice straw (RS) during each post-harvest campaign is a predominant agricultural practice in waste management and soil carbon sequestration in deltaic regions such as the Ebro. Rice straw is characterized by a high content (>50%) of organic matter (w/w) and (> 1%) of total nitrogen (w/w) and a low proportion of recalcitrant lignin (approximately 5-15% w/w) (Yuan et al., 2020.; Jin et al., 2023). The influence of RS addition on methane (CH_4) production in rice field microcosms has been extensively documented (Nan et al., 2020.; Yuan et al., 2020.; Martínez-Eixarch et al., 2018). Therefore, achieving efficient RS utilization while maintaining soil productivity and fertility is crucial for both soil health and the development of novel methane mitigation applications. RS decomposition commences immediately upon its introduction. The observed slowdown in CH_4 accumulation after day 45 likely signifies the depletion of readily degradable organic carbon within the RS, marking the culmination of the rapid decomposition phase. This observation aligns with previous research demonstrating a rapid initial decomposition rate followed by a significant decrease after 20 days (Yuan et al., 2020.; Jin et al., 2023).

Notably, the shifts in the microbial community following straw addition to microcosms aligned with beta-diversity patterns observed in the PCoA analysis (Bray Curtis distance at ASV level). This analysis revealed significant variation in the compositional structure of microbial communities attributable to the effects of the added rice straw (Figure 4). In contrast, alpha-diversity metrics did not detect significant differences in bacterial communities, although these differences were evident in archaeal communities. Furthermore, LEfSe analysis identified specific variations in species abundance between straw-amended and control microcosms, further supporting the beta-diversity trends (Table S8). Distinct bacterial community compositions across soils were likely driven by various factors, including pH, COD, and total nitrogen (Table S10). For example, higher soil COD content potentially explains the increased abundance of bacterial families affiliated with *Firmicutes*, particularly *Clostridia* species, which are well-known for their role in organic matter hydrolysis and fermentation (Kim and Liesack, 2015). Previous studies have also shown a rise in the relative abundance of several *Clostridia*-affiliated families with increased expression of glycosyl hydrolase transcripts, enzymes involved in cellulose and chitin breakdown upon RS addition (Wegner and Liesack, 2016). Additionally, the Bacteroidetes group, with a prominent representative like *Cytophaga xylanolytica*, known for degrading large macromolecules like cellulose, was depicted This bacterium is known for its ability to degrade large macromolecules such as xylose under anaerobic conditions (Haack and Breznak, 1993). While *Cytophaga xylanolytica* may not directly degrade cellulose or lignin, it's well-suited to utilize the hemicellulose fraction of RS. Furthermore, LEfSe analysis revealed enrichment of the of the *Cloroflexi* in *Anaerolineaceae* family in the straw treatment and the CMs with straw at the final time, they are likely important primary fermenters in anaerobic environments. These bacteria engage in fermentative metabolism, utilizing carbohydrates and proteinaceous carbon substrates under anaerobic conditions (Sun et al., 2016). Conversely, RS addition only resulted in a relative increase of *Methanobacteria* and *Methanosarcina* (Fig. 3b), as the dominant methanogenic archaeal groups in the rice soil samples, these archaeal groups were also the dominant methanogens in the rice soil samples, exhibiting a significant positive correlation with CH_4 production as revealed by Spearman's rank correlation test. Interestingly, the relative abundances of *Nitrososphaeraceae* were initially higher in both control soils (with and without straw) compared to the straw-amended microcosms at the final sampling time (130 days of incubation). This decrease suggests a potential reduction in their populations following RS addition. Our findings provide strong evidence for their potential role in the nitrification process of rice soil when O_2 is available (surface of paddy soils at the beginning of the postharvest season 2 weeks before rice straw incorporation, or under low organic loads). Notably, a previous study by Zhen et al. (2023) reported similar observations, highlighting the influence of salinity and ammonia concentration on *Nitrososphaeraceae* species (Zhen et al., 2023) in rice paddy fields.

4.2 Impact of Conductive Materials on Methane Production and Microbial Communities in Paddy Fields

Biochar

Compared to the control with straw and without CM, biochar amendments significantly reduced CH_4 emissions (10.3%) from rice paddy soils amended with rice straw. These findings align with previous research on paddy soils on biochar amendment (Feng et al., 2012; Nan et al., 2020, Han et al., 2020). Multiple factors influence CH_4 emissions in biochar-treated soils, but also the type of biomass used for pyrolysis, temperature during pyrolysis and inherent soil properties are important drivers for final GHG mitigation described (Lehmann et al., 2006). Studies report

contrasting findings. Feng et al. (2012) observed significant CH_4 reduction with biochars pyrolyzed at 300 and 500 °C, while Zhang et al. (2010) reported increased emissions. Our experiment aligns with Feng et al., demonstrating a 10.2% CH_4 reduction using 700 °C biochar. High pyrolysis temperatures impact functional groups (COOH−, OH−, COO−) but likely not the core carbon structure or conductive properties. Ji et al. (2020) observed an 18.1% reduction with 700 °C straw biochar, highlighting potential feedstock and soil type (mulched vs. paddy) influences. Further research is necessary to elucidate the stability of functional groups across pyrolysis temperatures and their effects on methane mitigation in various soil environments.

In our study we observed that biochar addition significantly increased the relative abundance of potential iron-reducing bacteria such as *Clostridia* species. This observation aligns with previous reports on the interaction between *Clostridia* and biochar (Ji et al., 2020; XU et al., 2023). Biochar's high surface area facilitates electron shuttling between microbes and insoluble electron acceptors, such as Fe(III) (oxyhydr) oxides, promoting Fe(II) reduction. This process may outcompete methanogens to utilize electrons under DIET interactions leading to a decrease of CH_4 emissions. One potential inhibition mechanism for methanogenesis involves competition for acetate or H_2 between methanogens and Fe(III)-reducing bacteria when biochar with high surface area is added. Notably, LEfSe analysis revealed a differential enrichment of specific *Clostridia* species ($p < 0.05$) including *Alkaliphilus* related to iron or sulfur reduction, and *Proteinivoracales_f_g* with hydrolytic and acidogenic abilities to produce VFAs and hydrogen (Figure 6). Also, LEfSe analysis revealed distinct biomarker of potential electroactive bacteria in biochar amended soil compared to the control and other treatments (Table S8). These inclu*ded Clostridium sensu stricto 1, Christensenellaceae R-7 group, Paraclostridium, and Bacillus* as identified using different LEfSe analyses. Furthermore, previous studies suggest that electroactive microbes within *Clostridia* could promote direct interspecies electron transfer (DIET) using biochar as electron conduits (Lim et al., 2020). Otherwise, biochar amendment did not inhibit methanogenic archaea in this study, consistent with previous observations (Feng et al., 2012). Syntrophy between direct interspecies electron transfer (DIET) species and the methanogenic archaeal community appeared to be unaffected by biochar addition. *Methanobacterium,* a strictly hydrogenotrophic methanogen, was the most abundant archaeal group. Interestingly carbon isotope signatures were related to methyltrophic-aceticlastic pathway, which could be explained by a specific signature of DIET interaction with hydrogenotrophic methanogens. *Methanobacterium* can potentially partner with hydrogen-producing acetogens like *Clostridium* to convert H_2 and CO_2 to acetate, thereby competing for substrates with other hydrogenotrophic methanogens (Dykstra and Pavlostathis, 2017). The presence of *Methanosarcina* interacting with DIET-capable *Clostridium* species has also been reported in biochar-amended paddy fields (Ji et al., 2018). In addition, conductive particles stimulated syntrophic oxidation of acetate together with CO_2-reductive methanogenesis involving *Geobacter* and *Methanosarcina* (Nozhevnikova et al., 2020).

Carbon and hydrogen isotopic analysis of CH_4 and CO_2 revealed that these systems were dominated by aceticlastic-methylotrophic metabolisms. This conclusion is supported by the higher abundances of *Methanobacterium* and *Methanosarcina*, key methanogens in rice field soils. The existence of non-hydrogenotrophic pathway during methanogenesis would imply that Methanobacterium (a strictly hydrogenotrophic methanogen) could be also active by means DIET with natural electron conduits in rice paddy soil (with and without the amendment of biochar) in the rice generation. Similar studies have observed this correlation between methanogen abundance and metabolic pathways (Feng et al., 2012). Interestingly, biochar amendment exhibited minimal impact on the composition of the methanogenic archaeal community. These observations suggest that biochar at neutral pH (6.61 ± 0.04), as observed in this study, does not

exert a significant effect on methanogenesis. This finding aligns with observations in paddy soils with neutral pH conditions. It is well established that biochar's stimulatory effect on methanogenesis is greater at lower pH compared to neutral conditions, as observed in this study (Lehmann, 2007; Liu et al., 2011). Besides, redundancy analysis (RDA) revealed a negative correlation between chemical oxygen demand (COD) and sulfate (SO_4) concentrations n bacteria communities, while microbial activity and abundance were positively associated with bacterial populations and total nitrogen content, implying that microorganisms were actively involved in the degradation of organic matter and sulfate when biochar was amended into the soil. Therefore, biochar amendment likely influences pH regulation, potentially due to its conductive properties. This hypothesis is further supported by our redundancy analysis (RDA) which revealed a negative association between biochar application, archaeal abundance, and neutral pH. This observed association might be attributed to the complex interactions between fermentative bacteria and methanogenic archaea within syntrophic relationships, along with the intricate regulation of redox conditions within the rice paddy soil system. However, to elucidate the precise influence of pH on methanogenesis in these systems, further studies are warranted.

Fungal melanin

This study explores the potential of fungal melanin, as an alternative biomaterial for biotechnological purposes, as a potential methane mitigation strategy in paddy fields. Fungal melanin possesses properties similar to humic acid, with a shared carbon structure rich in strong C-C bonds and π-π interactions, leading to enhanced electrical conductivity acting as a semiconductive material (Medina-Armijo, et al 2024). Additionally, the presence of functional groups like COO^-, OH, COOH, and NH^- facilitates interactions with both metallic and organic compounds (Hong and Simon, 2007) as well as enhancing the electroactive capability of *Geobacter* under in-vitro conditions (Medina-Armijo et al., 2024). Notably, fungal melanin exhibits a high surface area, analogous to biochar. This characteristic, previously recognized for its potential in supercapacitors and semi-conductor reactions, allows for the adsorption of free electrons within the system (Madkhali et al., 2020). Intriguingly, the present study has revealed a significant methane mitigation effect under anaerobic conditions, when by fungal melanin was amended, suggesting its potential as a natural material for mitigating methane emissions while simultaneously promoting soil fertility. This mitigation effect may be attributed to the recalcitrant nature of fungal melanin, similar to biochar, facilitating long-term carbon sequestration within rice paddy soils, and also the high porosity and negative surface charge of fungal melanin could promote nutrient and water retention, further enhancing soil fertility. Additionally, fungal melanin may act as an electron conduit, facilitating competition with alternative interspecies electron transfer (IET) metabolisms utilized by methanogens. This competition could contribute to the observed reduction in methane emissions.

Fungal melanin microcosms exhibited a significant association with *Geobacter* as revealed in LEfSe ($P = 0.021$) analysis when compared to the control (with rice straw without CM) and the other CM treatments. Previously, Medina-Armijo et al. (2024) demonstrated the electrochemical interaction through cyclic voltammetry of fungal melanin extracted from *Exophiala mesophila*, a black fungus, in co-culture with *Geobacter sulfurreducens*. Their results showed that *G. sulfurreduscens* can reduce the quinone-like compounds of melanin, generating new voltametric peaks possibly corresponding to semiquinones (Medina-Armijo et al., 2024). Interestingly, artificial quinone molecules have been described to act as extracellular electron acceptors, particularly in anaerobic methane oxidation (AOM), and can act as electron transfer mediators, with *Mentanosarcina acetivorans* (Holmes et al., 2019; Song et al., 2023).

Electroactive bacteria belonging to the genus *Geobacter* are also known to be quinone-reducing microorganisms, utilizing Fe(III) as their terminal electron acceptor (Lovley et al., 1998). Recent studies have demonstrated the occurrence of direct interspecies electron transfer (DIET) in co-cultures of *Geobacter* species and acetoclastic methanogens (e.g., *Methanosaeta* and *Methanosarcina*) (Rotaru et al., 2017). The majority of these studies highlight syntrophy between bacterial electron-reducing species and methanogenic archaea in methane production via DIET. However, competition for electron donors between methanogens and Fe(III)-reducing microorganisms, as well as melanin-reducing microorganisms, is a crucial factor in rice paddy soil microcosms. This competition likely arises due to the limited availability of electron donors for methanogenic respiration.

Fungal melanin can function as an alternative electron sink. In rice paddy soil, for instance, it can accept electrons from various sources such as sulfate (SO_4^{-2}), nitrates (NO^{-3}), Fe(III), Mn(II), and H_2, thereby creating competition with bacterial electron reducers and methanogenic archaea. Notably, fungal melanin also stimulates the presence of other electrobacteria like *Pseudopelobacter*, *Geotalea*, *Christensenellaceae_g*, and *Paraclostridium*, known for their Fe(III)-reducing capabilities. These bacteria could potentially compete with methanogens in alternative DIET-based metabolisms.

Intriguingly, fungal melanin appears to be correlated with an increase in the relative abundance of *Methanosarcina*. While the role of fungal melanin in DIET or syntrophic relationships with *Methanosarcina* has not been directly studied, others research has described a specific mechanism by which humic acid (similar to melanin) enhances the respiratory growth of *Methanosarcina acetivorans*. This mechanism involves pyrroloquinoline quinone (PQQ). When utilizing methanol or acetate as energy sources, humic acid reduction (analogous to melanin) promotes the growth of *M. acetivorans* beyond that attributed solely to methanogenesis, suggesting the utilization of both respiratory and fermentative modes of energy conservation, with less CH4 generation (Song et al., 2023), which could be a potential pathway promoted by the melanine availability under anaerobic conditions in soil microcosms, and in waterlogged flooded agroecosystems. .

Fungal melanin exhibited a delayed onset of methane production compared to the control and other treatments, despite not affecting methanogen growth (Figure 3). This observation suggests that fungal melanin may exert a strong electron-attracting effect, potentially altering pH, redox conditions, or nutrient availability, and creating a less favorable environment for methanogenesis. However, volatile fatty acid (VFA) analysis revealed that fungal melanin accelerated VFA degradation, potentially preventing VFA accumulation, which can compete with methanogenic activity. Previous reports have shown that conductive materials promote rapid VFA degradation and prevent VFA accumulation during anaerobic digestion (Qiu et al., 2019; Yin et al., 2020a). This phenomenon may be attributed to the fact that fermentation and acidification of complex organic substrates involve subsequent reaction steps and require high diverse microbial communities. Therefore, it is possible that fungal melanin modulates DIET between different syntrophic bacteria and methanogens, resulting in a shorter lag phase for CH_4 production but with lower emission rate.

Notably, we observed a significantly higher abundance of *Cladosporium* in treatments at the beginning of the incubation period compared to the control without straw addition (C2T0). *Cladosporium* is a black fungus known for its conspicuous production of melanin, primarily within its cell walls. This finding suggests that dead *Cladosporium* biomass could be an additional source of melanin in paddy soils. Consequently, it is highly plausible that the melanin content in our

Ebro Delta paddy field system is naturally augmented. This further implies that the presence of Cladosporium in rice straw plays a significant role in melanin incorporation and potentially influences microbial community dynamics within these soils.

Magnetite

In contrast to other conductive materials (CMs), magnetite promoted a non-significative increase of methane production in the microcosms. It exhibited a low and statistically non-significant methane production rate (-3%; P >0.05) compared to the control with rice straw and the treatments encompassing CM. Several studies on anaerobic digestion systems report the application of magnetite to enhance methane yields (Zhuang et al., 2018; Xia et al., 2019). Magnetite exhibited remarkable differences in *alpha* and *beta* microbial diversity compared to other conductive materials (CMs) and controls. Notably, magnetite displayed the lowest bacterial richness, while archaea showed a pattern of high richness. A distinctive pattern was also observed in beta diversity, with a significant difference attributed to the low dominance and abundance of bacteria (F-value: 16723; R2: 0.84078; P: 0.001) (Table S5). In contrast, magnetite treatments revealed a significant specific increase in *Methanobacteria* and uncultured *Bathyarchaeia* phyla, with a notable decrease in the *Methanosarcina* class.

The stimulation of *Methanobacteria* growth, a strictly hydrogenotrophic archaeon, might be the primary reason for the increased CH_4 production observed with magnetite, and we can infer that the methanogenic metabolic in these treatments is hydrogenotrophic. However, the isotopic signature of carbon and hydrogen in CH_4 and CO_2 reveals that the pathway in non-hydrogenotrophic but acetoclastic-methylotrophic, which could be explain by a specific alternative isotopic signature lined to DIET methanogenesis promoted by natural conduits, as well as the presence of magnetite. Nevertheless, the CH_4 production rate could be attributed to the dual nature of conductive materials: they can either promote extracellular electron exchange or exhibit cytotoxicity towards microbes. However, further studies are required to elucidate the specific effects of magnetite and its potential toxic impact on bacterial communities. While magnetite-driven interspecies electron transfer (DIET) can stimulate both anaerobic fermentative bacteria and methanogens, the detailed stimulating mechanisms may differ due to their particle sizes (Yin et al., 2020b). Liu et al (2015), proposed that nanoscale magnetite could serve as a substitute for the *OmcS* cytochrome associated with *e-pili* in extracellular electron transfer (Liu et al., 2015). Interestingly, in the present study magnetite showed a strong association (LefSE) with *Thiobacillus denitrificans* , which is widely studied for its role in the oxidation of inorganic sulfur compounds and the reduction of oxidized nitrogen compounds (such as nitrate, nitrite), as well as iron reduction (Yu et al., 2015; Kumar et al., 2020)(figure). Several studies have reported the electroactivity of *Thiobacillus denitrificans* species to utilize poised electrodes directly as sole electron donors for autotrophic denitrification in bioelectrochemical systems (Yu et al., 2015), and also in-vitro DIET interactions with *Geobacter* on magnetite materials (Kato et al., 2012) . In our study natural potential IET interactions between *Thiobacillus* and magnetite have been revealed in anoxic soil microcosms form paddy rice fields mimicking postharvest season.

Furthermore, in Lefse's analysis it has been observed that *Anaerolinea*, a typical rice soil bacterial genus, is an active nitrogen fixer in rice soil. LEfSe analysis also revealed a significant association with the electrogenic bacterium *Ruminiclostridium*. However, a precise connection between the stimulation of electrogenic bacteria and magnetite in paddy soil cannot be established based on the current data. RDA analysis further contrasted the observed microbial community patterns. A positive correlation with total nitrogen indicated that magnetite influenced nitrogen-fixing bacteria (*Anaerolinea*), and also autotrophic denitrifying *Thiobacillus denitrificans ASV5910* and

(Supplementary Table S7). Regarding archaea, intriguingly, magnetite stimulated uncultured *Batyarchaeia*, formerly known as the *miscellaneous Crenarchaeotal* group. *Batyarchaeota* members are apparently widespread in anoxic sediments and soils, with a diverse metabolisms including dissimilatory nitrate reduction to ammonium (Lazar et al., 2016) Additionally, *Batarchaeota* may also play a role in the methanogenesis by means methyl-coenzyme M reductase (*MCR*) complex (Evans et al., 2015).

5. Conclusión

This study demonstrates that incorporating natural conductive materials, biochar and fungal melanin, impacts CH_4 emissions in rice soil microcosms under anaerobic conditions during long-term incubation (130 days). Biochar and fungal melanin incorporation to the soil were related with a depletion in the total methane accumulated, while magnetite addition did not significantly reduce methane production. Conductive materials decreased the transient accumulation of acetate, during the degradation of rice straw, whereas altered the kinetic profile of CH_4 production, shifting the lag phase and methane production during the initial incubation period. The three conductive materials (CMs) could modify the microbial community in the soil microcosms under anaerobic conditions. Biochar and melanin, in particular, influence the electroactive bacterial communities, such as *Clostridium* and *Geobacter* spp. These CMs likely promote changes in redox potentials and electron flow, stimulating competition for electron acceptors with methanogenic archaea, primarily *Methanobacteria* and *Methanosarcina*. However, further research is needed to elucidate the specific mechanisms by which biochar and fungal melanin retard and inhibit methane production. Interestingly, all three CMs generally resulted in a decrease in methanogenic archaea, with magnetite differing from the others by exhibiting a greater relative abundance compared to biochar and fungal melanin.

Notably, this study observed a significantly higher abundance of *Cladosporium* in treatments containing rice straw, suggesting it's a common fungal associate of rice plants. *Cladosporium*, a black fungus known for its melanization process. This finding suggests the potential presence of abundant melanin polymers in Ebro Delta rice soils, potentially influencing the redox potential and interspecies electron transfer (DIET) within the microbial communities. Therefore, *Cladosporium* and its associated melanin production could be a significant factor to consider in future studies exploring the role of melanin in mitigating methane emissions from rice paddies and its impact on the resident microbial communities.

Supplementary materials

The following supporting information can be downloaded in anexo, Table S1. Kinetic Modeling of CH_4 and CO_2 Production in Anaerobic Microcosms under Different CM Treatments; Tabla S2. Isotopic compositional analysis of CH_4; Table S3. qPCR was used to quantify total bacteria (16S rRNA), dissimilatory sulfate-reducing bacteria (aprA), and methanogenic archaea (mcrA), along with their respective ratios. Statistical tests were performed to compare C2T0, C2TF, ME, BIO, and MAG treatments. The figure shows statistically significant differences determined using Tukey's HSD test (P-value < 0.05); Table S4. Bacteria and archaea community metrics: richness (ACE), diversity (Shannon) and dominance (Simpsom). Tukey HSD test, significance p-value (<0.05) letres indicate statistical differences by time and treatment; Table S5. PERMANOVA Pairwise Comparisons of Treatment Effects on Microbial Communities and Controls (High F-Values Indicate Significant Differences); Table S6. The relative abundance (RA) of fungal taxa using ITS amplicon sequencing. We present the taxonomic composition at the phylum and family level (top 10 most abundant) visualized with an image hetmap. Additionally, the fungal class

composition is explored through a separate bar plot showcasing the top 10 most abundant classes. Alpha and beta diversity metrics were employed to characterize community richness and composition, respectively. All biodiversity analyses were accompanied by statistical tests; Table S7. Taxonomic categories relative abundance (RA) of both bacteria and archaea kingdom; TableS8. Lefse analysys of bacteria communities; TableS9. Lefse analysys of archaeas communities; TableS10. Physicochemical properties measured after 130 days of incubation.

Author Contributions

CM-A: conceptualization, data curation, bioinformatics analysis, investigation, writing – original draft; BF: methane analytical work, help interpretation; YL, CM-A: laboratory experiments and analytical work, methodology; FP, MM-E, CA: help interpretation statistical data writing – review & editing; MG: project administration, funding acquisition; MV: conceptualization, project administration, supervision, writing – review & editing. All the Authors gave their critical contribution on the whole manuscript.

Funding

This research was funded by the Spanish Agencia Estatal de Investigación for funding (PID2019-111572RB-I00/AEI/10.13039/501100011033, MIC-RICE project), and the Consolidated Research Group SOSBIO (ref. 2021 SGR 01568) Generalitat de Catalunya). Cristy Medina-Armijo was the recipient of the fellowship Agencia Nacional de investigación y Desarrollo (ANID) from Chile.

Conflict of Interest

The authors declare that the research was conducted in the absence of any commercial or financial relationships that could be construed as a potential conflict of interest.

Acknowledgments

We acknowledge MSc studient Laura Martinez, from the Univerity of Barcelona, for laboratory assistance during her dergraduate intership.

6. References

Bray, J. R., and Curtis, J. T. (1957). An ordination of the upland forest communities of southern Wisconsin. *Ecol. Monogr.* 27, 325–349. doi: 10.2307/1942268.

Butler, M. J., Gardiner, R. B., and Day, A. W. (2005). Fungal melanin detection by the use of copper sulfide-silver. *Mycologia.* 97, 312–319. doi: 10.1080/15572536.2006.11832806.

Callahan, B. J., McMurdie, P. J., Rosen, M. J., Han, A. W., Johnson, A. J. A., and Holmes, S. P. (2016). DADA2: High-resolution sample inference from Illumina amplicon data. *Nat. Methods.* 13, 581–583. doi: 10.1038/nmeth.3869.

Cavalcante, W. A., Gehring, T. A., and Zaiat, M. (2021). Stimulation and inhibition of direct interspecies electron transfer mechanisms within methanogenic reactors by adding magnetite and granular actived carbon. *Chem. Eng. J.* 415, 1385–8947. doi: 10.1016/j.cej.2021.128882.

Chen, S., Rotaru, A. E., Shrestha, P. M., Malvankar, N. S., Liu, F., Fan, W., et al. (2014). Promoting Interspecies Electron Transfer with Biochar. *Sci. Reports*. 4, 1–7. doi: 10.1038/srep05019.

Choi, K. Y. (2021). Bioprocess of Microbial Melanin Production and Isolation. *Front. Bioeng. Biotechnol.* 9, 1–12. doi: 10.3389/fbioe.2021.765110.

Coleman, D. D., Risatti, J. B., and Schoell, M. (1981). Fractionation of carbon and hydrogen isotopes by methane-oxidizing bacteria. *Geochim. Cosmochim. Acta* 45, 1033–1037.

Conrad, R., Claus, P., and Casper, P. (2009). Characterization of stable isotope fractionation during methane production in the sediment of a eutrophic lake, Lake Dagow, Germany. *Limnol. Oceanogr.* 54, 457–471. doi: 10.4319/lo.2009.54.2.0457.

Duc Phung, L., Miyazawa, M., Pham, D. V., Nishiyama, M., Masuda, S., Takakai, F., et al. (2021). Methane mitigation is associated with reduced abundance of methanogenic and methanotrophic communities in paddy soils continuously sub-irrigated with treated wastewater. *Sci Rep*. 1;11(1):7426. doi: 10.1038/s41598-021-86925-5.

Dykstra, C. M., and Pavlostathis, S. G. (2017). Methanogenic biocathode microbial community development and the role of bacteria. doi: 10.1021/acs.est.6b04112.

Evans, P. N., Boyd, J. A., Leu, A. O., Woodcroft, B. J., Parks, D. H., Hugenholtz, P., et al. (2019). An evolving view of methane metabolism in the Archaea. *Nat. Rev. Microbiol. 2018 174* 17, 219–232. doi: 10.1038/s41579-018-0136-7.

Evans, P. N., Parks, D. H., Chadwick, G. L., Robbins, S. J., Orphan, V. J., Golding, S. D., et al. (2015). Methane metabolism in the archaeal phylum *Bathyarchaeota* revealed by genome-centric metagenomics. *Science* 350, 434–438. doi: 10.1126/science.aac7745.

Feng, Y., Xu, Y., Yu, Y., Xie, Z., and Lin, X. (2012). Mechanisms of biochar decreasing methane emission from Chinese paddy soils. *Soil Biol. Biochem.* 46, 80–88. doi: 10.1016/j.soilbio.2011.11.016.

Gu, X., Weng, S., Li, Y., and Zhou, X. (2022). Effects of water and fertilizer management practices on methane emissions from paddy soils: Synthesis and perspective. *Int. J. Environ. Res. Public Health* 19. doi: 10.3390/ijerph19127324/s1.

Haack, S. K., and Breznak, J. A. (1993). *Cytophaga xylanolytica* sp. nov., a xylan-degrading, anaerobic gliding bacterium. *Arch. Microbiol.* 159, 6–15. doi: 10.1007/bf00244257.

Han, X., Sun, X., Wang, C., Wu, M., Dong, D., Zhong, T., et al. (2016). Mitigating methane emission from paddy soil with rice-straw biochar amendment under projected climate change. *Sci Rep.* 2016;6:24731. doi: 10.1038/srep24731.

Holmes, D. E., Shrestha, P. M., Walker, D. J., Dang, Y., Nevin, K. P., Woodard, T. L., & Lovley, D. R. (2017). Metatranscriptomic evidence for direct interspecies electron transfer between Geobacter and Methanothrix species in methanogenic rice paddy soils. *Applied and environmental microbiology*, 83(9), e00223-17.

Holmes, D. E., Ueki, T., Tang, H. Y., Zhou, J., Smith, J. A., Chaput, G., et al. (2019). A membrane-bound cytochrome enables *Methanosarcina acetivorans* to conserve energy from extracellular electron transfer. *MBio* 10: 10:10.1128/mbio.00789-19. doi: 10.1128/mbio.00789-19.

Hong, L., and Simon, J. D. (2007). Current understanding of the binding sites, capacity, affinity, and biological significance of metals in melanin. *J. Phys. Química.* 28, 7938–7947. doi: 10.1021/jp071439h.

Hong, L., and Simon, J. D. (2006). Insight into the binding of divalent cations to sepia eumelanin from IR absorption spectroscopy. *Photochem. Photobiol*. 82, 1265. doi: 10.1562/2006-02-23-ra-809.

Ji, M., Zhou, L., Zhang, S., Luo, G., and Sang, W. (2020). Effects of biochar on methane emission from paddy soil: Focusing on DOM and microbial communities. *Sci Total Environ*. 743,140725. doi: 10.1016/j.scitotenv.2020.140725.

Ji, Y., Liu, P., and Conrad, R. (2018). Response of fermenting bacterial and methanogenic archaeal communities in paddy soil to progressing rice straw degradation. *Soil Biol. Biochem.* 124, 70–80. doi: 10.1016/j.soilbio.2018.05.029.

Jin, S., Huang, Y., Dong, C., Bai, Y., Pan, H., and Hu, Z. (2023). Effects of different straw returning amounts and fertilizer conditions on bacteria of rice's different part in rare earth mining area. *Sci Rep.* 13, 412. doi: 10.1038/s41598-023-27553-z.

Kato, S., Hashimoto, K., and Watanabe, K. (2012). Microbial interspecies electron transfer via electric currents through conductive minerals. P*roc. Natl. Acad. Sci. U.S A.* 109, 10042–10046. doi: 10.1073/pnas.1117592109/suppl_file/pnas.201117592si.pdf.

Kim, B. R., Shin, J., Guevarra, R. B., Lee, J. H., Kim, D. W., Seol, K. H., et al. (2017). Deciphering diversity indices for a better understanding of microbial communities. *J. Microbiol. Biotechnol.* 27, 2089–2093. doi: 10.4014/jmb.1709.09027.

Kim, Y., and Liesack, W. (2015). Differential assemblage of functional units in paddy soil microbiomes. *PLoS One* 10, e0122221. doi: 10.1371/journal.pone.0122221.

Klindworth, A., Pruesse, E., Schweer, T., Peplies, J., Quast, C., Horn, M., et al. (2013). Evaluation of general 16S ribosomal RNA gene PCR primers for classical and next-generation sequencing-based diversity studies. *Nucleic Acids Res*. 41. doi: 10.1093/NAR/GKS808.

Kumar, M., Zeyad, M. T., Choudhary, P., Paul, S., Chakdar, H., and Rajawat, M. V. S. (2020). *Thiobacillus*. *Benef. Microbes Agro-Ecology Bact. Fungi*, 545–557. doi: 10.1016/B978-0-12-823414-3.00026-5.

Lazar, C. S., Baker, B. J., Seitz, K., Hyde, A. S., Dick, G. J., Hinrichs, K. U., et al. (2016). Genomic evidence for distinct carbon substrate preferences and ecological niches of *Bathyarchaeota* in estuarine sediments. *Environ. Microbiol.* 18, 1200–1211. doi: 10.1111/1462-2920.13142.

Lehmann, J., Gaunt, J., and Rondon, M. (2006). Biochar sequestration in terrestrial ecosystems-a review. Mitigation and Adaptation Strategies for Global Change. 11: 403-427. doi: 10.1007/s11027-005-9006-5

Lehmann, J. (2007). Bio-energy in the black. *Front. Ecol. Environ.* 5:381-387. doi: 10.1890/060133.

Li, P., Li, W., Sun, M., Xu, X., Zhang, B., and Sun, Y. (2018). Evaluation of biochemical methane potential and kinetics on the anaerobic digestion of vegetable crop residues. *Energies 2019.* 12, 26. doi: 10.3390/en12010026.

Lim, E. Y., Tian, H., Chen, Y., Ni, K., Zhang, J., and Tong, Y. W. (2020). Methanogenic pathway and microbial succession during start-up and stabilization of thermophilic food waste anaerobic digestion with biochar. *Bioresour Technol*. 314:123751. doi: 10.1016/j.biortech.2020.123751.

Liu, C., Cui, Y., Li, X., & Yao, M. (2021). microeco: an R package for data mining in microbial community ecology. *FEMS microbiology ecology*. 97(2), fiaa255.

Liu, F., Rotaru, A. E., Shrestha, P. M., Malvankar, N. S., Nevin, K. P., and Lovley, D. R. (2015). Magnetite compensates for the lack of a pilin-associated c-type cytochrome in extracellular electron exchange. *Environ. Microbiol.* 17, 648–655. doi: 10.1111/1462-2920.12485.

Liu, F., Rotaru, A. E., Shrestha, P. M., Malvankar, N. S., Nevin, K. P., and Lovley, D. R. (2012). Promoting direct interspecies electron transfer with activated carbon. *Energy Environ. Sci.* 5, 8982–8989. doi: 10.1039/c2ee22459c.

Liu, L., Cheng, M., Yang, L., Gu, X., Jin, J., and Fu, M. (2023). Regulation of straw decomposition and its effect on soil function by the amount of returned straw in a cool zone rice crop system. Sci Rep 13, 15673. doi: 10.1038/s41598-023-42650-9.

Liu, Y., Yang, M., Wu, Y., Wang, H., Chen, Y., and Wu, W. (2011). Reducing CH_4 and CO_2 emissions from waterlogged paddy soil with biochar. *J. Soils Sediments* 11, 930–939. doi: 10.1007/s11368-011-0376-x/figures/8.

Lovley, D. R. (2017). Syntrophy goes lectric: Direct interspecies electron transfer. *Annu. Rev. Microbiol.* 71, 643–664. doi: 10.1146/annurev-micro-030117-020420.

Lovley, D. R., Fraga, J. L., Blunt-Harris, E. L., Hayes, L. A., Phillips, E. J. P., Coates, J. D., et al. (1998). Humic substances as a mediator for microbially catalyzed metal reduction. *Acta Hydrochim. hydrobiol* 26, 3.

Lu, Y., Liu, Q., Fu, L., Hu, Y., Zhong, L., Zhang, S., et al. (2022). The effect of modified biochar on methane emission and succession of methanogenic archaeal community in paddy soil. *Chemosphere*. 304, 0045–6535. doi: 10.1016/j.chemosphere.2022.135288.

Ma, J., Xu, H., Yagi, K., and Cai, Z. (2008). Methane emission from paddy soils as affected by wheat straw returning mode. *Plant Soil.* 313, 167–174. doi: 10.1007/S11104-008-9689-y/tables/2.

Madkhali, N., Alqahtani, H. R., Alterary, S., Albrithen, H. A., Laref, A., and Hassib, A. (2020). Characterization and electrochemical deposition of natural melanin thin films. *Arab. J. Chem.* 13, 4987–4993. doi: 10.1016/j.arabjc.2020.01.021.

Martínez-Eixarch, M., Alcaraz, C., Viñas, M., Noguerol, J., Aranda, X., Xavier Prenafeta-Boldú, F., et al. (2018). Neglecting the fallow season can significantly underestimate annual methane emissions in Mediterranean rice fields. *PLoS One* 13(5): e0198081. doi: 10.1371/journal.pone.0198081.

McKnight, D. T., Huerlimann, R., Bower, D. S., Schwarzkopf, L., Alford, R. A., and Zenger, K. R. (2019). Methods for normalizing microbiome data: An ecological perspective. *Methods Ecol. Evol.* 10, 389–400. doi: 10.1111/2041-210X.13115.

McMurdie, P. J., and Holmes, S. (2013). phyloseq: An R package for reproducible interactive analysis and graphics of microbiome census data. *PLoS One* 8, e61217. doi: 10.1371/journal.pone.0061217.

Medina-Armijo, C., Yousef, I., Berna, A., Puerta, A., Esteve-Núñez, A., Viñas, M., et al. (2024). Characterization of melanin from *Exophiala mesophila* with the prospect of potential biotechnological applications. *Front. Fungal Biol*. 5, 1390724. doi: 10.3389/ffunb.2024.1390724.

Nan, Q., Wang B, C., Yi, Q., Zhang, L., Ping, F., Thies, J. E., et al. (2020.). Biochar amendment pyrolysed with rice straw increases rice production and mitigates methane emission over successive three years. *Waste Management*. 118, 1–8. doi: 10.1016/j.wasman.2020.08.013.

Nozhevnikova, AN, Russkova, YI, Litti, YV et al. (2020). Sintrofia y transferencia de electrones entre especies en comunidades microbianas metanogénicas. *Microbiología.* 89 , 129-147. doi: 10.1134/S0026261720020101

Penning, H., and Conrad, R. (2007). Quantification of carbon flow from stable isotope fractionation in rice field soils with different organic matter content. *Org. Geochem.* 38, 2058–2069. doi: 10.1016/j.orggeochem.2007.08.004.

Qiu, L., Deng, Y. F., Wang, F., Davaritouchaee, M., and Yao, Y. Q. (2019). A review on biochar-mediated anaerobic digestion with enhanced methane recovery. *Renew. Sustain. Energy Rev.* 115, 109373. doi: 10.1016/j.rser.2019.109373.

Rotaru, A. E., Shrestha, P. M., Liu, F., Markovaite, B., Chen, S., Nevin, K. P., et al. (2014). Direct interspecies electron transfer between *Geobacter metallireducens* and *Methanosarcina barkeri*. *Appl. Environ. Microbiol.* 80, 4599–4605. doi: 10.1128/aem.00895-14/asset/de9d6f24-9c8b-4d33-adc0-76c2364ec6fc/assets/graphic/zam9991055120004.jpeg.

Rotaru, A. E., Shrestha, P. M., Liu, F., Shrestha, M., Shrestha, D., Embree, M., et al. (2013). A new model for electron flow during anaerobic digestion: direct interspecies electron transfer to *Methanosaeta* for the reduction of carbon dioxide to methane. Energy Environ. Sci. 7, 408–415. doi: 10.1039/c3ee42189a.

Ruff, S. E., Humez, P., de Angelis, I. H., Diao, M., Nightingale, M., Cho, S., et al. (2023). Hydrogen and dark oxygen drive microbial productivity in diverse groundwater ecosystems. *Nat. Commun.* 2023 141 14, 1–17. doi: 10.1038/s41467-023-38523-4.

Schievano, A., Berenguer, R., Goglio, A., Bocchi, S., Marzorati, S., Rago, L., & Esteve-Núñez, A. (2019). Electroactive biochar for large-scale environmental applications of microbial electrochemistry. *ACS sustainable chemistry & engineering*. 7, 18198-18212.

Singh, N. K., Patel, D. B., and Khalekar, G. D. (2018). *M*ethanogenesis and Methane Emission in Rice / Paddy Fields. *In: Lichtfouse, E. (eds) Sustainable Agriculture Reviews 33. Sustainable Agriculture Reviews, vol 33. Springer, Cham. https://doi.org/10.1007/978-3-319-99076-7_5* Smith, P., Reay, D., & Smith, J. (2021). Agricultural methane emissions and the potential formitigation. *Philosophical Transactions of the Royal Society* A, 379(2210), 20200451.

Song, Y., Huang, R., Li, L., Du, K., Zhu, F., Song, C., et al. (2023). Humic acid-dependent respiratory growth

of *Methanosarcina* acetivorans involves pyrroloquinoline quinone. *ISME J.* 17, 2103–2111. doi: 10.1038/s41396-023-01520-y.

Stams, A. J. M., and Plugge, C. M. (2009). Electron transfer in syntrophic communities of anaerobic bacteria and archaea. *Nat. Rev. Microbiol. 2009 78* 7, 568–577. doi: 10.1038/nrmicro2166.

Sun, L., Toyonaga, M., Ohashi, A., Matsuura, N., Tourlousse, D. M., Meng, X. Y., et al. (2016). Isolation and characterization of flexilinea flocculi gen. Nov., sp. Nov., a filamentous, anaerobic bacterium belonging to the class *anaerolineae* in the phylum c*hloroflexi*. *Int. J. Syst. Evol. Microbiol.* 66, 988–996. doi: 10.1099/ijsem.0.000822/cite/refworks.

Thauer, R. K., Kaster, A. K., Seedorf, H., Buckel, W., and Hedderich, R. (2008). Methanogenic archaea: ecologically relevant differences in energy conservation. *Nat. Rev. Microbiol. 2008 68* 6, 579–591. doi: 10.1038/nrmicro1931.

Toju, H., Tanabe, A. S., Yamamoto, S., and Sato, H. (2012). High-Coverage ITS Primers for the DNA-Based Identification of *Ascomycetes* and *Basidiomycetes* in Environmental Samples. *PLoS One 7*, e40863. doi: 10.1371/journal.pone.0040863.

Wang, L. Y., Nevin, K. P., Woodard, T. L., Mu, B. Z., and Lovley, D. R. (2016). Expanding the Diet for DIET: Electron donors supporting direct interspecies electron transfer (DIET) in defined co-cultures. *Front. Microbiol.* 7. doi: 10.3389/fmicb.2016.00236.

Wegner, C. E., and Liesack, W. (2016). Microbial community dynamics during the early stages of plant polymer breakdown in paddy soil. *Environ. Microbiol.* 18, 2825–2842. doi: 10.1111/1462-2920.12815/SUPPINFO.

White T J, Burns T, Lee S, Taylor J. Amplification and sequencing of fungal ribosomal RNA genes for phylogenetics. In: Innis MA, Gelfand D H, Sninsky J J, White T J, editors. PCR protocols. A guide to methods and applications. San Diego, Calif: Academic Press, Inc.; 1990. pp. 315–322.

Whiticar, M. J. (1999). Carbon and hydrogen isotope systematics of bacterial formation and oxidation of methane. *Chem. Geol.* 161, 291–314. doi: 10.1016/S0009-2541(99)00092-3.

Whiticar, M. J., Faber, E., and Schoell, M. (1986). Biogenic methane formation in marine and freshwater environments: CO_2 reduction vs. acetate fermentation—Isotope evidence. *Geochim. Cosmochim. Acta* 50, 693–709. doi: 10.1016/0016-7037(86)90346-7.

Xia, X., Zhang, J., Song, T., and Lu, Y. (2019). Stimulation of Smithella-dominating propionate oxidation in a sediment enrichment by magnetite and carbon nanotubes. *Environ. Microbiol. Rep.* 11, 236–248. doi: 10.1111/1758-2229.12737.

Xiao, L., Lichtfouse, E., and Senthil Kumar, P. (2021). Advantage of conductive materials on interspecies electron transfer-independent acetoclastic methanogenesis: A critical review. *Fuel* 305, 121577. doi: 10.1016/J.fuel.2021.121577.

Xu, M., Lin, Y., Ma, J., Long, L., Chen, C., Yang, G., et al. (2023). Biochar regulates biogeochemical cycling of iron and chromium in paddy soil system by stimulating *Geobacter* and *Clostridium*. *Pedosphere*. doi: 10.1016/j.pedsph.2023.07.013.

Xu, J., Zhuang, L., Yang, G., Yuan, Y., & Zhou, S. (2013). Extracellular quinones affecting methane production and methanogenic community in paddy soil. *Microbial ecology*. 66, 950-960.

Yin, Q., Gu, M., and Wu, G. (2020). Inhibition mitigation of methanogenesis processes by conductive materials: A critical review. *Bioresource Technology*. 317, 123977. doi: 10.1016/j.biortech.2020.123977.

Yu, L., Yuan, Y., Chen, S., Zhuang, L., and Zhou, S. (2015). Direct uptake of electrode electrons for autotrophic denitrification by *Thiobacillus denitrificans*. *Electrochem. commun.* 60, 126–130. doi: 10.1016/j.elecom.2015.08.025.

Yuan, Q., Huang, X., Rui, • Junpeng, Qiu, S., and Conrad, R. (2020). Methane production from rice straw carbon in five different methanogenic rice soils: rates, quantities and microbial communities. *Acta Geochim* 39 , 181–191. doi: 10.1007/s11631-019-00391-5.

Zhang, A., Cui, L., Pan, G., Li, L., Hussain, Q., Zhang, X., et al. (2010). Effect of biochar amendment on yield and methane and nitrous oxide emissions from a rice paddy from Tai Lake plain, China. *Agric. Ecosyst. Environ.* 139, 469–475. doi: 10.1016/j.agee.2010.09.003.

Zhen, Z., Li, G., Chen, Y., Wei, T., Li, H., Huang, F., et al. (2023). Accelerated nitrification and altered community structure of ammonia-oxidizing microorganisms in the saline-alkali tolerant rice rhizosphere of coastal solonchaks. *Appl. Soil Ecol.* 189, 104978. doi: 10.1016/j.apsoil.2023.104978.

Zhuang, L., Ma, J., Yu, Z., Wang, Y., and Tang, J. (2018). Magnetite accelerates syntrophic acetate oxidation in methanogenic systems with high ammonia concentrations. *Microb. Biotechnol.* 11, 710–720. doi: 10.1111/1751-7915.13286.

General discussion

Melanin is a natural pigment found across the tree of life that possesses a unique combination of properties that could be of interest for novel practical applications in biotechnology. Photoprotection is the most obvious function of melanin, but metal chelation and electrical conductivity are also important. In chapter 1 we provide a detailed state-of-the-art on the prospects of melanin-based biotechnology. The bibliography on melanin is quite extensive but most published papers are related to human and animals (usually to the ink of *Sepia officinalis*)[1]. Melanin-analogues have also been synthetized in the laboratory and are commercialized as speciality chemicals, but both natural and synthetic melanins have a very high cost ranging 470 to 800€/g respectively [2]. Hence, animal-derived and synthetic melanins face limitations in terms of sustainability for large-scale production, in what concerns technical, economic, environmental, and bioethical (animal wellbeing) constraints. Consequently, the lack of a readily available melanin source hinders the advancement of scientific-technical research on the potential applications of melanin.

The research described in this dissertation has explored a relatively neglected source of melanin produced by the so-called black fungi. These microorganisms are characterized by an intense and complete melanization of their mycelium and reproductive structures. Building upon previous pioneering research on melanin extracted from black fungi (Zhan et al., 2011; Suwannarach et al., 2019), the present work focuses on the characterization of functional and physicochemical aspects of melanin from black fungi, both in whole cells and in purified extracts, as a potentially scalable melanin source. Two processes of melanized fungal biomass and melanin extracts that can be engineered into practical applications have been explored in more detail: the binding of toxic heavy metals and metalloids and as a bioelectroconductive material that could mediate in electroactive microbial communities.

When looking for alternative sources of melanin, black fungi (often referred to as black yeasts or dematiaceous fungi in the mycology literature) are strong candidates because of their intense melanization and the possibility of cultivation as industrial microorganisms. Black fungi belong to various taxonomic groups, but they are predominant in the ascomycetous orders *Chaetothyriales* (class *Eurotiomycetes*), as well as *Asterinales*, *Capnodiales*, *Cladosporiales*, *Dothideales*, *Mycospharellales*, and *Venturiales* (class *Dothideomycetes*). They can be isolated from a wide range of natural and anthropized environments. Some black fungi are opportunistic pathogens (predominantly in the *Chaetothyriales*), capable of causing infections in humans and other animals, while others thrive under an array of extreme environmental conditions including environments that are polluted with toxic organic chemicals and heavy metals. Melanin seems to play an

[1] Web of Science (https://www.webofscience.com/wos/woscc/basic-search): Searches on "melanin" have yielded 36,254 entries in the Core Collection database, versus 29,340 on "(human OR animal) AND melanin", performed during April 2024.

[2] Sigma-Aldrich catalogue of chemicals (https://www.sigmaaldrich.com/ES/en/search): 1 gram of synthetic melanin is commercialized at 796€, while 1 g of natural melanin from *Sepia officinalis* costs 467€.

important role in both virulence and extremotolerance, but the exploitation potential of the melanin from black fungi has yet to be investigated in detail.

To this end, in Chapter 3 we describe the screening a collection of black fungi, isolated previously from environments that were polluted with petroleum hydrocarbons and other toxic chemicals for their tolerance to hexavalent chromium and pentavalent arsenic (Cr(VI) and As(V), respectively), selected as models for an environmentally relevant heavy metal and metalloid. In total, 34 strains belonging to 21 distinct species, predominantly from the Chaetothyriales but which also included some representatives from the Asterinales, Cladosporiales, Dothideales, Mycospharellales, and venturiales, were screened. Quantitative toxicity parameters, such as the tolerance index (TI) and the 50% inhibitory concentration (IC_{50}) were determined on growing cultures. The results showed a high inter- and intraspecific variability in metallotolerance (Chapter 3), suggesting that there must be other physiologic mechanisms to cope with the toxic effects of toxic metals and metalloids, rather than relying solely on melanization. This issue has been covered from a molecular perspective in Chapter 5, as discussed further below).

Four strains of the species *Cyphellophora olivacea*, *Rhinocladiella similis*, *Exophiala crusticola* and *Exophiala mesophila* (Chaetothyriales) were identified as hyper-metallotolerant (Chapter 3). The latter two species, *Rhinocladiella similis* and *E. mesophila*, were relatively easy to cultivate under laboratory conditions and were subjected to further tests to determine the biosorption capacity of whole cells (dead and alive liquid cultures) and, for *E. mesophila*, also melanin extracts. These results revealed significant differences in the absorption capacity of live and dead fungal biomass during Cr(VI) and As(V) bioabsorption. Arsenic As(V) exhibited reduced toxicity and absorption capacity compared to chromium Cr(VI). This observation was attributed to the electrostatic repulsion between the negatively charged fungal cell wall surface and arsenate, which also carries negative charges. Interestingly, even when the pH was lowered to 4.0, approaching the fungal biomass point of zero charge (pzc), arsenate absorption remained suboptimal. This finding suggests that arsenic forms less stable complexes with fungal cell components compared to other heavy metals, such as cadmium, lead, and mercury. This reduced affinity limits its uptake and accumulation within the cell.

Dead biomass displayed a higher capacity compared to living biomass, probably because of cell lysis and the higher accessibility of metals to melanin, whereas living cells deploy defensive active strategies (physical barriers, transport systems, etc.) to minimize the intracellular accumulation of toxic metals. While both live and dead biomass offer potential for metal removal, they require optimization through different approaches. Furthermore, metal binding to melanin likely necessitates deprotonation, resulting in pH dependence. This was observed with Cr(VI) biosorption experiments, where a higher metal removal efficiency was achieved at pH 4. When fitting these results to different sorption isotherms and kinetic models, a rather high Cr(VI) biosorption capacity was observed with whole cells in combination with low sorption rates, when compared to those of extracted melanin. This difference could be explained by an evolved strategy of the fungus to, firstly, minimize the penetration of toxic metals into the cell and, secondly, sequester those that would eventually leak into the cytoplasm. The molecular response of *E. mesophila* to toxic concentrations of Cr(VI) and As(V) is discussed in more detail in Chapter 5.

In Chapter 4 we deepened our research on the characteristics and function of the fungal melanin extracted from *E. mesophila*. For this purpose, we adapted and optimized a melanin extraction protocol in search for a more cost-effective alternative, thereby overcoming the limitations

associated with conventional production methods. This approach offers a more cost-effective strategy for the production of natural melanin production, achieving a significant reduction in cost compared to animal-derived sources (a preliminary cost estimate performed under laboratory conditions amounted approximately 87 euros per gram of melanin; results not shown). It is not easy to find specific data on the relative amount or the yield of melanin from different sources of biomass. Zou et al. (2010) used an optimized ultrasound-assisted extraction technique on dried mushrooms from the basidiomycete *Auricularia auricula*, and the observed melanin yield was 1.2 mg per gram of dry biomass (0.12% d.w. yield). A recent study reported an increase of the melanin yield extraction of an *Aspergillus nidulans* mutant strain from 10.0 to 22.5% d.w. upon a lengthy optimization process of the growth conditions (Campanhol et al. 2023). In this respect, the melanin extraction yield of 15.5% d.w. that was obtained during this study from cultures of the black fungus *E. mesophila* is promissing.

Once sufficient amounts of extracted and purified fungal melanin were obtained, further steps were taken to the physicochemical characterization of this biomaterial (Chapter 4). This is important considering that natural melanins are commonly classified according to their precursor molecules and macroscopic characteristic into three major groups (Pralea et al. 2019): i) Brown-black eumelanin, biosynthesized from L-tyrosine that is converted into L-3,4-dihydroxiphenylalanine (DOPA-melanin). ii) Brown-red phaeomelanin is also produced from the precursor molecule L-tyrosine, but its biochemical pathway involves the addition of cysteine to form benzothiazine intermediates. iii) Allomelanin is a very heterogenous group of nitrogen-free polymers that include red pyomelanin, which is obtained through the catabolic pathway of L-tyrosine. Also, within this last group, most ascomycetes synthetize melanin through the polyketide pathway, using 1,8-dihydroxynaphthalene as precursor (DHN-melanin). Instead, basidiomycetes generally produce eumelanin (DOPA-melanin) in a pathway resembling that of animal melanin biosynthesis.

Once sufficient yields of purified fungal melanin were available, we performed a comprehensive physicochemical characterization of *E. mesophila* melanin in order to obtain further insights into its structural features and functions concerning metal-binding and conductive behavior (Chapter 4). Inhibitory studies on whole cells with the specific DHN-melanin inhibitor tricyclazole indicated that *E. mesophila* produces melanin primarily via the DHN pathway. The structure of the *E. mesophila* melanin was elucidated and compared to existing literature (Eisenman and Casadevall, 2012; Gonçalves et al., 2012; Suwannarach et al., 2019; Elsayis et al., 2022) employing techniques such as electron paramagnetic resonance (EPR), Fourier-transform infrared (FTIR) spectroscopy, and UV spectroscopy. These results were consistent with the hypothesized DHN-melanin main type of *E. mesophila*. Such conclusion does not preclude the possibility that minor amounts of other melanin types are also biosynthesized by the fungus, as discussed in Chapter 5.

Biosorption experiments with melanin extracts showed that this material exhibits a remarkable capacity to bind heavy metal, as demonstrated with Cr(VI) ions in liquid batch experiments. Previous studies already showed that natural melanins sequester several reactive heavy metals like Pb(II), Cd(II), Fe(III) and Cu(II), and also mitigate the detrimental effects of reactive oxygen species generated by the exposure to toxic metals (Liu et al., 2004; Tran-Ly et al., 2020). This multifaceted metal-binding feature of melanin stems from the presence of diverse functional groups within its structure. These include carboxyl, amine, hydroxyl (phenolic), quinone, and semiquinone groups, which can all serve as potential metal binding sites (Manirethan et al., 2020; Mota et al., 2020; Fahry et al., 2023). Such complex binding mechanisms often involve more than

one functional group coordinating with the same metal ion, and each specific binding site may heavily depend on the nature of the metal itself (Hong and Simon, 2007). This phenomenon can lead to competition between functional groups and different metal ions during the remediation of complex metal mixtures, potentially affecting sorption efficiency. During this study, we determined that the main functional groups of *E. mesophila* melanin extracts that bind with Cr(VI) in are OH- and COOH-, but multiple mechanisms, such as chemisorption, complexation, electrostatic capacitance, reduction, π-metal interaction and cationic exchange could also affect the sorption process. Further research into these metal-binding site interactions is needed to fully harness the potential of fungal melanin for metal remediation.

The Chapter 4 also focuses on the characterization of semiconducting potential of *E. mesophila* melanin extracts. This section reports the observation of reversible redox couples attributable to the oxidation and reduction processes involving quinone moieties within the melanin structure. These interactions are consistent with previous studies on eumelanin (derived from DOPA), where melanin's redox processes are linked to the π-electron conjugation present in its aromatic rings (Gonzáles et al., 2009; Kumar et al., 2016). Significantly, in the present study this interaction is corroborated by investigating the combined system of fungal melanin (DHN-melanin) and the electroactive bacterium *Geobacter sulfurreducens* (GS). The results demonstrate a strong relationship between GS and quinone redox processes (semiquinone/hydroquinone redox transformations), showing an interaction that leads to a non-reversible electrochemical behavior. Here, we propose that if quinones are indeed facilitating extracellular electron transfer from GS to the electrode, their reduction (electron gain) would be hindered when GS prioritizes the electrode as the electron acceptor. In this scenario, the typical reduction peak associated with quinones would be absent in the electrochemical signature, explaining the observed "non-reversible behavior". These findings unveil an electron transfer mechanism between GS and melanin, suggesting a semiconducting potential of fungal melanin and its role as an electron sink in natural environments. This electron transfer process could facilitate interactions between melanin and native electroconductive microorganisms in soil under anaerobic conditions. Electron transfer processes using melanin extracts in complex microbial communities are discussed in Chapter 6.

Building upon the exceptional metallotolerance of *E. mesophila* discussed in Chapter 3, Chapter 5 delves into the underlying molecular mechanisms of this phenomenon. High throughput biochemical profiling by SR-FTIR and transcriptome sequencing were conducted for an exhaustive analysis of its biochemical alterations and gene expression patterns of *E. mesophila* cultures, in response to the exposure to concentrations of As(V) and Cr(VI) equivalent to the IC_{50} values determined previously (Chapter 3). To investigate the relationship between melanization and metal exposure, we continued the study on the inhibition of DHN-melanin with tricyclazole, as discussed in Chapter 4, to artificially generate a negative control for melanization. To elucidate the role of melanin in As(V) and Cr(VI) exposure, the hyaline cells resulting from the treatment with tricyclazole, were analyzed for associated biochemical and supramolecular changes. These effects were seen as major alterations in protein, DNA, and lipid conformational structures, similar to previously reported observations (Liang and Zhou, 2007; Bárcena et al., 2015; Hu et al., 2016; Zhan et al., 2016). These alterations likely influence the organization of complexes responsible for producing secondary metabolites like flaviolin and 2-hydroxy juglone, potentially facilitating the fungus's survival against tricyclazole toxicity and DHN-melanin inhibition (Lee et al., 2003; Bárcena et al., 2015). SR-FTIR analysis revealed changes in aromatic ring vibrations and

C=O stretching, characteristic of quinoid structures typically found in melanin, confirming the inhibition of DHN-melanin biosynthesis. Concerning the exposure of *E. mesophila* to As(V), this metalloid did not significantly affect the cell biochemistry. Observed metabolic changes could be attributed to increased phosphate hydration, potentially influencing metal transport to the cytoplasm and subsequent binding to functional groups. Instead, Cr(VI) exposure resulted in a comparatively stronger impact on *E. mesophila* biochemistry across various cellular components, including the cell wall, proteins, DNA, and polysaccharides.

Notably, the combined tricyclazole plus Cr(VI) exposure resulted in dramatic alterations in the lipid structure of fungal cells, which likely leads to cell lysis. Besides the inherent toxicity of tricyclazole, the lack of the melanin's protective action, by enabling free radical and peroxide detoxification, heavy metal sequestration, and the neutralization of electrophilic metabolites (Sarna and Plonka, 2006), may exacerbate the biochemical disruptions associated to Cr(VI) exposure. Supporting this notion, Zhan et al. (2016) demonstrated a dramatic decrease in *Exophiala pisciphila's* tolerance to cadmium upon inhibition of DHN-melanin synthesis with tricyclazole (Zhan et al., 2016).

To further investigate the mechanisms underlying the high tolerance to As(V) and Cr(VI) exhibited by *E. mesophila*, we extended our study to analyze the biochemical and gene expression changes in native cells exposed to these toxicants. SR-FTIR analysis of *Exophiala mesophila* cells exposed to As(V) suggested a primary impact on proteins at the supramolecular level. This effect could be attributed to the generation of reactive oxygen species (ROS) upon contact with As(V) ions (Robinson et al., 2021). The observed alterations were attributed to modifications in hydrogen bonding within protein amide groups and/or potential As(V) binding to these groups. Additionally, As(V) exposure induced changes in the spectral signature of phosphodiester group, indicative of localized conformational alterations. These alterations could involve pyrimidine dimers, DNA-DNA cross-links, or protein-DNA cross-links. These finding aligns with observations from similar studies, suggesting that As(V) exposure can induce amide-level effects on cells (Kasemets et al., 2009; Giannousi et al., 2014).

The transcriptomic analysis of As(V)-exposed cells of *E. mesophila*, provided further insights on the fungal response to this metalloid. The observed upregulation of genes associated with transport regulation, including those encoding ATP-binding cassette (ABC) transporters, Na^+/K^+, Fe^{2+}, and Ca^{2+} transporters, aligns remarkably well with the SR-FTIR data. This suggests a potential mechanism to maintaining cellular integrity by facilitating the controlled homeostasis (influx/efflux of various ions Na^+, K^+, Ca^{2+}) across the cell membrane of *E. mesophila*. Notably, similar observations of upregulated transport regulation in response to As(V) stress have been reported in *Aspergillus oryzae* (Liang et al., 2021). By downregulating these transporters, the fungus might limit the As(V) influx into the cell membrane, which is consistent with the low As(V) uptake rates discussed in Chapter 3. Moreover, the upregulation of transporters like the vacuolar calcium ion transporter suggests a more complex regulatory network. This transporter might facilitate the movement of arsenic ions into the vacuole, potentially sequestering them away from sensitive cellular components.

Exophiala mesophila could potentially confine As(V) into citoplasm through Hemerythrin/HHE (Hr), a protein transport of oxygen that has iron (Fe^{2+}) composites that might bind to As(V). In *Cryptococcus neoformans*, hemerythrin/HHE cation-binding domains have been implicated in nitric oxide response, suggesting an alternate ligand configuration (Chow et al., 2007). Literature on Hr proteins expressed in fungi and their role in metal detoxification via intracellular

sequestration, including metal segregation into vacuoles and ROS production restriction in conjunction with antioxidant enzymes like superoxide dismutase (SOD) and catalase (CAT) remains scarce (Bellini et al., 2020). *Exophiala mesophila* also exhibits upregulation of superoxide dismutase (SOD) genes in response to As(V) exposure such as, defense mechanism against the increased reactive oxygen species (ROS) generated by As(V)-induced stress.

The metabolic pathways associated to As(V) exposuree (KEGG analysis) revealed additional adaptation strategies employed by *E. mesophila*. These include alterations in pyrimidine metabolism, indicative of prioritized RNA synthesis, likely for the production of new proteins or enzymes necessary for stress response and adaptation. Additionally, upregulated genes associated with oxidative phosphorylation suggest an effort to maintain energy production despite the stress induced by As(V). Finally, increased proteasome function implies an enhanced protein turnover process, which might be crucial for eliminating misfolded or damaged proteins resulting from As(V) exposure (Sigler et al., 1999; Poljsak et al., 2010). A striking concordance exists between these metabolic pathways and the SR-FTIR biochemical analyses presented in this study. *Exophiala mesophila* exhibits morphological changes in response to As(V) exposure, including colony shape alterations, stronger dark pigmentation, irregular in shape and displayed coarser edges under stressful conditions (as discussed in Chapter 3). However, a discrepancy with gene expression analysis in this study did not reveal significantly upregulated expression of melanin synthesis genes. Gene expression analysis suggests that osmotic changes could be the primary drivers of the observed meristematic alterations in As(V)-exposed cells. These osmotic changes might involve dehydration and depletion of essential ions (Na^+, K^+, Ca^{2+}). While oxidative stress undoubtedly plays a role, dedicated studies on osmotic stress responses in fungal cells are crucial to definitively validate this hypothesis.

In contrast to tricyclazole exposure, Cr(VI) exerts its toxic effects on *E. mesophila* at the cellular level, causing significant damage to the cell wall, proteins, DNA, polysaccharides, and overall cellular integrity. The potential mechanism of chromium toxicity appears to involve disruption of protein synthesis and metal binding within the cell. One of the fungus's defense strategies against chromium toxicity involves the increased generation of ROS. However, the subsequent oxidative stress triggered by Cr(VI) exposure can ultimately lead to apoptosis or autophagy through mechanisms like mitochondrial damage, cytochrome c release, DNA fragmentation, phosphatidylserine exposure, and metacaspase activation. Exposure to Cr(VI) triggers rapid changes in gene expression, contrasting with the significant supramolecular differences observed through SR-FTIR analysis. Notably, genes associated with cellular detoxification are upregulated, including those encoding NADPH dehydrogenase quinone, and peroxisomal catalase (CAT). This suggests the activation of defense mechanisms against chromium-induced stress. NADPH is observed consistent with the reduction of chromium (ChrR) under aerobic conditions typically associated with soluble chromate reductases that utilize NADH or NADPH as cofactors (Viti et al.,2022). This NADPH-dependent reduction of Cr(VI) to Cr(II) generates ROS intermediates, which are potentially controlled by the action of catalase (CAT). Additionally, quinols produced by quinone reduction confer tolerance to ROS. Therefore, ROS generated by ChrR activity during Cr(VI) reduction are likely neutralized by quinols formed by the quinone reductase activity of the same enzyme (NADPH dehydrogenase quinone) (Gonzalez et al., 2005). Furthermore, Cr(VI) exposure disrupts various amino acid metabolic pathways, particularly those linked to glutathione, a cellular antioxidant crucial for detoxification, osmoprotection, and energy metabolism. Additionally, chromium disrupts protein synthesis, actin cytoskeleton regulation, and autophagy. Pathways like glycolysis, the pentose phosphate pathway, oxidative phosphorylation, and fatty acid degradation, all essential for energy production, might also be

disrupted by Cr(VI) exposure. Finally, Cr(VI) exposure impacts purine and pyrimidine metabolism, which provides building blocks for DNA and RNA synthesis. These combined effects highlight the widespread cellular disruption caused by exposure to this highly toxic metal species (Poljsak et al., 2010).

Intriguingly, Cr(VI) exposure appears to induce the metabolic activity of tyrosine, tryptophan, and phenylalanine, ultimately leading to melanin production via the DOPA-melanin pathway. This finding contrasts with the previously observed tricyclazole-induced inhibition of DHN-melanin synthesis in *E. mesophila*, as supported by the relevant literature on this fungal strain. This observation suggests that *E. mesophila* possesses the ability to produce melanin through distinct pathways depending on the specific environmental stress encountered. However, it is essential to acknowledge that increased tyrosine metabolism cannot be definitively linked solely to melanin synthesis. It could also contribute to protein synthesis for fungal growth or, alternatively, tyrosine degradation could serve as an energy source during nutrient scarcity. Interestingly, previous studies have reported the overexpression of tyrosine metabolism in *Exophiala pisciphila*, but a connection to DOPA-melanin production was not established in that instance (Zhao et al., 2015). Another study revealed a marked enhancement of melatonin synthesis enzymes in *Exophiala pisciphila*, driven by tryptophan hydroxylase activity (Yu et al., 2021). Further sutdies are thus needed to verify the capacity of *E. mesophila* to produce DOPA-melanin, even if in minor amounts.

Finally, in Chapter 5 the effect of fungal melanin, and other (semi)conductive materials (biochar and magnetite), was tested for the mitigation of methane emissions in anaerobic soil microcosms, mimicking the postharvest season of flooded rice paddies. The hypothesis was that the mitigation of methane emission could be achieved due to the biostimulation effect on the electroactive bacteria and archaea by means of (direct) interspecies electron transfer (IET). During IET conductive materials could act as solid extracellular electron acceptors, outcompeting non-electroactive methanogens. However, it also could stimulate specific electroactive methanogens by means of DIET mechanisms, when an electroactive bacteria could act as electron donor by transferring the electrons from the oxidation of VFA and H_2 to a conductive material, that could act as conduit, being the electrons uptaken by specific electroactive methanogens to produce CH_4 (Rotaru et al., 2014). In this experiment the ability of fungal melanin, compared with other conductive materials, to influence the composition on soil microbiota form paddy soil, specifically focusing on its suppressive effect a (and from other conductive materials) on methane (CH_4) production. The present study revealed that fungal melanin exhibits a significant affinity for electrobacteria like *Geobacter*, *Pseudopelobacter*, and methanogenic archaea such as *Metanosarcina*. This strong interaction suggests the occurrence of direct interspecies electron transfer (DIET) within co-cultures of *Geobacter* species and acetoclastic methanogens (e.g., *Methanosaeta* and *Methanosarcina*) and methylotrophic methanogens (*Methanosarcina and Methanobacterium*), as observed in previous studies (Rotaru et al., 2014; Holmes et al., 2017; Zheng et al., 2020). The extensive surface area of melanin facilitates electron transfer between microorganisms (i.e. *Geobacter*) and insoluble electron acceptors such as Fe(III) (oxyhydr)oxides. This promotes the reduction of Fe(III) to Fe(II). This process may compete with methanogenesis for available electrons, potentially leading to a decrease in methane (CH_4) emissions. In comparison to two other conductive materials, biological-biochar and inorganic-magnetite, melanin exhibited a superior capacity to mitigate methane under the conditions studied. This enhanced methane mitigation potential of melanin is likely attributed to its larger surface area and abundance of quinone structures, which, during their reduction processes, facilitate electron transfer between microorganisms. It is noteworthy that under quinone availability in paddy soil a specific DIET

interaction of *Geobacter* and *Methanosarcina*, at the expenses of *Methanobacterium*, was depicted with methane formation from acetate (Xu et al., 2013). Li et al (2014) also observed DIET interaction in SIP experiments among Geobacteriaceae, *Syntrophomonadaceae* and methanogens (*Methanosarcinaceae*. *Methanobacteriales* and *Methanocellales*) from butyrate oxidation with the amendment of iron nanoparticles (nanoFe_3O_4) in paddy soil microcosms (Li et al., 2014). Interestingly, in our study biochar addition also demonstrated a substantial methane mitigation effect, comparable to that of melanin. Biochar is known to possess a high surface area, which has been observed to induce competition for acetate or H_2 between methanogens and Fe(III)-reducing bacteria (Feng et al., 2012; Sriphirom et al., 2021). However, potential differences arising from biochar manufacturing process temperature, and the source of carbon biomass, could lead to the loss of certain functional groups, thereby diminishing its electron transfer or its redox interactions capacity with other molecules and exoelectrogenic microbial populations (Schievano et al., 2019).

Furthermore, the observed interaction hints at a potential electron-attracting effect exerted by fungal melanin. This effect could potentially alter environmental factors like pH, redox conditions, or nutrient availability, creating an environment less conducive to methanogenesis. Consequently, fungal melanin may modulate DIET between different syntrophic bacteria and methanogens, resulting in a shortened lag phase for CH4 production, but lower cumulative Ch4 emission. This thesis presents the first investigation of fungal melanin for mediating electron transfer through electroactive bacteria in a strategy for methane reduction within rice field soils. This finding holds significant implications. Natural melanin exhibits a high affinity for *Geobacter* species, a key electroactive bacterium. Furthermore, melanin possesses favorable environmental biocompatibility due to its recalcitrant C=C structures, which also contribute to carbon sequestration processes, hampering catabolic rate and mineralization of edible carbon. Therefore, fungal melanin offers a potential dual benefit: promoting methane reduction and a potential promotion of carbon storage in flooded soils such as rice paddy fields during postharvest season, when rice straw is incorporated to the soil.

General conclusions

Chapter 3.

Black fungi exhibited hyper-metallotolerance towards As(V) and Cr(VI), with a substantial inter- and intraspecies variability in tolerance levels. The highly tolerant strains displayed slower sorption rates compared to other fungi. This suggests a two-step protective mechanism: an initial barrier provided by the outer cell wall and melanin binding with As(V) and Cr(VI), followed by the internal biosorption of leaked metals by melanin. Biomass of *Exophiala mesophila* and *Rhinocladiella similis* exhibited a remarkable biosorption potential, particularly for Cr(VI), under oligotrophic growth conditions, demonstrating their potential as fungal agents for bioremediation of heavy metal polluted streams.

Chapter 4.

The extraction and purification of natural melanin from the metallotolerant black fungus *Exophiala mesophila* presents a promising approach for enhancing industrial melanin production processes, offering both economic and sustainability advantages over previous similar attempts. An indepth physico-chemical characterization revealed that fungal melanin possesses a unique molecular structure composed of chromophore molecules and functional groups, endowing it with exceptional metal chelating abilities, semiconductor-like properties and promising applications. Fungal melanin exhibited superior Cr(VI) sorption performance compared to the fungal biomass of *Exophiala mesophila* and *Rhinocladiella similis*. The binding mechanism in fungal melanin occurs initially by the attachment of Cr(VI) to OH- and COO- functional groups, indicating chemisorption. This is followed by interactions with C=O functional groups, suggesting complexation and electrostatic (π-bond) mechanisms. The disappearance of peaks associated with metal binding in FTIR spectra suggests possible reduction or precipitation mechanisms.

The strong inhibition of dihydroxynaphthalene (DHN)-melanin biosynthesis by tricyclazole in *E. mesophila* alters protein, DNA, and lipid supramolecular structures in fungal cells, but it appears to have a minimal impact on the overall fungal growth. Furthermore, tricyclazole application resulted in a reduction in the intensity of the aromatic band in the spectra of fungal cells, further supporting the predominant DHN-melanin content in non-inhibited cells.

Chapter 5.

Biochemical profiling (SR-FTIR) and gene expression analysis (transcriptome) during the exposure of cells of E. mesophila to As(V) and Cr(VI) revealed strong correlation between SR-FTIR analysis and gene expression patterns, indicating the complementary utility of these

techniques in elucidating the diverse tolerance mechanisms employed against high concentrations of As(V) and Cr(VI).

The As(V)-exposed fungi revealed significant alterations in amide groups associated with protein synthesis and degradation, while lipid supramolecular changes were less pronounced. Gene expression profiling highlighted an adaptive strategy centered on As(V) transport, with upregulation of genes involved in protein transport mechanisms, including transporters potentially facilitating As(V) sequestration into vacuoles. Notably, the induction of SOD enzymes emerged as a crucial protective mechanism against ROS generation.

Chromium exposure elicited profound effects on the proteome, DNA, polysaccharides and lipids of exposed cell, demonstrating a marked distinction from native cell. Gene expression analysis revealed that the primary detoxification strategy involves the activation of NADPH pathways to reduce Cr(VI) to less toxic Cr(III) forms. This mechanism is complemented by the activation of catalase to scavenge reactive oxygen species (ROS) within the cell. Additionally, various metabolic processes related to osmoregulation, energy metabolism, protein synthesis, autophagy, phosphorylation, and pyrimidine synthesis were upregulated to enhance tolerance and survival upon chromium exposure. The expression genes in *E. mesophila* indicated alternative melanin production pathways in stress-Cr(VI), for the expression tyrosine-based route leading to DOPA-melanin, cannot be entirely excluded.

Chapter 6.

The incorporation of fungal melanin into rice soil significantly reduced total methane accumulation. Fungal melanin decreased the accumulation of volatile fatty acids (VFAs) during rice straw degradation, thereby altering the kinetic profile of CH_4 production. This resulted in a shift in the lag phase and methane production during the initial incubation period. The proposed mechanism for fungal melanin-mediated methane mitigation involves the stimulation of electrogenic bacteria such as *Geobacter* or *Pseudopelobacter.* This potentially facilitates direct interspecies electron transfer (DIET), possibly mediated by competition for electrons between methanogenic archaea against electroactive bacteria and certain electroactive methanogens which could emit less methane when conductive materials are available within anaerobic rice straw-soil systems.

These findings highlight the potential of fungal melanin as a promising biomaterial, paving the way for the development of novel biotechnological applications. Potential areas of exploration include bioremediation of environmental pollutants, sensor development, nanoparticle synthesis, ion transfer, and bioelectrochemical processes.

Reference

Anh, N., Ly, T., Fink, S., and Linder, M. (2022). Fungal melanin and its composites for water remediation and wood treatment. Thesis, ETH Zúrich. doi.org/10.3929/ethz-b-000574615

Bárcena, A., Petroselli, G., Velasquez, S. M., Estévez, J. M., Erra-Balsells, R., Balatti, P. A., et al. (2015). Response of the fungus *Pseudocercospora griseola* f. mesoamericana to Tricyclazole. *Mycol. Prog*. 14. doi: 10.1007/s11557-015-1102-7.

Bellini, E., Maresca, V., Betti, C., Castiglione, M. R., Fontanini, D., Capocchi, A., et al. (2020). The moss Leptodictyum riparium counteracts severe cadmium stress by activation of glutathione transferase and phytochelatin synthase, but slightly by phytochelatins. *Int. J. Mol. Sci. Artic. Int. J. Mol. Sci.* 2020, 1583. doi: 10.3390/ijms21051583.

Broxton, C. N., and Culotta, V. C. (2016). SOD Enzymes and microbial pathogens: Surviving the oxidative storm of infection living with ROS through superoxide dismutase Enzymes. *PLoS Pathog* 12(1): e1005295. doi: 10.1371/journal.ppat.1005295.

Cao, W., Zhou, X., McCallum, N. C., Hu, Z., Ni, Q. Z., Kapoor, U., et al. (2021). Unraveling the structure and function of melanin through synthesis. *J. Am. Chem. Soc.* 143, 2622–2637. doi: 10.1021/jacs.0c12322/asset/images/medium/ja0c12322_0012.gif.

Campanhol, B.S., Ribeiro, B.D., Casellato, F., Medina, K.J.D. and Sponchiado, S.R.P. (2023) Improvement of DOPA-melanin production by *Aspergillus nidulans* using eco-friendly and inexpensive substrates. *Journal of Fungi.* 9(7), 714.

Chow, E. D., Liu, O. W., O'Brien, S., and Madhani, H. D. (2007). Exploration of whole-genome responses of the human AIDS-associated yeast pathogen *Cryptococcus neoformans* var grubii: Nitric oxide stress and body temperature. *Curr. Genet*. 52, 137–148. doi: 10.1007/S00294-007-0147-9/figures/6.

De La Rosa, J. M., Martin-Sanchez, P. M., Sanchez-Cortes, S., Hermosin, B., Knicker, H., and Saiz-Jimenez, C. (2017). Structure of melanins from the fungi *Ochroconis lascauxensis* and *Ochroconis anomala* contaminating rock art in the Lascaux Cave. Sci. Reports 2017 71 7, 1–11. doi: 10.1038/s41598-017-13862-7.

Eisenman, H. C., and Casadevall, A. (2012). Synthesis and assembly of fungal melanin. *Appl. Microbiol. Biotechnol*. 93, 931–940. doi: 10.1007/S00253-011-3777-2/figures/2.

Elsayis, A., Hassan, S. W. M., Ghanem, K. M., and Khairy, H. (2022). Optimization of melanin pigment production from the halotolerant black yeast *Hortaea werneckii* AS1 isolated from solar salter in Alexandria. *BMC Microbiol*. 22, 1–16. doi: 10.1186/s12866-022-02505-1.

Fahry, Kh., Ghoniem, A. A., Al-Otibi, F. O., Helmy, Y. A., El Hersh, M. S., Elattar, K. M., et al. (2023). A Comparative Study of Cr(VI) Sorption by *Aureobasidium pullulans* AKW biomass and its extracellular melanin: Complementary modeling with equilibrium isotherms, kinetic studies, and decision. *Tree Modeling. Polymers* (Basel). 15. doi: 10.3390/polym15183754.

Feng, Y., Xu, Y., Yu, Y., Xie, Z., and Lin, X. (2012). Mechanisms of biochar decreasing methane emission from Chinese paddy soils. *Soil Biol. Biochem*. 46, 80–88. doi: 10.1016/j.soilbio.2011.11.016.

Giannousi, K., Sarafidis, G., Mourdikoudis, S., Pantazaki, A., and Dendrinou-Samara, C. (2014). Selective synthesis of Cu_2O and Cu/Cu_2O NPs: antifungal activity to yeast *Saccharomyces cerevisiae* and DNA interaction. *Inorg. Chem*. 53, 9657–9666. doi: 10.1021/ic501143z.

Gonçalves, R. C. R., Lisboa, H. C. F., and Pombeiro-Sponchiado, S. R. (2012). Characterization of melanin pigment produced by *Aspergillus nidulans. World J. Microbiol. Biotechnol*. 28, 1467–1474. doi: 10.1007/s11274-011-0948-3.

Gonzalez, C. F., Aekerley, D. F., Lynch, S. V., and Matin, A. (2005). ChrR, a soluble quinone reductase of *Pseudomonas putida* that defends against H_2O_2. *J. Biol. Chem.* 280, 22590–22595. doi: 10.1074/jbc.M501654200.

Gonzáles,O. A., Gimeno, Y., Creus, A. H., Grumelli, D., Vericat, C., Benitez, G., et al. (2009). Electrochemical preparation of metal-melanin functionalized graphite surfaces. *Electrochim*. 54, 1589–1596. doi: 10.1016/j.electacta.2008.09.046.

Hong, L., and Simon, J. D. (2007). Current understanding of the binding sites, capacity, affinity, and biological significance of metals in melanin. *J. Phys. Chem.* B 111, 7938–7947. doi: 10.1021/jp071439h/asset/images/large/jp071439hf00009.jpeg.

Holmes, D. E., Shrestha, P. M., Walker, D. J., Dang, Y., Nevin, K. P., Woodard, T. L., & Lovley, D. R. (2017). Metatranscriptomic evidence for direct interspecies electron transfer between *Geobacter* and *Methanothrix* species in methanogenic rice paddy soils. *Applied and environmental microbiology*. 83, e00223-17.

Hu, X. J., Liu, Z. X., Wang, Y. Di, Li, X. N., Hu, J., and Lü, J. H. (2016). Synchrotron FTIR spectroscopy reveals molecular changes in *Escherichia coli* upon Cu^{2+} exposure. *Nucl. Sci. Tech*. 27, 1–8. doi: 10.1007/s41365-016-0067-9.

Jacobson, E. S., and Tinnell, S. B. (1993). Antioxidant function of fungal melanin. *J. Bacteriol*. 175, 7102–7104. doi: 10.1128/jb.175.21.7102-7104.1993.

Kasemets, K., Ivask, A., Dubourguier, H. C., and Kahru, A. (2009). Toxicity of nanoparticles of ZnO, CuO and TiO_2 to yeast Saccharomyces cerevisiae. *Toxicol. Vitr*. 23, 1116–1122. doi: 10.1016/j.tiv.2009.05.015.

Kumar, P., Di Mauro, E., Zhang, S., Pezzella, A., Soavi, F., Santato, C., et al. (2016). Melanin-based flexible supercapacitors. *J. Mater. Chem*. C 4, 9516–9525. doi: 10.1039/c6tc03739a.

Lee, J. K., Jung, H. M., and Kim, S. Y. (2003). 1,8-Dihydroxynaphthalene (DHN)-melanin biosynthesis inhibitors increase erythritol production in Torula corallina, and DHN-melanin inhibits erythrose reductase. *Appl. Environ. Microbiol*. 69, 3427–3434. doi: 10.1128/AEM.69.6.3427-3434.2003.

Liang, J., Liu, J., Cheng, T. Q., and Song, W. (2021). Comparative Transcriptome Analysis Providing Resistance Mechanism of *Aspergillus oryzae* Under Arsenate Stress. *Geomicrobiol. J*. 38, 426–435. doi: 10.1080/01490451.2021.1877854.

Liang, Q., and Zhou, B. (2007). Copper and manganese induce yeast apoptosis via different pathways. *Mol. Biol. Cell.* 18, 4741–4749. doi: 10.1091/mbc.E07-05-0431.

Liu, Y., Hong, L., Kempf, V. R., Wakamatsu, K., Ito, S., and Simon, J. D. (2004). Ion-exchange and adsorption of Fe(III) by Sepia melanin. *Pigment Cell Res*. 17, 262–269. doi: 10.1111/j.1600-0749.2004.00140.x.

Manirethan, V., Raval, K., and Balakrishnan, R. M. (2020). Adsorptive removal of trivalent and pentavalent arsenic from aqueous solutions using iron and copper impregnated melanin extracted from the marine bacterium *Pseudomonas stutzeri*. *Environ. Pollut*. 257, 113576. doi: 10.1016/j.envpol.2019.113576.

Meredith, P., and Riesz, J. (2004). Radiative relaxation quantum yields for synthetic Eumelanin. *Photochem. Photobiol*. 79, 211–216. doi: 10.1111/J.1751-1097.2004.tb00012.x.

Micillo, R., Panzella, L., Koike, K., Monfrecola, G., Napolitano, A., and D'Ischia, M. (2016). "Fifty Shades" of black and red or how carboxyl groups fine tune eumelanin and pheomelanin properties. *Int. J. Mol. Sci*. 17, 746, 746. doi: 10.3390/ijms17050746.

Mota, E. A., Felestrino, É. B., Leão, V. A., and Guerra-Sá, R. (2020). Manganese (II) removal from aqueous solutions by *Cladosporium halotolerans* and *Hypocrea jecorina*. *Biotechnol. Reports*. 25, e00431. doi: 10.1016/j.btre.2020.e00431.

Poljsak, B., Pócsi, I., Raspor, P., and Pesti, M. (2010). Interference of chromium with biological systems in yeasts and fungi: a review Introduction. *J. Basic Microbiol*. 50, 21–36. doi: 10.1002/jobm.200900170.

Pralea, I. E., Moldovan, R. C., Petrache, A. M., Ilieș, M., Hegheș, S. C., Ielciu, I., et al. (2019). From extraction to advanced analytical methods: The challenges of melanin analysis. *Int. J. Mol. Sci*. 20. doi: 10.3390/ijms20163943.

Robinson, J. R., Isikhuemhen, O. S., and Anike, F. N. (2021). Fungal-Metal Interactions: A review of toxicity and homeostasis. doi: 10.3390/jof7030225.

Rotaru, A. E., Shrestha, P. M., Liu, F., Markovaite, B., Chen, S., Nevin, K. P., et al. (2014). Direct interspecies electron transfer between *Geobacter metallireducens* and *Methanosarcina barkeri*. *Appl. Environ. Microbiol*. 80, 4599–4605. doi: 10.1128/aem.00895-14.

Sarna, T., and Plonka, P. M. (2006). Biophysical Studies of Melanin. Biomed. EPR, Part A Free Radicals, Met. *Med. Physiol*. 125–146. doi: 10.1007/0-387-26741-7_7.

Sigler, K., Chaloupka, J., Brozmanová, J., Stadler, N., and Höfer, M. (1999). Oxidative stress in microorganisms. *I. Folia Microbiol*. 1999 446 44, 587–624. doi: 10.1007/bf02825650.

Schievano, A., Berenguer, R., Goglio, A., Bocchi, S., Marzorati, S., Rago, L., ... & Esteve-Núñez, A. (2019). Electroactive biochar for large-scale environmental applications of microbial electrochemistry. *ACS sustainable chemistry & engineering*. 7, 18198-18212.

Smith, D. F. Q., and Casadevall, A. (2019). The role of melanin in fungal pathogenesis for animal hosts. Curr. Top. *Microbiol. Immunol*. 422, 1–30. doi: 10.1007/82_2019_173.

Sriphirom, P., Chidthaisong, A., Yagi, K., Tripetchkul, S., Boonapatcharoen, N., and Towprayoon, S. (2021). Effects of biochar on methane emission, grain yield, and soil in rice cultivation in Thailand. *Carbon Manag.* 12, 109–121. doi: 10.1080/17583004.2021.1885257.

Suwannarach, N., Kumla, J., Watanabe, B., Matsui, K., and Lumyong, S. (2019). Characterization of melanin and optimal conditions for pigment production by an endophytic fungus, *Spissiomyces endophytica* SDBR-CMU319. *PLoS One 14*, 1–15. doi: 10.1371/journal.pone.0222187.

Tran-Ly, A. N., Ribera, J., Schwarze, F. W. M. R., Brunelli, M., and Fortunato, G. (2020a). Fungal melanin-based electrospun membranes for heavy metal detoxification of water. *Sustain. Mater. Technol*. 23, e00146. doi: 10.1016/j.susmat.2019.e00146.

Tran-Ly, A. N., Ribera, J., Schwarze, F. W. M. R., Brunelli, M., and Fortunato, G. (2020b). Fungal melanin-based electrospun membranes for heavy metal detoxification of water. *Sustain. Mater. Technol*. 23, e00146.

Xu, J., Zhuang, L., Yang, G., Yuan, Y., & Zhou, S. (2013). Extracellular quinones affecting methane production and methanogenic community in paddy soil. *Microbial ecology*. 66, 950-960. doi:10.1016/j.susmat.2019.E00146.

Verma, S., Verma, P. K., Meher, A. K., Dwivedi, S., Bansiwal, A. K., Pande, V., et al. (2016). A novel arsenic methyltransferase gene of *Westerdykella aurantiaca* isolated from arsenic contaminated soil: phylogenetic, physiological, and biochemical studies and its role in arsenic bioremediation. *Metallomics.* 8, 344–353. doi: 10.1039/c5mt00277j.

Viti, C.; Marchi, E.; Decorosi, F.; Giovannetti, L. (2014). Molecular mechanisms of Cr (VI) resistance in bacteria and fungi. *FEMS Microbiology Reviews*. 38, 633–659; DOI:10.1111/1574-6976.12051.

Yu, Y., Teng, Z., Mou, Z., Lv, Y., Li, T., Chen, S., et al. (2021). Melatonin confers heavy metal-induced tolerance by alleviating oxidative stress and reducing the heavy metal accumulation in *Exophiala pisciphila*, a dark septate endophyte (DSE). *BMC Microbiol*. 21, 40 (2021). doi.org/10.1186/s12866-021-02098-1

Zhan, F., He, Y., Yang, Y., Li, Y., Li, T., and Zhao, Z. (2016). Effects of tricyclazole on cadmium Tolerance and accumulation characteristics of a dark septate endophyte (DSE), *Exophiala pisciphila*. *Bull. Environ. Contam. Toxicol*. 96, 235–241. doi: 10.1007/s00128-015-1676-4.

Zhan, F., He, Y., Zu, Y., Li, T., and Zhao, Z. (2011). Characterization of melanin isolated from a dark septate endophyte (DSE), *Exophiala pisciphila*. *World J. Microbiol. Biotechnol*. 27, 2483–2489. doi: 10.1007/s11274-011-0712-8.

Zhao, D., Li, T., shen, M., Wang, J., and Zhao, Z. (2015). Diverse strategies conferring extreme cadmium (Cd) tolerance in the dark septate endophyte (DSE), *Exophiala pisciphila*: Evidence from RNA-seq data. Microbiol. Res. 170, 27–35. doi: 10.1016/j.micres.2014.09.005.

Zou, Y., Xie, C., Fan, G., Gu, Z., Han, Y., 2010. Optimization of ultrasound-assisted extraction of melanin from *Auricularia auricula* fruit bodies. *Innov. Food Sci. Emerg. Technol*. 11, 611–615. https://doi.org/10.3390/molecules21010018.

Anexos

Table S1. Kinetic Modeling of CH_4 and CO_2 Production in Anaerobic Microcosms under Different CM Treatments

		Gompertz		
base: gCOD-straw	mLCH4/ gDQO	mLCH4/ gDQO·d	days	R^2
Treatment	Am	μm_g (mLCH4/ gDQO·d)	λ	
C2TF	227.286993	5.427	8.954	0.985
BIO	191.046178	5.348	7.231	0.997
ME	148.847026	4.167	10.916	0.986
MAG	221.996946	4.282	6.036	0.974

Tabla S2. Isotopic compositional analysis of CH4.

	$\delta^{13}C$-CH_4		**$\delta^{2}H$-CH_4**		**$\delta^{13}C$-CO_2-DIC**		***Alpha_C***
Treatment	**delta13_AVG**	**delta13_des**	**delta2_AVG**	**delta2_des**	**CO_2_AVG**	**CO_2_des**	
C2TF	-57.7	0.1	-370	1	-21.3	0.1	1,039
C2TF	-56.5	0.1	-366	1	-20.3	0.1	1,038
C2TF	-51.8	0.5	-369	1	-17.6	0.5	1,036
C2TF	-54.7	0.1	-368	2	-18.84	0.01	1,036
ME	-54	0.1	-357	2	-20.22	0.02	1,036
ME	-62.8	0.5	-362	2	-22	0.5	1,044
ME	-57.33	0.02	-360	2	-21.07	0.02	1,038
ME	-51.6	0.5	-356	1	-20.3	0.5	1,033
BIO	-50.29	0.05	-364	2	-19.81	0.02	1,032
BIO	-50.6	0.5	-362	2	-19.8	0.5	1,032
BIO	-51.3	0.5	-353	1	-19.3	0.5	1,034
BIO	-51.4	0.01	-365	2	-19.7	0.1	1,033
MAG	-52.9	0.5	-355	2	-19.4	0.5	1,035
MAG	-51.7	0.5	-355	1	-19.1	0.5	1,034
MAG	-51.8	0.2	-358	2	-19.63	0.04	1,034
MAG	-51.3	0.5	-357	2	-19.1	0.5	1,034
C1TF	-57.7	0.1	-370	1	-21.3	0.1	1,039
C1TF	-56.5	0.1	-366	1	-20.3	0.1	1,038
C1TF	-51.8	0.5	-369	1	-17.6	0.5	1,036
C1TF	-54.7	0.1	-368	2	-18.8	0	1,038

Table S3. qPCR was used to quantify total bacteria (16S rRNA), dissimilatory sulfate-reducing bacteria (aprA), and methanogenic archaea (mcrA), along with their respective ratios. Statistical tests were performed to compare C2T0, C2TF, ME, BIO, and MAG treatments. The figure shows statistically significant differences determined using Tukey's HSD test (P-value < 0.05).

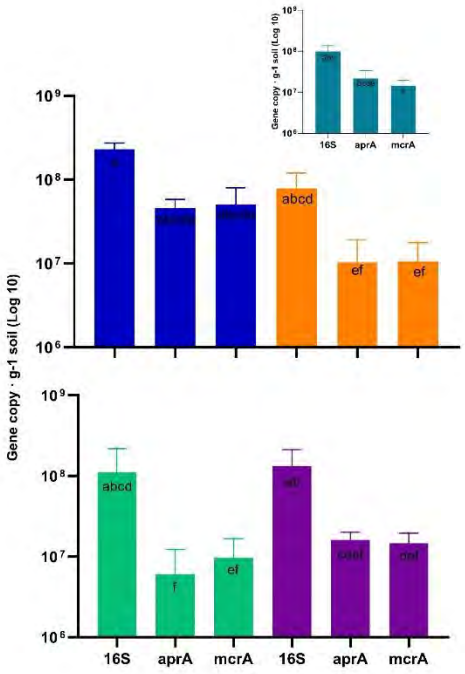

Figure 1. Copy number quantification of bacterial 16S rRNA, sulfate reducer aprA and methanogenic mcrA genes (qPCR) in the soil slurries over the 130-day incubation period. Data are means ± SE (n = 4). Differences between two incubation time points were determined using TUKEY HSD test (P-value < 0.05). The exact copy numbers per gram of dry paddy soil are shown in Tables S3. Insert (green) is control C2T0 with Straw/CM; blue is control C2TF without Straw/CM; orange is fungal melanin; green is biochar and purple is magnetite treatment.

Table S4. Bacteria and archaea community metrics: richness (ACE), diversity (Shannon) and dominance (Simpsom). Tukey HSD test, significance p-value (<0.05) letters indicate statistical differences by time and treatment.

Kingdom	Straw presence	Time	Fertilization treatments	Shannon	Simpsom	ACE
Bacteria	Without Straw (WS)	Inital	C1T0	7.13±0,05 **a**	0,998±1.08E-04 **a**	2613.71±188.4 **a**
			C1TF	7,0±0,14 **a**	0,998±1.40E-03 **ab**	2660.40±131,4 **a**
		Final	C2T0	7.06±0,02 **a**	0.998±8.9E-05 **ab**	2671.50±18,4 **a**
			C2TF	7.0±0.08 **a**	0.998±1,94E-04 **a**	2363.39±386,1 **a**
			BIO	7.01±0,08 **a**	0.998±3.38E-04 **ab**	2525.32±14,3 **a**
			ME	7,02±0,09 **a**	0.998±3.83E-04 **ab**	2654,25±100,0 **a**
	Straw (S)		MAG	6.56±0,11 **b**	0.996±4.33E-04 **b**	1506,42±336,8 **b**
Kingdom	**Plant presence**	**Time**	**Fertilization treatments**	**Shannon**	**Simpsom**	**ACE**
Archaea	Without Straw (WS)	Inital	C1T0	2.64±0.15 **a**	0.913±0.01 **a**	19±3,65 **c**
			C1TF	2.84±0,1 **a**	0.921±0.01 **a**	25.8±1,50 **c**
		Final	C2T0	2,64±0.13 **a**	0.914±0.009 **a**	19±3,56 **c**
			C2TF	2.59±0.10 **a**	0.846±0.03 **b**	39,89±2,43 **b**
			BIO	2,83±0.26 **a**	0.896±0.04 **ab**	44.69±3.24 **ab**
			ME	2.61±0.06 **a**	0.853±0.01 **b**	38,89±4.61 **b**
	Straw (S)		MAG	2.79±0.06 **a**	0.858±0.01 **b**	53.13±2.83 **a**

Table S5. PERMANOVA Pairwise Comparisons of Treatment Effects on Microbial Communities and Controls (High F-Values Indicate Significant Differences)

Bacteria

	pairs	Df	F.Model	R2	p.value	p.adjusted
1	C2T0 vs C1TF	0.007	4,360	0.421	0.065	1
2	C2T0 vs C2TF	0.078	67,594	0.919	0.037	0.777
3	C2T0 vs BIO	0.054	41,365	0.892	0.031	0.651
4	C2T0 vs MAG	0.075	68,065	0.919	0.027	0.567
5	C2T0 vs ME	0.059	51,069	0.895	0.022	0.462
6	C2T0 vs C1T0	0.01	11,818	0.663	0.037	0.777
7	C1TF vs C2TF	0.059	29,385	0.830	0.026	0.546
8	C1TF vs BIO	0.040	17,091	0.774	0.035	0.735
9	C1TF vs MAG	0.056	28,764	0.827	0.025	0.525
10	C1TF vs ME	0.042	21,040	0.778	0.035	0.735
11	C1TF vs C1T0	0.01	5,940	0.498	0.023	0.483
12	C2TF vs BIO	0.007	4,247	0.459	0.03	0.63
13	C2TF vs MAG	0.023	16,261	0.730	0.027	0.567
14	C2TF vs ME	0.008	5,409	0.474	0.032	0.672
15	C2TF vs C1T0	0.063	57,361	0.905	0.035	0.735
16	BIO vs MAG	0.017	10,361	0.674	0.034	0.714
17	BIO vs ME	0.009	5,420	0.520	0.034	0.714
18	BIO vs C1T0	0.043	34,499	0.873	0.031	0.651
19	MAG vs ME	0.039	28,344	0.825	0.037	0.777
20	MAG vs C1T0	0.058	55,278	0.902	0.025	0.525
21	ME vs C1T0	0.046	41,684	0.874	0.029	0.609

Archaea

pairs	Df	F.Model	R2	p.value	p.adjusted
C2T0 vs C1TF	0.059	18,729	0.757	0.033	0.693
C2T0 vs C2TF	0.546	350,217	0.983	0.024	0.504
C2T0 vs BIO	0.342	66,844	0.930	0.038	0.798
C2T0 vs MAG	0.489	459,132	0.987	0.039	0.819
C2T0 vs ME	0.432	75,222	0.926	0.027	0.567
C2T0 vs C1T0	0.001	0.50	0.091	0.84	1
C1TF vs C2TF	0.362	108,358	0.948	0.034	0.714
C1TF vs BIO	0.203	27,987	0.848	0.029	0.609
C1TF vs MAG	0.312	109,584	0.948	0.032	0.672
C1TF vs ME	0.271	35,977	0.857	0.029	0.609
C1TF vs C1T0	0.045	13,121	0.725	0.046	0.966
C2TF vs BIO	0.014	2,676	0.349	0.138	1
C2TF vs MAG	0.016	13,121	0.686	0.031	0.651
C2TF vs ME	0.008	1.30	0.178	0.318	1
C2TF vs C1T0	0.450	293,125	0.983	0.035	0.735
BIO vs MAG	0.019	4,054	0.448	0.027	0.567
BIO vs ME	0.008	0.745	0.130	0.494	1
BIO vs C1T0	0.287	47,901	0.923	0.1	1
MAG vs ME	0.018	3,265	0.352	0.038	0.798
MAG vs C1T0	0.403	426,317	0.988	0.028	0.588
ME vs C1T0	0.357	54,178	0.916	0.032	0.672

Table S6. The relative abundance (RA) of fungal taxa using ITS amplicon sequencing. We present the taxonomic composition at the phylum and family level (top 10 most abundant) visualized with an image hetmap. Additionally, the fungal class composition is explored through a separate bar plot showcasing the top 10 most abundant classes. Alpha and beta diversity metrics were employed to characterize community richness and composition, respectively. All biodiversity analyses were accompanied by statistical tests.

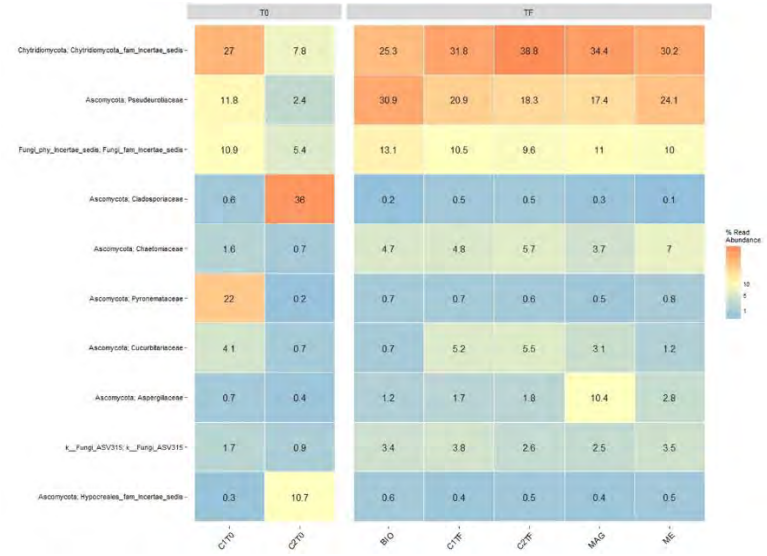

Figure 6a. Heatmap average relative abundance (RA) of fungi phyla-family, in different sample types (control initial (C1T0/C2T0); control 130 days of incubation (C1TF/C2TF); and treatments 130 days of incubation (biochar: BIO, melanin: ME, magnetite: MAG).

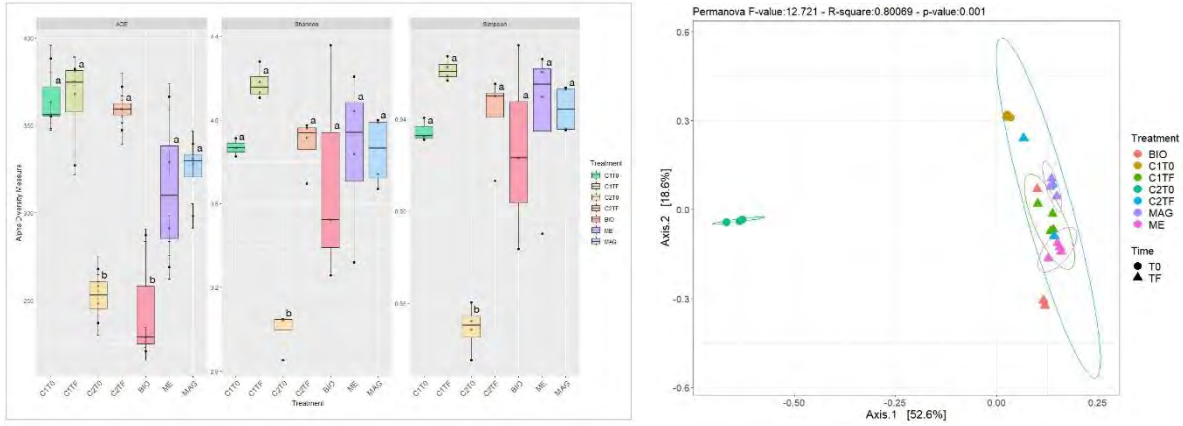

Figure 6b. Fungi community metrics: richness (Chao1), diversity (Shannon), and relative dominance index (Simpsom). Significance p-value $p < 0.05$, letter indicate statistical differences according to Tukey HSD test between the CM treatments (BIO: biochar; ME: fungal melanin MAG: magnetite); Control: C2T0 (time 0 incubation) and C2TF (final time) both withou CM and with straw (Left panel). Principal coordinate analysis (PCoA) plots based on Bray-Curtis dissimilarities at ASV level, illustrating the beta-diversity of Fungi communities (rigth panel) . PERMANOVA test results of all groups are displayed in the corresponding headers.

Table S7. Taxonomic categories relative abundance (RA) of both bacteria and archaea kingdom.

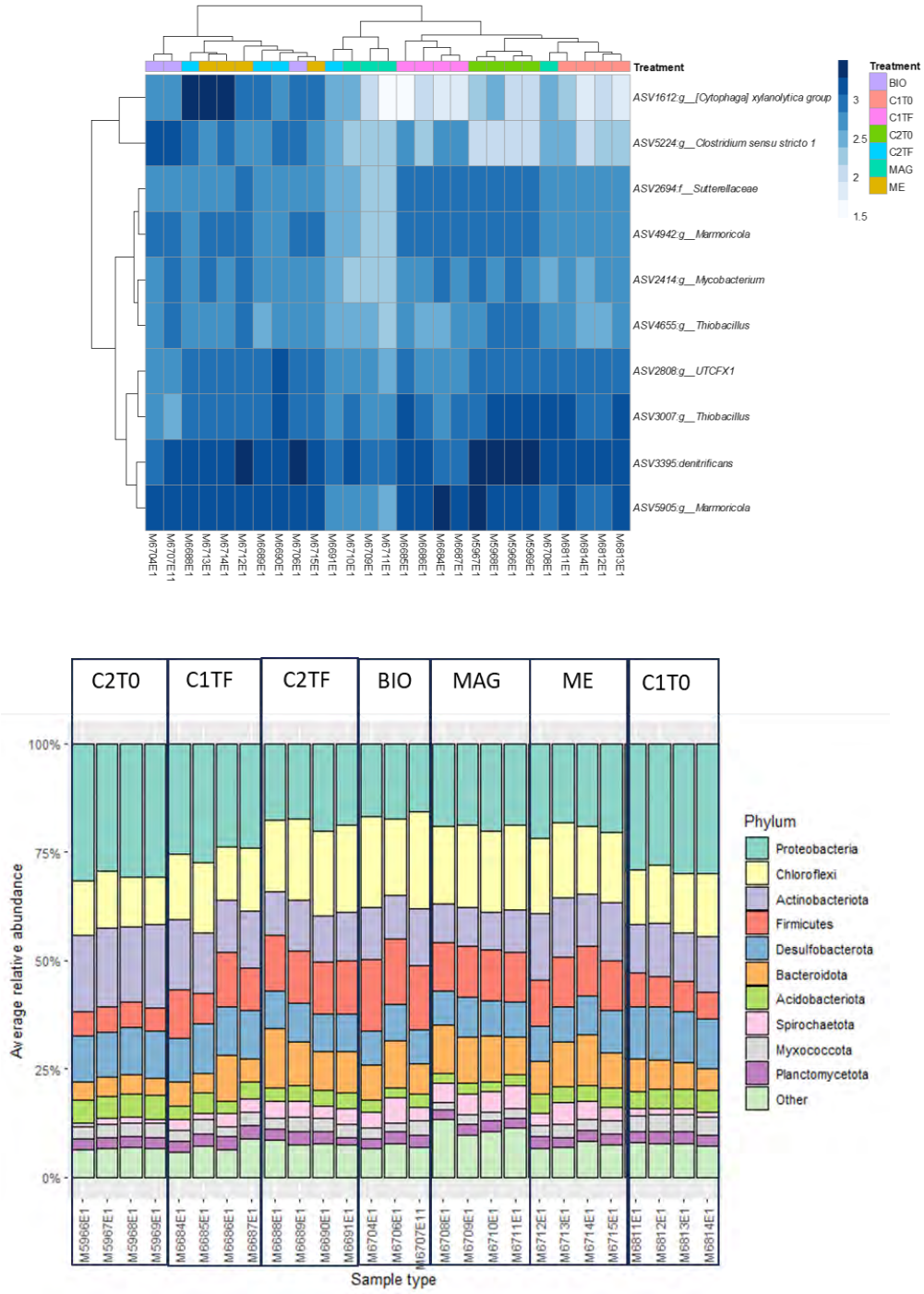

Figure 7a. Bacteria community composition based on the relative abundance of ASV. Values are averaged across treatments. Only taxa with a relative abundance above 0.1% are shown. Up, Heat-map and clustering of the soil microbial community composition of the ASV taxa with major relative abundance. Down, Bacterial community composition of the soil microbial community composition.

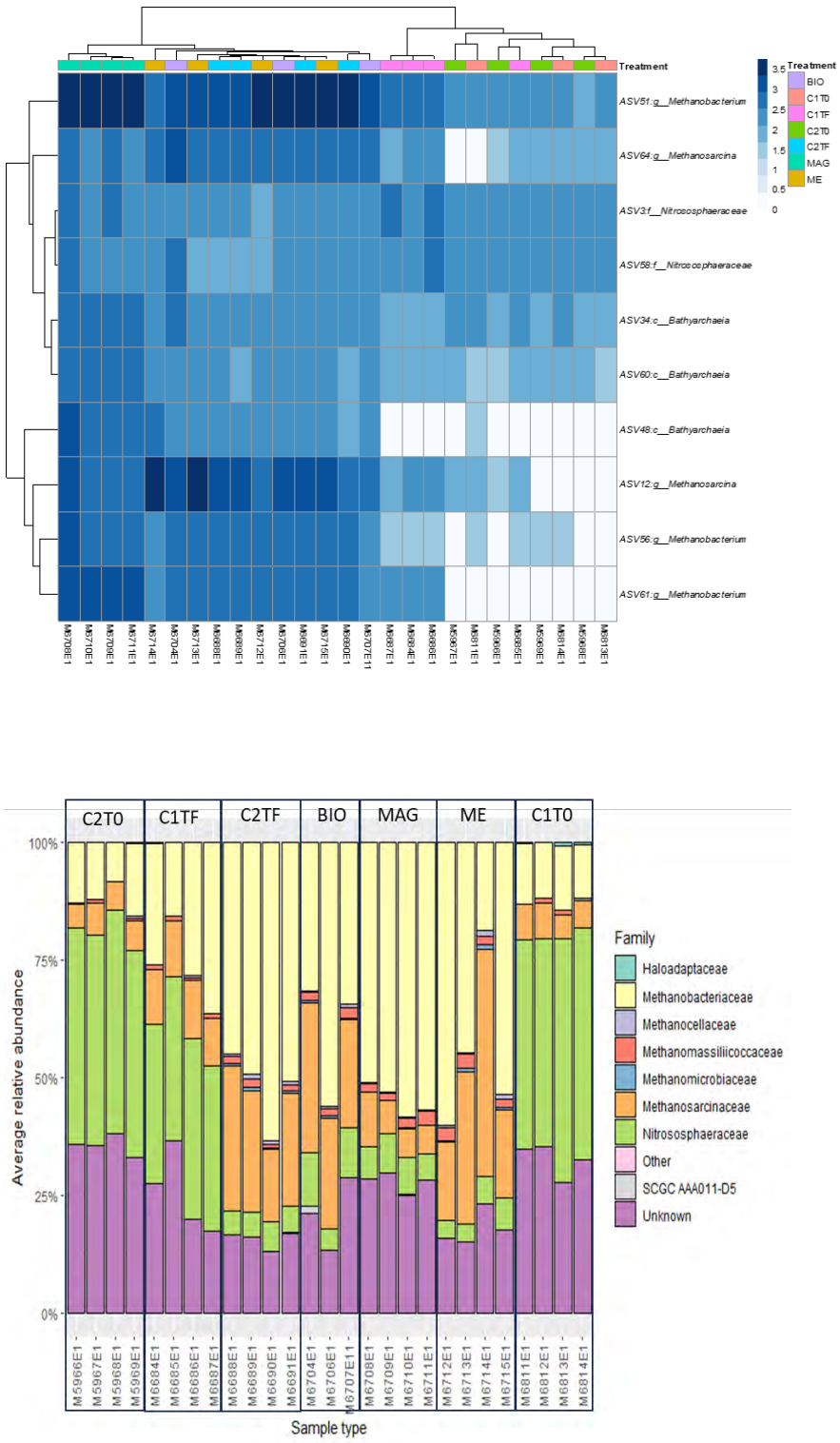

Figure 7b. Archaea community composition based on the relative abundance of ASV. Values are averaged across treatments. Only taxa with a relative abundance above 0.1% are shown. Up, Heat-map and clustering of the soil microbial community composition of the ASV taxa with major relative abundance. Down, Archaea community composition of the soil microbial community composition.

TableS10a. Physicochemical properties measured after 130 days of incubation.

	pH	EC(µS/cm)	NH_3 (µ/ml)	COD (mg O_2/Kg)	N (mg N/Kg)	SO_4 (mg/L)
C1T0	7.20±0.21	1.13±0.0	3.13±0.31	1517.75±962.48	405.5±107.72	406±6.78
C1TF	7.59±0.36	12.36±0.84	51.91±5.65	13659.25±642.56	540±38.13	17.5±13.58
C2T0	9.38±0.07	4.46±0.3	26.25±2.14	19062.75±5641.47	411±69.73	266.75±13.6
C2TF	6.72±6.71	9.14±10.31	33.81±33.81	19334±18716.25	690±593	28±25.25
ME	6.76±0.05	9.39±0.1	23.49±2.43	25602.75±6036.81	626.5±15.46	162.25±195.46
BIO	6.61±0.04	8.7±0.75	21.9±13.46	28391.75±2985.01	662±46.77	463.25±513.21
MAG	6.68±0.05	8.49±0.17	35.32±2.83	18730.25±1420.83	704.25±18.84	104.75±11.17
p-value	1.00E-15	2.20E-16	5.70E-07	4.50E-05	1.90E-05	0.031

TablesS10b. Statistical Analysis of Environmental and Treatment Variables (C2TF, C1TF, BIO, ME, MAG) using Redundancy Analysis (RDA) with Spearman Correlation

	Bacteria				Archaea		
	Variance	**F**	**R^2**		**Variance**	**F**	**R^2**
pH	0.0009212	1.96	0.093**.**	**pH**	0.0008512	0.38	0.804
NH3	0.0006951	1.48	0.177	**NH_3**	0.0014064	0.63	0.615
COD	0.0008805	1.87	0.100	**DQO**	0.0014195	0.63	0.606
N_total	0.0020525	4.36	0.008**	**N_total**	0.00791	3.52	0.029*
SO4	0.0006074	1.29	0.240	**SO_4**	0.0019007	0.85	0.444
CH4	0.0015221	3.23	0.024*	**CH_4**	0.0183968	8.20	0.001***
CO2	0.0001236	0.27	0.939	**CO_2**	0.0072907	3.25	0.05*

Signif. codes: 0 '*' 0.001 '**' 0.01 '*' 0.05 '.' 0.1 ' ' 1**